SYNTHESIS AND CHARACTERIZATION OF FISH SCALES (*Oreochromis niloticus*) DERIVED BIOCHAR AND MAGNETIC COMPOSITES AND THEIR APPLICATION IN REMOVAL OF ANIONIC INDIGO CARMINE AND CATIONIC CRYSTAL VIOLET DYES FROM SYNTHETIC AND INDUSTRIAL WASTEWATER

BY

GEORGE OINDO ACHIENG'

A THESIS SUBMITTED IN FULFILLMENT OF THE REQUIREMENTS FOR THE DEGREE OF DOCTOR OF PHILOSOPHY IN CHEMISTRY

SCHOOL OF PHYSICAL AND BIOLOGICAL SCIENCES

MASENO UNIVERSITY

DECLARATIONS

I affirm that this thesis has never been submitted for examination and award of a degree at Maseno University or another higher learning institution. Work presented herein is novel and all sources of information have been supported by relevant references.

	Signature	**Date**
Student: George Oindo Achieng' Reg. No.: PHD/SC/00076/2015 Maseno University	……	…….
Supervisors: Prof. Chrispin O. Kowenje Maseno University	……..	…….
Prof. Joseph O. Lalah The Technical University of Kenya	……..	……..
Prof. Stephen O. Ojwach University of Kwa-Zulu Natal	…….	……

ACKNOWLEDGEMENT

I first acknowledge the divine protection and provision from Almighty Living God this far. It has been a long research journey under the fruitful supervision of my supervisors Prof. Chrispin Kowenje and Prof. Joseph Lalah who were always available for intellectual contributions whenever I was in need. I acknowledge the overwhelming contribution to the success of this work by my host supervisor, Prof. Stephen Ojwach, in the School of Chemistry at the University of KwaZulu-Natal (UKZN) Pietermaritzburg Campus. Numerous assistances offered by Dr. Lorika Beukes, Dr. Vishal Bharuth and Ms. Cynthia Matyumza of School of Life Sciences, Microscopy & Microanalysis Unit (MMU) during SEM-EDX and TEM characterizations, Ms. Clark and Ms. Jessica offered a working space, thus, are highly appreciated. Fellow students from Prof. Ojwach's, Prof. Jaganyi's and Prof. Ajibade's research groups in the School of Chemistry, UKZN-Pietermaritzburg Campus are acknowledged for their contributions. Mr. Ephraim Chauke, a PhD Biochemistry student in the School of Life Sciences is appreciated for always being at my disposal whenever I needed to access the building during sample preparations and batch adsorption experiments. Colleagues in the School of Chemistry and Material Science (formerly Department of Chemical Science and Technology) at the Technical University of Kenya (TUK), especially Dr. James Jorum Owuor and Mr. Daniel Ouma Nyangoro are thanked for their unconditional help during biomass collection, preparation, pulverization and charring. Immense contributions made by Dr. Victor Odhiambo Shikuku, a colleague from Prof. Kowenje's Maseno University Chemistry Department research group, Prof. Dickson Mubera Andala and colleagues at CSI International Ltd are highly recognized and appreciated. Dr. James

Ochieng' Ochieng' is appreciated for assisting in characterization of some research materials. I recognize and appreciate the efforts of my brother, Mr. Alfred Omondi Achieng', for assisting in sampling of industrial dye wastewater. National Research Foundation (NRF-Kenya) and DAAD-Excellent Center for Development Cooperation (Exceed-Swindon) are acknowledged for their financial support.

DEDICATION

This work is dedicated to the family of Naphtali Achieng' Atina.

ABSTRACT

The global and regional increase in demand for textile products have led to increased quantities of dye wastewater in the environment, which is a potential source of carcinogenic compounds. This situation not only hampers photosynthetic activities of benthic plants but also affects aesthetic quality of water sources. Apart from many available wood biomass, fish scales of Tilapia (*Oreochromis niloticus*) are also abundant wastes in the environment that can be processed and applied as materials in abstraction of indigo carmine (IC) and crystal violet (CV) dyes from wastewater. Nevertheless, physical and chemical characteristics of raw fish scales and their biochars are not known. The main objective of this study was to synthesize and characterize fish scale biochars (FSB) and magnetic composites (FSB@Fe_3O_4) at varying temperatures and apply them in remediation of industrial dye effluents. Pulverized raw fish scales (RFS) were pyrolysed over temperature of 200 ºC - 800 ºC and magnetic composites, FSB@400 ºC-Fe_3O_4, FSB@600 ºC-Fe_3O_4 and FSB@800 ºC-Fe_3O_4, were synthesized by chemical co-precipitation method. The adsorbents were characterized for peak optical absorbance, functional groups, magnetic strength, surface morphology, particle size, elemental compositions, surface charge, surface area, thermal stability and crystallinity. The potential of pulverized RFS, FSB and FSB@Fe_3O_4 compared to activated charcoal (AC) for abstraction of IC and CV dyes from aqueous solutions was determined as a function of initial dye concentration, contact time, dye solution pH, adsorbent dosage and temperature. Peak optical absorbance was 252-320 nm with FSB@600 ºC posting the lowest peak of all the magnetic composites studied. The adsorbents contained CO_3^{2-}, PO_4^{3-}, Fe-O and -OH as confirmed by EDX and XRD analysis. TEM results displayed spotted ring-like patterns on the surface of FSB and catenation of identical spherically shaped flowers was observed on FSB@Fe_3O_4. Magnetization values for VSM analysis ranged between 8 to 10 emu/g, sufficient for adsorbent recovery with a magnet. The pH_{pzc} ranged between 3.80-8.42, while TGA showed that a rise in temperature led to a rise and a decline in weight loss for RFS, FSB and FSB@Fe_3O_4, correspondingly. BET surface areas were 94.05 and 102.67 m^2/g for FSB@600 ºC and FSB@600 ºC-Fe_3O_4, respectively. Adsorption results demonstrated that the quantity (q) of the dyes adsorbed by FSB and FSB@Fe_3O_4 increased with initial dye concentration, material load and solution temperature. Lower quantities of IC and higher quantities of CV were recorded at higher pH levels. Statistics fitted *pseudo*-second-order kinetic models while the Langmuir isotherm presented the best fit of all the models tested. The optimum pH 2 and pH 8-10 were favourable for adsorption of IC and CV, respectively. Wastewater remediation data revealed that for location A, FSB@600 ºC significantly reduced IC and CV by 72.00% and 96.96%, correspondingly. Reusability results showed that the adsorbents conserved their initial adsorption capacities for the abstraction of IC for five consecutive cycles without significant depletion. However, substantial decrease in adsorption capacities at the fifth regeneration cycle was observed for CV. Fish scale biomass can be applied in the synthesis of adsorbents that can be adopted as easily accessible materials for remediation of industrial dye wastewater.

TABLE OF CONTENTS

ABBREVIATIONS AND ACRONYMS

ANOVA- Analysis of variance

BET - Brunauer-Emmett-Teller

CV - Crystal violet

EDX - Energy Dispersive X-ray

FSB - Fish Scales Biochar

FT-IR- Fourier-Transform Infrared

IC - Indigo carmine

pzc - Point of zero charge

SAS - Statistical Analysis System

SEM - Scanning Electron Microscopy

TEM - Transmission Electron Microscopy

VSM - Vibrating Sample Magnetometry

XRD - X-Ray Diffraction

DEFINITION OF TERMS

AC – Activated charcoal

RFS – Raw fish scale

Fe_3O_4 – Magnetite

FSB – Fish Scale Biochar

HAp – Hydroxyl apatite

H – Magnetic field

KHz – kilohertz

K_L – Langmuir constant indicating the energy of adsorption

K_F – Freundlich constant

LSD – Least significant difference

M – Magnetization

M_s – Magnetization saturation

n – Freundlich model constant that expresses the strength of the adsorbate removal process

O – Oersted, units for measuring magnetization

P – P value, a measure of statistical significance

pH_i – Initial pH of solution

pH_f – Final pH of solution

R_L – dimensionless separation factor illustrating the favourability of an adsorption process

TGA – Thermogravimetric analysis

UV-Vis – Ultra violet visible

VSM – Vibrating sample magnetometry

q_m – Langmuir maximum monolayer adsorption capacity

%R – Percent removal efficiency

ΔH – Changes enthalpy

ΔG – Changes in Gibb's free energy entropy

ΔS – Changes energy entropy

LIST OF TABLES

LIST OF FIGURES

LIST OF APPENDICES

CHAPTER ONE

INTRODUCTION

1.1 Background

Dyes are materials that, when applied to a substrate, impart colour via a process that momentarily changes any crystal arrangement of the coloured substrates (Bafana *et al*., 2011). Dyes are largely used in a variety of industries which include but not limited to textile, pharmaceutical, food, cosmetics and paper (Carneiro *et al*., 2010) and are capable of adsorbing onto compatible surfaces through covalent bonding, physical adsorption or mechanical retention (Bafana *et al*., 2011). Classification of dyes is based on their application and chemical structure, whereby colour is ascribed to different functional groups such as azo, methine, nitro, and carbonyl found within the dye structure, which are known as chromophores. In addition, electron withdrawing or donating substituents referred to as auxochromes are included to strengthen the colour of the chromophores. The most common auxochromes are amine, carboxyl, sulfonate and hydroxyl (Dos Santos, 2005; Prasad & Rao, 2010). The increased need for textile products and the relative increase in their manufacture has led to the application of artificial dyes such as anionic indigo carmine (IC) and cationic crystal violet (CV), subsequently, contributing to dye wastewater pollution in the environment, since there is either intentional discharge of raw wastewater or inefficiency of the treatment systems. The levels of IC and CV dyes in the industrial wastewater from Nairobi are not known, yet they are potential disease causing compounds, can hamper the photosynthetic activities of benthic plants and affect the aesthetic quality of water sources. Therefore, this calls for remediation process to aid in reducing the level of industrial dyes in the wastewater.

In order to treat dye wastewater, a number of adsorbents have been used some of which are carbon materials derived from either plant or animal biomass, which are naturally abundant and renewable (Xiu *et al*., 2017). Important focus has been given to a variety of plant biomass such as energy crops, agricultural remains, and woody biomass (Xie *et al*., 2015; Kimosop *et al*., 2017). Numerous researches have been done on plant biomass (Ngeno *et al*., 2016) while little research output exists on the feasibility of animal biomass compared to the latter. A noble example is fish scales, which are considered as wastes that lack clear economic significance (Rustad, 2003; De Gisi *et al*., 2016; Nnaemeka *et al*., 2016; Nia *et al*., 2017; Temesgen *et al*., 2018; Fegousse *et al*., 2019; Lafi *et al*., 2019). Despite their sustainable abundance, fish scales are a suitable alternative worth exploring in the treatment of dye wastewater instead of laying in the environment and decompose leading to pollution of available water resources and ambient air. Application of fish scales as adsorbents for the abstraction of copper from water was reported by Huang (2007). The researcher utilized Tilapia *Niloticus Linnaeus* fish scales instead of Atlantic cods' scales, alluding to the fact that tilapia is cheaper and more available compared to Atlantic cod. In addition, it has been shown that applying fish scales as an adsorbent displayed a more feasible substitute for abstraction of metals from wastewater compared to wool since fish scales are already a waste generated resource material from fish markets and households (Villanueva-Espinosa *et al*., 2001; Huang, 2007). Rustad (2003) reported that about 91 million tons of fish and shellfish from both inland and marine waters were captured worldwide and 50 - 60 % were consumed by human and the rest were discarded as waste. Despite the increase in the world human

population and fish aquaculture, statistics have shown that there is no significant reduction in number of fish captured (Delgado *et al*., 2003; Mohammed *et al*., 2008), and this supports the sustainable accessibility of fish scales as a source for manufacture of commercial adsorbents.

Adsorption characteristics of RB5G dye onto fish scales in the presence of NaCl and protein (SP) mixtures were studied by Neves *et al*. (2018) and the results showed favorable kinetics and high adsorption capacity for the dye hence providing useful base data for the design, optimization and scaling up of the adsorption processes for commercial application. Bamukyaye and Wanasolo (2017) confirmed that the abstraction of chromium (VI) by processed fish-scales was highly viable for remediation of effluents from Tannery Industries. Related work was also reported by Mustafiz (2003) with fish scales from Atlantic cods. Villanueva-Espinosa *et al*. (2001) examined the suitability of thermally pre-treated fish scales, from Mojarra Tilapia variety, for metal ion remediation and observed that the processed adsorbent was effective in the removal of Cu^{2+} ions from wastewater. Similarly, other researchers have investigated the application of fish scales on sequestration of pollutants from wastewater and confirmed their feasibility hence recommended them for removal of metal ions and dyes (Chowdhury *et al*., 2012; Ho *et al*., 2012; Begum & Kabir, 2013; Zhu *et al*., 2013; Abdullah & Vo, 2014; Othman *et al*., 2016; Ooi *et al*., 2017; Ahmadifar & Koohi, 2018; Gholami *et al*., 2018; Kwaansa-Ansah *et al*., 2019). In this regard, raw fish scales can be applied in adsorption of IC and CV dyes from the industrial wastewater; however, their physical and chemical properties such as surface area, particle

size and inorganic carbon content may not be sufficient to give good adsorption output. However, these properties can be enhanced through charring of the raw fish scales in order to obtain a biochar.

Biochar, a product from thermally converted biomass, has been considerably applied in abstraction of many contaminants owing to its economical and abundance benefits (Xiu *et al*., 2017). Studies have ascertained that charring improves the surface characteristics that aid in increasing the adsorption capacity of a biochar (Zhao *et al*., 2017; Noor *et al*., 2019), consequently adsorption increases with increase in charring temperature (Luo *et al*. (2018; Nnadozie & Ajibade, 2021). However, it is not known whether the physical and chemical properties of the characterized fish scale biochar will be improved by different charring temperatures to make it a better adsorbent than the raw fish sacles.

The removal efficiencies and adsorption capacity of the dyes by the adsorbents are usually influenced by several factors such as adsorbent dosage, initial pH of the adsorbate, temperature, contact time e.t.c. and the adsorption process is governed by mechanisms and kinetics (Dutta *et al*., 2021). Patel & Vashi (2010) established that Freundlich isotherm was the most applicable in describing the adsorption process of crystal violet. In another study, Azari *et al*. (2021) investigated dye removal from raw textile wastewater by magnetic multi-walled carbon nanotubes-loaded alginate. The data fitted the Langmuir isotherm and *pseudo*-second-order kinetics. However, it is not known how adsorbent dosage, initial pH of the adsorbate, temperature, and contact time will affect the adsorption parameters of FSB, and

FSB@Fe_3O_4. In addition, the reaction kinetics and isothermal mechanisms that will govern the adsorption of dye by FSB, and FSB@Fe_3O_4 are not known.

Recovery and subsequent regeneration and reuse/recycling of adsorbent are important attributes of an adsorption process from economy and environmental point of view (Kulkarni & Kaware, 2014). In this case, anchoring/immobilizing of magnetic particles into the biochar has aided in separating adsorbents from aqueous media through the introduction of an external magnetic field, thus, increasing efficacy and limiting chances for secondary pollution by used adsorbents (Yu *et al*., 2013; Wu *et al*., 2016). Researchers have justified the inclusion of magnetic particles in composite preparations since they confer beneficial properties such as easy recovery, cost-effectiveness, ease of synthesis, absence of secondary contamination, environmental friendliness and high surface area (Ebrahimian Pirbazari *et al*., 2016; Gholami *et al*., 2018; Mushtaq *et al*., 2019). Subsequently, stability/leaching effect and the recyclability of a magnetite-impregnated adsorbent are essential properties in qualifying it for application in adsorption process under considered experimental conditions (Song *et al*., 2014; Rangabhashiyam *et al*., 2018). However, it is not known if the fish scale biochars will exhibit magnetic properties sufficient for their recovery, stability to resist leaching effect in adsorption conditions and withstand regeneration for reuse/recycling after adsorption process.

Indigo carmine (IC) is an artificial anionic dye that has been applied as an antiseptic material, biotic pigment, dermatological material and preservative to poultry feedstuff. It is also a

potential cancer causing chemical which is intractable and lethal to animal cells (Owens, 2002). Crystal violet (CV) is an important triphenylmethane cationic dye commonly applied in colouring paper, cotton, silk and leather. It is also used as a disinfectant and antiseptic in pharmaceutical industry. Exposure to crystal violet leads to serious disease (Guz *et al*., 2014). Contamination pathway involves effluent discharge from conventional treatment plants where the dyes bioaccumulate in sediments and soil and eventual flow into public water supply systems (Vikrant *et al*., 2018). The chemical structures of the IC and CV dyes are given in Figures 1.1a and b, respectively.

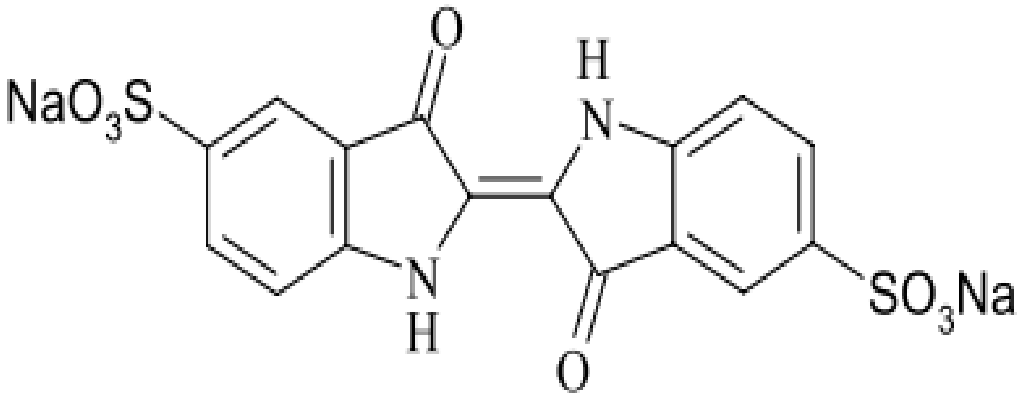

Figure 1.1a: Indigo Carmine (Ramesh & Pavagada Sreenivasa, 2015)

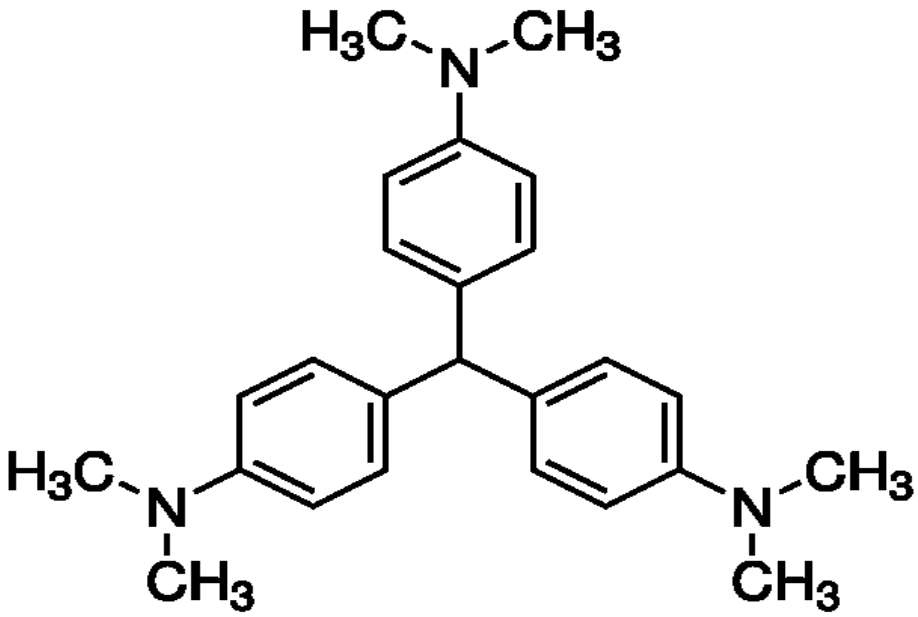

Figure 1.1b: Crystal Violet (Song *et al*., 2016)

Different adsorbents have been used to effectively sequester the colour of dye wastewater; for example, Elango & Govindasamy (2018) used activated carbon derived from temple waste flowers to remove the colour of industrial wastewater. In another study, Panhwar *et al*. (2020) employed activated carbon to reduce the colour of textile wastewater samples. However, it is not known whether the application of RFS, FSB, and FSB@Fe_3O_4 will be effective in reducing the colour of industrial dye wastewater.

The aim of this study was to employ an abundant and disregarded local environmental pollutant, fish scales, from a local large-scale fish market in Gikomba in Nairobi, Kenya, in the remediation of dye-polluted effluent from some local textile industries. Preliminary findings for proof of the adsorption concept were demonstrated for pulverized raw fish scales and their biochars to rationalize the significance of carrying out the biomass thermo-chemical conversion process. The potential of the adsorbents for the abstraction of indigo

carmine and crystal violet dyes from synthetic wastewater was also determined as a function of initial dye concentration, contact time, adsorbent dose, dye solution pH and temperature.

1.2 Statement of the problem

Effluents from textile industries are categorized as the most contaminating of all the industrial sector waters, owing to its quantity and composition. In addition, the increased need for textile products and the relative increase in their manufacture, and the application of artificial dyes have contributed to dye wastewater being one of the general sources of contamination problems in modern times. The existence of very minor concentration of dyes in the water, which are usually noticeable, influences the aesthetic quality and clearness of water sources such as lakes, and rivers leading to damage to the marine environment. In addition, dyes are potent carcinogens, toxic to mammalian cells, mutagenic, able to absorb and reflect sunlight in water hence diminishing photosynthetic process of benthic plants hence affecting negatively the aquatic food chain. Although adsorption is a proven technology for the removal of dye, it has a major limitation to its application due to the associated high cost. Thus, there is need to device green and sustainable technology to assist in the removal of dyes from the polluted water. Numerous researches have been done on plant biomass while very diminutive information exists on the feasibility of animal biomass, for example, fish scales, which are viewed as wastes that do not have a clear economic significance and pose, environmental menace especially when they decompose.

Raw fish scale is expected to exhibit lower surface area than the counterpart biochar. Thermal conversion of raw fish scale to biochars at different temperatures is a better

transformation to improve its nature and guarantee longevity. Anchoring the biochar in magnetic particles can aid in its recovery from the treatment vessel after removal using an external bar magnet, subsequently its regeneration and reuse/recycling. It is uncertain how the morphological and chemical properties of the adsorbents prepared at different temperatures would vary as characterized using various techniques. The overall behavior of the adsorbents during dye removal from the aqueous media is subject to mixed influences of dye concentration, pH and temperature of the media, contact time between the adsorbent and the media, and the adsorbent dose. Besides, the removal efficiencies of the dyes by the adsorbents is expected to be governed by mechanisms and kinetics. The magnetic composites can easily contaminate the treated dye wastewater through leaching of the iron metal if the adsorbent is unstable under reaction conditions such as pH.

1.3 Objectives

1.3.1 General objective

To synthesize and characterize fish scales derived biochar and magnetic composites, and determine their removal efficiencies of anionic indigo carmine (IC) and cationic crystal violet (CV) dyes from synthetic and industrial wastewaters.

1.3.2 Specific objectives

i. To synthesize fish (Tilapia) scale biochar (FSB) at 200 ºC, 300 ºC, 400 ºC, 600 ºC and 800 ºC and characterize them for surface charges, surface area, thermal stability, crystallinity, surface morphology and functional groups.

ii. To determine the removal capacities and efficiencies of raw fish scales (RFS), FSB (200 ºC, 300 ºC, 400 ºC, 600 ºC and 800 ºC) biochars and activated charcoal (AC) in dye removal at ambient temperature.

iii. To synthesize and characterize fish scale biochar magnetic composites (FSB@Fe_3O_4) for surface charges, optical absorbance, thermal stability, crystallinity, magnetic properties, surface area, surface morphology and functional groups.

iv. To determine the effects of initial dye concentration, pH, contact time, temperature and adsorbent dosage on the removal of IC and CV dyes onto FSB and FSB@Fe_3O_4 compared to activated carbon.

v. To infer the removal mechanisms and adsorption kinetics of IC and CV dyes onto activated carbon, FSB and FSB@Fe_3O_4, assess the stability of the FSB@Fe_3O_4 under reaction conditions and determine their regeneration/recyclability frequency.

vi. To assess the efficiency of the adsorbents in the treatment of industrial dye wastewater.

1.4 Hypotheses (Null-H_o)

i. Different temperature ranges will not have effect on the Fish Scale Biochar (FSB) generated as characterized for surface charges, crystallinity, thermal stability, surface morphology, elemental composition, surface area, and functional groups.

ii. The raw fish scales (RFS), FSB (200 ºC, 300 ºC, 400 ºC, 600 ºC and 800 ºC) biochars and activated charcoal (AC) will not have significantly different IC, and CV dyes removal capacities and efficiencies at ambient temperature.

iii. Different temperature ranges will not have effect on the synthesized fish scale biochar magnetic composites (FSB@Fe_3O_4) as characterized for surface charges, peak optical absorbance, crystallinity, magnetic strength, surface morphology, elemental composition, surface area, and functional groups.

iv. Initial dye concentration, solution pH, contact time, solution temperature and adsorbent dosage will not influence the removal of IC and CV dyes by FSB, FSB@Fe_3O_4 and activated carbon.

v. The removal mechanisms and kinetics of IC and CV dyes onto activated carbon, FSB and FSB@Fe_3O_4 are not plausible. The magnetic composites will not be stable under the reaction conditions and their regeneration/recyclability frequency will not be plausible.

vi. The prepared adsorbents will not be effective in the treatment of industrial dye wastewater.

1.5 Justification of the study

The increased demand for textile products and the relative increase in their manufacture, and the application of artificial dyes have contributed to dye wastewater being one of the considerable sources of main effluence problems in present times. The ultimate negative effects e.g. their carcinogenicity to mammals and toxicity to aquatic organisms have been reported (Guz *et al*., 2014; Ismail *et al*., 2019; Owens, 2002; Ribeiro & Umbuzeiro, 2014). In this regard, purification of the polluted water would create a good environment for the living organisms. The entire endeavour would create an economical benefit of fish scales by using them sustainably, hence, reducing environmental pollution.

CHAPTER TWO

LITERATURE REVIEW

This section displays a review of academic sources related to the research. The preparation of the adsorbents, experimental conditions, kinetics and mechanisms of adsorption, stability and recyclability of the magnetic composites, and application in treatment of industrial dye wastewater are presented. Note that the images for raw fish scales, pulverized fish scales, fish scale biochar and magnetic composite were obtained from the current study.

2.1 Methods for preparation of fish scale biochars (FSB) and magnetic composites (FSB@Fe_3O_4)

Biochar is a product from biomass thermo-chemical conversion applied considerably in abstraction of a variety of contaminants owing to its economical and abundance benefits (Xiu *et al*., 2017). According to Teshale *et al*. (2020), the bio-adsorbent for removal of chromium (III) was prepared by washing the fish scale, soaking for 24 h with ordinary water, followed by cleaning with deionized water in order to eliminate the impurities. In order to make the washed fish scales moisture free and crispy; they were put in sundry for 48 h and open-air oven at 65 °C for 24 h. The dry scales were mechanically finely powdered and sieved on an octagon sieve while maintaining the portion size range of 125-200 μm. Acid and base activations were performed by separately mixing 10 g of fish scale powder with 150 mL of 0.1 M H_2SO_4 and 0.1 M NaOH solutions for 2½ h at 100-rpm on a rotatory shaker in ambient room temperature. The components were transferred to a vacuum filter to isolate the liquid portion, subsequently, washed severally with distilled water until a neutral pH

solution was achieved. Next, the sample was dried at room temperature for 2 h and in the oven at 80 °C. The researchers did not grind the product after drying before application in adsorption studies, since this would have ensured that the particles are not coalesced onto each other.

Sahoo *et al*. (2019) explored the preparation of activated carbon from fish scales for application in adsorption and catalysis. The researchers precarbonized clean and dry fish scale at 330 ºC for 3 h in air, mixed the resulting powder with KOH at a weight ratio of 1:1 and activated at 950 ºC for 1 h in N_2 ambience. In the elimination of present excess acid from the surface of the prepared adsorbent, the product was kept in 20 M of phosphoric acid and finally washed with deionized water. By precarbonizing the dry fish scales in air is expected to limit the amount of carbon since the amount of ash will increase due to oxygen gas, consequently, the adsorption potential will be low. Therefore, it would have been prudent for the precarbonization to occur in either limited oxygen or inert environment.

Zhu *et al*. (2013) employed *Tilapia* fish scales to make an adsorbent material for the adsorption of Ponceau 4R dye. In their method, the rinsed fish scales were dried in the sun until crisp, mixed with NaOH solution in a triangular flask and heated in an oil bath prior to cooling to room temperature. Resulting solid was filtered from solution and repeatedly rinsed with distilled water before drying in an oven at 50 ºC, ground to a powder and sieved via a 160-mesh to get the *Tilapia* fish scale adsorbent.

However, the researchers did not specify the quantities of fish scales and NaOH used and the period of reaction in their procedure. Uzunoğlu & Özer (2015) dried *Dicentrarchus Labrax* fish scales in shade for 48 h after washing them repeatedly in tap water to eliminate dust and solvable contaminants from their surface. The moisture was evaporated in the oven at 110 °C and the final product used directly as an adsorbent without grinding. In this procedure, the authors have not indicated the duration of oven drying. Moreover, using the adsorbent without grinding deprived it of key adsorption properties such as particle size and surface area sufficient to embolden high adsorption capacity.

Marrakchi *et al*. (2017) used an electrical furnace in N_2 (99.99%) at a flow and heating rates of 100 cm^3/min and 10 °C/min, respectively, to carbonize fish scales at 600 °C for 90 min in a tubular stainless steel reactor. The prepared material was cooled to room temperature in N_2 gas flow then washed with 1 M HCl in order to remove residual inorganic matters and open up its pores. The product was rinsed with hot distilled water until the filtrate attained neutral pH, dried at 105 °C for 24 h, subsequently ground and sieved to a fraction of fine particles through a mesh of 250-500 μm. In this method, by grinding and sieving the prepared adsorbent, ensured that the surface area and particle size were improved hence raising the potential of achieving high adsorption capacity.

Figure 2.1 shows (a) the raw fish scales, (b) pulverized fish scales, (c) fish scale biochar and (d) magnetic composite, from the current study.

(a) Raw fish scales (RFS)

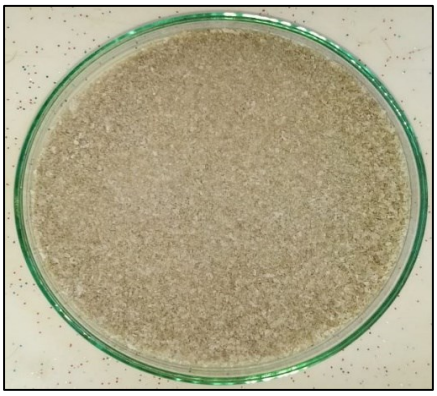

(b) Pulverized raw fish scales

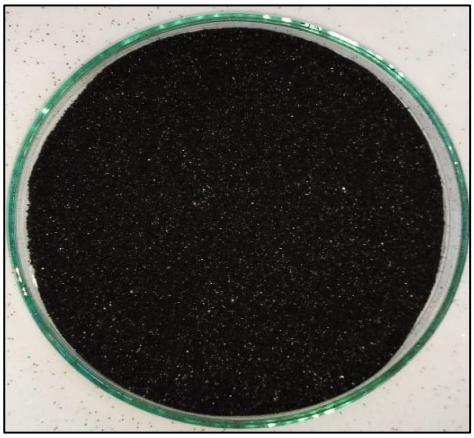

(c) Fish scale biochar (FSB)

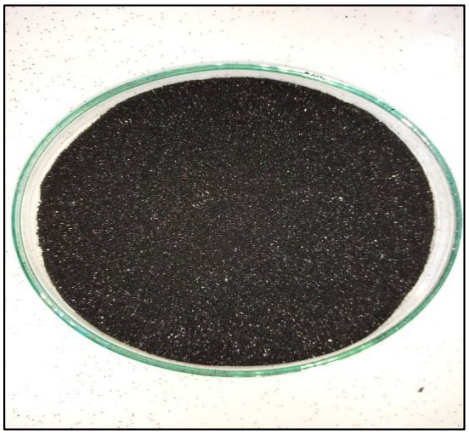

(d) Magnetic composite (FSB@Fe_3O_4)

Figure 2.1: The raw fish scales, pulverized fish scales, fish scale biochar and magnetic composite

Many investigators have reported methodologies for synthesis of magnetic composites. Datta *et al*. (2017) demonstrated the co-precipitation method for preparing Fe_3O_4/Activated Carbon Composite for adsorption of Malachite Green and

Rhodamine B dyes. In their procedure, Activated Carbon was oxidized using concentrated HNO_3 in an ultrasonic bath (35 kHz) for 100 min, the product sieved into Gooch crucible, washed with deionized water until neutral pH was attained prior to drying in a vacuum oven. A mixture of Fe^{2+} and Fe^{3+} in the ratio of 1:2 was spread in 200 mL of deionized water, and sonicated for 10 min with a mass ratio of 4:1 for the (Fe^{2+} + Fe^{3+}): Activated Carbon. At the co-precipitation step, 8 M of aqueous ammonia (NH_3) was added drop-wise while continuously stirring for 30 min at 50 °C until the mixture achieved a pH of 11-12. Consequently, the prepared magnetic composite was filtered, washed with deionized water and ethanol, and dried at 60 °C in a vacuum oven. In this procedure, the researchers did not indicate the duration of drying the materials in oven at the respective stages. This is necessary since drying a magnetic composite beyond confines of the recommended duration would lead to gradual decomposition culminating into insufficient magnetic properties needed for adsorbent recovery after adsorption process.

In another procedure for the preparation of Fe_3O_4@fish scale nanocomposites for Methylene Blue dye abstraction, Gholami *et al*. (2018) rinsed fish scales with tap water followed by NaOCl solution (5% wt) to remove any dirt, in which the fish scales were freshened and degreased in the process. The raw materials were rinsed with distilled water, dried at 80 °C for 24 h, crushed and sieved to 100-500 μm particle size range, and conserved in desiccators. The chemical precipitation technique was applied to generate the magnetic composite. Precisely, 3.2 g of

$FeSO_4.7H_2O$ and 6.2 g of $FeCl_3.6H_2O$ (Fe^{3+} : Fe^{2+} molar ratio of 2:1) were dissolved in 160 mL of distilled water with vigorous stirring in an inactive ambience to obtain 4 g of magnetic particles. Aqueous NH_3 solution (20 mL of 25 %) was added while heating the solution to 80 °C during which the colour changed from light brown to black. The solution was left for ten minutes to facilitate the eventual development of the nanoparticle crystals, then 20 g of powdered fish scales was added to the solution, and the reaction allowed to progress for 70 min at 80±1 °C with continuous stirring. Lastly, the suspension was cooled to room temperature, washed repeatedly with distilled water to eliminate un-reacted chemicals. The ratio of the weights of Fe^{3+} : Fe^{2+} salts used in preparation of the magnetic composites was 1.9375:1 which is against the stoichiometric requirement of 2:1. On the other hand, the researchers did not mention if the magnetic composites were dried before use in the subsequent assessments.

2.2 Effects of biochar preparation temperatures on their physical and chemical properties

Adsorbents prepared at different carbonization temperatures are expected to exhibit varying physical and chemical properties, which ultimately influence their adsorptive behaviours. Nnadozie & Ajibade (2021) reported that the *C. Odorata* biochar prepared at 800 °C posted optimal abstraction efficacy for indigo carmine (IC) dye. The researchers ascribed the adsorption behaviour of *C. Odorata* biochar to its organic content. Moreover, the enhanced removal of anionic I.C. dye was attributed to the strengthening of functional group and high cations composition in the biochar at high temperature as witnessed in other studies by Luo *et al*. (2018). It was also

noted that rise in charring temperature reduced the number of organic moieties (Nnadozie & Ajibade, 2021). The surface area of the biochar determined by BET was 244.31 ± 6.54 m^2/g, with pore volume and pore size of 0.00693 cm^3/g and of 5.10 nm, respectively.

The influence of pyrolysis temperature on the yield and characteristics of biochar via slow charring of coconut flesh waste was investigated (Noor *et al*., 2019). The temperature was varied between 350 °C to 600 °C at a steady heating rate of 5 °C/min whereby reduction in biochar yield from 23.54 wt % to 13.97 wt % was observed. The level of ash in the biochar was augmented from 4.63 wt % to 19 wt %, the fixed carbon level increased from 45.20 wt % to 79.09 wt % and carbon content rose from 72.70 wt % to 83.25 wt %. Moreover, the volatile matter and oxygen content of biochar were decreased from 50.17 wt % to 12.71 wt % and 13.86 wt % to 10.99 wt %, respectively, while the surface area of coconut flesh waste biochar (CFWB) was slowly increased from 0.3971 m^2/g to 0.6619 m^2/g as the pyrolysis temperature was elevated from 350 °C to 500 °C. Increase in surface area was attributed to the loss of organic compound or enhanced devolatilization, which created void within the biochar matrix (Wang *et al*., 2013). In addition, the SEM micrograph of CFWB biochar prepared at 400 °C showed pores that were more obvious and the cell walls that were moderately rebuilt, hence, enlarging its shape. Further temperature increase to 600 °C not only deepened and enlarged the pores of CFWB but also shrunk and totally reconstructed the cell walls of the coconut flesh.

Das *et al*. (2021) observed similar findings on biochar yield whereby the yield declined considerably with pyrolysis temperature. Lower biochar yield was witnessed at 600 ^{o}C and was ascribed to the emanation of CH_4, CO, and CO_2. Precisely, biochar yield followed the trend; 400 ^{o}C > 500 ^{o}C > 600 ^{o}C. The researchers concluded that less of volatile matter is lost at lower pyrolysis temperature, consequently, strengthening the secondary char. Moreover, phenolic, surface carboxylic, lactonic and total acidic functional groups declined from 400 to 600 ^{o}C. The FT-IR band strength of the C=O/OH, -CH_n and –OH stretching diminished with rise in pyrolysis temperature due to de-polymerization and loss of moisture content. On the other hand, thermogravimetric analysis posted weight loss with rise in temperature from 0 to 600 ^{o}C. Heitkötter & Marschner (2015) reported that biochars produced at 600 °C were characterized with higher ash contents and higher pH. The high pH level was attributed to the accumulation of alkali and alkaline earth metals (K, Mg and Ca), formation of carbonates, and concentration of biomass-derived carbonates as a function of temperature.

Effect of heating time (30, 60, 90, and 120 min) and temperature (350, 450, and 600 °C) on the chemical features of biochar from Poultry Manure (PM) was studied by Cimò *et al*. (2014). The findings showed that the biochar produced at the highest temperature contained aromatic structures whose chemical characteristics seemed unaffected by heating time. Thermogravimetric analysis displayed disparities in the

thermo-oxidative strength of the aromatic spheres in the as-synthesized biochars. Precisely, the PM biochar prepared at 600 ºC exhibited less stability relative to those prepared at 350 ºC and 450 ºC, a consequence attributable to a protective effect of the alkyl groups.

Zhao *et al*. (2017) explored the possible consequence of temperature on the structural and physicochemical features of biochar with apple tree branches under pyrolysis temperatures of 300, 400, 500 and 600 ºC. The findings showed that rise in temperature improved the carbon content and inorganic minerals such as K, P, Fe, Zn, Ca, and Mg. Notably, biochar yield, volatile matter, O, H, CEC, O:C and H:C ratios declined, whereas biochar produced at 500 ºC exhibited the highest pH and ash content. On the other hand, the magnitude of carboxylic functional groups declined, while thermal stability, BET surface area and pore volume increased with rise in pyrolysis temperature. The observation made on BET surface area and pore volume were attributed to the rise in micropore surface area and micropore volume. Furthermore, Zhao *et al*. (2017) reported that the SEM image of biochar at 300 ºC displayed a softened, melted and fused material owing to release of volatile gases from the biomass, culminating to a biochar whose morphology presented a number of pore structure at 400 ºC. For the biochar at 500 ºC, portions of the skeletal structure appeared brittle due to the decomposition of more components. The fracture phenomenon also appeared within the pore structure for the biochar at 600 ºC.

The effect of pyrolysis temperature on physicochemical properties of *miscanthus* biochar (obtained at 350, 360, 370, 400 and 450 ºC) revealed that thermal and biological stability are affected by pyrolysis temperature in a nonlinear manner (Mimmo *et al*., 2014). Increase in the biochar pH with increasing pyrolysis temperature from 6.36 to 9.25 for the feedstock and the biochar produced at 450 ºC. The largest increase in biochar pH as a function of pyrolysis temperature was observed between 360 ºC and 370 ºC. However, this study sets to unveil the possible effects of charring temperatures 400, 600, and 800 ºC on the physicochemical properties of the fish scale biochars (FSB) since the effects are not known.

2.3 Effects of experimental conditions on adsorbent performance in adsorption process

Adsorption reaction conditions are fundamentally initial adsorbate concentration, initial pH of the adsorbate, contact time between adsorbate and adsorbent, temperature of the contents in the reaction vessel and the adsorbent dosage. Presented herein are conditions used by researchers in previous adsorption studies. Gholami *et al*. (2018) performed batch kinetic experimentations by separately adding 0.3 g of both fish scales and magnetic composites into 50 mL of the Methyl Blue dye solution at constant initial concentration of 200 mg/L at 303 K, pH of 8 and agitating for 160 minutes. Optimal amount of adsorbent was obtained by addition of varied quantities of magnetic fish scales (0.05 - 0.5 g) into 50 mL of 200 mg/L dye solution at a fixed pH of 8 at 303 K. The experiment revealed that the adsorption capacity improved as a function of contact time until 60 minutes for both fish scales and magnetic fish

scales, and optimal adsorbent dosage was 0.3 g. However, the speed at which the contents were shaken was not specified in the batch experiments.

The influence of pH, temperature, dosage and initial concentration of Methylene blue (MB) and Rhodamine B (RB) dyes on adsorption behaviour of Pongamia glabra seed cover (PGSC) biochar prepared at 550 ºC were investigated (Bordoloi *et al*., 2018). Different amounts of adsorbent were incubated individually for adsorption of MB and RB from 50-ppm aqueous solutions. In order to obtain the peak adsorption of MB and RB, 50 g/L and 30 g/L of biochars, respectively, were required. The tubes were incubated at 28 ºC for 24 h in a shaker at 60 rpm. The researchers concluded that at 50-ppm concentration, adsorption of both MB and RB required an optimal biochar concentration of 50 g/L and 30 g/L, respectively. In addition, dye abstraction was independent of solution pH, but was optimum at 28 ºC, while an optimal point for adsorption for both dyes was rapidly reached within a range of 20 to 50 minutes.

Senthil Kumar *et al*. (2014) investigated the influence of temperature on the removal of methylene blue dye from its aqueous solution onto sulfuric acid-treated orange peel. The experimental conditions, which include solution pH, amount of adsorbent, initial MB dye concentration, and contact time, were evaluated in the process. Batch adsorption studies indicated that the maximum removal of MB dye was 99.29% for 50 mg/L of MB dye level at optimal conditions of pH 8, contact time of 45 minutes, adsorbent dose of 0.4 g, and temperature of 30 ºC. The removal of crystal violet (CV)

dye from synthetic wastewater by corn stalks magnetic biochar (MBC) was examined by Sun *et al*. (2015). The adsorption capacity of 349.40 mg/g was registered within 5 minutes for an initial CV level of 400 mg/L, pH of 6 and temperature of 40 °C. However, influence of adsorbent dose on adsorption of CV dye was not studied. In another study by Vanitha (2014), removal of CV by carbon material prepared from bamboo tree leaf was investigated. The study reported that the optimal conditions for the experiment were 0.10 g of the adsorbent, basic pH, equilibration time of 30 minutes, initial dye concentration of 150 ppm and a temperature of 30±1 ºC.

Different concentrations (0.05 mg to 0.25 mg/10 mL) of indigo carmine dye solutions were prepared and examined for removal efficiencies using different amounts of magnesium oxide (20 mg, 40 mg, 60 mg, and 80 mg) as an adsorbent (Ramesh & Sreenivasa, 2015). The influence of temperature on the abstraction of IC dye solutions at different pH levels at a fixed dose of 40 mg was also assessed for a dwell time of 50 minutes at pH ranges 6-7 and 12-13. The results displayed that maximum removal efficiency of approximately 81% was witnessed when 80 mg of $Mg(OH)_2$ was used for 50 minutes. Furthermore, adsorption was maximum at 333 K, with initial dye concentration of 0.25 mg/10 mL and pH range 6-7. In the current study, the appropriate experimental conditions that will yield maximum removal efficiencies of indigo carmine and crystal violet dyes onto the fish scale biochars, magnetic composites and activated carbon are not known. The surveyed literatures will avail

the necessary information for explaining the observations that will be made in the current study.

2.4 Mechanisms of adsorption: Kinetics and isothermal modelling

Kinetics of adsorption by a typical adsorbent is principally obtained by fitting contact time data at varying initial adsorbate concentrations onto reaction simulations such as intra-particle diffusion, *pseudo*-first and *pseudo*-second-orders. Thermodynamic factors, which include changes in Gibb's free energy (ΔG), enthalpy (ΔH), and entropy (ΔS), are also computed to determine the possibility of the adsorption process, the effect of solution temperature on adsorption and degree of randomness of collision of particles at the boundary. Isothermal simulations are essential theories of adsorbate removal process that describe adsorbate-adsorbent interface (Nia *et al*., 2017). Specifically, models such as Langmuir, Freundlich among others are ordinarily engaged to fit the adsorption statistics. Consequently, some quantities are calculated, these are q_m, K_L, R_L, K_F and n which are, respectively, defined as Langmuir maximum monolayer adsorption capacity (mg/g), Langmuir constant indicating the energy of adsorption (L/mg), dimensionless separation factor illustrating the favourability of an adsorption process, Freundlich constant (mg/g. $Lmg^{-1/n}$) and Freundlich model constant that expresses the strength of the adsorbate removal process. The *pseudo*-first-order, *pseudo*-second-order, and intra-particle diffusion models are given in equations 1, 2 and 3, correspondingly.

$$\log\left(q_e - q_t\right) = \log\, q_e - \frac{k_1}{2.303} t \qquad (1)$$

$$\frac{t}{q_t} = \frac{1}{k_2 q_e^2} + \frac{t}{q_e} \quad (2)$$

$$q_t = k_p t^{0.5} + I \quad (3)$$

Where, q_e is equilibrium quantity of dye abstracted (mg/g), q_t is the quantity of indigocarmine dye abstracted at time t (mg/g), k_1, k_2 and k_p are abstraction rate constants, I is intercept whose values provide an understanding on the width of border layer, and t is time (min). Thermodynamic functions such as a change in Gibb's free energy (ΔG), enthalpy (ΔH) and entropy (ΔS) were computed on equations 4-7, correspondingly.

$$\Delta G = -RT \ln K \quad (4)$$

$$K = \frac{C_o - C_e}{C_e} \quad (5)$$

$$\log K = \frac{\Delta S}{2.303\,R} - \frac{\Delta H}{2.303\,RT} \quad (6)$$

$$\Delta G = \Delta H - T\Delta S \quad (7)$$

Where, T is temperature (Kelvin), R is the universal gas constant (8.314 J/mol/K), and K denotes thermodynamic equilibrium constant. Equilibrium adsorption isotherm data were evaluated using Langmuir and Freundlich models (Langmuir, 1916; Freundlich, 1907). Langmuir model is appropriate in describing adsorptive behavior of homogeneous surfaces. Mathematical representations of linear Langmuir and Freundlich adsorption models are presented in equations 8 and 9, correspondingly.

$$\frac{t}{q_e} = \frac{1}{q_m K_L} \cdot \frac{1}{C_e} + \frac{1}{q_m} \quad (8)$$

$$\log_{10} q_e = \log_{10} K_F + \frac{1}{n} \log_{10} C_e \quad (9)$$

Where K_L is Langmuir equilibrium constant (Lmg^{-1}), K_F represents Freundlich adsorption constant (Lmg^{-1}) and q_m is maximum adsorption capacity of adsorbent (mg/g). Dimensionless separation factor (R_L) given in equation 10 is the main feature used to express Langmuir isotherm. Therefore, an isotherm is favorable if $0< R_L<1$; unfavorable if $R_L >1$; linear if $R_L =1$ and irreversible if $R_L = 0$ (Yuan *et al*., 2015).

$$R_L = \frac{1}{1 + K_L C_O} \quad (10)$$

The Temkin isotherm (Temkin & Pyzhev, 1940) integrates the influence of adsorbate-adsorbate interactions and postulates that the heat of adsorption (ΔH_{ads}) of the adsorbate in the layer decreases linearly with a rise in surface coverage. The model is illustrated in equations 11 and 12.

$$q_e = B_T\left(A_T C_e\right) \quad (11)$$

$$B_T = \frac{RT}{b_T} \quad (12)$$

Where $B_T \ln(A_T)$ is the adsorption energies ($kJ\ mol^{-1}$) and b_T denotes the type of sorption mechanism (Rahangdale & Kumar, 2018).

The Sips isotherm is a combination of both Freundlich and Langmuir models (Sips, 1948). This model envisages adsorption onto heterogeneous sites where the adsorbate can be fixed onto more than one adsorption site but with no lateral interactions between adsorbed molecules. The Sips isotherm is given in equation 13.

$$q_e = \frac{q_{ms} a_s C_e^{B_s}}{1 + a_s C_e^{B_s}} \tag{13}$$

The Toth isotherm model (Toth, 1971) was derived to improve the fitness of the Langmuir isotherm to experimental data at low and high adsorbate concentrations. The Toth correlation is presented in equation 14.

$$q_e = \frac{q_{mT} C_e}{\left(a_T + C_e^z\right)^{1/z}} \tag{14}$$

Where parameter *z* is an index of the system's heterogeneity.

The Redlich-Peterson isotherm (Redlich & Peterson, 1959) similarly integrates the Langmuir and the Freundlich isotherm constants and allows for both homogeneous and heterogeneous adsorption processes. The isotherm is defined in equation 15.

$$q_e = \frac{K_R C_e}{1 + a_R C_e^g} \tag{15}$$

Where K_R (L/g) and a_R $(mg/L)^{-g}$ are the Redlich-Peterson constants and *g* (dimensionless) is a factor whose magnitude lies between 0 and 1 for heterogeneous sorption (Allen *et al*., 2003).

The Hill equation (Foo & Hameed, 2010) postulates the binding of different species onto a homogeneous surface. The model is given in equation 16.

$$q_e = \frac{q_{SH} C_e^{n_H}}{K_D + C_e^{n_H}} \tag{16}$$

The Hill isotherm hypothesizes that adsorption is a cooperative phenomenon. The parameters n_H>1, n_H=1 and n_H<1 represent positive cooperativity, non-cooperative, and negative cooperativity in binding, respectively.

Concerning the models, a review of literature on isotherms and reaction mechanisms of adsorption is hereby presented. Mtshatsheni *et al*. (2020) studied the characterization of grafted acrylamide onto pine magnetite composite (GACA) for the abstraction of Methylene Blue dye from effluent. It is important to note that only Langmuir and Freundlich isotherm simulations were examined in which Langmuir isotherm model presented the best equilibrium fit. Freundlich model constant, n values, observed across the temperature range of 299 K to 319 K, were averagely greater than 2 (i.e. n>2), depicting a good adsorption strength for the dye abstraction process. However, the thermodynamic parameters and the dimensionless separation factor (R_L) illustrating the favourability of the adsorption process were not examined in this study.

The abstraction of CV and MB as cationic dyes by magnetic nanoparticles loaded Fig leaves (MNLFL) and Azolla (MNLA) as natural cheap sources of adsorbent materials was examined (Alizadeh *et al*., 2017). The dye removal process followed the *pseudo*-second-order kinetic model, suggesting chemisorption. Langmuir model displayed a better fit of MNLFL and MNLA for MB and CV than Freundlich and Temkin isotherms hence depicting the formation of a monolayer cover of the adsorbate at the

outer space of the adsorbent. However, this study did not investigate thermodynamic factors such as changes in Gibb's free energy (ΔG), enthalpy (ΔH), and entropy (ΔS).

Pre-source biochar (p-Biochar) and milled biochar (m-Biochar) derived from rice straw were inspected for abstraction of MB and CV dyes from aqueous solutions (Abd-Elhamid *et al*., 2020). The findings revealed that p-Biochar exhibited poor adsorptive behaviour. On the other hand, the adsorption isotherm data evaluated on m-Biochar was better described by Langmuir model than Freundlich, with the peak abstraction capacity of 90.91 and 44.64 mg/g for MB and CV dyes, correspondingly. Comparison of correlation coefficient R^2 values of the two simulations established that the adsorption of MB and CV dyes on the surface of m-Biochar followed Langmuir model implying that dye removal occurred as a monolayer on a uniform active sites. Additionally, *pseudo*-second-order model best defined the kinetics data of the two dyes whereas the R_L values were within 0.0 - 1.0 demonstrating a favourable removal of MB and CV onto m-Biochar. The study also reported that the removal of MB and CV onto m-Biochar was not influenced by rise in temperature and NaCl dose.

Azari *et al*. (2021) investigated dye removal from raw textile wastewater by magnetic multi-walled carbon nanotubes-loaded alginate (CNT-Alg-Fe_3O_4). The researchers demonstrated that the data fitted the Langmuir isotherm ($r^2 = 1$, $x^2 = 0.012$) and *pseudo*-second-order kinetics ($r^2 = 0.993$, $x^2 = 0.015$) signifying that dye removal was

monolayer and chemical in nature. The thermodynamic parameters $\Delta H° > 0$, $\Delta S° > 0$, and $\Delta G° < 0$ showed that dye removal was spontaneous and endothermic.

Bordoloi *et al*. (2018) evaluated adsorption kinetics of MB and RB dyes by Pongamia glabra seed cover (PSC) derived biochar. The findings confirmed that the equilibrium data well fitted on Dubinin-Radushkevich (D-R) and Langmuir isotherms for MB and RB dyes, respectively, with adsorption capacities of 1.385 mg/g and 0.683 mg/g, in that order. In addition, *pseudo*-second-order kinetics well described the abstraction of the two dyes by PGSC biochar. However, thermodynamic parameters were not examined in this research.

Dastgerdi *et al*. (2019) analysed the adsorption of IC dye by carbon nanotubes (CNTs). The kinetic study established that the adsorption data best fitted *pseudo*-second-order model. The abstraction efficiency (%R) of IC dye by pure and COOH-functionalized CNTs was 84% and 98.7%, correspondingly, for 15 minutes. On the other hand, Langmuir isotherm model posted a well fitting for the equilibrium data, whereas, CNT and COOH-CNT registered adsorption capacities of 88.5 and 136 mg/g, correspondingly. The adsorption mechanism of pure CNT was through π–π interaction between IC dye molecules and adsorbent while IC dye abstraction by COOH-CNT proceeded via the formation of hydrogen bonding. Notably, the researchers did not study the thermodynamic parameters.

Magnetic graphene oxide/chitin nanocomposites were investigated for effective removal of MB and CV from aqueous solutions (Gautam & Hooda, 2020). The as-synthesized material displayed superb adsorption capacity especially towards CV and MB with optimal adsorption capacities of 403.78 and 332.61 mg/g, correspondingly. Zeta potential and pH studies showed that electrostatic, $\pi - \pi$, and hydrogen-bonding interactions were the dominating parameters in the removal mechanism of the dyes. Kinetic studies revealed that the *pseudo*-second-order model presented a better simulation for elucidating the abstraction of dye molecules onto the magnetic graphene oxide/chitin nanocomposites. Gautam & Hooda (2020) further reported that when the temperature of the system was augmented from 298 to 348 K, the value of ΔG_0 also amplified for both dyes, signifying that a low temperature was more favourable for the removal of dye molecules. A negative value of ΔH_0 showed that the dye abstraction process is exothermic, and a negative value of ΔS_0 depicted a more organized arrangement of the adsorbent surface after the interaction between dyes and adsorbent molecules. Synthesis and assessment of a novel hemoglobin/iron oxide composite (Hb/Fe_3O_4) was explored for the abstraction of indigo carmine, naphthol blue black, tartrazine, erythrosine, eriochrome black T and bromophenol blue dyes (Essandoh & Garcia, 2018). The researchers reported a high removal efficiency whose adsorption mechanism was dominated by electrostatic interaction. Dye removal followed *pseudo*-second order kinetic model and linear Langmuir isotherm. The

posted Langmuir monolayer removal capacities for the dyes were between 80 and 178 mg/g. The Hb/Fe_3O_4 composite also exhibited added benefit of being easily sequestered from aqueous suspension by an external magnet.

Nnadozie & Ajibade (2021) evaluated the adsorption of indigo carmine dye onto *C. odorata* biochar and reported 94.7% removal efficiency of 75 mg/L indigo carmine dye after 2 h contact time at 30 °C. The study revealed that Langmuir isotherm posted a better goodness-of-fit than the non-linear model for the adsorption process with R^2 value of 0.92. Linear Langmuir adsorption capacity (q_o) was 98.8 mg/g after 3 h of equilibration time. On the other hand, the results showed that the adsorption process followed *pseudo*-second order reaction kinetics with R^2 values of 0.87. Moreover, the research concluded that the adsorption process was largely by physio-sorption rather than chemisorption owing to the evidence from the spectra that the functional groups present in the biochar were unaltered after the adsorption process. Nevertheless, the kinetics, thermodynamics and mechanisms of adsorption of indigo carmine and crystal violet dyes onto fish scale biochars (FSB), magnetic composites and activated charcoal in the current study are not known.

2.5 Applications of various adsorbents in remediation of dye contaminated wastewater

Dye wastewater is potentially detrimental to humans, fauna and flora, therefore, requires remediation to circumvent the associated risks. Researchers have employed low cost adsorbents derived from different readily available biomass in attempt to reduce dyes from artificial and industrial wastewater. The Photo-Fenton discoloration

of IC dye from synthetic wastewater catalyzed by magnetite reduced graphene oxide (Fe_3O_4/RGO) composite displayed positive results (Gonçalves *et al*., 2020). Remarkably, total indigo carmine discoloration was achieved within 5 minutes of reaction, without pH correction before the tests, or any additional adjustment.

Application of activated carbon and alum to reduce the colour of textile wastewater samples generated positive outcome (Panhwar *et al*., 2020). The sample was initially characterized by 3406 HU colour units before treatment, a value which was above the limit of Environmental Protection Agency (EPA). The colour decreased to 1614 HU on addition of alum and significantly 1owered to 15 HU after addition of activated carbon, thus, affording EPA permissible levels.

In another study by Elango & Govindasamy (2018), the colour of industrial wastewater was effectively removed by activated carbon derived from temple waste flowers. Normally, the removal efficiencies (%R) attained by the adsorbents for the environmental wastewater are expected to be higher than synthetic dye wastewater from the laboratory batch experiments. This observation is attributed to nitrite ions in the wastewater and organic materials adsorbed onto the adsorbent. Konan *et al.* (2020) reported high removal efficiencies of 2, 4-dimethylphenol from wastewater onto activated carbon due to nitrite ions and organic materials. The efficiency of orange peel as an adsorbent for the abstraction of dyes from wastewater was investigated (Popuri *et al*., 2016) and established the maximum percentage of colour removal of 47.23, 52.59, 66.34 and 88.04 % for the textile dyeing industry effluent respectively

under optimum conditions of 90 rpm, 120 min, adsorbent dose of 2.5 g/L and pH of 10. The study concluded that removal technique is the most suitable process for treatment of effluent from dyeing industry. It is not known whether the adsorbents in the current study would be efficient in abstraction of IC and CV dyes from industrial wastewater.

2.6 Stability and regeneration/recyclability of the magnetic composites (FSB@Fe_3O_4)

The stability and regeneration/recyclability of an adsorbent containing magnetic materials is an essential property in qualifying an adsorbent for application in adsorption process under considered experimental conditions. Song *et al*. (2014) investigated the stability of water-soluble polyacrylamide coated-Fe_3O_4 magnetic composites (Fe_3O_4@PAM) and reported <1% leaching of Fe in 0.02 mol/L HCl solution for 96 hours, demonstrating that PAM coat prevented the dissolution of Fe_3O_4. This observation confirmed the stability of Fe_3O_4@PAM composites under the aforementioned experimental conditions. Similar findings were reported by Essandoh & Garcia (2018) on a novel hemoglobin/iron oxide composite (Hb/Fe_3O_4). Zheng *et al*. (2020) reported insignificant loss of Fe from anionic polyacrylamide-modified-chitosan magnetic (Fe_3O_4) composite (FS@CS-PAA) nanoparticles in the entire tested pH range signifying that FS@CS-PAA had good stability. The researchers proved that the leaching of Fe was effectively prevented at extremely acidic condition due to the protection of SiO_2 and anionic polyacrylamide-modified-chitosan (CS-PAA). Conversely, the stability of the *Tilapia* fish scale biochar magnetic composites in the current study is not known.

A study by Gautam & Hooda (2020) on adsorption of MB and CV from aqueous solutions onto magnetic Graphene Oxide/Chitin nanocomposite showed excellent regeneration capacity as adsorption efficiency was largely retained even after nine successive cycles of the adsorption-desorption process. Zhang *et al*. (2020) reported that the prepared porous carbon/Fe_3O_4-600 composite retained an excellent adsorption capacity for the removal of methyl orange dye after four cycles, therefore, qualifying it as an outstanding material for recyclable dye adsorbent. Four adsorption and regeneration cycles on a novel hemoglobin/iron oxide composite (Hb/Fe_3O_4) established that the adsorption capacity for IC dye reduced by 2% of the initial capacity (Essandoh & Garcia, 2018). Nonetheless, the researchers noted that the regeneration treatment was not effective for 300 mg/L dye solution leading to loss of reusability. Recycle adsorption experiments using calcination method also showed that the prepared monodisperse porous silica nanospheres (SiO_2 NSs) were recycled at least six times while the removal efficiencies for Alcian blue (AB) and methylene blue (MB) dyes had no significant decrease (Lv *et al*., 2018). In another study, reusability of fish (Dicentrarchus labrax) scales (FS) in the adsorption of Acid Blue (AB) 121 dye was surveyed (Uzunoğlu & Özer, 2016). The findings indicated that the adsorbed AB 121 amount by FS in the first and eighth cycles were 98.5 and 39.9 mg/g, respectively. Since FS displayed high structural stability even after multi-cycles use, the researchers concluded that it could be considered as an adsorbent in the removal of the dye anions. Rangabhashiyam *et al*. (2018) investigated the reusability of *Carica*

papaya wood (CPW) for five successive cycles in the biosorption of methylene blue (MB) and malachite green (MG) dyes from simulated wastewater. However, the recyclability frequency of *Tilapia* fish scale biochar magnetic composites is not known.

2.7 Summary of the literature review

The reviewed literature indicated that raw biomass materials were first washed in tap water then rinsed using distilled or deionized water. The rinsed materials were dried for 48 - 72 h and dried in oven between 60 – 110 ^{o}C to evaporate moisture content. Preparation of biochar and magnetic composites was done in neutral ambience (in argon or nitrogen gas) at a flow rate of 100 cm^3 per minute, 10 ^{o}C per minute for 60 – 180 minutes, and temperatures of 80 – 950 ^{o}C. The prepared materials were rinsed till neutral pH of the effluent and dried in oven at 60 – 120 ^{o}C for 1 – 24 h. Adsorption conditions were as follows: pH of 2 - 13, adsorbent dosage of 0.04 – 50 g, initial adsorbate concentration of 2 – 400 mg/L, contact time of 1 – 24 h, and temperature of 298 - 333 K. Adsorption kinetics such as *pseudo* first and second orders, and intraparticle diffusion models were evaluated. Isothermal models included Langmuir and Freundlich, and thermodynamic parameters such as ΔG, ΔH, and ΔS were explored. Moreover, the researchers evaluated the stability, regeneration/recovery, and reuse/recyclability of the prepared magnetic composites. In this regard, the current study settled on 200 to 800 ^{o}C for biochar preparation and the following adsorption condition: pH of 2 - 10, adsorbent dosage of 0.05 – 0.25 g, initial adsorbate

concentration of 5 – 200 mg/L, contact time of 1 – 5 h, rotation speed of 200 rpm and temperature of 298 - 333 K.

CHAPTER THREE

MATERIALS AND METHODS

3.1 Materials and instrumentation

Tilapia (*Oreochromis niloticus*) fish scales were obtained in March 2017 from a local fish market, Gikomba, in Nairobi, Kenya, and extra-pure activated charcoal (99.57%) was purchased from FINAR Limited. The chemicals and solvents were of analytical grade and were used as procured. Indigo carmine and crystal violet dyes were bought from BDH Chemicals Ltd, Poole, UK. All the solutions for adsorption studies were prepared in deionized water (product 18.2 MΩcm, Ultra 370 Series YOUNGLIN). The instruments: a pH meter (Hanna Instruments Microprocessor pH Meter 211), and an infrared spectrophotometer (Cary 630 FT-IR) were used. Surface morphology and particle size of the materials were determined using SEM (Zeiss Evo LS 15 SEM) and TEM (JEOL JEM-1400), respectively. Thermal degradation profiles were done on a TGA Thermo plus (Evo2 TG-DTA/H) and TA Instruments (SDT Q600 thermal analyser). Crystallinity test was carried out on an XRD, while residual dye concentration was quantified by a UV-Vis spectrophotometer (UVmini-1240-Shimadzu). Other adsorbent properties were evaluated using specific techniques as further elaborated herein.

3.2 Preparation of Raw Fish Scales (RFS) and Fish Scale Biochars (FSB): pulverization and charring

Fresh Tilapia (*Oreochromis niloticus*) fish scales were first washed with tap water at 25 ºC to eliminate all the dirt, and rinsed several times with de-ionized water before air-drying under shade for 3 days. The dried material was then pulverized at 30 ºC and 100 Pa (HERZOG HSM-H). The pulverized fish scales (25.0 g) were placed in a porcelain

combustion boat (50 mL), covered with an appropriate lid and subjected to slow pyrolysis in an inert environment (N_2 flow of 100 mL/min) at a heating rate of 10 ºC per minute to 200 ºC, 300 ºC, 400 ºC, 600 ºC and 800 ºC, then for a residence time of 60 minutes in a furnace (WiseTherm). The samples were allowed to cool and washed with deionized water until the effluents were neutral (pH 6.7) to litmus paper and finally oven-dried at 100 ºC for 2 h (Bordoloi *et al*., 2018). The adsorbents were stored in airtight glass vials. Percent (%) yields of the adsorbents were calculated as shown in Equation 17.

$$\%Yield = \frac{Yield\ weight\,(g)}{weight\ of\ biomass\,(g)} \times 100 \tag{17}$$

3.3 Preparation of Fish Scales Biochar magnetic composites (FSB@Fe_3O_4)

Magnetite (Fe_3O_4) particles were prepared by the conventional co-precipitation method. Briefly, 1.208 g of $FeCl_3.6H_2O$ and 0.604 g of $FeCl_2.4H_2O$ (Merck, Germany) were separately dissolved in 50 mL of deionized water and heated for 1 h at a constant temperature of 85 °C in a nitrogen ambience with energetic automated stirring (500 rpm). Using a 6-mL syringe, 10 mL of 25 % aqueous NH_3 solution was added to the solution while vigorously stirring the content with a magnetic stirrer. Additional drops of ammonia solution were added until a black precipitate of magnetite was formed and further stirred for another 1h. The mixture was cooled to room temperature, put into centrifuge tubes and washed numerous times with 50 mL of deionized water and twice with 20 mL of ethanol while centrifuging at 10,000 rpm for 10 minutes. The magnetite was dried in the oven at 60 ºC, ground using pestle and mortar, and stored in airtight glass vials ready for characterization (Keypour *et al*., 2017). For the magnetic

composites, 1.208 g of $FeCl_3.6H_2O$ and 0.604 g of $FeCl_2.4H_2O$ were separately dissolved in 50 mL of deionized water and heated on a hot plate for 1h at a constant temperature of 85 ºC under nitrogen atmosphere with vigorous mechanical stirring at 500 rpm. Using a 6-mL syringe, 10 mL of 25 % of aqueous NH_3 solution was added into the solution while vigorously stirring the contents with a magnetic stirrer. Extra ammonia solution was dropped until a black precipitate of magnetite was formed. At this point, 5.0 g of the fish scale biochar (FSB) was added and stirring done for a further 1h. The mixture was cooled to room temperature, put into centrifuge tubes and washed five times with 50 mL de-ionized water and twice with 20 mL of ethanol while centrifuging at 10,000 rpm for 10 minutes. The magnetic biochar composite was dried in the oven (PROLAB) at 60 ºC for 12 h, ground using pestle and mortar, and stored in airtight glass vials ready for characterization and adsorption experiments (Keypour *et al*., 2017). The three as-synthesized magnetic biochars were assigned FSB@400 ºC-Fe_3O_4, FSB@600 ºC-Fe_3O_4 and FSB@800 ºC-Fe_3O_4. Percent (%) yields of the magnetic composites were computed as presented in equation 18.

$$\% \text{ Yield} = \text{Yield Weight (g) x100/weight of starting reacted salts (g)} \quad (18)$$

3.4 Characterization of the adsorbent

3.4.1 Determination of point of zero charge pH (pH_{pzc}) of the adsorbents

The pH_{pzc} was determined by weighing 0.3 g of the adsorbents on an analytical balance and mixing with 30 mL of de-ionized water at 25 ^{o}C. Solutions of 0.1 M HCl and NaOH were employed to regulate the pH_i (initial pH) levels from 2 to 10, while using a pH meter to obtain the pH_i readings. After agitating the contents at 200 rpm for 5h, the suspensions were sieved on Whatman filter paper of grade 595, and the pH_f (final pH) values were measured. A plot of pH_f–pH_i values against pH_i was obtained; therefore, the point of interception of the resultant curve was the pH_{pzc} of the adsorbent. The magnetic composites and de-ionized water were combined in the ratio of 1:5 and their pH levels read on a calibrated pH meter (Dai *et al*., 2013).

3.4.2 Characterization of Fish Scale Biochars (FSB@400 ^{o}C, FSB@600 ^{o}C, FSB@800 ^{o}C, magnetite (Fe_3O_4), FSB@400 ^{o}C- Fe_3O_4, FSB@600 ^{o}C-Fe_3O_4 and FSB@800 ^{o}C-Fe_3O_4)

3.4.2.1 Optical absorbance

Characteristic maximum absorption wavelengths (λ_{max}) of magnetite and magnetic composites were assessed on a UV-Vis spec, in which about 0.05 g of prepared magnetite (Fe_3O_4) and magnetic composites (FSB@Fe_3O_4) were put into clean Eppendorf tubes containing 2 mL of methanol and sonicated at 10,000 rpm for 10-15 minutes. Components were filtered through cotton wool to remove undissolved/suspended particulates and scanned on UV-Vis spec to determine optical absorbance of magnetite and magnetic composites.

3.4.2.2 Functional group identification

A pinch (0.05 g) of each sample (Raw Fish Scale-RFS, Fish Scale Biochars, magnetite and magnetic composites) were analyzed on FT-IR and their spectra obtained between 400 cm^{-1} and 4000 cm^{-1} to find the existing functional groups.

3.4.2.3 Structural thermal stability

Thermo-gravimetric analysis (TGA) was performed by heating samples at 10 °C/min under flowing air (100 mL/min) up to 1000 °C.

3.4.2.4 Surface morphology, structure and chemical composition

A pinch (0.05 g) of the sample was smeared onto a carbon tape with the aid of a spatula, fixed on a clean SEM stub and forwarded for SEM-EDX examination. High-resolution SEM micrographs were obtained using high vacuum secondary electron detector with accelerating voltage of 20 kV where gold coating was essential to reduce charging between sample and stream of electrons, consequently, allowing improved transmittance. The gold coating was prepared for five minutes on Quorum Coater machine. Transmission Electron Microscopy images were obtained as follows; ethanol was midway filled into Eppendorf tube, a sample was parsimoniously added and homogenized for 10-15 minutes on a sonicator. The Eppendorf tube was allowed to stand for 30 seconds; subsequently the grid was floated into the sample dispersant using tweezers then cautiously placed on a clean Whatman filter paper to dry before taking images, analyzing particle sizes and diffraction patterns on TEM equipment.

3.4.2.5 Magnetic properties

Magnetic properties of magnetite (Fe_3O_4) and magnetic composites (FSB@Fe_3O_4) were measured at 300 K on a vibrating sample magnetometer (VSM) equipped with a superconducting magnetic coil. Measurements were done on powder forms of the samples after vacuum drying.

3.4.2.6 Textural Analysis

The Brunauer-Emmett-Teller (BET) method was employed to measure the surface areas of the adsorbents. The total pore volume was calculated from nitrogen uptake at close to saturation pressure while t-plot analysis was used to assess micropore surface area and volume.

3.5 Assessment of the adsorbents on artificial wastewater for dye removal

Accurately weighed 0.1 grams of each of the adsorbents of pulverized Raw Fish Scales (RFS), activated charcoal (AC), Fish Scale Biochars (FSB) and magnetic composites (FSB@Fe_3O_4) were mixed, separately, with 30 mL of prepared standard dye solutions (at 5, 15, 25, 50, 75 and 100 mg/L) into capped reaction vessels. The vessel components were agitated for 4 h in an Orbital Shaker/Incubator at 200 rpm set at 298 K and the residual dye concentrations were detected using a UV-Vis Spectrophotometer (UVmini-1240-Shimadzu) at wavelengths of 588 and 611 nm for crystal violet and indigo carmine dyes, respectively.

3.6 Batch Adsorption Experiments

Batch experiments were performed to probe the effects of solution pH (2-10), initial adsorbate concentration (25-100 mg/L), adsorbate contact time (0-180 min), adsorbent dosage (0.05-0.25 g/30 mL solution) and solution temperature (298-323 K) for dyes on adsorption kinetics using pulverized raw fish scales, biochar materials prepared at different temperatures (FSB@400 ºC, FSB@600 ºC, and FSB@800 ºC) and magnetic composites (FSB@400 ºC-Fe_3O_4, FSB@600 ºC-Fe_3O_4 and FSB@800 ºC-Fe_3O_4) without pH adjustment. Adsorption mixtures in triplicates were shaken at 200 rpm for 180 minutes in an orbital shaker, and residual dye levels were sensed and quantified on UV-Vis Spectrophotometer at wavelengths of 588 and 611 nm for crystal violet and indigo carmine dyes, respectively, as determined by experimental scans on UV-Vis spectrophotometer. The dyes (IC and CV) and distilled water used in the experiments were also characterized for metal concentrations. A standard activated charcoal (99.9% purity) was used as a control adsorbent to evaluate the performance of the RFS and the generated biochars. The percent removal (%R) and the amount of dye adsorbed per unit mass of adsorbent were calculated using equations 19 and 20, respectively.

$$\%R = \frac{C_o - C_e}{C_o} \times 100 \tag{19}$$

$$q_e = \frac{C_o - C_e}{m} \times V \tag{20}$$

Where q_e, C_o, C_e, m and V are the amount of dye adsorbed (mg/g), initial dye concentration (mg/L), equilibrium dye concentration (mg/L), the mass of the adsorbent (g) and volume of the dye solution (L), respectively.

3.7 Stability and regeneration/recyclability of the magnetic (FSB@Fe_3O_4) composites

Leaching studies were carried out following Zheng *et al*. (2020) with a few modifications. Precisely, 20 mg of the magnetic composites were dispersed in 30 mL of distilled water at pH 2, pH 8-10 and 313 K. The mixture was gently swirled using an orbital shaker for 2 hours. After magnetic separation, Atomic Absorption Spectrophotometer (SPECTRA AA-5, USA) was used for the analysis of Ca, Mg, Na, and Fe concentrations in the supernatant. These elements were also assessed in 25 mg/L of IC and CV dyes. Recyclability/regeneration study was done by separating spent adsorbents from the adsorption mixture using an external magnet. The used adsorbents were then washed three times with 10 mL of ethyl-alcohol and dried in the oven. The adsorption experiment was repeated five times by dispersing 0.2 g of the adsorbents in 30 mL of 25 mg/L indigo carmine (IC) and crystal violet (CV) dye solutions.

3.8 Sampling, treatment and analysis of industrial dye wastewater

Wastewater samples were collected from five different locations situated within industrial areas in Nairobi-Kenya in July 2020, whose identities are concealed for confidentiality reasons. The choice of sampling locations (Figure 3.8) was guided by the application of textile dyes in the colouring of fabrics. Triplicate samples were collected in 500 mL glass bottles at the exit points from locations A (S 01º 18’07.46’’, E 036º 52’10.75’’), B (S 01º 18’21.29’’, E 036º 52’24.37’’), C (S 01º 19’31.68’’, E 036º 52’06.02’’), D (S 01º 14’12.0’’, E 036º 52’34.8’’) and E (S 01º 22’51.4’’, E 036º 56’24.6’’) and transported to the laboratory in cooler boxes packed with icepacks. The American Public Health Association (APHA, 2005) method was used to characterize the

samples for physical and chemical parameters with the aid of bench meters (pH, portable thermometer and colourimeter) and ultra-violet visible spectrophotometer. The temperature and pH levels of the raw dye wastewater were measured in *situ*. Approximately 30 mL of the collected wastewater samples were mixed with 0.2 g of pulverized raw fish scales (RFS), activated charcoal (AC), fish scale biochars (FSB@400 ^{o}C, FSB@600 ^{o}C, and FSB@800 ^{o}C), and magnetic biochar composites (FSB@400 ^{o}C-Fe_3O_4, FSB@600 ^{o}C-Fe_3O_4, and FSB@800 ^{o}C-Fe_3O_4). The reaction vessels containing the mixtures were agitated for 3 hours on an orbital shaker at ambient temperature and without pH adjustment. Subsequently, the treated samples were examined for pH, residual indigo carmine (IC) and crystal violet (CV) dye concentrations.

Figure 3.8: Sampling locations for industrial dye wastewater samples

3.9 Recovery of the spent magnetic composite

Recovery of the used/spent magnetic composite was done by placing a bar magnet on the surface of the adsorption reaction vessel. The spent adsorbent was attracted to the bar magnet due to the created magnetic field. Subsequently, the treated wastewater was separated from the spent magnetic composite.

3.10 Data Analysis

Significant differences in the treatments at 95 % confidence ($P \leq 0.05$) level were obtained using Statistical Analysis Software (SAS System for Windows Version 8) and the findings summarized in Analysis of Variance (ANOVA) Tables and Figures obtained from Microsoft office Excel.

CHAPTER FOUR

RESULTS AND DISCUSSION

4.1 Synthesis of Fish Scale Biochars (FSB) and magnetic composites (FSB@Fe_3O_4)

The Fish scale biochars (FSB) were prepared via slow pyrolysis at different temperatures of 200 ºC (FSB@200 ºC), 300 ºC (FSB@300 ºC), 400 ºC (FSB@400 ºC), 600 ºC (FSB@600 ºC) and 800 ºC (FSB@800 ºC). The percentage yields of each FSB prepared at a specified temperature are given in Table 4.1. From the results, it was noted that biochar yields declined significantly with rise in pyrolysis temperatures, an observation attributed to liberation of volatile matters such as water, carbon dioxide, ammonia, carbon monoxide, $C_xH_yO_z$ and hydrogen cyanide during pyrolysis (Xu & Chen, 2013).

Xu & Chen (2013) also reported that the mineral component in the biochar functions as a barrier to the diffusion of heat, causing the release of the volatile components during the charring process, an observation that is in agreement with several other previous reports (Uchimiya *et al*., 2011; Jindo *et al*., 2014; Liu *et al*., 2015; Li *et al*., 2016; Bordoloi *et al*., 2018). The rise in pyrolysis temperature from 350 °C to 600 °C on coconut flesh waste reduced the biochar yield from 23.54 % to 13.97 % (Noor *et al*., 2019), attributed to the volatile matter and oxygen content of biochar that decreased from 50.17 % to 12.71 % and 13.86 % to 10.99 %, correspondingly. Das *et al*. (2021) observed similar findings on biochar yield whereby the yield declined (20.69%) significantly with increase in pyrolysis temperature. The lower yield of biochar was witnessed at higher charring temperature (600 ºC) and was ascribed to the release of CH_4, CO, and CO_2. Precisely, optimal biochar yield was achieved at 400 ºC (average of all feedstock was

32.63%) charring temperature followed by 500 ºC (29.20%) and minimum at 600 ºC (25.88%). The researchers concluded that low temperature pyrolysis reduces the volatile matter losses and strengthens the secondary char creating pyrolysis mechanism. Zhao *et al*. (2017) explored the possible influence of temperature on apple tree branches as feedstock material under pyrolysis temperatures of 300, 400, 500 and 600 ºC, and reported a decrease in biochar yield with rise in temperature.

Magnetic composites were prepared by chemical co-precipitation method as illustrated in the following chemical reaction equation:

$$\mathbf{Fe^{2+}(aq) + 2Fe^{3+}(aq) + 8OH^{-}(aq) + FSB(s) \rightarrow FSB@Fe_3O_4(s) + 4H_2O(l)}$$

The percentage yields of the magnetic composites are given in Table 4.1.

Table 4.1: Percent (%) yields of the materials

Adsorbent	**% Yield**
Raw Fish Scales (RFS)	-
Activated charcoal	-
FSB@200 ºC	77±0.84
FSB@300 ºC	57±0.92
FSB@400 ºC	53±1.08
FSB@600 ºC	51±0.69
FSB@800 ºC	46±0.20
Fe_3O_4	31±2.05
FSB@400 ºC-Fe_3O_4	61±1.86
FSB@600 ºC-Fe_3O_4	48±1.40
FSB@800 ºC-Fe_3O_4	50±1.62

The data showed that the increase in pyrolysis temperature led to a decline in biochar yield. Similar reports have been documented in literature (Noor *et al*., 2019; Das *et al*., 2021).

4.2 Characterization of Fish Scale Biochars (FSB) and magnetic composites (FSB@Fe_3O_4)

4.2.1 Determination of point of zero charge pH (pH_{pzc}) and pH of the adsorbents

Point of zero charge (pH_{pzc}) of a material predicts the net charge on the surface of an adsorbent at a given solution pH (Gholami *et al*., 2018). Thus, the adsorbent surface becomes positively charged when the solution pH is less than the pH_{pzc}. Therefore, high values of pH_{pzc} promote adsorption of anionic adsorbates. Conversely, an adsorbent bears a negative surface charge and effectively adsorbs cations if the solution pH values are greater than the pH_{pzc} (Gholami *et al*., 2018). The values for the point of zero charge pH (pH_{pzc}) and pH of the materials are highlighted in Table 4.2.1, while the plots are given in Figure 4.2.1.

Table 4.2.1: Point of zero charge pH (pH_{pzc}) and pH $_{(H2O)}$ of materials

Adsorbent	pH_{pzc}	pH $_{(H2O)}$
Raw Fish Scales (RFS)	8.42±0.02	7.65±0.02
Activated charcoal	3.80±0.01	7.37±0.02
FSB@200 ºC	7.67±0.02	6.29±0.01
FSB@300 ºC	7.36±0.01	7.25±0.02
FSB@400 ºC	7.27±0.02	7.05±0.02
FSB@600 ºC	6.97±0.02	7.95±0.02
FSB@800 ºC	6.48±0.03	8.05±0.02
FSB@400 ºC-Fe_3O_4	7.11±0.03	6.15±0.02
FSB@600 ºC-Fe_3O_4	7.77±0.02	6.20±0.02
FSB@800 ºC-Fe_3O_4	7.27±0.03	5.99±0.02

In this study, the pH_{pzc} values of the adsorbents ranged from 6.48 to 8.42, depicting a decrease from RFS to FSB@800 ºC with rise in pyrolysis temperature. The pH(H_2O) values of the RFS and FSB ranged between 6.29 and 8.05, without a definite trend. On the other hand, pH_{pzc} levels of the magnetic composites were reported in the range of 7.11 to 7.77, inferring that the adsorbents would be positively and negatively charged in acidic and alkaline pH, respectively. In addition, it was observed that the magnetic composites registered acidic pH (H_2O) levels.

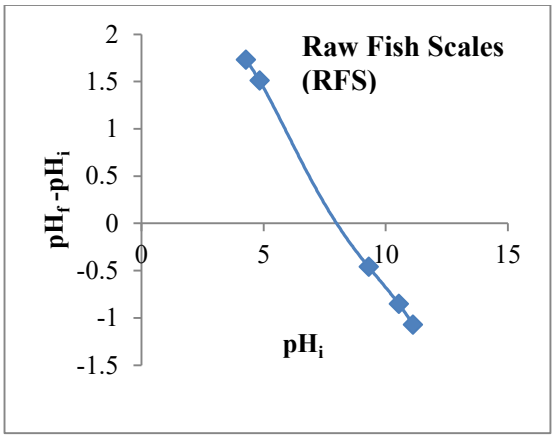

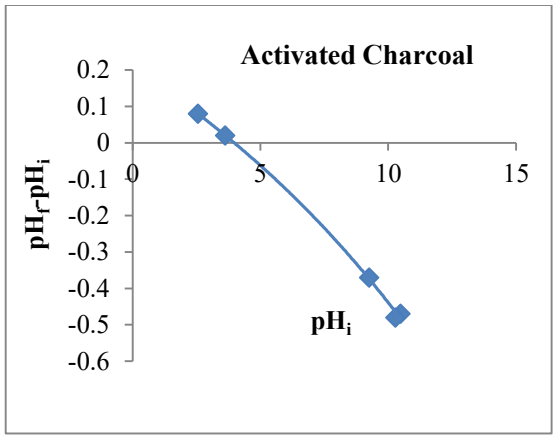

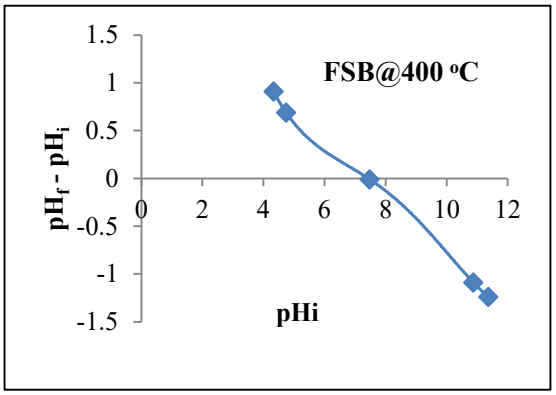

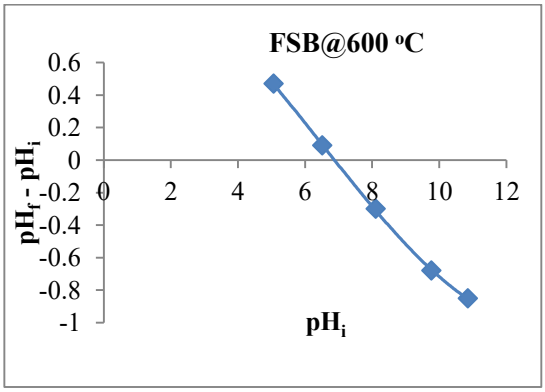

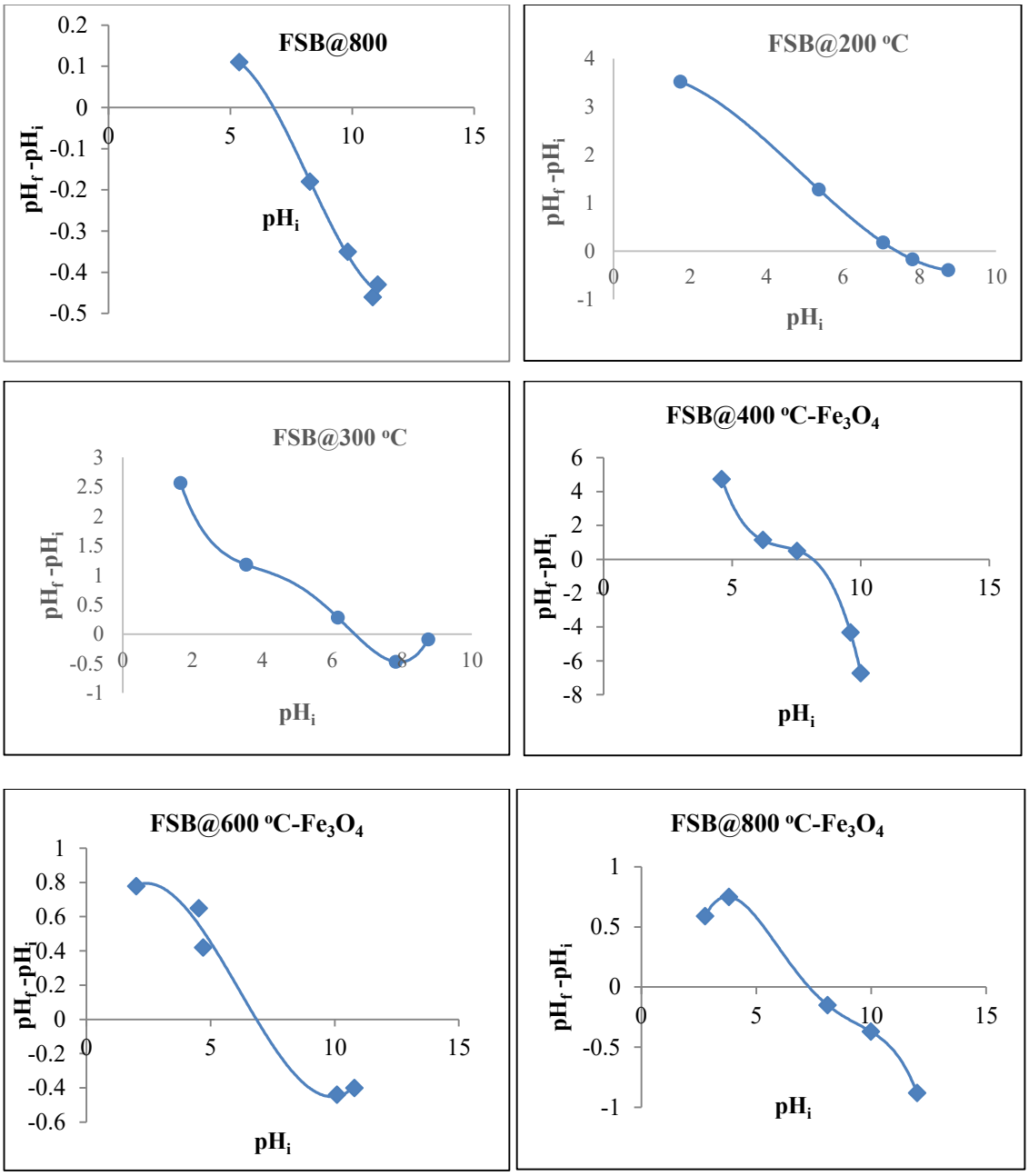

Figure 4.2.1: Point of zero charge pH (pH_{pzc}) for the adsorbents

Magnetic composite (Fe_3O_4@BC/APTES) functionalized with 3-aminopropyl triethoxysilane (APTES) prepared by capping magnetite nanoparticles with biochar from the *C. odorata* root for application in adsorption, recorded pH and pH_{pzc} of 9.45 and 12.8, respectively (Nnadozie and Ajibade, 2020). Gholami *et al*. (2018) reported a pH_{pzc} of 7.2 for magnetic fish scales (MFS). Uchimiya *et al*. (2011) recorded values of 3.5 to 10.1 for biochar adsorbents derived from cottonseed hulls prepared at temperatures between 200 ^oC to 800 ^oC. In the current study pH_{pzc} values indicate that the surface of the adsorbents would acquire either positive or negative charges in an adsorbate solution depending on the solution pH. Similar findings were reported for activated surface of banana and orange peels adsorbents (Temesgen *et al*., 2018). In the current study, the $pH_{(H2O)}$ levels posted by the biochars increased with pyrolysis temperature and decrease in %H contents. Rafiq *et al*. (2016) also reported a decrease in %H contents of the biochars as pH and pyrolysis temperature increased. Heitkötter & Marschner (2015) showed that biochars produced at 600 °C were characterized with higher ash contents and higher pH. The high pH level was attributed to the accumulation of alkali and alkaline metals (K, Mg and Ca), formation of carbonates, and concentration of biomass-derived carbonates as a function of temperature. In the current study, it was observed that pH of the biochar rose with increase in preparation temperature.

Zhao *et al*. (2017) explored the possible influence of temperature on the structural and physicochemical characteristics of biochar with apple tree branches as feedstock

material under pyrolysis temperatures of 300, 400, 500 and 600 ºC, and reported the highest pH in biochar produced at 500 ºC. In another study, increase in pH of the biochar with increasing pyrolysis temperature (obtained at 350, 360, 370, 400 and 450 ºC) from 6.36 to 9.25 for the feedstock and the biochar formed at 450 ºC, correspondingly (Mimmo *et al*., 2014). The highest increase in biochar pH as a function of pyrolysis temperature was recorded in the range 360 ºC - 370 ºC. In the current study, it can be concluded that pyrolysis temperature has an influence on pH_{pzc} and pH (H_2O) of the resulting biochar.

4.2.2 Functional group identification

The FT-IR spectra of the FSB are given in Figure 4.2.2a. These adsorbents were majorly composed of C, O, Ca and P. The band at 3955 cm^{-1} correspond to -OH stretching vibrations attributed to alcoholic functional group (Zainon *et al*., 2012; Slimani *et al*., 2014; Paul *et al*., 2017) while those at 1582 cm^{-1} characterized the amides as reported by Zainon *et al*. (2012) and Paul *et al*. (2017). Carbonate group stretching frequencies were assigned to the bands at 1455 cm^{-1} and 1413 cm^{-1} while those at 1017 cm^{-1} correspond to C-O stretching vibrations; peak of PO_4^{3-} groups of hydroxyapatite was assigned at wavenumber in the range of 962 cm^{-1}, corroborating previous reports (Zainon *et al*., 2012; Slimani *et al*., 2014; Paul *et al*., 2017). Absorption band of the carboxylate group on the surface of activated charcoal was evidenced by the band at 1582 cm^{-1} (Bagtash & Zolgharnein, 2018). Das *et al*. (2021) reported that the concentration of different surface functional groups like phenolic, surface carboxylic, lactonic and total acidic functional groups lessened with rise in pyrolysis temperature from 400 to 600 ºC.

The pyrolysis of feedstocks at higher temperature released more volatile substances and carbonaceous gases that led to lower total acidic functional groups. The researchers further observed a decreased FT-IR band strength of the C=O/OH, -CH_n and –OH stretching with rising pyrolysis temperature due to de-polymerization and dehydration processes.

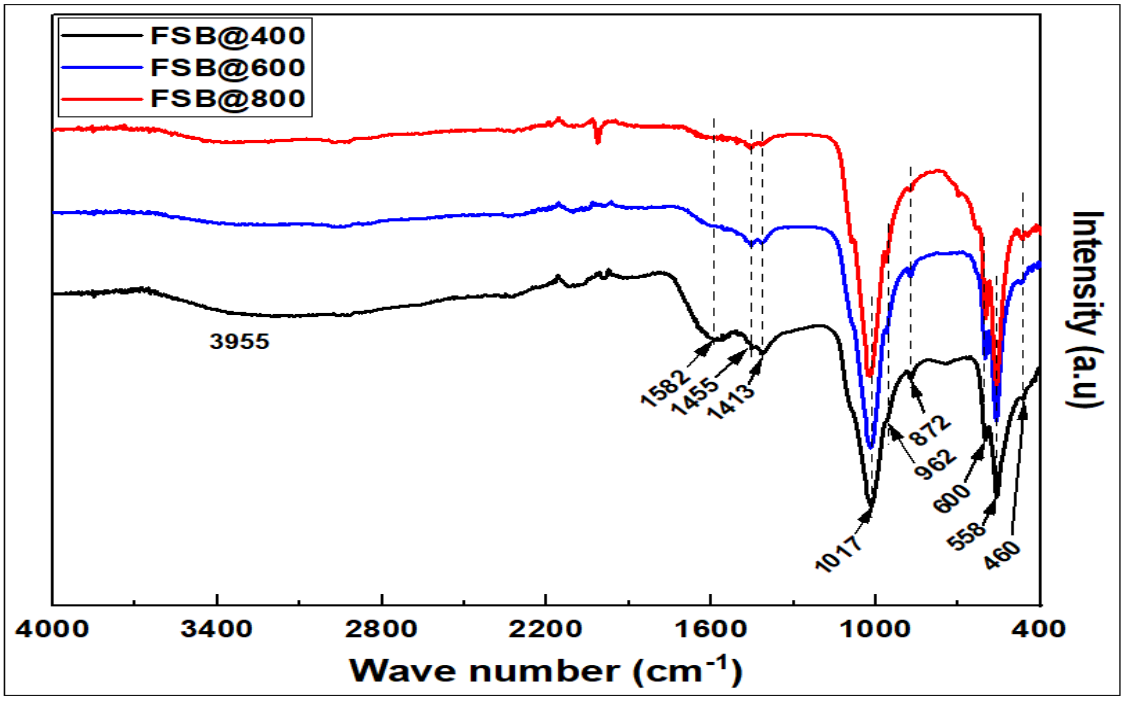

Figure 4.2.2a: FT-IR spectra of the adsorbents (FSB@400 ºC, FSB@600 ºC and FSB@800 ºC)

FT-IR spectra of the magnetic composites are displayed in Figures 4.2.2b and c. The bands between 3375 cm^{-1} and 3350 cm^{-1} correspond to –OH stretching vibration attributed to alcoholic functional group and OH group in the reduction process of magnetite and magnetic composite generation as reported by other researchers (Mahdavi *et al*., 2013; Slimani *et al*., 2014). Carbonate group stretching and folding was assigned to peaks at 1455 cm^{-1} and 872 cm^{-1} whereas the band at 1017 cm^{-1} corresponded to C-O stretching vibration. These observations are in harmony with published work (Slimani *et al*., 2014; Nnadozie & Ajibade, 2020). C–H distortion vibration at 1413 cm^{-1} indicates the presence of alkanes, whereas the presence of magnetite was characterized by absorption bands between 600 cm^{-1} and 465 cm^{-1} that correspond to Fe-O bond in magnetite and magnetic composite. Similar findings were reported in other studies (Bordoloi *et al*., 2018; Srivastava, 2012; Sun *et al*., 2015; Mahdavi *et al*., 2013; Fraga *et al*., 2019).

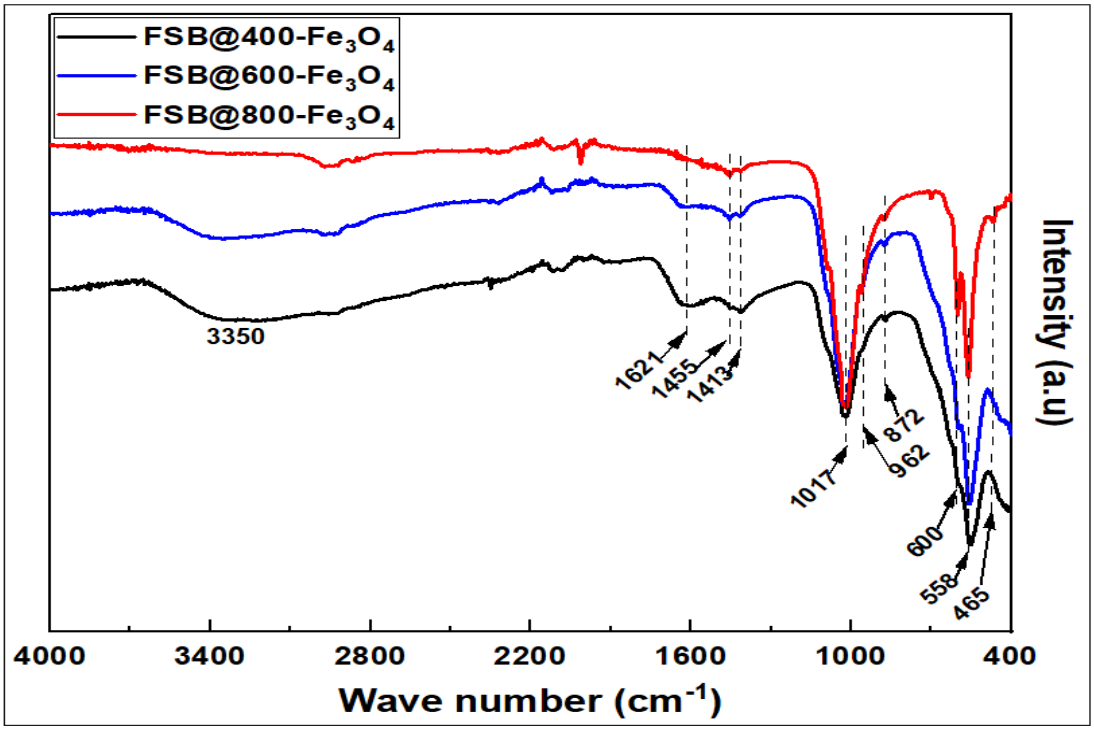

Figure 4.2.2b: FT-IR spectra for FSB@400 ºC-Fe_3O_4, FSB@600 ºC-Fe_3O_4 and FSB@800 ºC-Fe_3O_4

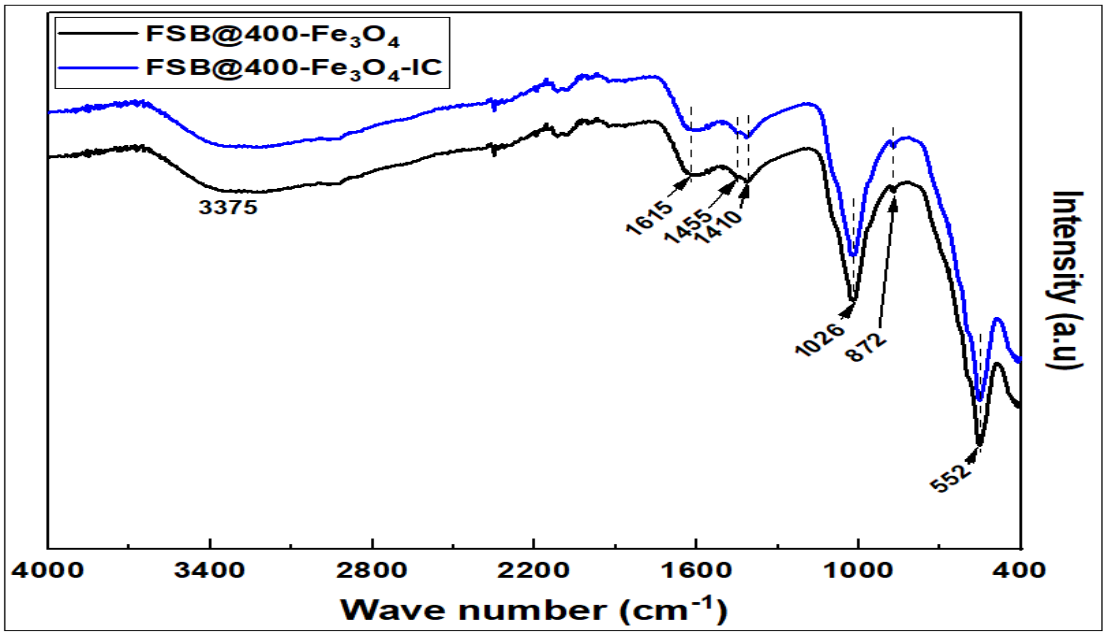

Figure 4.2.2c: FT-IR spectra for FSB@400 ºC-Fe_3O_4, and FSB@400 ºC-Fe_3O_4-I.C.

4.2.3 Surface morphology and structure of the adsorbents and chemical composition of the adsorbents

The morphology, structure, particle size and surface area of the FSB adsorbents were studied using Scanning Electron Microscopy (SEM-EDX), Transition Electron Microscopy (TEM), BET and powder X-ray diffraction (PXRD). The SEM micrographs showed the charred fish scales appearing more compact compared to the pulverized raw fish scales, a consequence of thermal conversion of RFS to FSB (Figures 4.2.3a and b). This is confirmed by difference in the image of the activated charcoal (Figure 4.2.3c) which is also a product of thermo-chemical conversion. Zhao *et al*. (2017) reported that the SEM image of biochar (from apple tree branches as feedstock material) at 300 ^{o}C revealed that the biomass had softened, liquefied and fused into a mass of vesicles which were the consequence of volatile gases released within the biomass. As temperatures rose, more volatile gases were released from the biomass, the vesicles on the surface of biochar at 400 ^{o}C busted after cooling, thus the morphology of biochar at 400 ^{o}C exhibited a number of pore structure. For the biochar at 500 ^{o}C, portions of the skeletal structure appeared brittle due to the decomposition of more components. The fracture phenomenon also appeared within the pore structure for the biochar at 600 ^{o}C. SEM images (Figures 4.2.3g and h) demonstrated spherical shapes of magnetite (Fe_3O_4) particles on the surface of synthesized material as reported in other studies (Srivastava, 2012; Dada *et al*., 2014; Chaki *et al*., 2015; De León-Condés *et al*., 2019). This observation was confirmed in

FT-IR spectra (Figure 4.2.2b), in which the Fe_3O_4 particles appeared uniformly spread within the composite matrix (Dada *et al*., 2014).

The TEM micrograph of the FSB@400 ^oC, FSB@600 ^oC and FSB@800 ^oC (Figures 4.2.3d, i and j) adsorbents displayed spotted ring-like patterns with particle sizes of 24.21 nm, 17.43 nm and 22.92 nm, respectively. The surface of magnetite particles as captured in TEM micrographs (Figure 4.2.3m) was visibly subjugated by catenation of identical and spherically shaped flowers whose average diameter is 7.40 nm (Dada *et al*., 2014; Chaki *et al*., 2015; Sun *et al*., 2015; Bordoloi *et al*., 2018; Mtshatsheni *et al*., 2020) which appeared dispersed and diminishing, though noticeable, in the case of magnetic composite (Figures 4.2.3k, l and n) owing to magnetic and Van der Waals forces in zero-valent iron particles (Mahdavi *et al*., 2013; Dada *et al*., 2014).

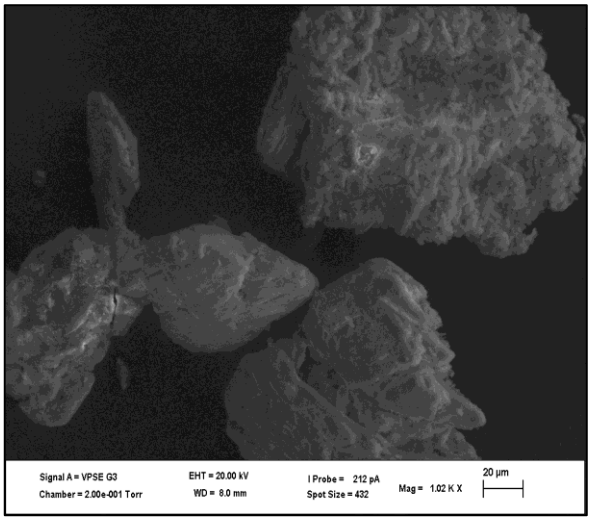

(a) SEM Raw Fish Scales

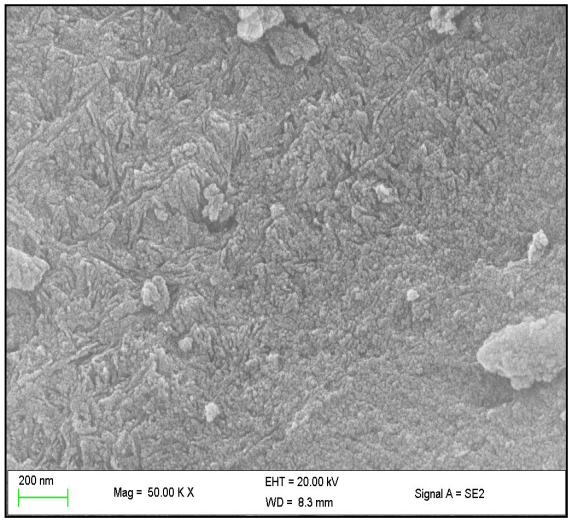

(b) SEM FSB@400 ºC

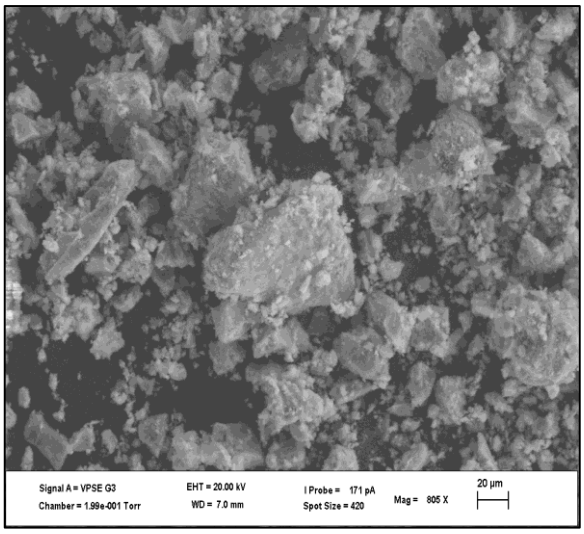

(c) SEM Activated charcoal (AC)

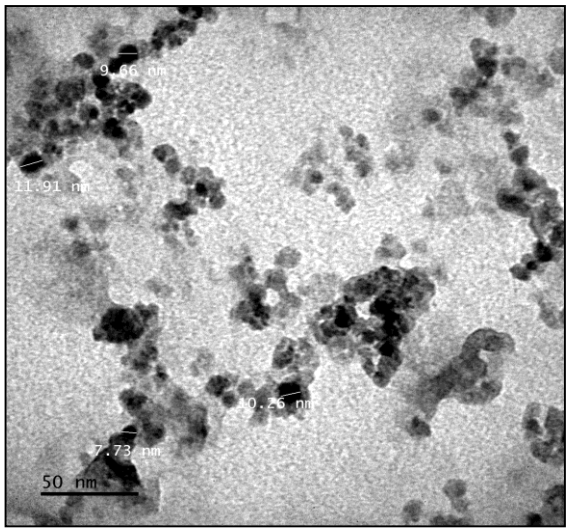

(d) TEM FSB@400 ºC

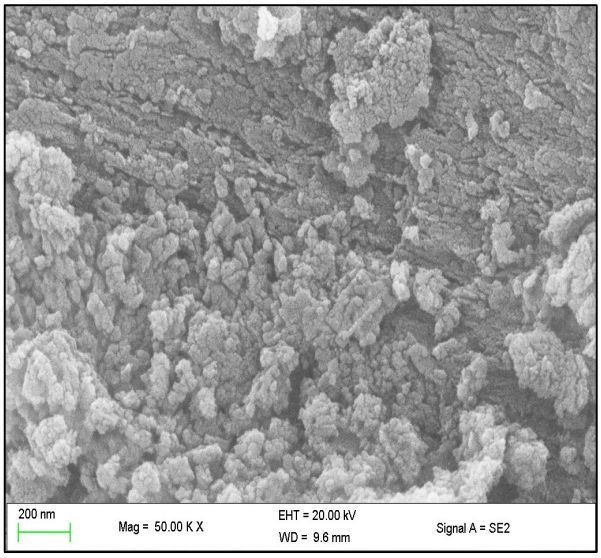

(e) SEM FSB@600 ºC

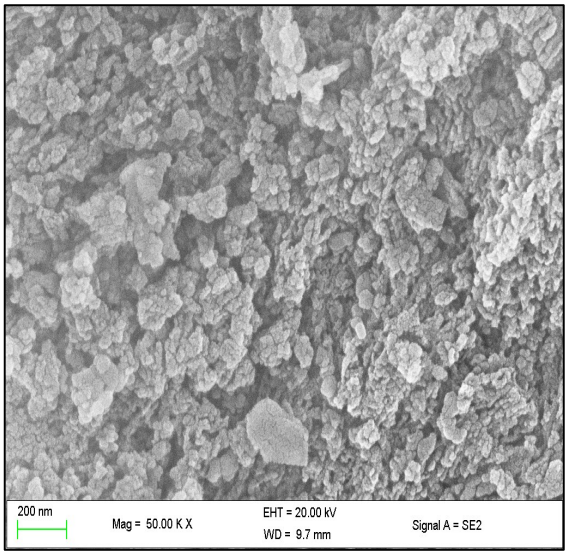

(f) SEM FSB@800 ºC

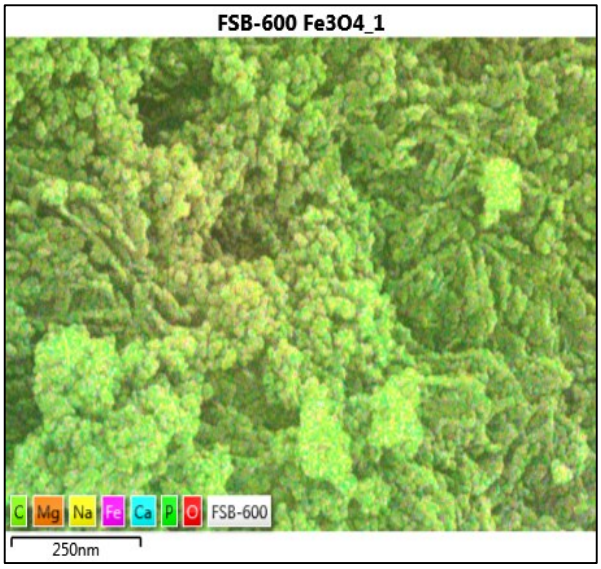

(g) SEM FSB@600 ºC-Fe_3O_4

(h) SEM FSB@800 ºC-Fe_3O_4

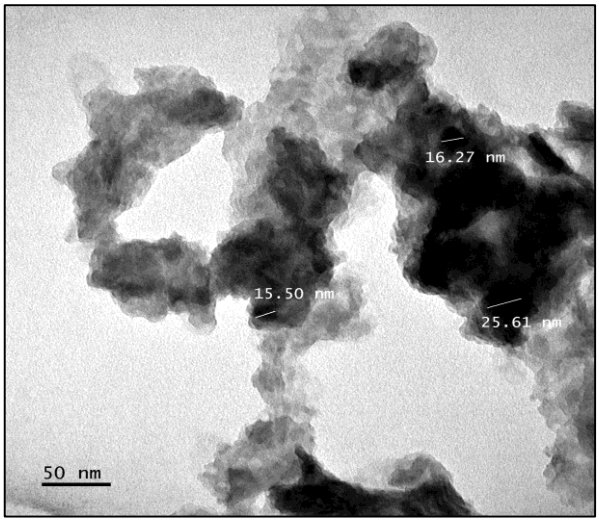

(i) TEM FSB@600 ºC

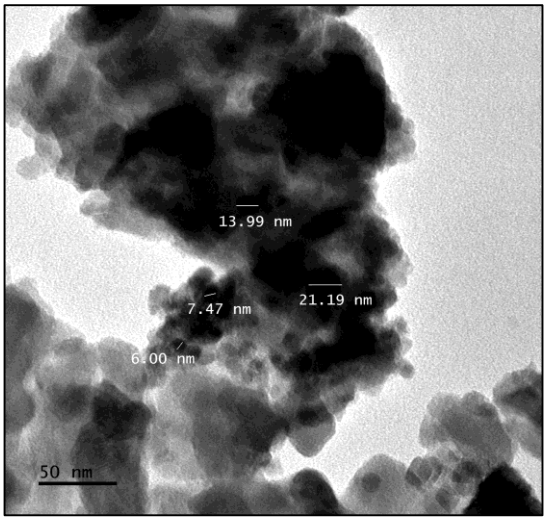

(j) TEM FSB@800 ºC

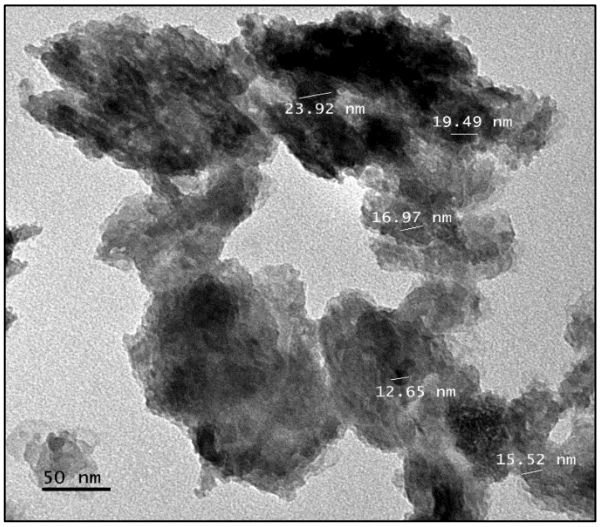

(k) TEM FSB@600 ºC-Fe_3O_4

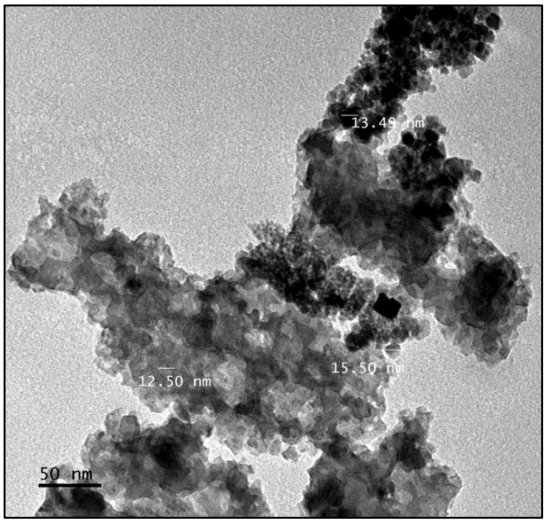

(l) TEM FSB@800 ºC-Fe_3O_4

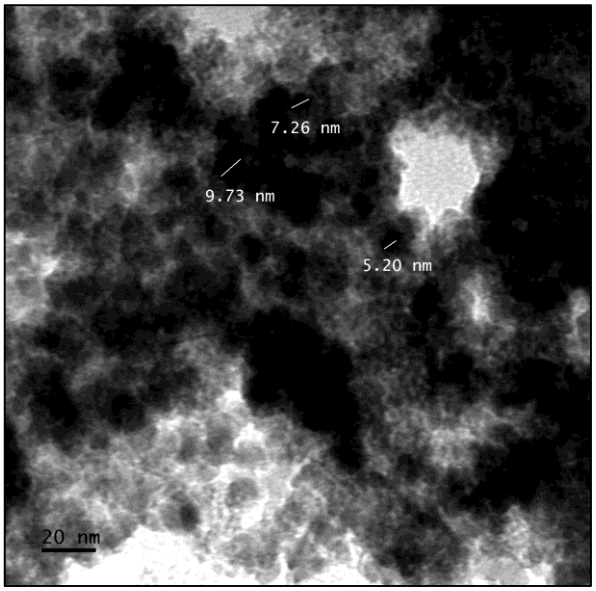

(m) TEM Fe_3O_4

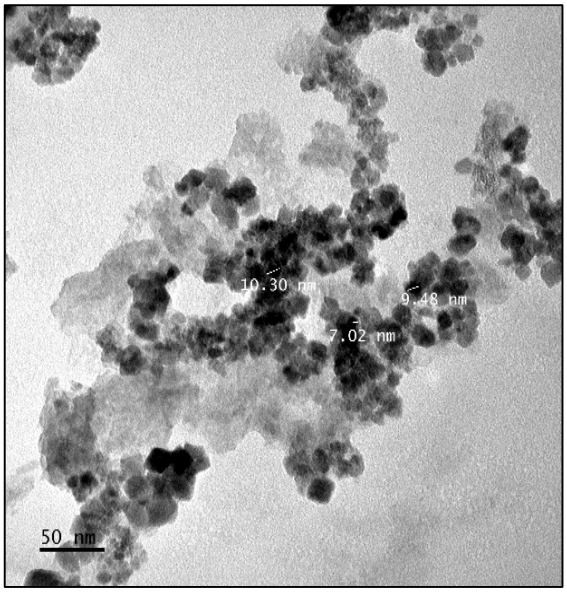

(n) TEM FSB@400 ^oC-Fe_3O_4

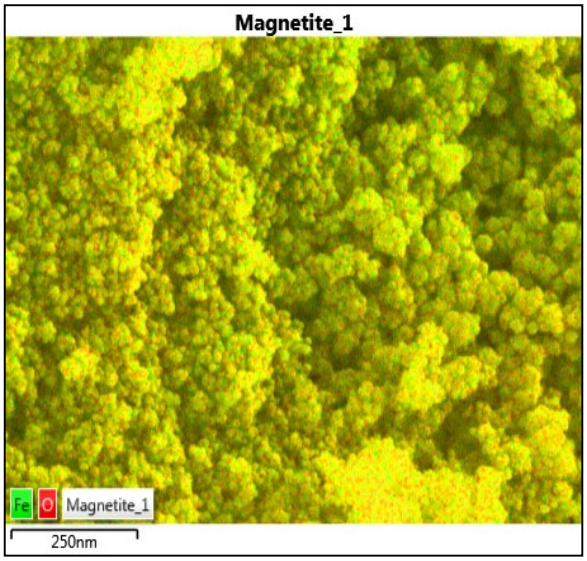

(o) SEM Fe_3O_4

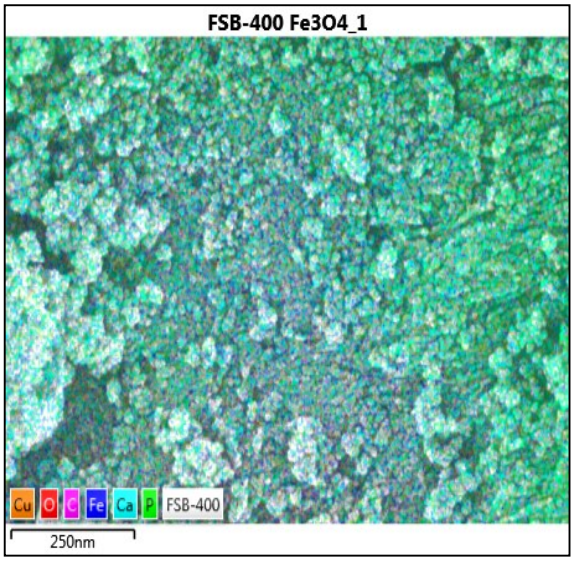

(p) SEM FSB@400 ^oC-Fe_3O_4

Figure 4.2.3: SEM and TEM images of Raw fish scales, fish scale biochars (FSB), activated charcoal (AC), magnetite (Fe_3O_4) and magnetic composites (FSB@Fe_3O_4)

4.2.4 Chemical compositions of the adsorbents

The chemical compositions of the materials are summarized in Table 4.2.4 and Figure 4.2.4. Activated carbon had the highest carbon content of 84.40% followed by FSB@600 ºC, FSB@800 ºC, FSB@400 ºC and raw fish scales. High carbon contents observed in the biochars were attributed to inorganic carbon as a function of pyrolysis. Other elements such as P, Ca, Na and Mg also increased with pyrolysis temperature while N, O and H exhibited declining trends. This observation is in agreement with the findings of Rafiq *et al*. (2016). In another study, Zhao *et al*. (2017) explored the possible influence of temperature on the structural and physico-chemical characteristics of biochar with apple tree branches as feedstock material under pyrolysis temperatures of 300, 400, 500 and 600 ºC. The results showed that rise in temperature improved the content of fixed carbon (C), the C content and inorganic minerals (K, P, Fe, Zn, Ca, Mg), while O and H decreased. Heitkötter & Marschner (2015) reported that biochars produced at 600 °C exhibited higher accumulation of metals (K, Mg and Ca), confirming that the concentration of alkaline metals is a function of biochar preparation temperature. Moreover, Luo *et al*. (2018) reported rich cations composition in the biochar at elevated temperature.

There were slight deviations of Na, Mg, Ca, P and O levels in FSB@400 ºC and FSB@400 ºC-IC. However, concentrations of N, C, H and S significantly increased in FSB@400 ºC-I.C. and FSB@400 ºC-C.V. confirming the adsorption of indigo carmine and crystal violet dyes. Magnetite registered percent compositions of 70.13 % and 27.18 % for Fe and O, respectively, which compared relatively well with findings from previous studies, Fe (72.36

%) and O (27.64 %) (Srivastava, 2012; Chaki *et al*., 2015), implying that there was successful coupling of FSB and Fe as was seen in the spectra of the composites (Dada *et al*., 2014; Zheng *et al*., 2020; Mtshatsheni *et al*., 2020). It has been observed that the pyrolysis temperature has an influence on the levels of elemental composition of the produced biochars.

Table 4.2.4: Elemental composition of the adsorbents

Adsorbents	**C%**	**N%**	**H%**	**O%**	**Ca%**	**P%**	**Mg%**	**Na%**	**Fe%**	**S%**	**Cl%**
Raw fish scales	6.8	16.03	-	37.74	15.20	8.97	0.34	0.16	-	0.08	-
Activated charcoal	84.40	8.26	-	6.78	0.26	-	-	-	-	-	-
FSB@400 ºC	12.51	4.07	1.07	40.51	27.38	12.98	0.39	0.34	-	-	-
FSB@600 ºC	18.41	0.37	0.06	43.74	29.08	13.89	0.46	0.32	-	-	-
FSB@800 ºC	14.72	0.50	0.01	37.04	32.28	14.90	0.42	0.20	-	-	-
Fe_3O_4	-	-	-	27.18	-	-	-	-	70.13	-	-
FSB@400 ºC-Fe_3O_4	13.76	1.92	0.92	41.68	23.37	14.57	-	-	3.75	-	-
FSB@600 ºC-Fe_3O_4	18.21	0.34	0.05	42.22	25.34	12.01	0.42	-	1.18	-	-
FSB@800 ºC-Fe_3O_4	11.47	0.46	0.01	40.95	28.34	14.42	0.64	0.20	4.19	-	-
FSB@400 ºC-I.C.	35.50	16.74	1.14	40.48	27.34	12.92	0.38	0.28	-	0.06	-
FSB@400 ºC-C.V.	34.03	20.70	0.82	27.00	12.43	5.84	-	-	-	-	0.03
FSB@400 ºC-Fe_3O_4-I.C	35.72	15.72	0.94	41.57	23.05	13.73	-	0.19	3.74	0.01	-
FSB@400 ºC-Fe_3O_4-C.V.	33.91	10.56	0.72	31.66	11.60	5.42	-	-	6.57	-	0.27

I.C.-Indigo Carmine; C.V.-Crystal Violet; FSB-fish scale biochar

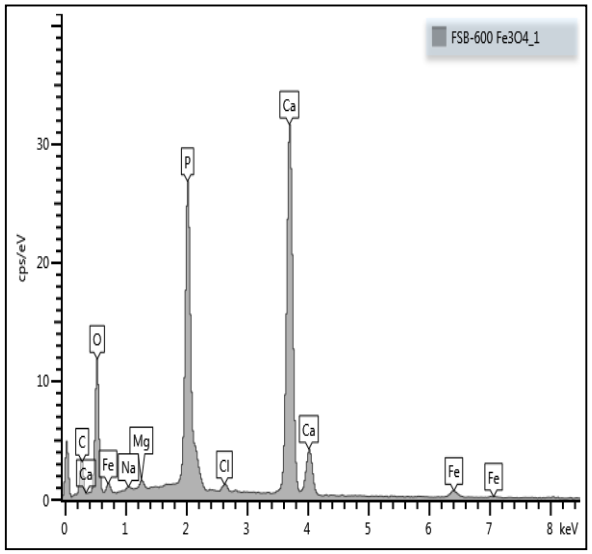

(a) FSB@600 ºC-Fe_3O_4

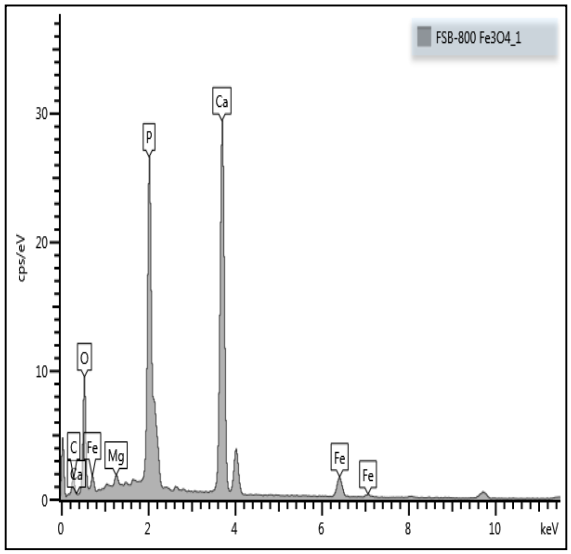

(b) FSB@800 ºC-Fe_3O_4

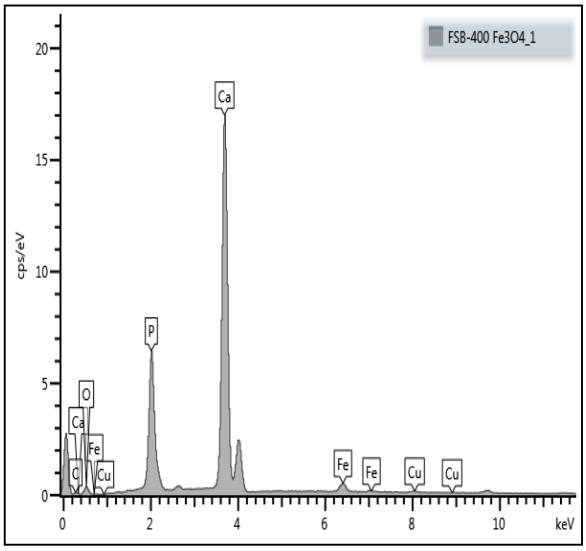

(c) FSB@400 ºC-Fe_3O_4

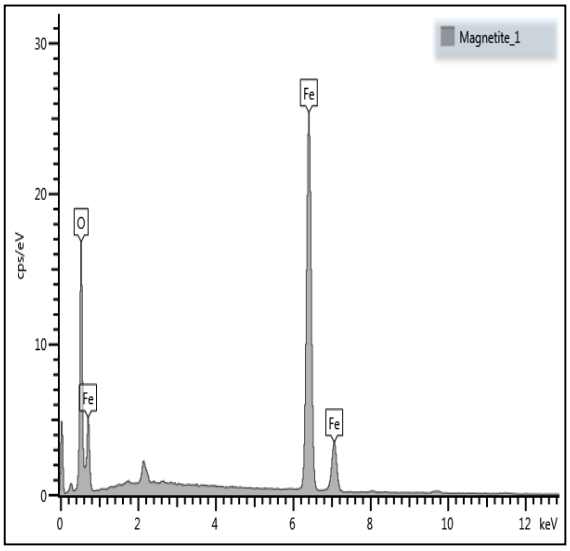

(d) Fe_3O_4

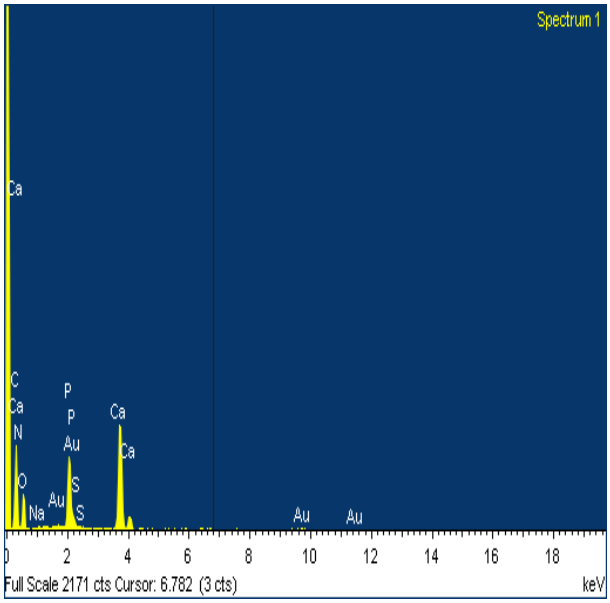

(e) FSB@400 ºC-I.C.

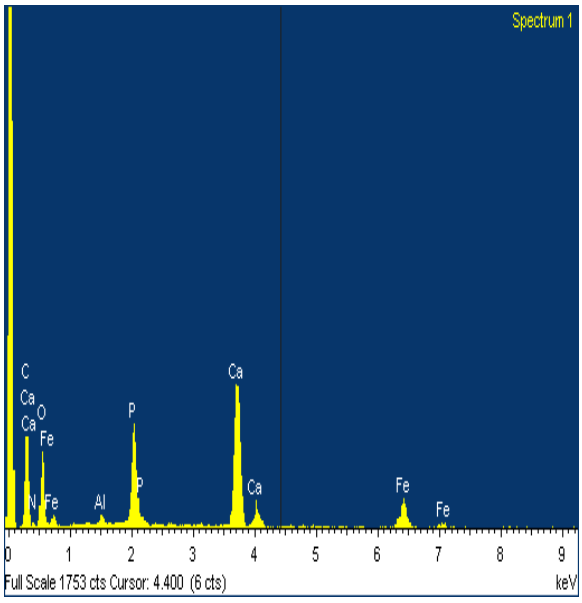

(f) FSB@400 ºC-Fe_3O_4-I.C.

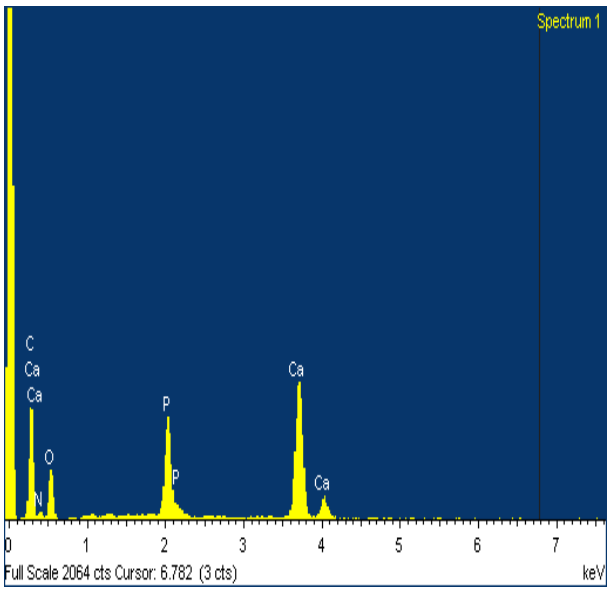

(g) FSB@400 ºC-C.V.

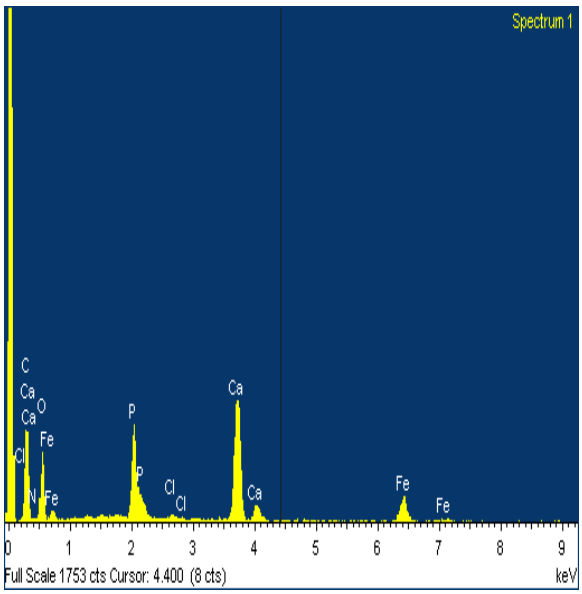

(h) FSB@400 ºC-Fe_3O_4-C.V.

Figure 4.2.4: EDX of fish scale biochars (FSB), magnetic composites (FSB@Fe_3O_4) and spent adsorbents

4.2.5 Mineral compositions and phase purity of the adsorbents

The mineral composition and phase purity of the fish scale biochars (FSB) and the magnetic composites (FSB@Fe_3O_4) were studied by X-ray diffraction (XRD) and the diffraction patterns are presented in Figures 4.2.5a-f. The fish scale Biochars (FSB@400 ºC, FSB@600 ºC, and FSB@800 ºC) are mainly composed of hydroxyl apatite, $Ca_5(PO_4)_3(OH)$, phase (Zainon *et al*., 2012; El Haddad *et al*., 2013a; Slimani *et al*., 2014; Scapin *et al*., 2015; Paul *et al*., 2017). Such results were also reported by Othman *et al*. (2016). The results showed that fish scale biochar at 400 ºC (FSB@400 ºC) exhibit broader peaks compared to FSB@600 ºC and FSB@800 ºC, whose peaks are sharper, and more intense. This difference is attributed to the presence of proteins and incomplete decomposition of organic matter at 400 ºC (Paul *et al*., 2017). Sharp and robust reflection XRD peaks were observed on the magnetic composites, implying that the biochar matrix was well crystallized (Figure 4.2.5d).

Magnetite was identified as the main crystalline phase in biochar as characterized with diffraction peaks at 2θ of 29.98º, 37.21º, 41.38º, 58.00º, and 62.50º, corresponding to five indexed planes (220), (311), (400), (511), and (440) (Figure 4.2.5d). These findings are in harmony with data reported by other researchers (Zhang *et al*., 2013; Mahdavi *et al*., 2013; Srivastava, 2012; Machala *et al*., 2011; Zheng *et al*., 2020; Goncalves *et al*., 2020; Zhang *et al*., 2020). The presence of Fe in the materials as characterized by XRD supports SEM, EDX, TEM, VSM and FT-IR results. It is concluded that pyrolysis temperature had an influence on the characteristics of the resulting biochars.

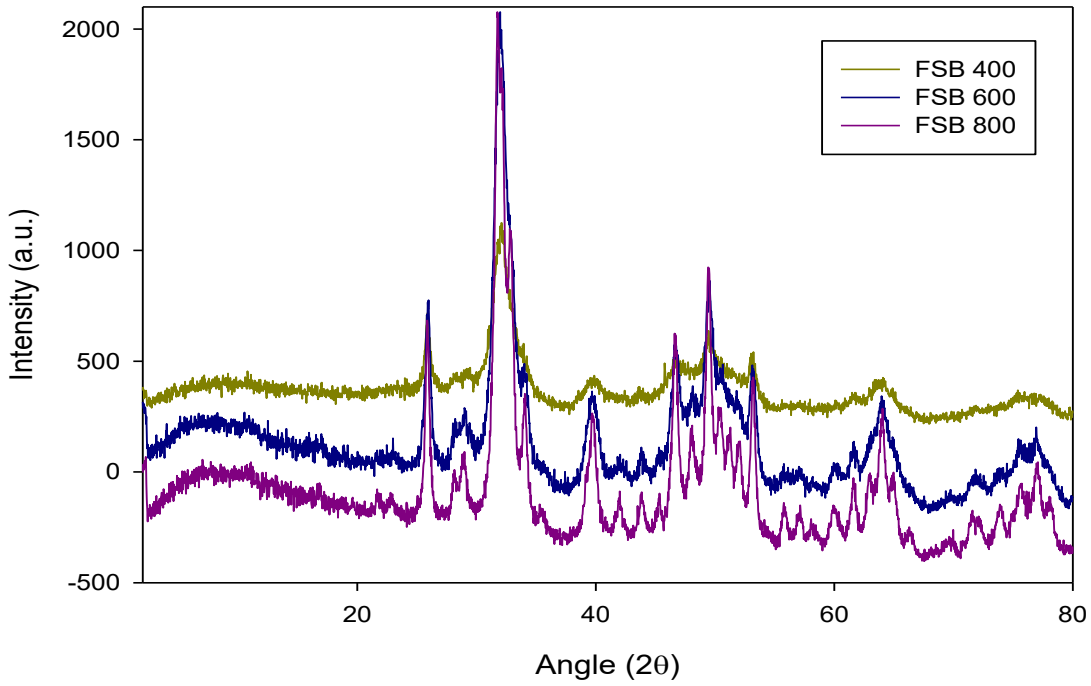

Figure 4.2.5a: Powder X-ray Diffractograms for Biochars prepared at 400 ºC, 600 ºC and 800 ºC

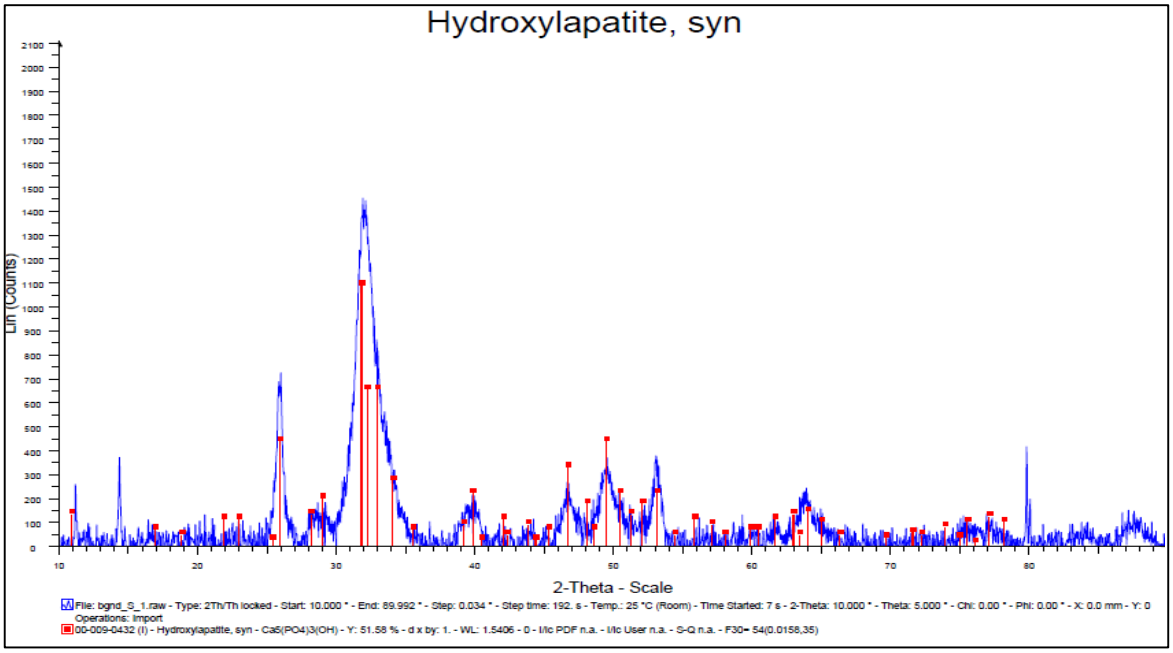

Figure 4.2.5b: Powder X-ray Diffractogram for FSB@400 ºC

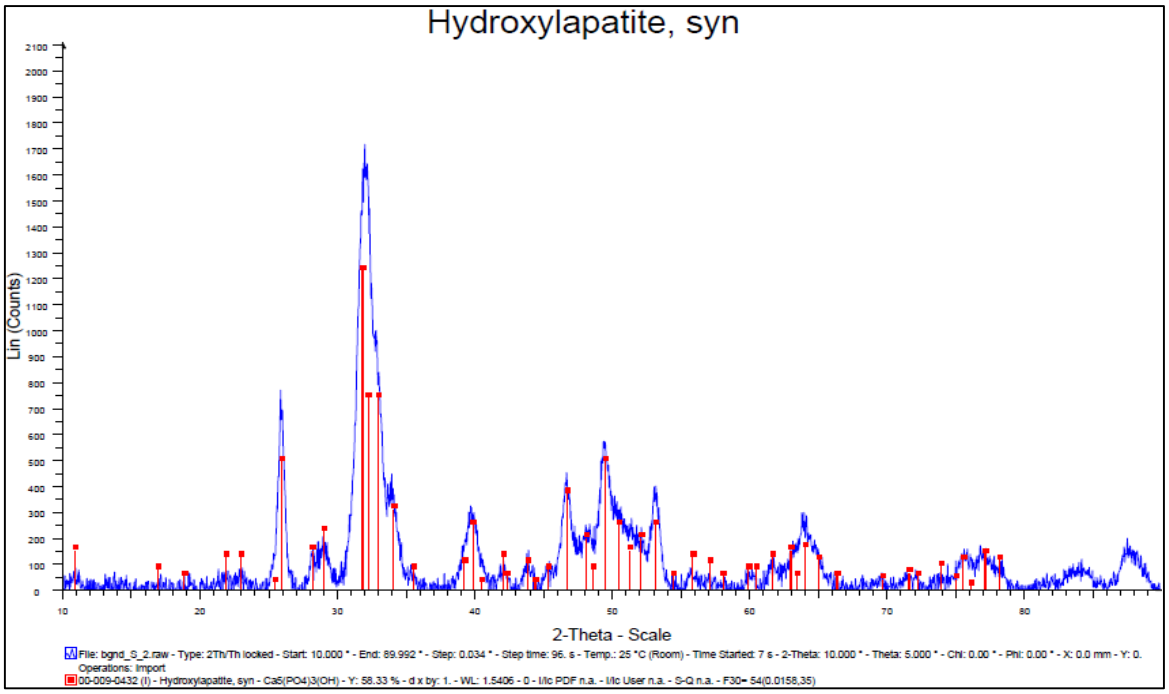

Figure 4.2.5c: Powder X-ray Diffractograms for FSB@600 ºC

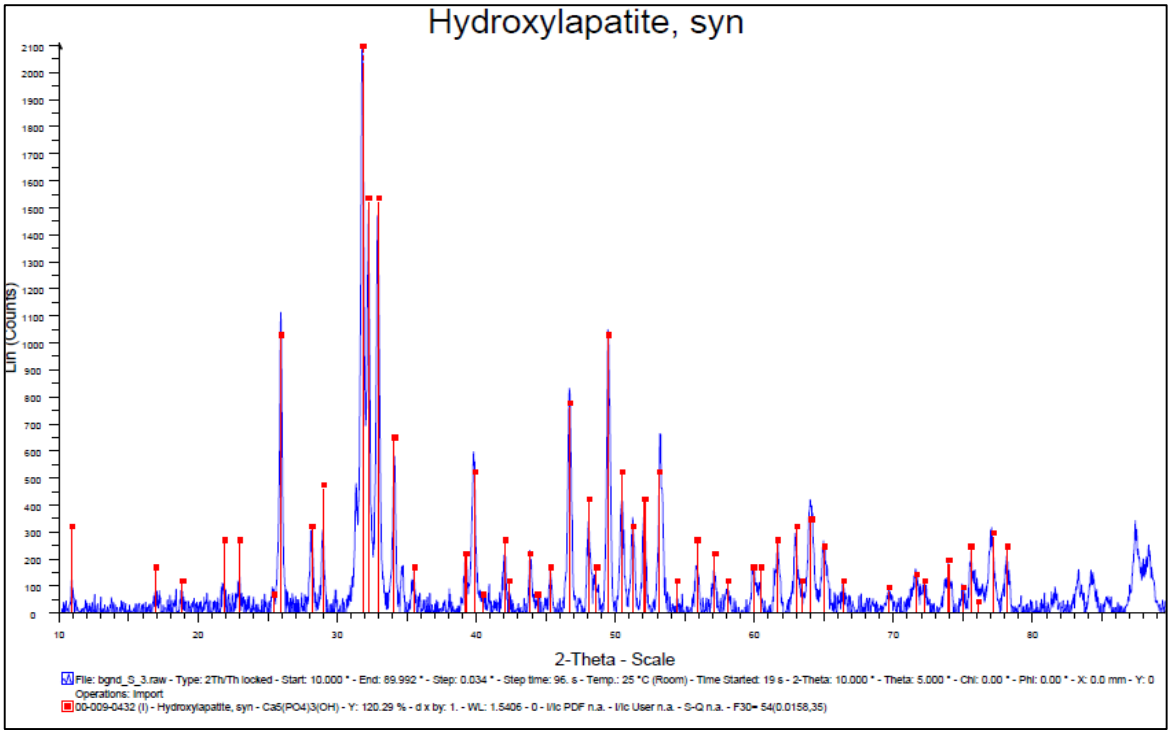

Figure 4.2.5d: Powder X-ray Diffractograms for FSB@800 ºC

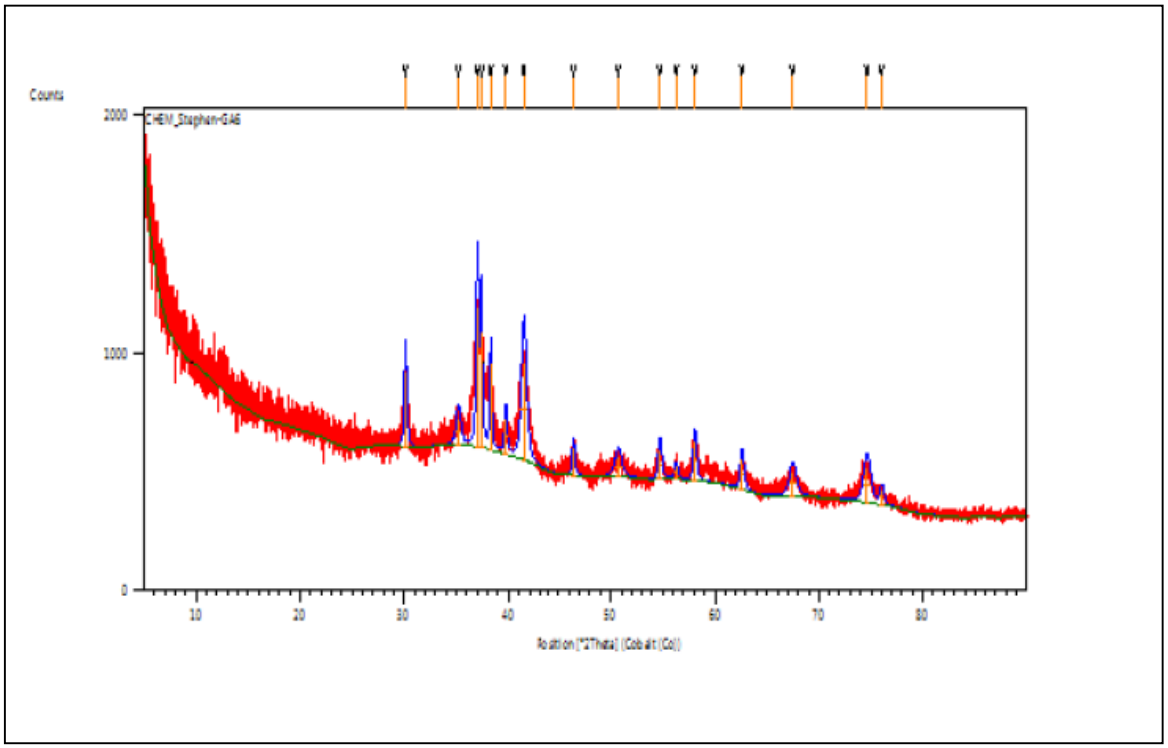

Figure 4.2.5e: Powder X-ray Diffractograms for FSB@600 ºC-Fe_3O_4

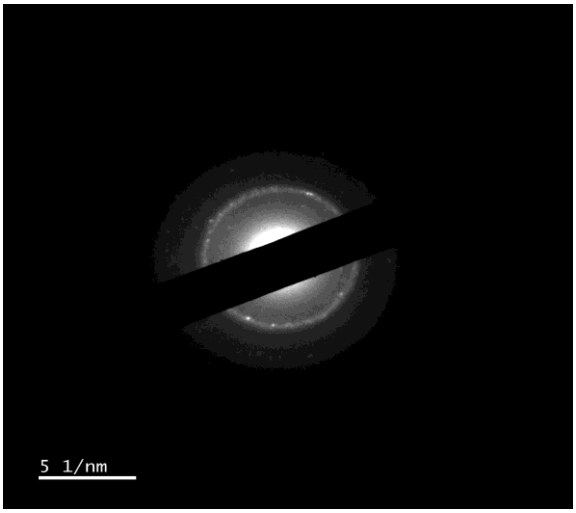

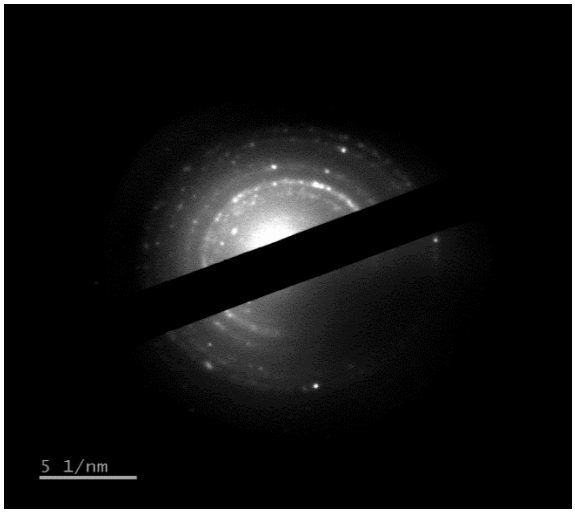

(f) FSB@600ºC FSB@600 ºC-Fe_3O_4

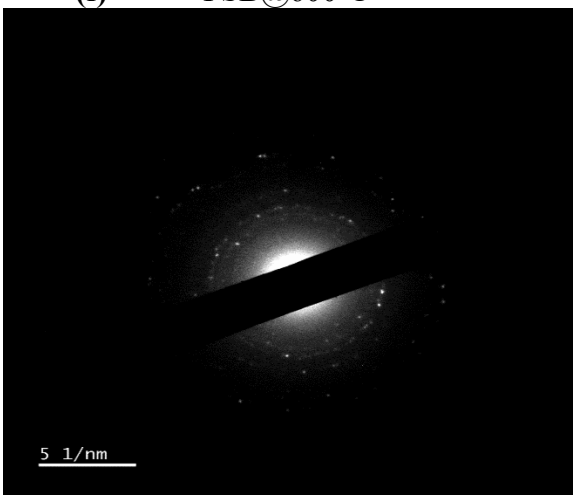

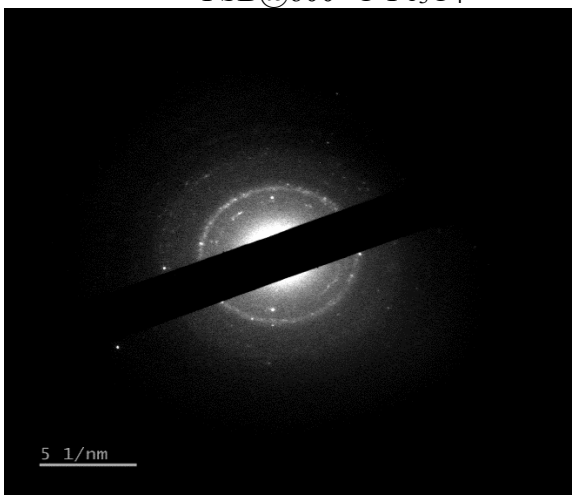

(g) FSB@400 ºC FSB@400 ºC-Fe_3O_4

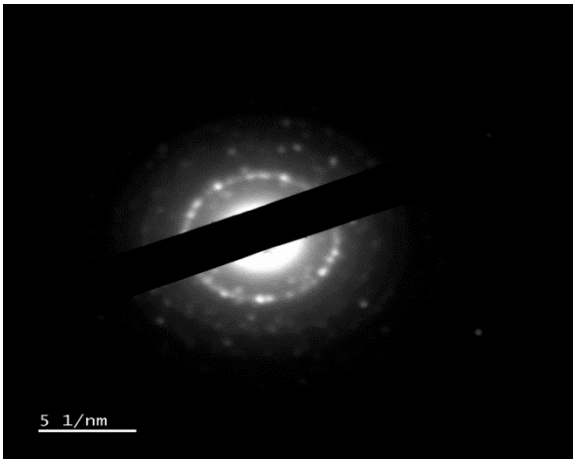

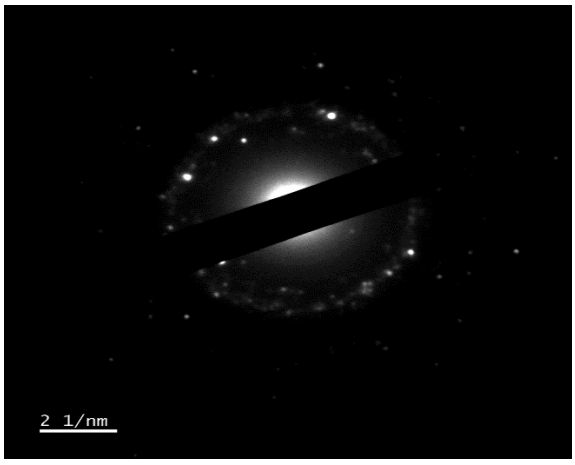

(h) FSB@800 ºC FSB@800 ºC-Fe_3O_4

Figure 4.2.5f-h: Diffraction patterns for FSB and FSB@Fe_3O_4

4.2.6 Surface areas, pore volumes and particle sizes of the adsorbents

Brunauer-Emmett-Teller (BET) surface areas, Barrett-Joyner-Halenda (BJH) pore volumes, and particle sizes, which are some of the critical adsorptive characteristics of an adsorbent, were examined, and the findings were as given in Table 4.2.6, Figures 4.2.64a and b.

Table 4.2.6: Surface areas and pore volumes of the adsorbents

Adsorbent	Surface Area (Micropore Surface Area), $m^2\ g^{-1}$	Pore Volume (Micropore Volume), $cm^3\ g^{-1}$	Particle size (nm)
Raw Fish Scales	2.8±0.07	0.002±0.001	444.13
Activated Charcoal	1024±27.41	0.71±0.03	3.8×10^{-8}
FSB@400 ºC	40.79±1.09	0.11±0.01	22.92
FSB@600 ºC	94.05±2.52	0.23±0.01	17.43
FSB@800 ºC	47.77±1.28	0.20±0.01	24.21
FSB@400 ºC-Fe_3O_4	102.23±2.74	0.25±0.01	19.26
FSB@600 ºC-Fe_3O_4	102.67±2.75	0.16±0.01	16.15
FSB@800 ºC-Fe_3O_4	96.89±2.60	0.22±0.01	19.03

The results displayed an increase in both surface area and pore volume as the pyrolysis temperature increased up to 600 ºC, thereafter decreased at 800 ºC. Precisely, raw fish scales and Activated Charcoal, recorded the least and the highest surface area and pore volume, respectively. This finding suggests that, in general, pyrolysis improves the surface area of a biomass adsorbent (Rafiq *et al*., 2016). Noor *et al*. (2019) reported that the surface area of coconut flesh waste biochar (CFWB) slowly increased from 0.3971 m^2/g to 0.6619 m^2/g as the pyrolysis temperature was increased from 350 °C to 500 °C. The increment of surface area is attributed to the loss of organic compound or enhanced devolatilization, which created void within the biochar matrix (Wang *et al*., 2013). At a higher temperature, the Brunauer–Emmett–teller (BET) surface area and pore volume are higher mostly due to the increase of the micropore surface area and micropore volume (Zhao *et al*., 2017). The surface area of the magnetic composites was in the order FSB@800 ºC-Fe_3O_4 < FSB@400 ºC-Fe_3O_4 < FSB@600 ºC-Fe_3O_4. On the other hand, FSB@400 ºC-Fe_3O_4 and FSB@600 ºC-Fe_3O_4 displayed the largest and the least pore volumes, respectively. In addition, FSB@600 ºC-Fe_3O_4 recorded the least particle size of the three magnetic composites. These results justify that loading of Fe_3O_4 particles on fish scale biochar (FSB) has a significant bearing on the improvement of specific surface area as shown by Gholami *et al*. (2018) for fish scales (FS) (0.65 m^2/g) and magnetic fish scales (MFS) (4.86 m^2/g). It is concluded that pyrolysis temperature has an effect on the surface area, pore volume and particle size of the biochar.

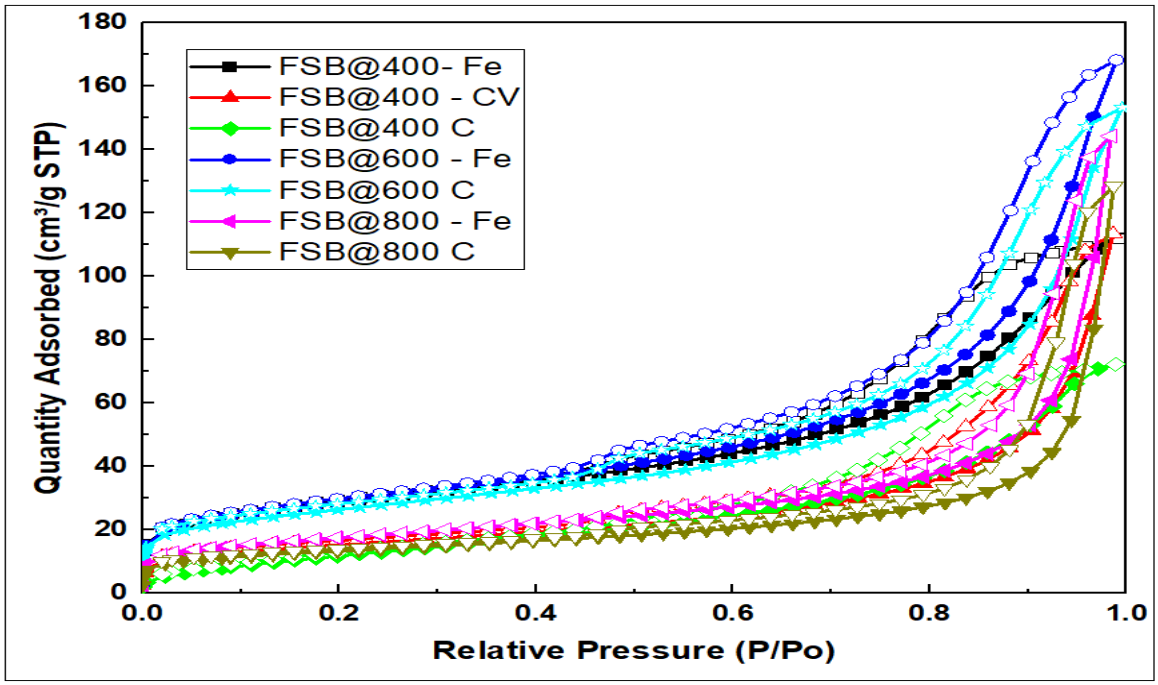

(a) Nitrogen sorption isotherms

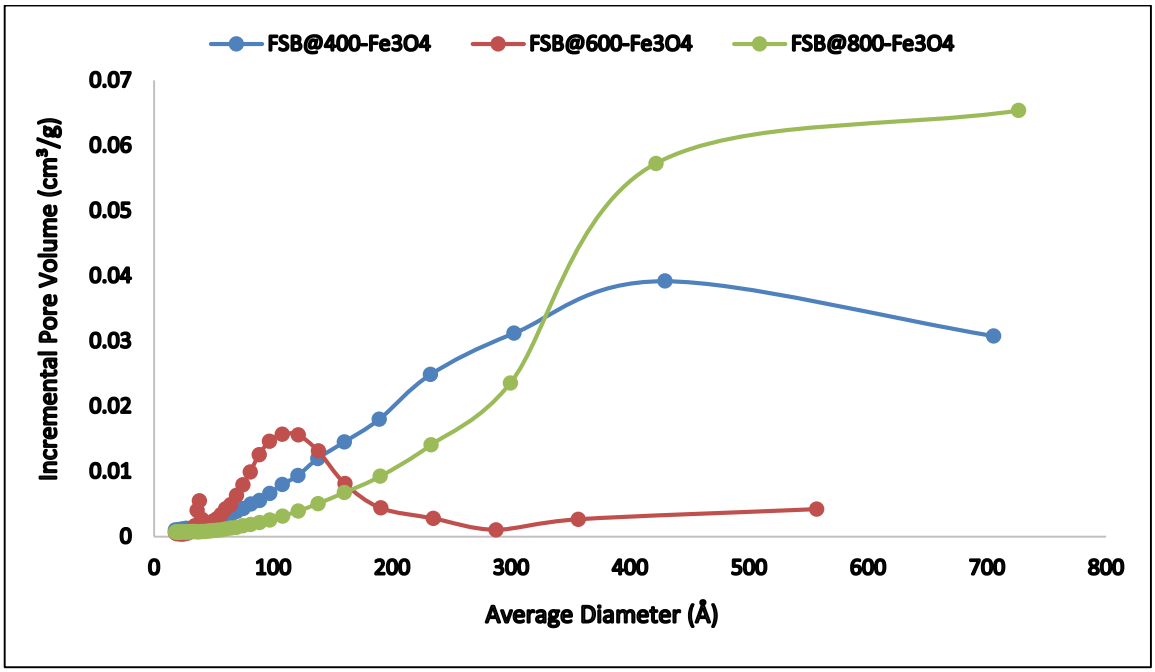

(b) Pore size distribution curves

Figure 4.2.6a and b: BET analysis of synthesized adsorbents (FSB and FSB@Fe_3O_4); Nitrogen sorption isotherms and Pore size distribution curves

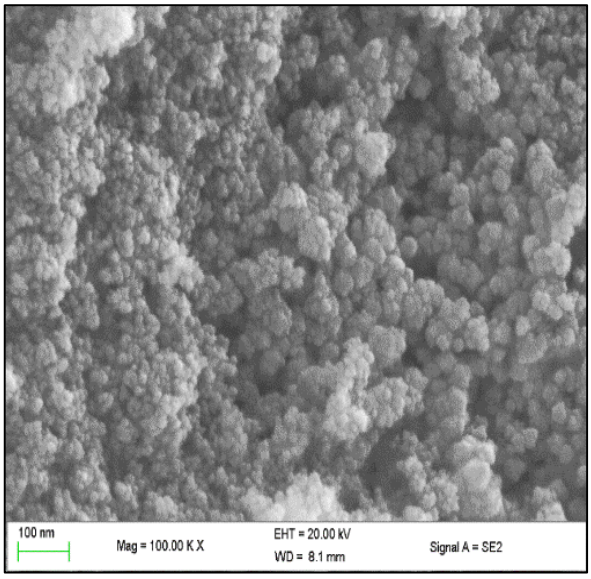

(c) Fe_3O_4

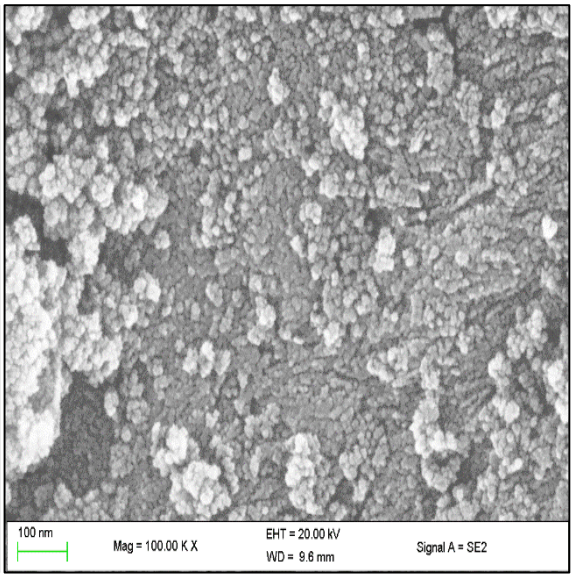

(d) FSB@400 ºC-Fe_3O_4

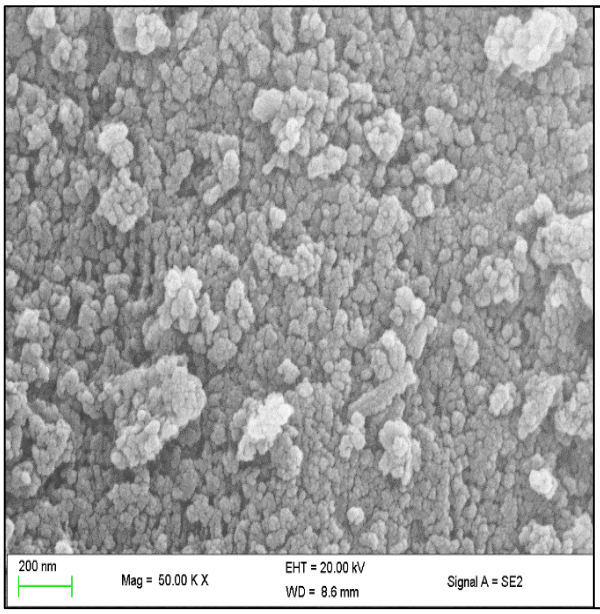

(e) FSB@400 ºC-C.V.

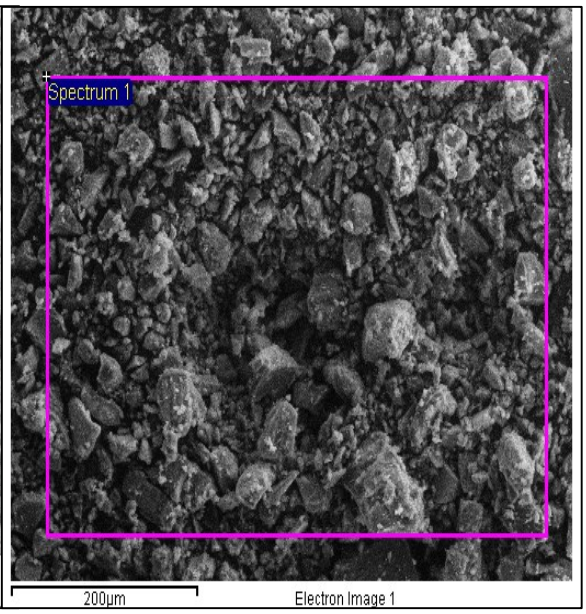

(f) FSB@400 ºC-Fe_3O_4 -I.C.

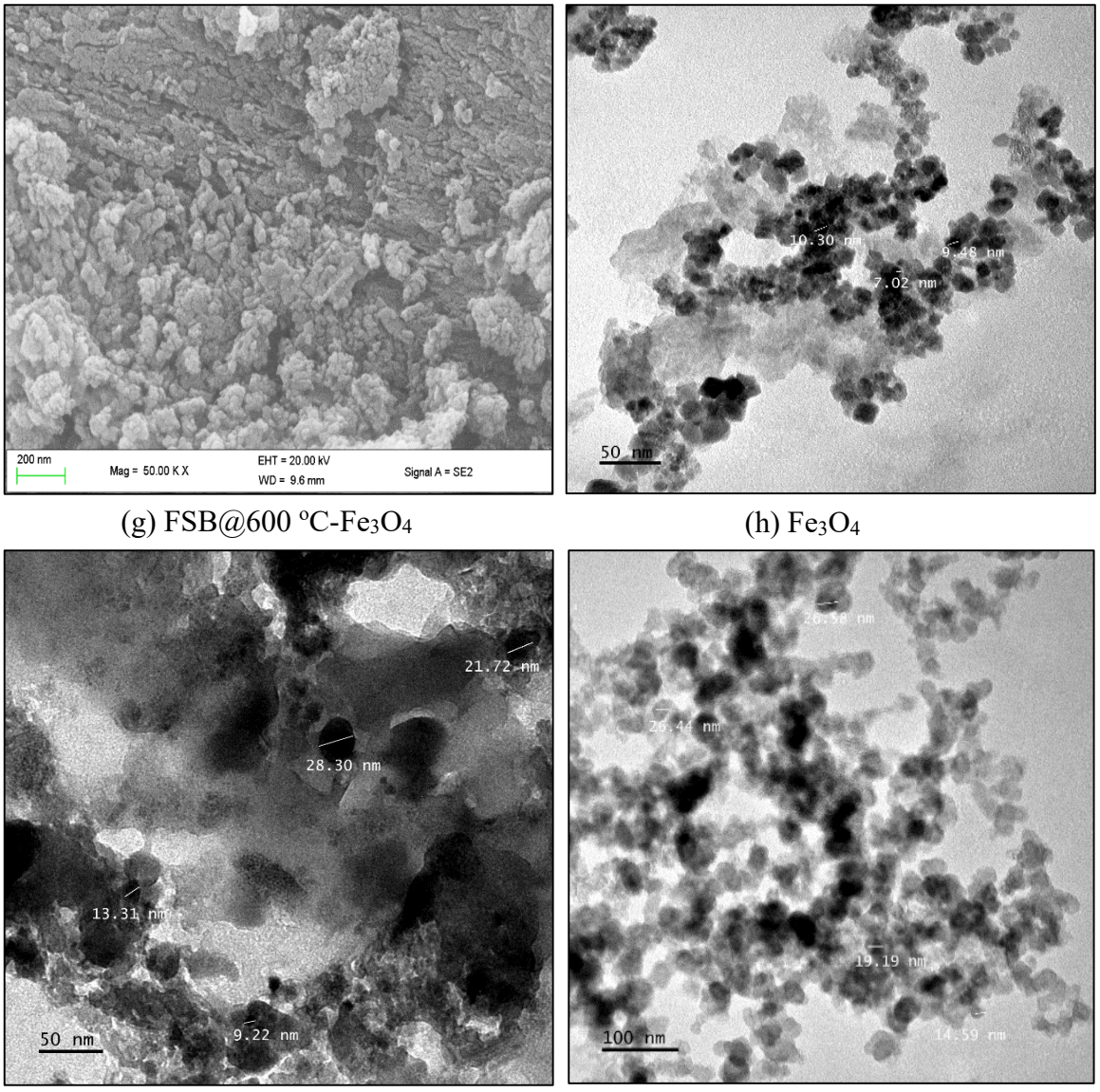

(g) FSB@600 ºC-Fe_3O_4 (h) Fe_3O_4

(i) FSB@600 ºC-Fe_3O_4 -C.V. (j) FSB@400 ºC-Fe_3O_4

Figure 4.2.6c-j: SEM micrographs of (c) Fe_3O_4, (d) FSB@400 ºC-Fe_3O_4, (e) FSB@400 ºC-C.V., (f) FSB@400 ºC-Fe_3O_4-I.C. and (g) FSB@400 ºC-Fe_3O_4; TEM micrographs of (h) Fe_3O_4, (i) FSB@600 ºC-Fe_3O_4 and (j) FSB@400 ºC-Fe_3O_4

4.2.7 Thermal properties and stability of Raw Fish Scale (RFS), Fish Scale Biochars (FSB) and magnetic composites (FSB@Fe_3O_4)

The thermal properties and stability of the adsorbents were investigated using thermo-gravimetric analysis (Figures 4.2.7a-l). The humps and the dents displayed by the derivative of heat flows characterize the exothermic and endothermic nature of the process, respectively. Heat is absorbed when there is weight loss and levels out when there is no loss in weight. For instance, loss of moisture from a material during TGA analysis is an endothermic process. The recorded initial weight loss above 100 ^oC is due to loss of moisture from the fish scales, while the subsequent sharp drop in weight between 200 ^oC and 700 ^oC (Figures 4.2.7a, b and c) could be ascribed to the elimination of organic matter and dehydration of HPO_4^{2-} yielding hydroxyl apatite (HAp) ($Ca_5(PO_4)_3(OH)$) (Zainon *et al*., 2012; Paul *et al*., 2017). In addition, there was a minor drop in weight at 780 ^oC, owing to the elimination of glycine and other organic proteins from the fish scale, beyond which there was no noticeable significant change (Zainon *et al*., 2012; Paul *et al*., 2017). For the biochars, thermal degradation profiles revealed that percent weight loss was inversely proportional to the temperature of pyrolysis (Figure 4.2.7j). Das *et al*. (2021) reported that thermogravimetric analysis mass loss (weight %) occurred on a declining manner with rise in temperature from 0 to 600 ^oC. In another study, the effect of pyrolysis temperature on physicochemical properties of *miscanthus* biochar (obtained at 350, 360, 370, 400 and 450 ^oC) revealed that thermal and biological stability are affected by pyrolysis temperature in a nonlinear manner (Mimmo *et al*., 2014).

On the contrary, Cimò *et al*. (2014) study on thermogravimetry demonstrated disparities in the thermo-oxidative stability of the aromatic domains in the different poultry manure (PM) biochars. The PM biochar produced at the highest temperature appeared less stable than those prepared at the lowest temperatures. This difference was elucidated by a protective effect of the alkyl groups, which are still present in chars formed at lower temperature. In our study, the weight reduction during thermal analysis did not exceed 10% for both FSB@600 ºC and FSB@800 ºC; however, approximately 30% decrease in weight was recorded for FSB@400 ºC. This trend was also observed by Jindo *et al*. (2014) for biochars derived from different agricultural residues.

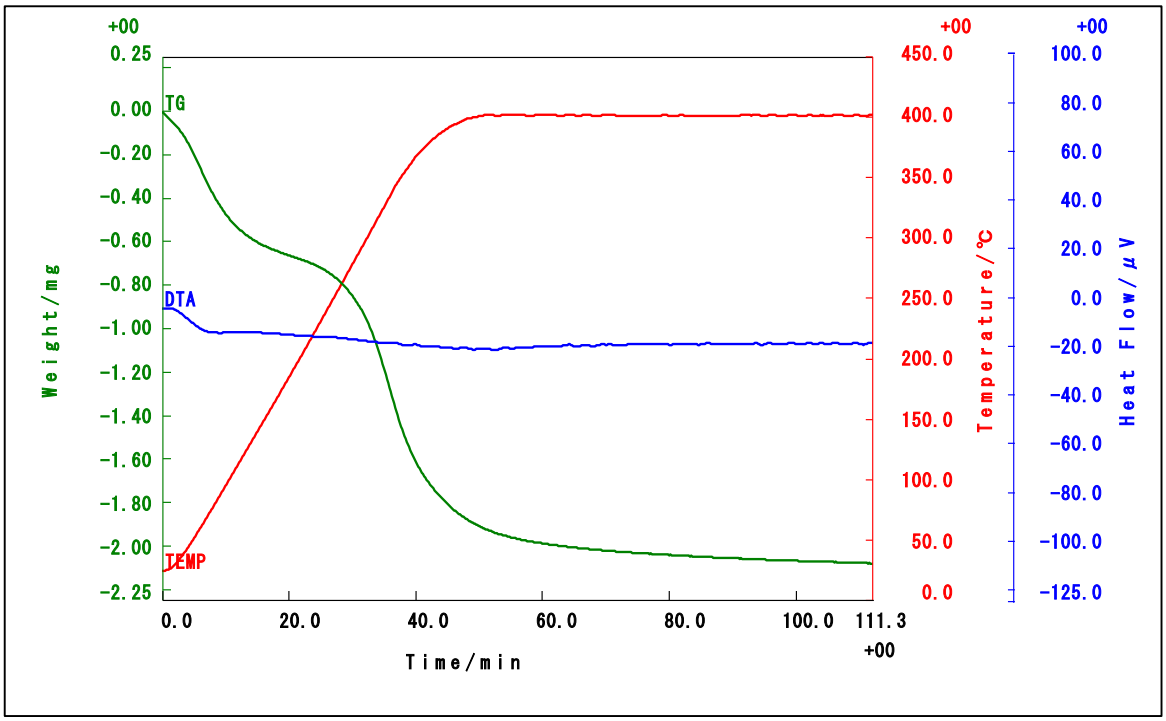

Figure 4.2.7 (a): TGA analysis of RFS at 400 ºC

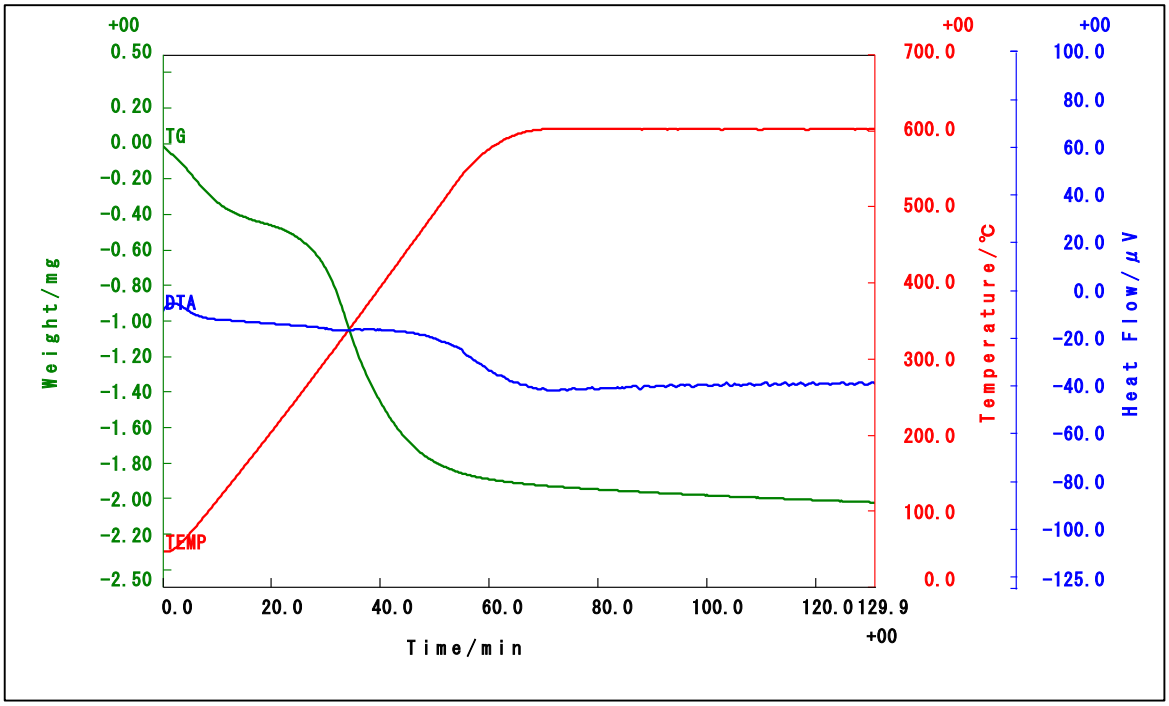

Figure 4.2.7 (b): TGA analysis of RFS at 600 ºC

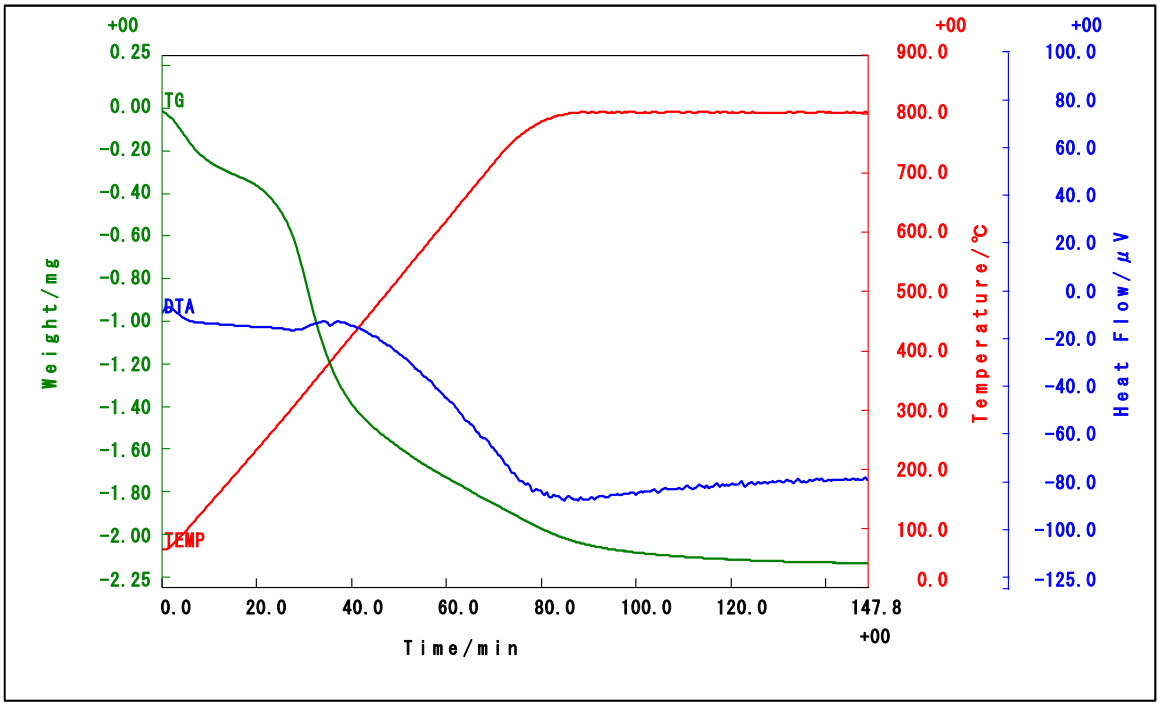

Figure 4.2.7 (c): TGA analysis of RFS at 800 ºC

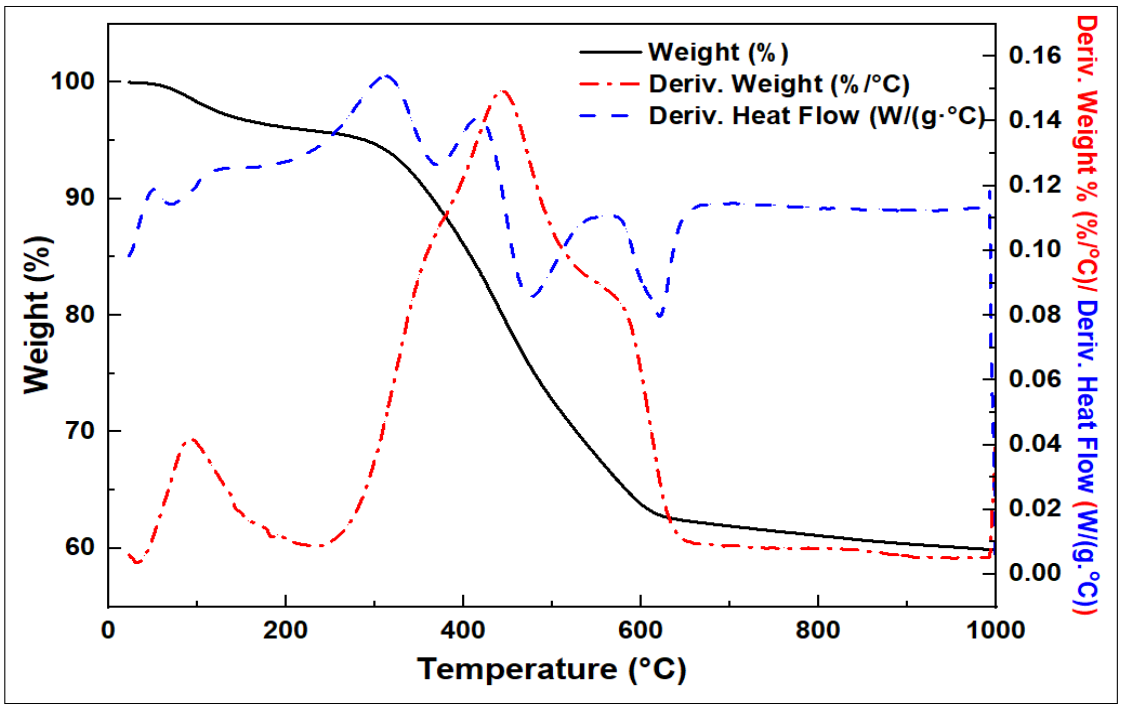

Figure 4.2.7 (d): TGA analysis of FSB@400 ºC

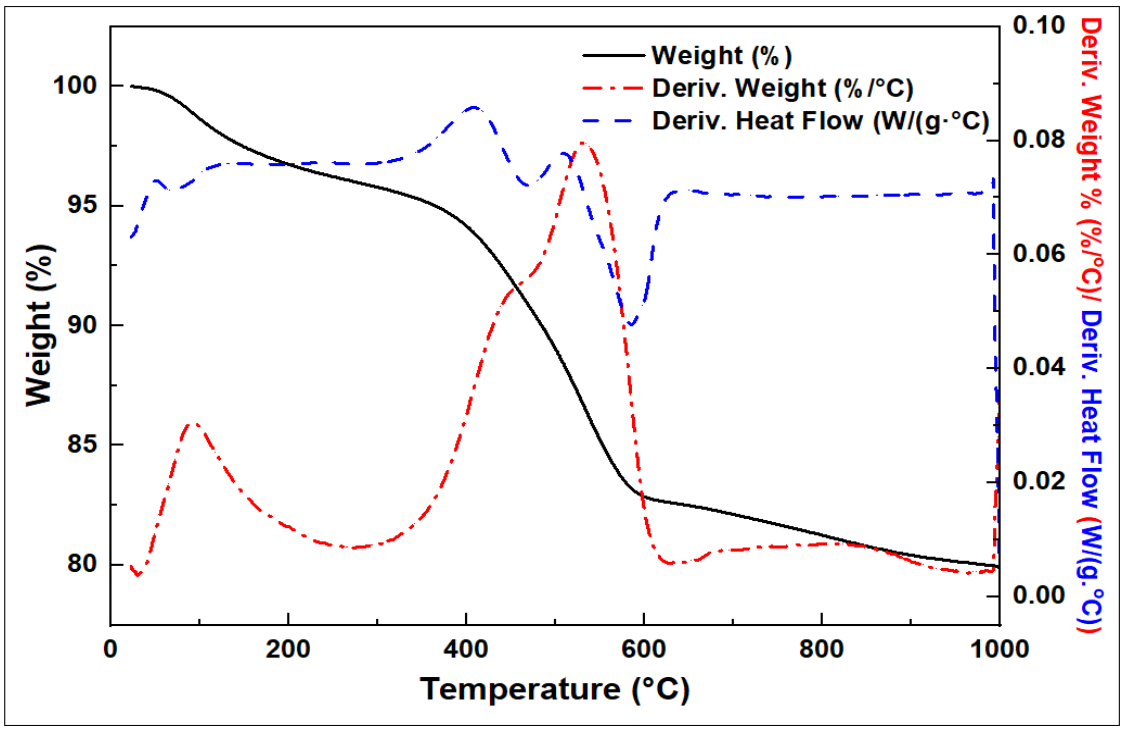

Figure 4.2.7 (e): TGA analysis of FSB@600 ºC

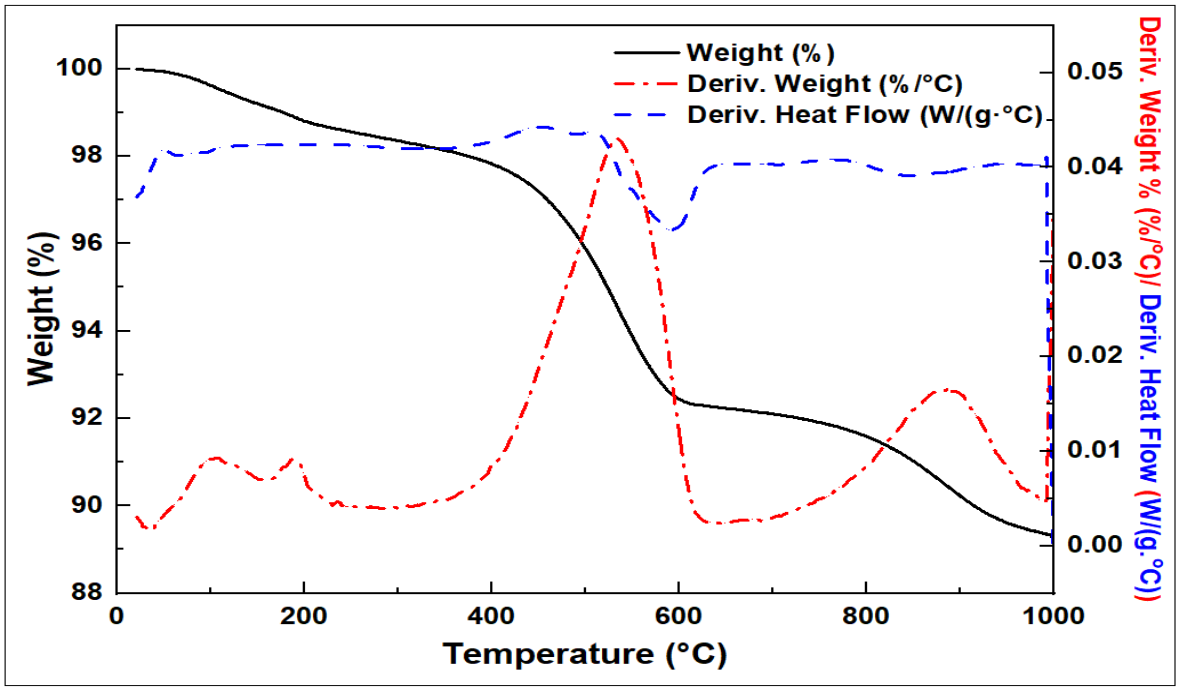

Figure 4.2.7 (f): TGA analysis of FSB@800 ºC

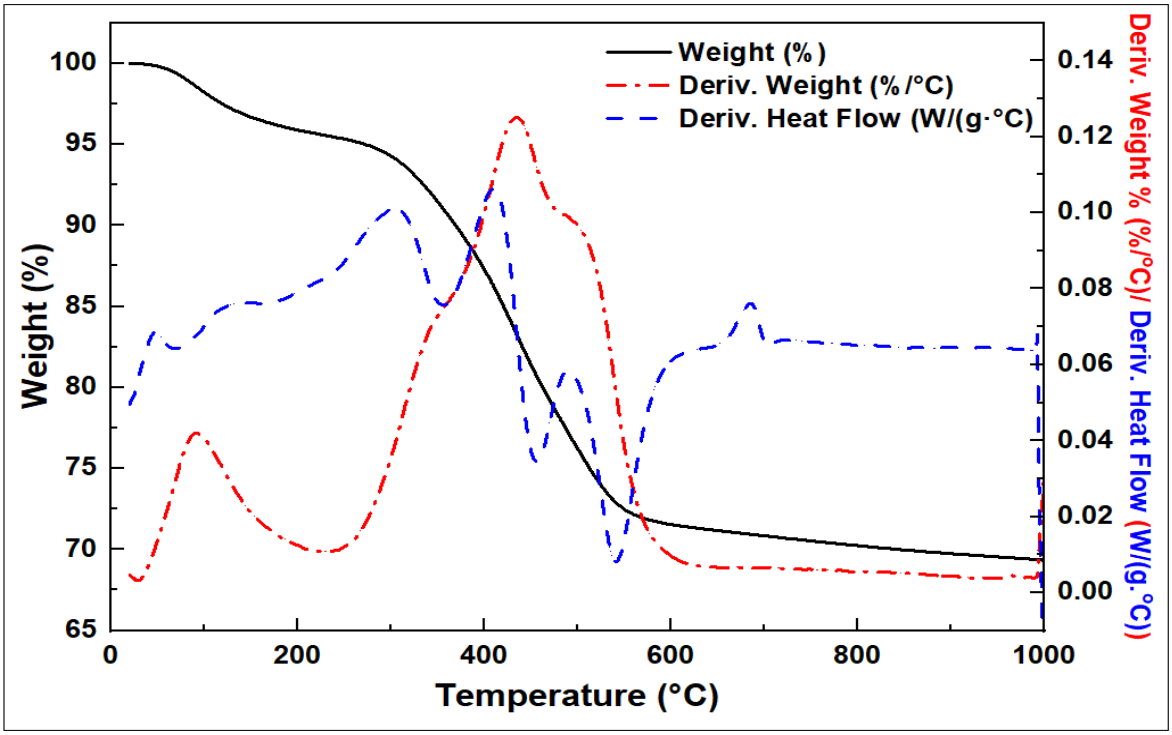

Figure 4.2.7 (g): TGA analysis of FSB@400 ºC-Fe_3O_4

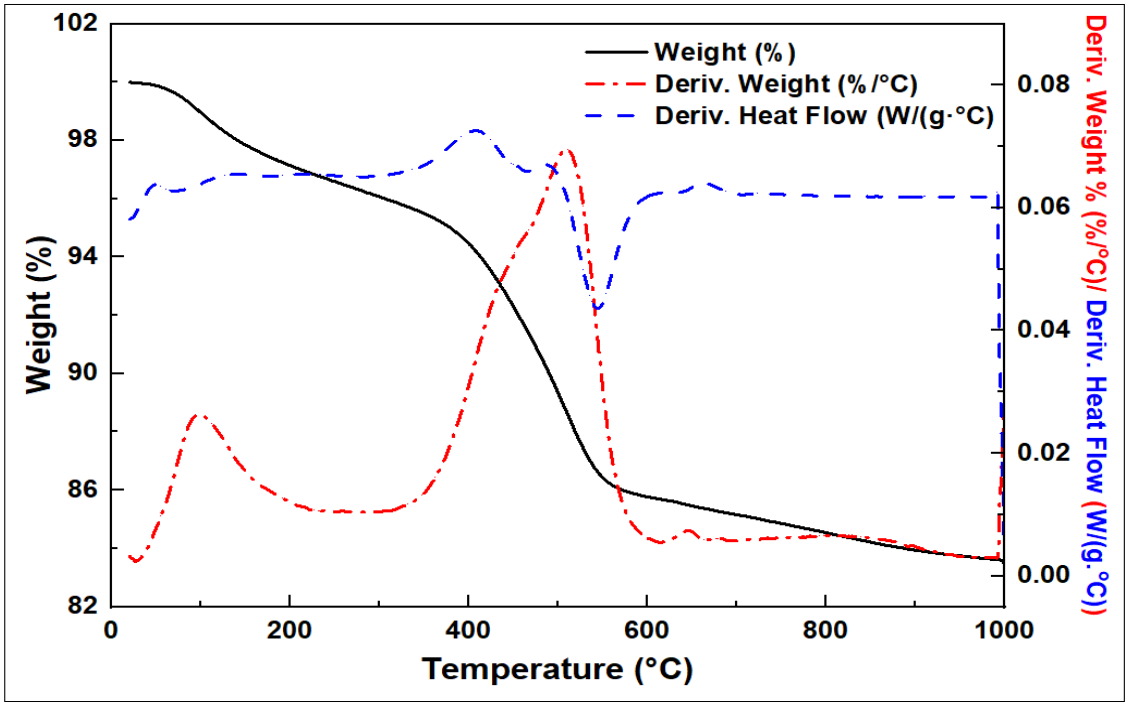

Figure 4.2.7 (h): TGA analysis of FSB@600 ºC-Fe_3O_4

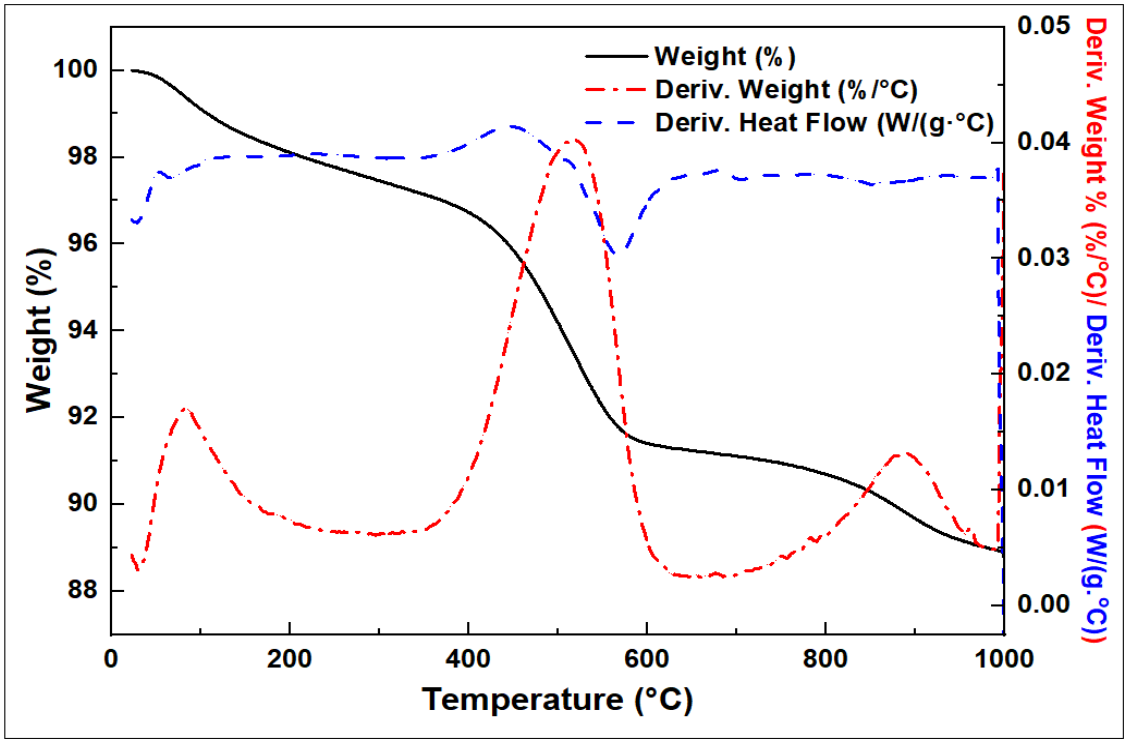

Figure 4.2.7 (i): TGA analysis of FSB@800 ºC-Fe_3O_4

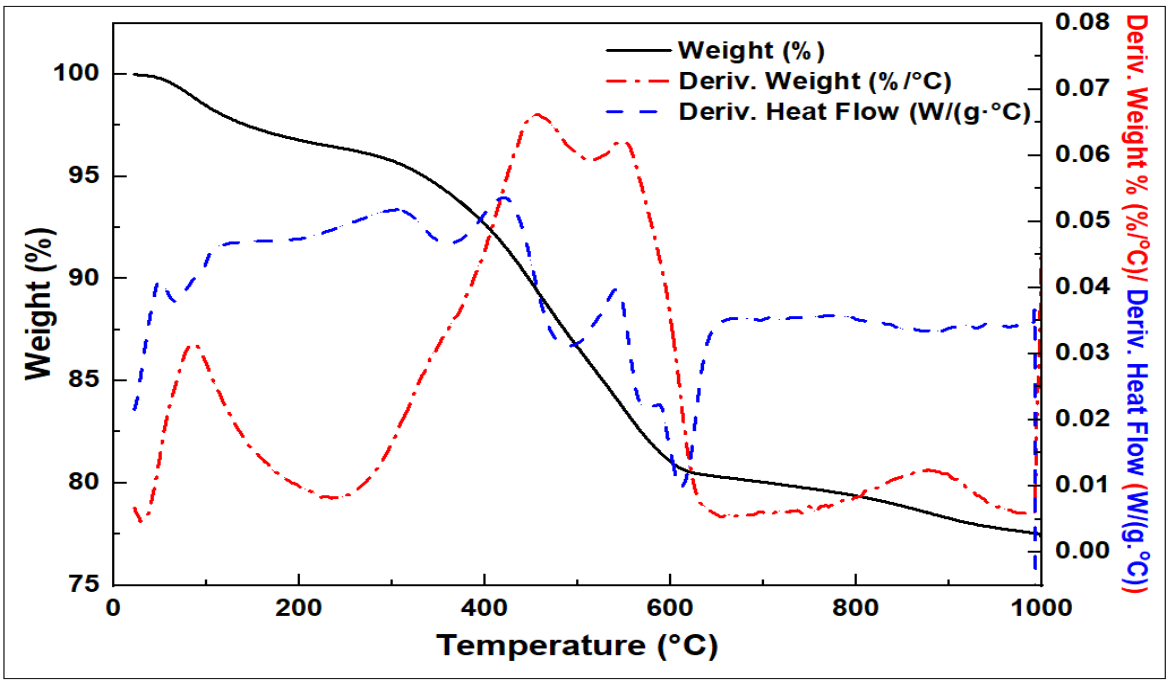

Figure 4.2.7 (j): TGA analysis of FSB@400 ºC-C.V.

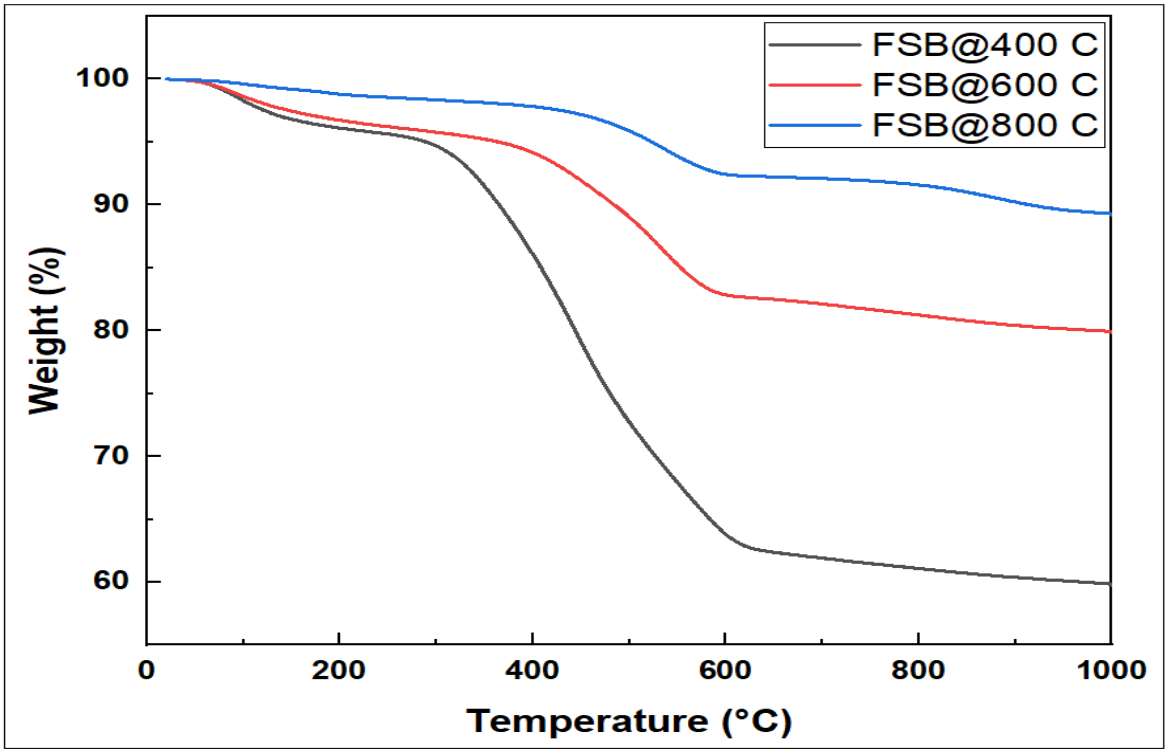

Figure 4.2.7 (k): TGA analysis of Fish scale biochars (FSB)

Thermal characteristics and stability of the magnetic composites were inspected on thermogravimetric analysis (TGA) equipment (Figure 4.2.7g-i and l). The initial weight loss at a temperature below 150 ºC refers to the evaporation of physically adsorbed water (Song *et al*., 2014; Essandoh & Garcia, 2018; Zheng *et al*., 2019). Weight loss in the temperature range 300 ºC - 600 ºC is ascribed to the decomposition of the biochar in the magnetic composite while the further decrease in weight from 700 ºC - 1000 ºC is due to reduction of Fe_3O_4 to metallic ion or a lower oxidation state oxide (Essandoh & Garcia, 2018). The temperature at which the FSB@Fe_3O_4 composites started further decomposition is lower than that of fish scale biochar (FSB), indicating that the thermal stability of FSB could have been reduced to some magnitude by Fe_3O_4-loading (Yu *et al*., 2013). Thermal degradation profiles showed that percent weight loss was indirectly related to pyrolysis temperatures at which the biochars were prepared (Jindo *et al*., 2014). Percent decline in weights of the magnetic composites during thermal analysis was approximately 30.69 %, 17.50 %, and 11.15 % for FSB@400 ºC-Fe_3O_4, FSB@600 ºC-Fe_3O_4, and FSB@800 ºC-Fe_3O_4, respectively. It is concluded that higher pyrolysis temperatures result into more thermally stable biochars.

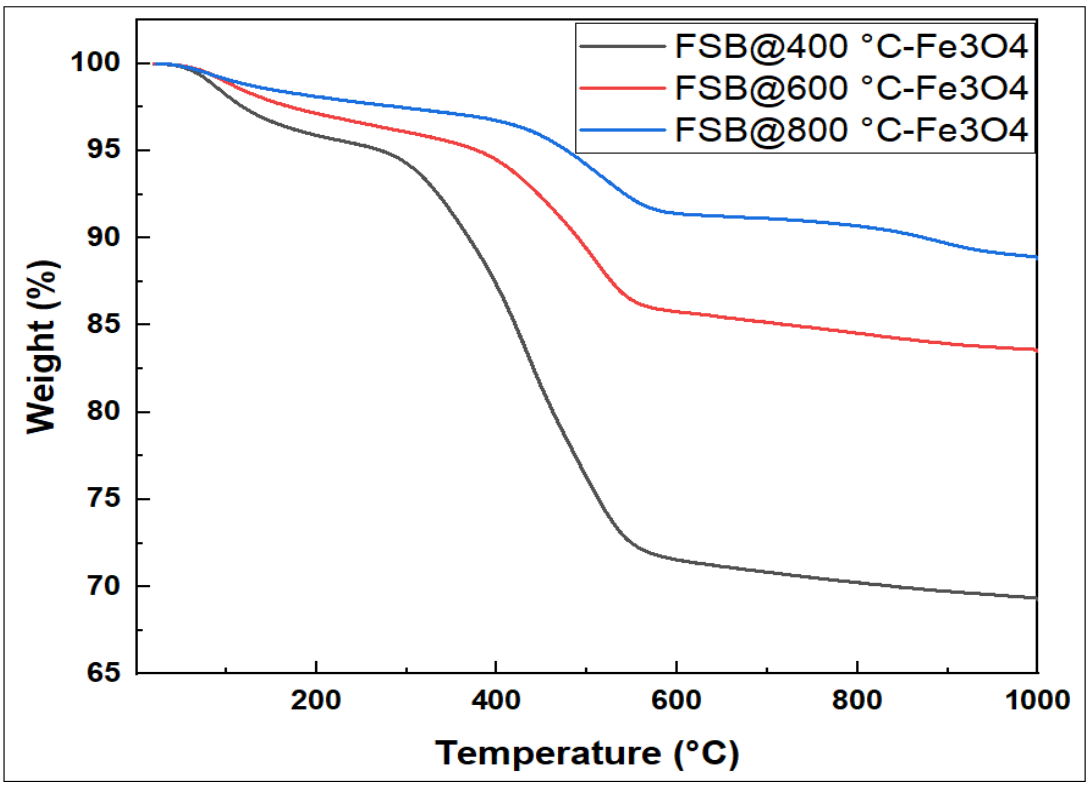

Figure 4.2.7 (l): TGA thermograms of the magnetic composites (FSB@Fe_3O_4)

4.2.8 Vibrating sample magnetometry (VSM)

Magnetic properties of the as-synthesized magnetite and composites were studied with the aid of VSM. Magnetization (M) varied with the applied magnetic field (H) measured at 300 K and saturated at higher magnetic fields (Figures 4.2.8a).

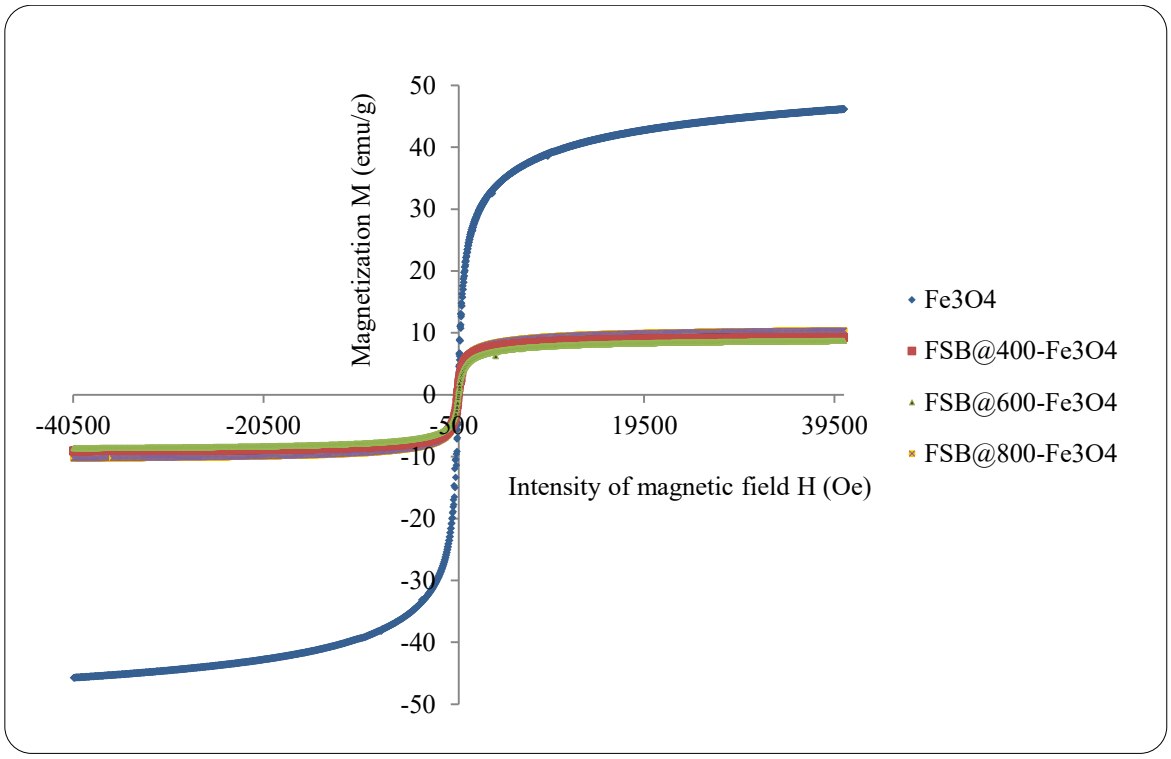

Figure 4.2.8a: Magnetic Hysteresis Loop of the magnetically supported fish scale biochars

Magnetization saturation (M_s) attained by magnetite (Fe_3O_4), FSB@400 ºC-Fe_3O_4, FSB@600 ºC-Fe_3O_4 and FSB@800 ºC-Fe_3O_4 were 46.19085, 9.21265, 8.70198 and 10.36903 emu/g, respectively. Noteworthy, magnetite and magnetic composites exhibited ferromagnetic and paramagnetic properties since they recorded coercivity of -500 Oe (oersted or ampere per meter units), zero remanence magnetization and a random flip of the magnetization under temperature effect. This observation is in agreement with

the findings made by Yu *et al*. (2013) and Wu *et al*. (2016). At higher magnetic fields, magnetic moments of the particles align themselves along the applied field direction culminating into the saturation of magnetization. The magnetization values displayed by the magnetic composites are sufficient for adsorbent recovery after adsorption; however, they are low compared to the value for bare magnetite indicating the presence of FSB which weakened the magnetic property (Xu & Wang, 2012; Zheng *et al*., 2020). Fish scale biochar impregnated with magnetic particles (FSB@Fe_3O_4) exhibited a magnetic feature in the presence of a magnetic field. The magnetic composite was tested by placing a magnet on the surface of the adsorption reaction vessel as shown in Figure 4.2.8b and c.

(b) Dye wastewater

(c) Adsorbent + Dye wastewater

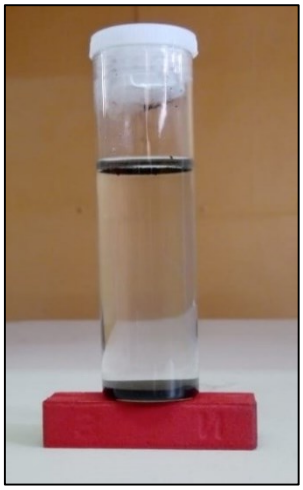

(d) Adsorbent recovery using a magnet

Figure 4.2.8b, c and d: Recovery of the spent adsorbent from aqueous system

The spent adsorbent was attracted by the magnet and when applied magnetic force was withdrawn, the magnetic composite easily dispersed by simple shaking. Therefore, the magnetic composite can be recovered from the medium with a bar magnet. These observations corroborate previous researches (Mahdavi *et al*., 2013; Zhang *et al*., 2013; Sun *et al*., 2015; Han *et al*., 2016; Yadav *et al*., 2020; Malek *et al*., 2020; Goncalves *et al*., 2020; Zhang *et al*., 2020; Zheng *et al*., 2020). It is concluded that the spent magnetic composites were successfully recovered from the system using an external magnet.

4.2.9 Optical absorbance spectrophotometry

Optical absorbance spectra of the as-synthesized magnetite and magnetic composites were assessed on UV-Vis spectrometer (Figure 4.2.9) to determine the peak absorbance of the materials.

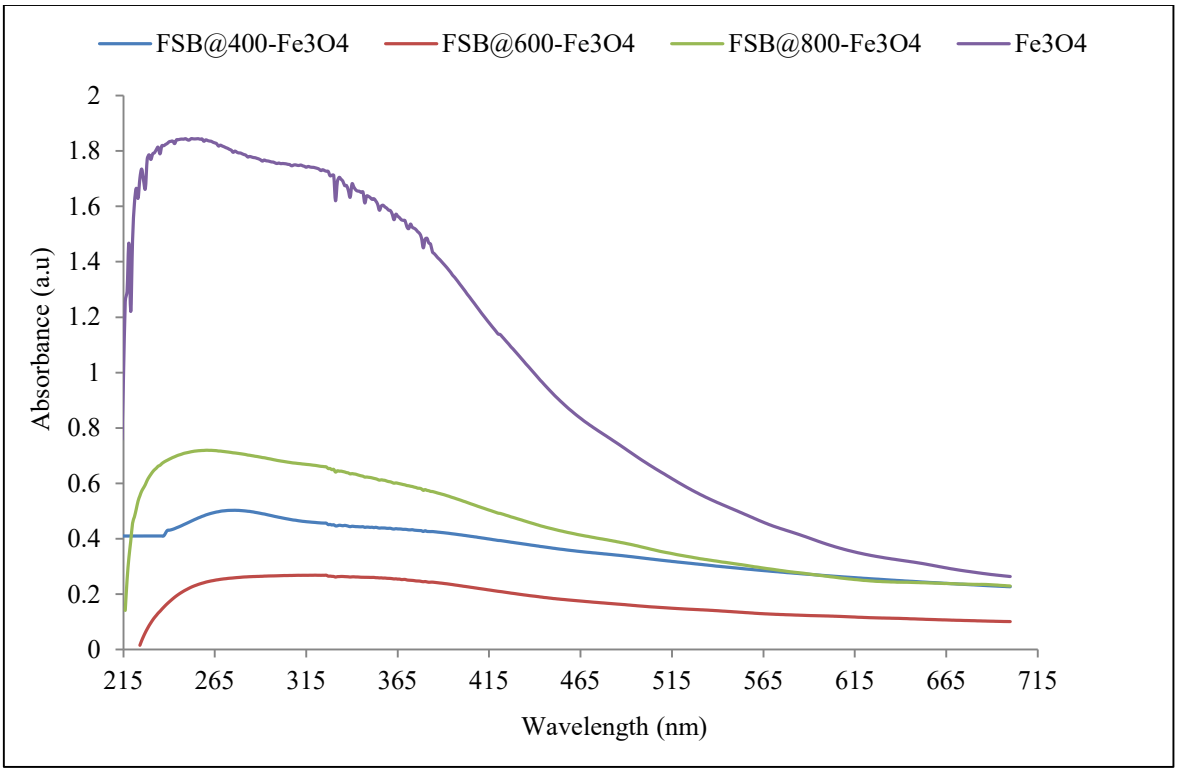

Figure 4.2.9: Optical absorbance spectra of as-synthesized magnetic composites (FSB@Fe_3O_4) at ambient temperature

Peak absorbance for magnetite, FSB@400 ^oC-Fe_3O_4, FSB@600 ^oC-Fe_3O_4 and FSB@800 ^oC-Fe_3O_4 were observed at 252 nm, 261 nm, 320 nm and 276 nm, respectively. Dada *et al*. (2014) found peaks between 280 nm - 350 nm for Fe nano-particles with maximum absorbance at 340 nm. Chaki *et al*. (2015) reported similar findings. The concept of peak absorbance of an adsorbent is explained in terms of conduction and valence bands of metals; precisely, conduction and valence bands in metals usually lie adjacent to one another, thus, electrons can move freely leading to a surface resonance absorption band attributable to a combined oscillation of electrons in tone with lightwave (Monalisa & Nayak, 2013). The absorption peak of FSB@600 ^oC-Fe_3O_4 is lower than that of the other magnetic composites signifying a higher adsorption

capacity of FSB@600 ºC-Fe_3O_4 (Figure 4.2.9). Suffices to infer that the FSB@600 ºC-Fe_3O_4 has the highest specific surface area among the as-prepared magnetic composites hence exhibited a better mesoporous filling for adsorption of crystal violet and indigo carmine dyes. Zhang *et al*. (2020) also reported this observation on composite C-600-Fe_3O_4 prepared from waste cigarette filters.

4.3 Assessment of the adsorbents for dye removal from aqueous solution

4.3.1 Assessment of the adsorbents for indigo carmine dye removal

The wavelength for the experiment was obtained as 611 nm as illustrated in Figure 4.3.1a.

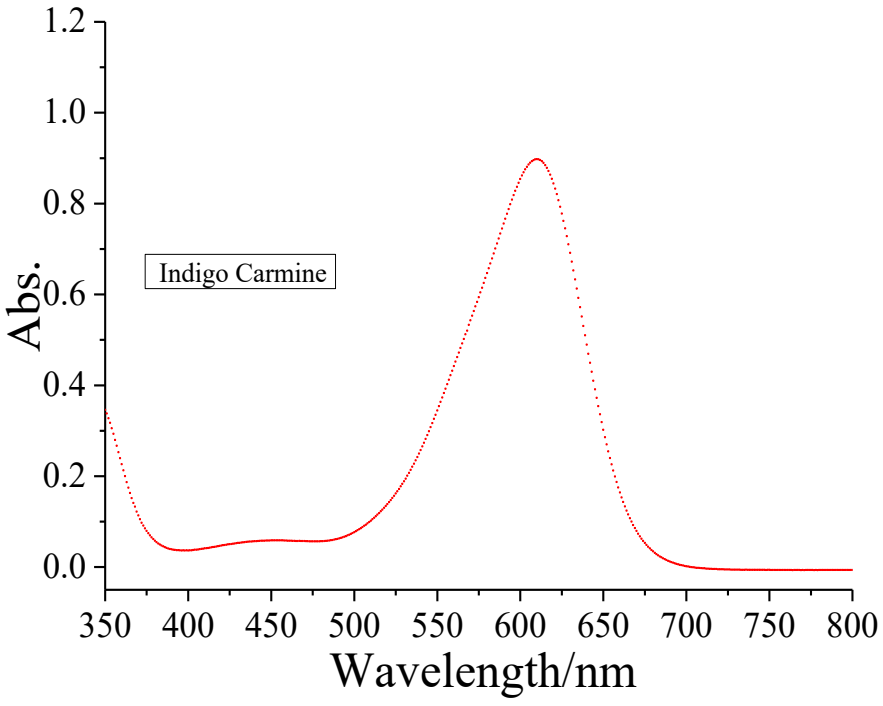

Figures 4.3.1a: Wavelength for indigo carmine dye experiments

The results of metal concentrations in the dyes (IC and CV) and distilled water used in the experiments are given in Table 4.3.1a.

Table 4.3.1a: Concentrations of metal ions (mg/L) in distilled water, indigo carmine and crystal violet dyes

Metal ion	Concentration (mg/L)		
	Distilled water	Indigo carmine	Crystal violet
Ca	0.01±0.00	1.43±0.05	1.55±0.04
Mg	0.0±0.00	0.53±0.02	0.62±0.02
Na	0.01±0.00	14.14±0.82	0.02±0.00
Fe	0.0±0.00	0.0±0.00	0.0±0.00
Zn	0.0±0.00	0.0±0.00	0.0±0.00
Pb	0.0±0.00	0.0±0.00	0.0±0.00
Cu	0.0±0.00	0.0±0.00	0.0±0.00

Distilled water registered negligible Ca and Na concentrations while the appreciably high Na concentration in IC dye is attributed to its inherent metal constituent. Al-Deffeeri (2013) analyzed the quality of distilled water produced through distillation process and reported 2.4 and 3.4 ppb for Fe and Cu, respectively. In another study, Edwin & Sekhar (2015) obtained 0.6 and 1.1 ppm for Ca and Mg, respectively, in distilled water produced from saline water solar distillation system. Considering the values reported in these studies with reference to the current study, it is worth mentioning that the quality of distilled water was sufficient in giving positive results.

The pulverized raw fish scales (RFS) and fish scale biochars were investigated as adsorbents in the removal of indigo carmine from aqueous solution at room (ambient) temperature using adsorbent dosage of 0.1 g, solution volume of 30 mL and pH of 8.5. The results for all the adsorbents are summarized in Tables 4.3.1b and c.

Table 4.3.1b: Adsorption capacities of raw fish scales, fish scale biochars (FSB) and activated charcoal (AC) for removal of indigo carmine dye

Adsorbents	**Indigo carmine (IC) concentrations**					
	5 mg/L	**15 mg/L**	**25 mg/L**	**50 mg/L**	**75 mg/L**	**100 mg/L**
Raw fish scales (RFS)	0.2085^{f}	0.6156^{f}	1.31625^{f}	2.5755^{f}	4.97925^{f}	7.242^{g}
FSB@200 ºC	0.30615^{e}	1.04175^{e}	1.70925^{e}	3.12^{e}	5.13675^{e}	8.187^{f}
FSB@300 ºC	0.38775^{d}	1.0953^{e}	1.93875^{d}	3.957^{d}	6.30225^{d}	9.579^{e}
FSB@400 ºC	0.51795^{c}	1.6434^{c}	2.78175^{c}	7.5855^{b}	10.4715^{c}	17.742^{d}
FSB@600 ºC	0.5934^{b}	1.91565^{b}	3.69225^{b}	7.6485^{b}	10.6785^{c}	17.943^{c}
FSB@800 ºC	0.5328^{c}	1.53855^{d}	2.8305^{c}	5.7525^{c}	10.4895^{c}	19.476^{b}
Activated Charcoal	1.24095^{a}	4.09545^{a}	6.61125^{a}	13.905^{a}	21.36825^{a}	28.713^{a}
CV%	6.13	3.35	2.88	2.95	0.45	0.37
LSD, p≤0.05	0.06	0.10	0.15	0.33	0.08	0.10

Adsorbent dosage 0.1 g, solution volume 30 mL, ambient temperature, contact time of 4 h; a, b, c, d, e, f, g signifies significant differences; LSD- least significant differences; CV- coefficient of variation

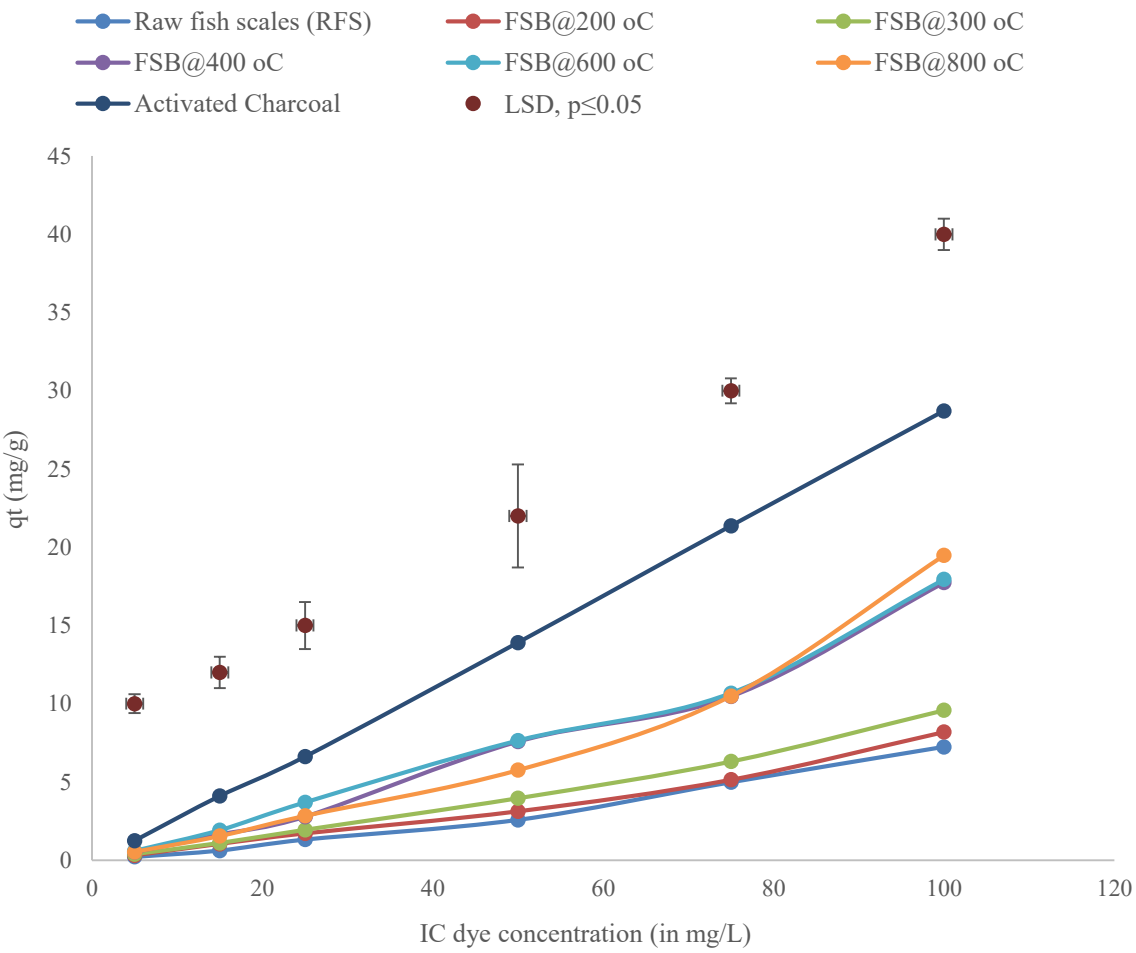

Figure 4.3.1b: Adsorption capacities of raw fish scales, fish scale biochars and activated charcoal for removal of indigo carmine dye

Table 4.3.1c: Percent removal (%R) of indigo carmine dye by raw fish scales, fish scale biochars and activated charcoal

Adsorbents	Indigo carmine (IC) concentrations					
	5 mg/L	**15 mg/L**	**25 mg/L**	**50 mg/L**	**75 mg/L**	**100 mg/L**
Raw fish scales (RFS)	13.90^{f}	13.68^{f}	17.55^{f}	17.17^{f}	22.13^{f}	24.14^{g}
FSB@200 ºC	20.41^{e}	23.15^{e}	22.79^{e}	20.80^{e}	22.83^{e}	27.29^{f}
FSB@300 ºC	25.85^{d}	24.34^{e}	25.85^{d}	26.38^{d}	28.01^{d}	31.93^{e}
FSB@400 ºC	34.53^{c}	36.52^{c}	37.09^{c}	50.57^{b}	46.54^{c}	59.14^{d}
FSB@600 ºC	39.56^{b}	42.57^{b}	49.23^{b}	50.99^{b}	47.46^{c}	59.81^{c}
FSB@800 ºC	35.52^{c}	34.19^{d}	37.74^{c}	38.35^{c}	46.62^{c}	64.92^{b}
Activated Charcoal	82.73^{a}	91.01^{a}	88.15^{a}	92.70^{a}	94.97^{a}	95.71^{a}
CV%	6.13	3.35	2.88	2.95	0.45	0.37
LSD, $p \leq 0.05$	3.87	2.22	2.00	2.20	0.34	0.33

Adsorbent dosage 0.1 g, solution volume 30 mL, ambient temperature, contact time of 4 h; a, b, c, d, e, f, g signifies significant differences; LSD- least significant differences; CV- coefficient of variation

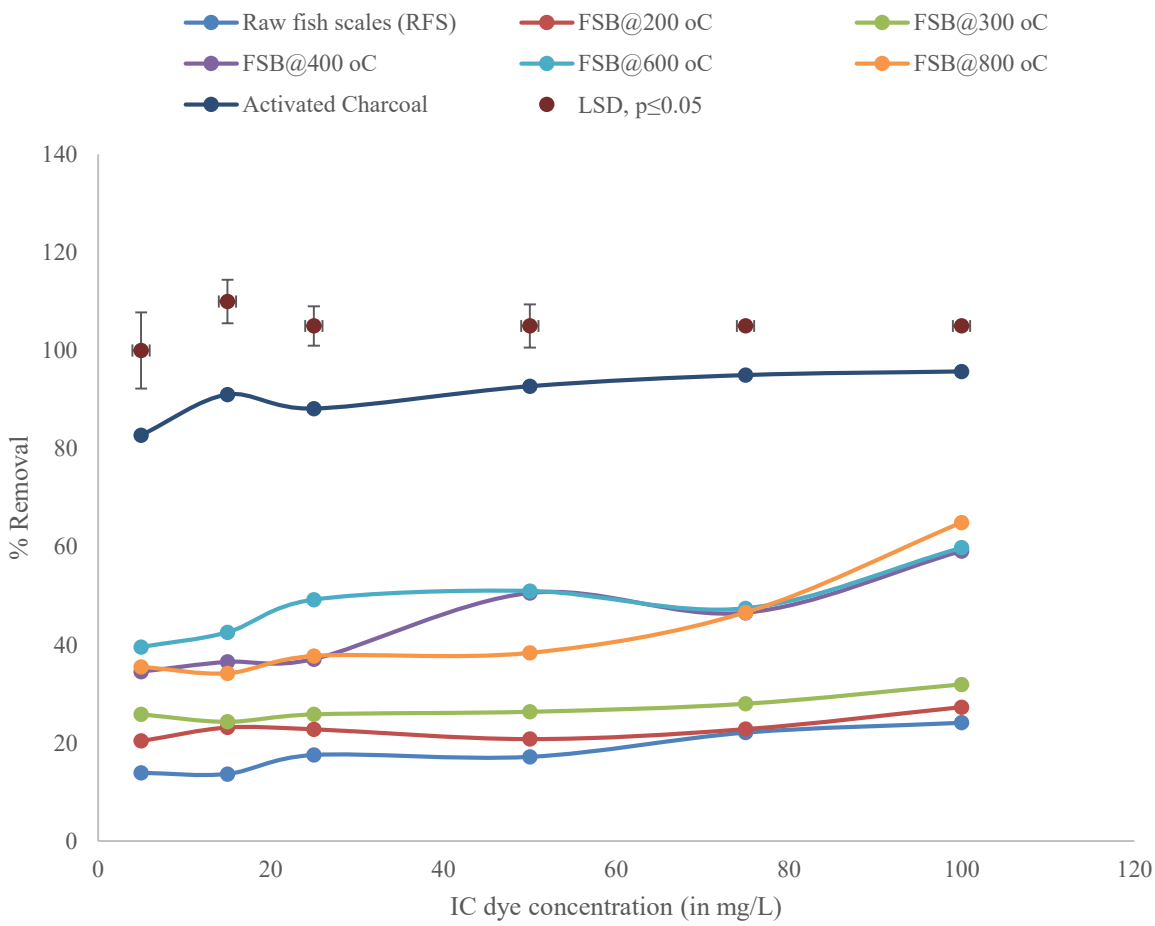

Figure 4.3.1c: Removal efficiency (%R) of raw fish scales, fish scale biochars and activated charcoal for removal of indigo carmine dye

The adsorbents recorded significantly different ($p \leq 0.05$) percent levels of dye removal efficiency (%R); with pulverized raw fish scales (RFS) and the biochar (FSB@600 ºC) performing the least (values between 13.68 at 15 mg/L and 24.14 at 100 mg/L) and the most effective (values between 39.56 at 15 mg/L and 59.81 at 100 mg/L), respectively. The trend of the mean performance of the adsorbents was RFS<FSB@400 ºC<FSB@800 ºC<FSB@600 ºC<Activated Charcoal (18.09, 22.88, 27.06, 44.07, 48.27

and 90.88%). The trend revealed that Fish scale biochars (FSB) performed better than pulverized raw fish scales (RFS) indicating that the surface characteristics of the biochar are different from those of the pulverized raw fish scale as influenced by the pyrolysis temperature. The observed consistent disparity in performance between raw fish scales and the biochars underscores the necessity of thermal conversion of the biomass, which improved the adsorbent surface characteristics such as surface area and pore volume, which are important for the adsorption process (Rafiq *et al*., 2016).

From the data in Table 4.2.6, surface area and particle size exhibited an inverse relationship. For example, as the particle size decreased from 22.92 nm in FSB@400 ºC to 17.43 nm in FSB@600 ºC (Table 4.2.6), the removal efficiency of 25 mg/L of IC dye increased from 37.09 to 49.23 % (Table 4.3.1c). The increase in removal efficiency with decreasing particle size is consistent with increase in the effective surface area (40.79 and 94.05 m^2/g) of adsorbents in the same order. Mashkoor *et al*. (2018) reported a decrease in adsorption of chromium (VI) on egg-shell and fish scale powder with the increase in particle size for all initial adsorbate concentrations. The poor adsorption witnessed on untreated fish scales was attributed to their non-porous surfaces (Kabir *et al*., 2019). It is concluded that thermal conversion of pulverized raw fish scales to biochars displayed improved surface properties. This observation justified the better performance of biochars than raw fish scales in the adsorption of anionic indigo carmine dye.

4.3.2 Assessment of the adsorbents for crystal violet dye removal

The pulverized raw fish scales (RFS) and fish scale biochars were also explored in the removal of crystal violet dye from aqueous solution using adsorbent dosage of 0.1 g, solution volume of 30 mL, pH of 8.5 at room temperature. The results for all the adsorbents are summarized in Tables 4.3.2a and b, and Figures 4.3.2a and b.

Table 4.3.2a: Adsorption capacities of raw fish scales, fish scale biochars and activated charcoal for removal of crystal violet dye

Adsorbents	Crystal violet (CV) concentrations					
	5 mg/L	**15 mg/L**	**25 mg/L**	**50 mg/L**	**75 mg/L**	**100 mg/L**
Raw fish scales (RFS)	0.27915^{g}	0.90045^{g}	1.62075^{g}	3.084^{f}	5.265^{f}	6.555^{g}
FSB@200 ^{o}C	0.39615^{f}	1.25055^{e}	2.00025^{f}	3.7125^{e}	6.03675^{e}	9.873^{f}
FSB@300 ^{o}C	0.46215^{e}	1.23795^{f}	2.16375^{e}	4.2645^{d}	7.0515^{d}	11.274^{e}
FSB@400 ^{o}C	0.54165^{c}	1.77525^{c}	3.168^{d}	7.2945^{c}	9.9585^{c}	15.09^{d}
FSB@600 ^{o}C	0.64125^{b}	1.83465^{b}	3.795^{b}	7.9815^{b}	10.0125^{c}	17.01^{b}
FSB@800 ^{o}C	0.5277^{d}	1.7433^{d}	3.29025^{c}	7.2615^{c}	10.2375^{b}	15.777^{c}
Activated Charcoal	1.29225^{a}	4.16295^{a}	6.88875^{a}	13.5885^{a}	20.6258^{a}	28.035^{a}
CV%	0.52	0.38	0.47	0.51	0.51	0.36
LSD, $p \leq 0.05$	0.01	0.01	0.03	0.05	0.09	0.11

Adsorbent dosage 0.1 g, solution volume 30 mL, ambient temperature, contact time of 4 h; a, b, c, d, e, f, g signifies significant differences; LSD- least significant differences; CV- coefficient of variation

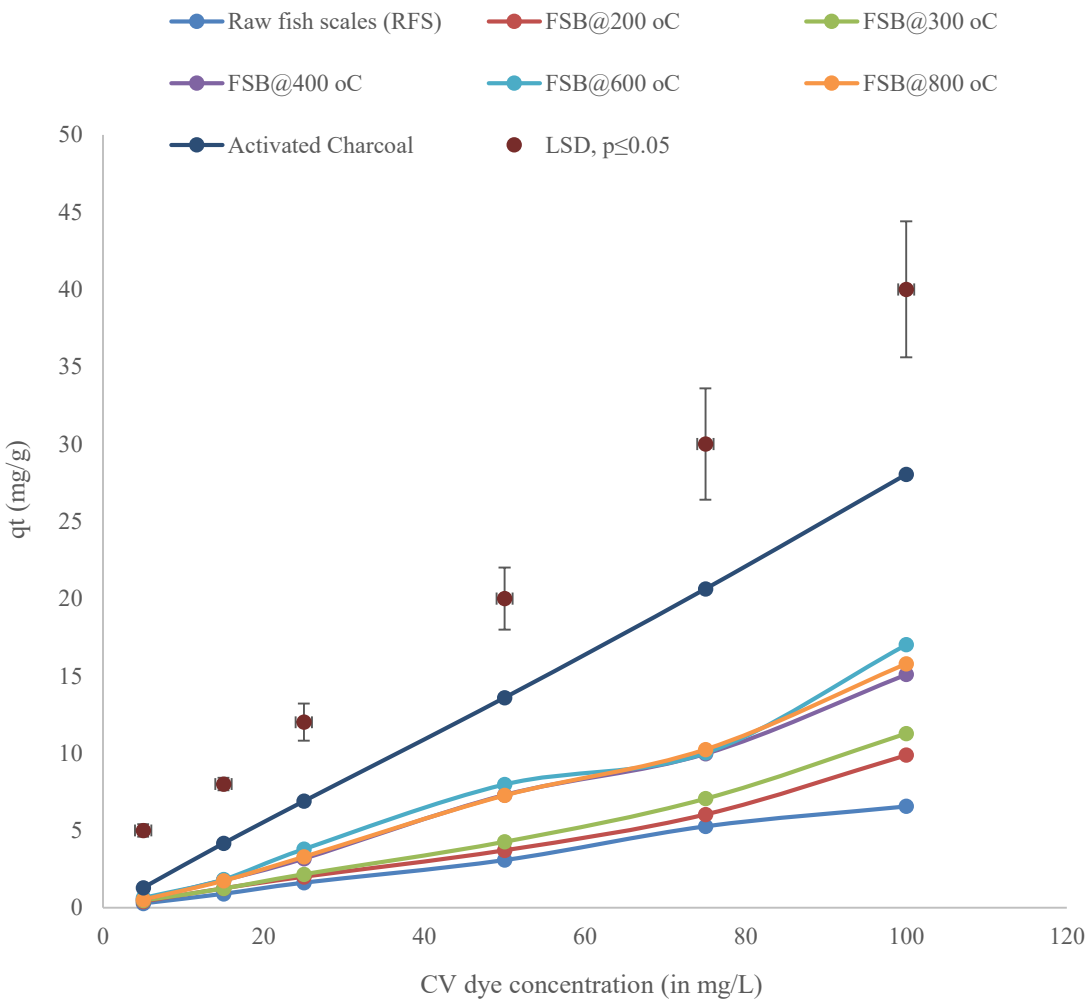

Figure 4.3.2a: Adsorption capacities of raw fish scales, fish scale biochars and activated charcoal for removal of crystal violet dye

Table 4.3.2b: Percent removal (%R) of crystal violet dye by raw fish scales, fish scale biochars and activated charcoal

Adsorbent	Crystal violet (CV) concentration					
	5 mg/L	**15 mg/L**	**25 mg/L**	**50 mg/L**	**75 mg/L**	**100 mg/L**
Raw Fish Scales	18.61^{g}	20.01^{g}	21.61^{g}	20.56^{f}	23.40^{f}	21.85^{g}
FSB@200 ^{o}C	26.41^{f}	27.79^{e}	26.67^{f}	24.75^{e}	26.83^{e}	32.91^{f}
FSB@300 ^{o}C	30.81^{e}	27.51^{f}	28.85^{e}	28.43^{d}	31.34^{d}	37.58^{e}
FSB@400 ^{o}C	36.11^{c}	39.45^{c}	42.24^{d}	48.63^{c}	44.26^{c}	50.30^{d}
FSB@600 ^{o}C	42.75^{b}	40.77^{b}	50.60^{b}	53.21^{b}	44.50^{c}	56.70^{b}
FSB@800 ^{o}C	35.18^{d}	38.74^{d}	43.87^{c}	48.41^{c}	45.50^{b}	52.59^{c}
Activated Charcoal	86.15^{a}	92.51^{a}	91.85^{a}	90.59^{a}	91.67^{a}	93.45^{a}
CV%	0.52	0.38	0.47	0.51	0.51	0.36
LSD, P≤0.05	0.36	0.28	0.36	0.32	0.39	0.31

Adsorbent dosage 0.1 g, solution volume 30 mL, ambient temperature, contact time of 4 h; a, b, c, d, e, f, g signifies significant differences; LSD- least significant differences; CV- coefficient of variation

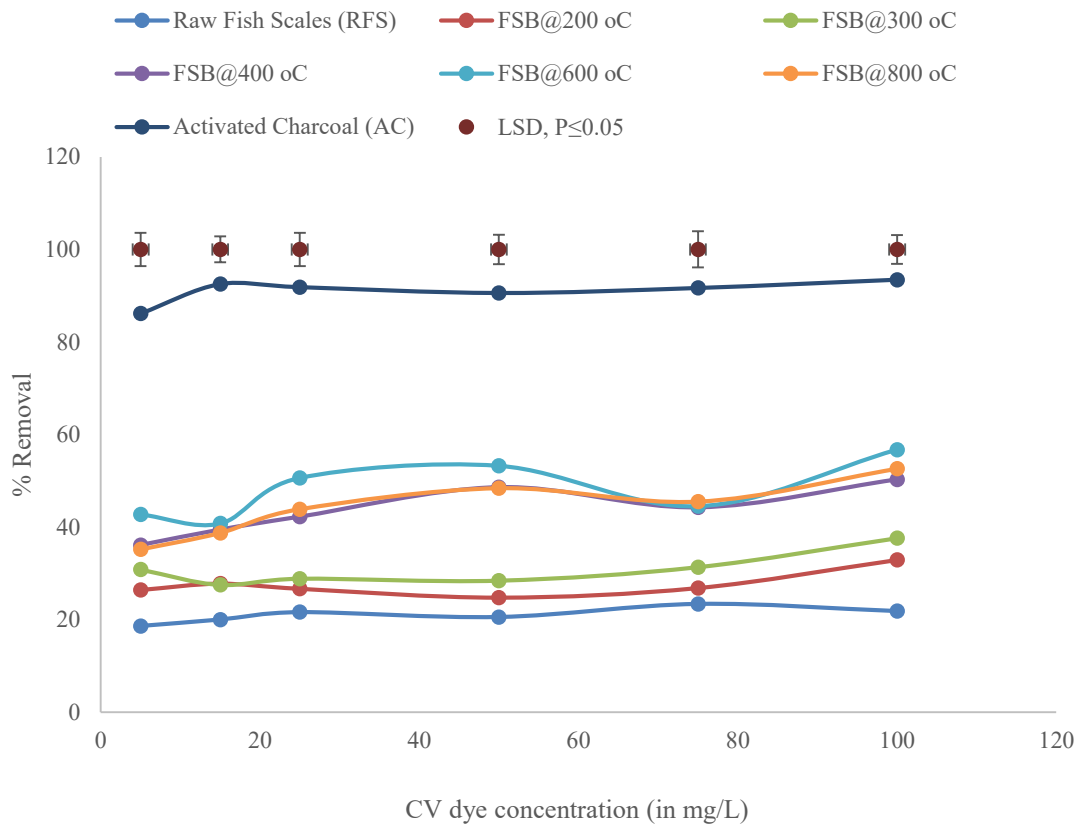

Figure 4.3.2b: Percent removal (%R) of raw fish scales, fish scale biochars and activated charcoal for removal of crystal violet dye

The adsorbents recorded significantly different efficiencies for removal of crystal violet dye in each concentration. Raw Fish Scales performed the least, while FSB@600 ºC afforded the highest removal efficiency of all the biochars and the raw fish scale studied. Notably, the removal efficiency increased with biochar preparation temperature until FSB@600 ºC, thereafter dropped at FSB@800 ºC, implying that charring improves the surface characteristics of a raw biomass. Considering the six initial concentrations of crystal violet dye, the highest concentration of dye removed was achieved with 100 mg/L. The standard commercial adsorbent, activated charcoal, achieved the highest

levels of removal efficiencies in all the initial dye concentrations assessed. The observations made herein are justified by the inverse relationship between particle size and surface area of the adsorbents, which, consequently, increases the removal efficiency. It is concluded that thermal conversion of pulverized raw fish scales to biochars displayed improved surface properties. This observation justified the better performance of biochars than raw fish scales in the adsorption of cationic crystal violet dye.

4.3.3 Effect of contact time, initial dye concentration, adsorbent dosage, solution pH and temperature on adsorption of indigo carmine

Batch adsorption experiments were carried out to determine the influence of contact time, initial dye concentration, adsorbent dosage, initial solution pH and temperature on the adsorption of indigo carmine dye. The effect of contact time and initial dye concentration on adsorption were studied using 25 mg/L, 50 mg/L, 75 mg/L and 100 mg/L of dye solutions at 298 K with FSB@600 ^{o}C dosage of 0.20 g/30 mL, 200 rpm from 0 to 180 minutes. Figure 4.3.3a shows plots of percentage dye removal over a period at different initial dye concentrations.

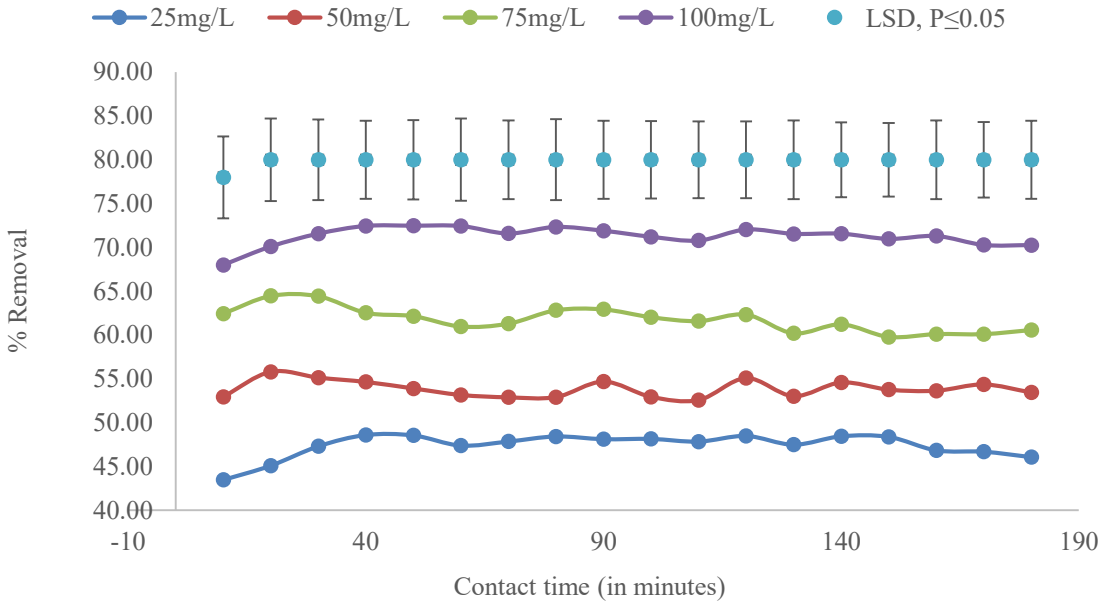

Figures 4.3.3a: Effects of contact time and initial IC dye concentration (FSB@600 ºC, 75 mg/L, 0.20 g/30 mL)

From Figure 4.4.1a, the adsorption process was very rapid during the initial stage, followed by a gradual phase as the system attained equilibrium. The equilibrium time varied with the initial dye concentration. For instance, dye dosages of 25 mg/L, 50 mg/L, 75 mg/L and 100 mg/L attained maximum adsorptions after 40 min, 10 min, 40 min and 50 min, respectively. In addition, more dye molecules were adsorbed at higher concentrations than at lower ones. For example, adsorption percentages of 48.59%, 52.95%, 62.54% and 72.47% were recorded for dye dosages of 25 mg/L, 50 mg/L, 75 mg/L and 100 mg/L, respectively. The fast initial adsorption rate is attributed to a large number of vacant adsorption sites available for occupancy by the adsorbate molecules (Slimani *et al*., 2014; Adeyi *et al*., 2019). The slow adsorption towards equilibrium point may be assigned to repulsive forces between the dye molecules in the bulk solution and

the adsorbed molecules (Shikuku *et al*., 2018) and reduced number of available binding sites. Notably, more dye was adsorbed at higher initial dye concentrations, compared to lower initial concentrations. At higher initial dye concentrations, there is significant driving force due to increased mass gradient that enables adsorption of dye molecules onto the adsorbents (El Haddad *et al*., 2013b; Slimani *et al*., 2014). These results are in agreement with previous findings of other researchers (Wagh & Shrivastava, 2015; Rangabhashiyam *et al*., 2018; Adeyi *et al*., 2019).

The effect of adsorbent dosage on the dye removal efficiency was studied by changing the dosage from 0.05 g/30 mL to 0.25 g/30 mL as given in Figure 4.3.3b. The results indicate that the removal efficiency (%R) varied directly and significantly with the amount of adsorbent used. As an illustration for FSB@600 ºC, the removal efficiency (%R) significantly ($p \leq 0.05$) increased from 52.70% at an adsorbent dose of 0.05 g to 74.40% at 0.20 g. This was expected due to increase in the number of active sites (Ngeno *et al*., 2016; Nnaemeka *et al*., 2016; Bordoloi *et al*., 2018; Temesgen *et al*., 2018; Adeyi *et al*., 2019; Badeenezhad *et al*., 2019; Fegousse *et al*., 2019; Tsolele *et al*., 2019).

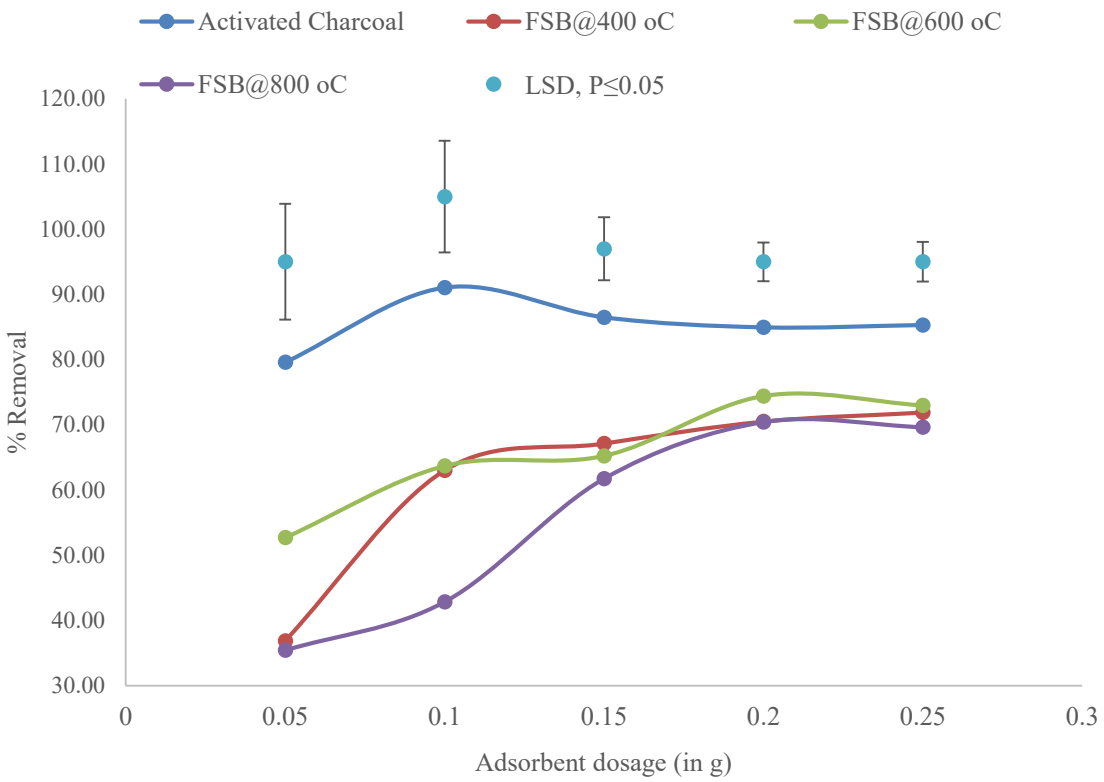

Figures 4.3.3b: Effects of adsorbent dosage on IC dye removal efficiency (%R)

Optimum adsorbent dosages were recorded as 0.10 g, 0.25 g, 0.20 g and 0.20 g per 30 mL, respectively, for activated charcoal, FSB@400 ºC, FSB@600 ºC, and FSB@800 ºC, respectively. Gholami *et al*. (2018) observed an optimum dosage of fish scale composites at 0.30 g in the removal of methyl blue dye. Decrease in dye removal beyond the optimum dosages could be due to adsorbent aggregation leading to decreased total surface area (Bamukyaye & Wanasolo, 2017; Gholami *et al*., 2018; Neves *et al*., 2018; Ayanda *et al*., 2019).

The influence of pH on dye adsorption was examined within the pH range of 2-10. In the current study, percent removal (%R) of indigo carmine dye from aqueous solution was

observed to decrease gradually with increase in solution pH for all the adsorbents (Figure 4.4.1c). Adsorbent FSB@600 ºC recorded a decrease in removal efficiency from 56.60% at pH 2 to 49.55% at pH 10. This can be accounted from the fact that at pH below 6, the adsorbents acquire net positive surface charges as predicted by point of zero charge pH (pH_{pzc}) (Table 4.2.1 and Figure 4.3.3d). Previous studies have established that adsorbent performance at various pH levels is controlled by surface charges, active sites and adsorption capacity of the adsorbent (Santhi *et al*., 2016).

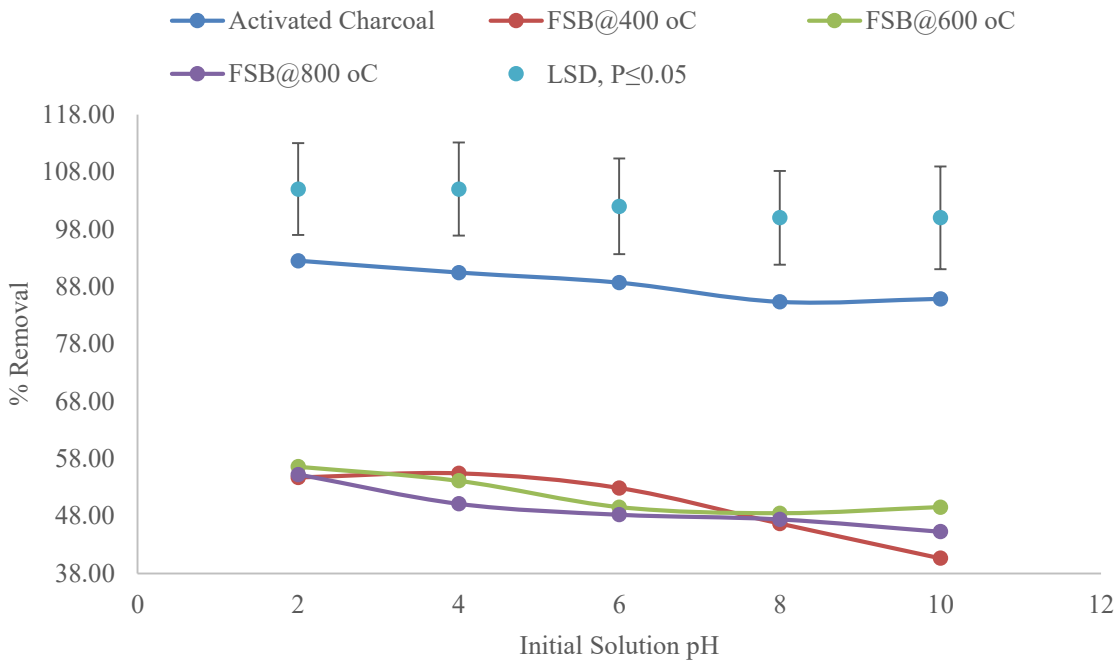

Figures 4.3.3c: Effects of initial solution pH on IC dye removal efficiency (%R)

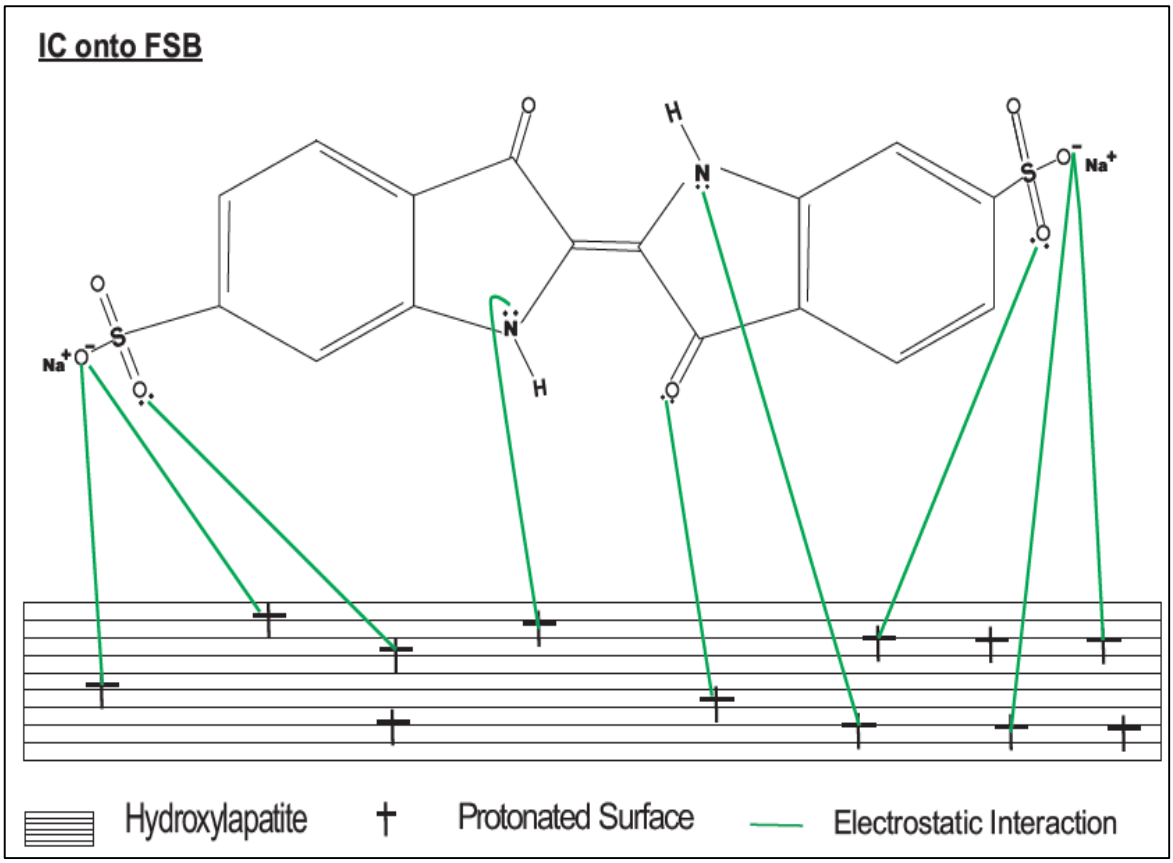

Figure 4.3.3d: Electrostatic interaction between IC dye molecules and FSB@400 ºC

Attractive coulombic forces occurred between the adsorbent and anionic indigo carmine dye molecules (Figure 4.4.1d), hence high adsorption capacity (Nnaemeka *et al*., 2016; Ayanda *et al*., 2019; Badeenezhad *et al*., 2019). On the other hand, at higher pH levels, the hydroxyl (OH^-) ions in the aqueous solution compete effectively with the dye anions causing a decrease in the percent removal (Slimani *et al*., 2014). In a previous study by Chakraborty *et al*. (2016), a higher pH of 8 resulted in lower removal efficiencies of methyl orange (MO) dye molecules. Noteworthy to state that the adsorption occurred quite uniformly within a wide range of pH demonstrating the potential of these

adsorbents for application in real environmental remediation for a variety of pollutants in industrial effluents (Bordoloi *et al*., 2018). The optimum pH 2 for dye removal in the present work is in agreement with the finding reported by Almoisheer *et al*. (2019).

In order to investigate the effect of temperature on the adsorption of indigo carmine dye, the adsorption experiments were carried out at 298 K, 303 K, 313 K and 323 K at different initial dye concentrations and at an initial solution pH 2, adsorbent dosage of 0.20 g/30 mL solution (Figure 4.3.3e). From the figure, it was evident that the amount of dye removed increased with increase in temperature for all the adsorbents, with an exception for activated charcoal at 323 K. For example, dye removal efficiency of FSB@600 ºC significantly ($p \leq 0.05$) increased from 45.69% at 298 K to 72.04% at 323 K. These findings suggest an endothermic nature of these adsorption processes (Kulkarni *et al*., 2017). Ho & McKay (2003) also reported that higher temperatures enhanced adsorption due to the increased kinetic energy of the adsorbate and adsorbent surface activity.

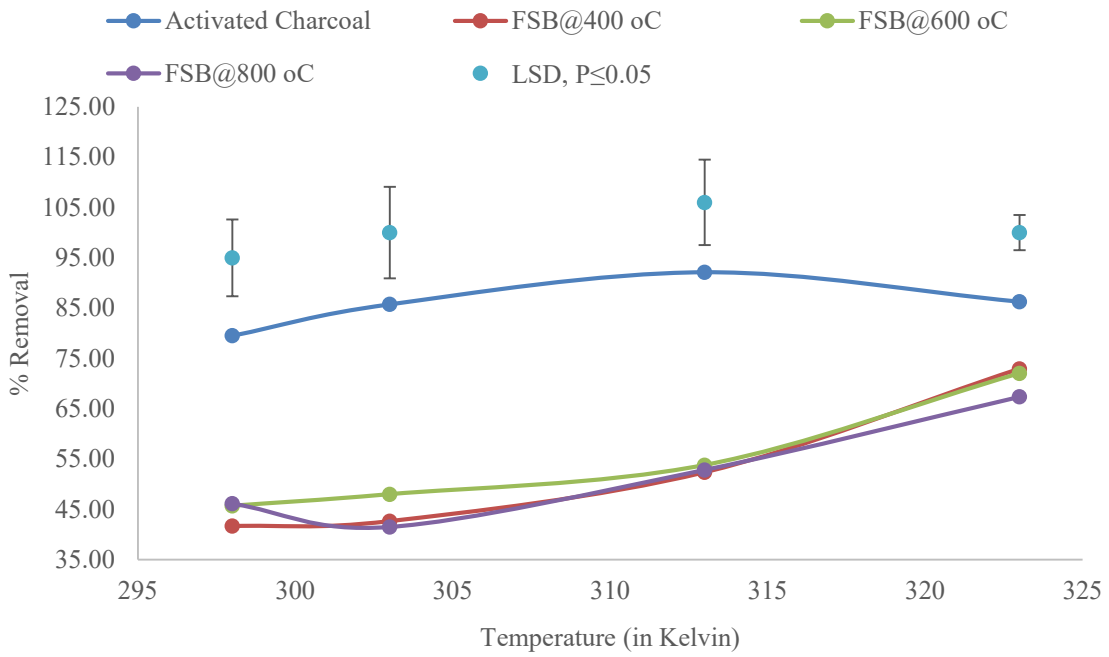

Figure 4.3.3e: Effects of temperature on adsorption of IC dye molecules

Potential of the magnetic composites for the uptake of indigo carmine from the water was examined as a function of contact time, initial dye concentration, adsorbent dose, initial solution pH and temperature. Influence of contact time and initial dye concentration on adsorption of indigo carmine dye onto magnetic composites were studied at 298 K using 25, 50, 75 and 100 mg/L of indigo carmine dye solutions with FSB@600 ºC-Fe_3O_4 dosage of 0.20 g/30 mL, at 200 rpm for 180 minutes. The results for the removal efficiency of indigo carmine dye over a predetermined period at selected initial dye concentrations are shown in Table 4.3.3a and Figure 4.3.3f.

Table 4.3.3a: Effect of contact time on adsorption of indigo carmine dye (mg/g) onto FSB@600 ºC-Fe_3O_4

	Indigo carmine concentrations (in mg/L)			
Time (in min)	**25**	**50**	**75**	**100**
20	1.39^{e}	3.43^{g}	4.46^{f}	6.47^{e}
40	1.51^{d}	3.73^{f}	5.03^{e}	6.94^{d}
60	1.56^{c}	3.97^{e}	$5.06^{c,d,e}$	7.26^{c}
80	1.57^{b}	$3.98^{c,d,e}$	$5.08^{b,c}$	7.64^{b}
100	1.58^{b}	$3.98^{c,d,e}$	5.13^{a}	$7.66^{a,b}$
120	1.58^{b}	$3.99^{b,c,d}$	5.09^{b}	7.65^{a}
140	1.59^{a}	4.02^{a}	$5.06^{b,c,d}$	7.65^{a}
160	1.58^{b}	4.00^{b}	$5.07^{b,c,d}$	7.65^{a}
180	1.58^{b}	$3.99^{b,c,d}$	$5.05^{d,e}$	7.65^{a}
CV%	0.49	0.23	0.35	0.07
LSD, P≤0.05	0.01	0.02	0.03	0.01

$^{a, b, c, d, e, f}$ Data with different letters are significantly different; CV-coefficient of variation; LSD-least significant difference

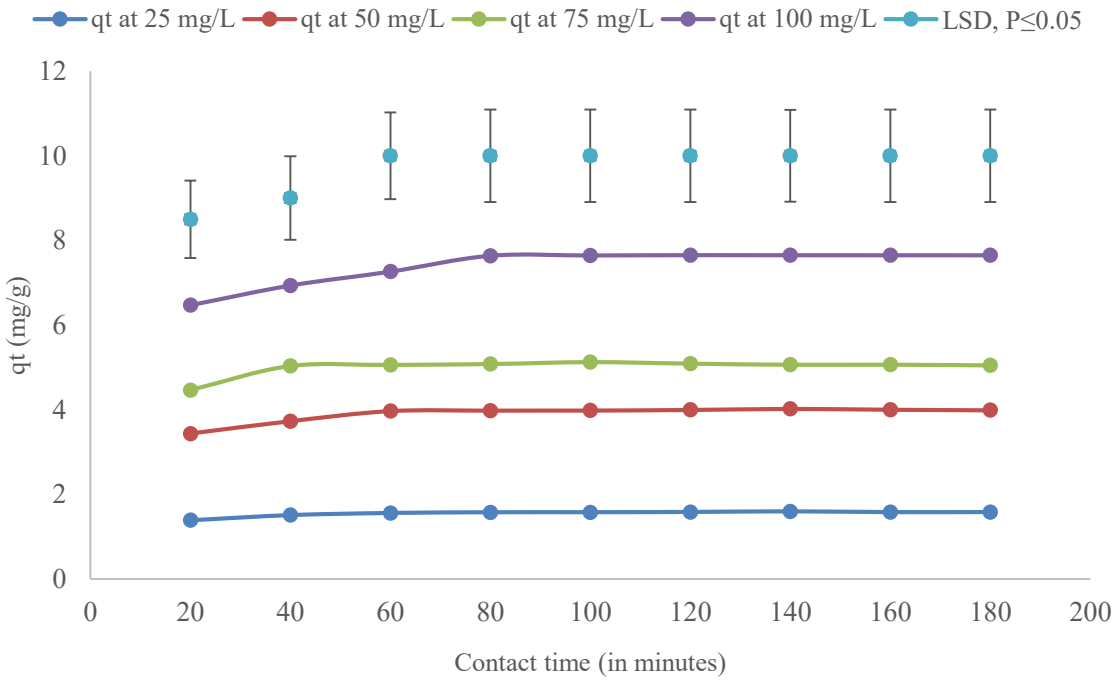

Figure 4.3.3f: Effects of contact time and initial concentration on IC dye removal by magnetic composite

Adsorption process occurred quite rapidly at the early stage, followed by a lag phase as the system approached equilibrium (Bouteraa *et al*., 2020; Ali & Gad, 2020). Dye concentrations of 25, 50, 75 and 100 mg/L reached optimum adsorptions after 140, 140, 100 and 120 minutes, correspondingly, indicating that equilibrium time is a function of initial dye concentration. Furthermore, higher initial dye concentrations recorded more adsorbed dye molecules than lower ones. Precisely, adsorption percentages and dye quantities of 42.52 % and 1.594 mg/g, 53.61 % and 4.021 mg/g, 45.57 % and 5.127 mg/g and 51.03 % and 7.654 mg/g were registered for indigo carmine dye concentrations of

25, 50, 75 and 100 mg/L, correspondingly. This observation is attributed to a significant driving force at higher initial dye concentration leading to an elevated mass gradient that permits adsorption of dye particles onto the adsorbents as reported by Slimani *et al*. (2014). The amount of methyl orange (MO) dye adsorbed by the magnetic composite (C-600-Fe_3O_4) increased with adsorption time and the dark orange colour of methyl orange solution became light orange after 300 min (Zhang *et al*., 2020). Adsorption of indigo carmine dye (75 mg/L to 250 mg/L) onto *C. odorata* biochar was investigated for 3 h using 10 mg of adsorbent dose (Nnadozie & Ajibade, 2021). The study reported a removal efficiency of 94.7% after 2 h contact time at 30 °C for the initial indigo carmine dye concentration of 75 mg/L.

Adsorption efficiency of dye as a function of adsorbent dosage was investigated by changing dosage from 0.05-0.25 g per 30 mL of dye solution as shown in Table 4.3.3b and Figure 4.3.3g.

Table 4.3.3b: Effect of adsorbent dose on adsorption efficiency (%R) of indigo carmine dye onto magnetic composites

	Adsorbent dosage (in g)				
Adsorbents	**0.05**	**0.10**	**0.15**	**0.20**	**0.25**
FSB@400 ^{o}C-Fe_3O_4	28.71^{b}	36.91^{a}	44.56^{a}	47.89^{a}	44.94^{b}
FSB@600 ^{o}C-Fe_3O_4	31.91^{a}	36.60^{a}	44.12^{a,b}	44.97^{b}	45.47^{a}
FSB@800 ^{o}C-Fe_3O_4	28.46^{b}	34.91^{b}	43.84^{b}	43.14^{c}	42.04^{c}
CV%	0.70	0.74	0.57	0.37	0.42
LSD, P≤0.05	0.42	0.53	0.50	0.34	0.37

$^{a, b, c}$ Data with different letters are significantly different; CV-coefficient of variation; LSD-least significant difference

The findings demonstrate that removal efficiency (%R) of an adsorbent was dependent on adsorbent dosage. With respect to the composite FSB@800 ^{o}C-Fe_3O_4, the amount of dye removed considerably rose from 28.46 % at an adsorbent quantity of 0.05 g to 42.04 % at 0.25 g usually attributed to the rise in quantity of energetic sites on the adsorbent's surface (Zhang *et al*., 2016; Ali & Gad, 2020). Peak dosages of adsorbents were obtained as 0.20 g, 0.25 g and 0.15 g per 30 mL, correspondingly, for FSB@400 ^{o}C-Fe_3O_4, FSB@600 ^{o}C-Fe_3O_4 and FSB@800 ^{o}C-Fe_3O_4. The decline in removal efficiency of indigo carmine dye past the adsorbents peak dosages was attributable to the accumulation of dye molecules leading to reduced total surface area (Ayanda *et al*., 2019).

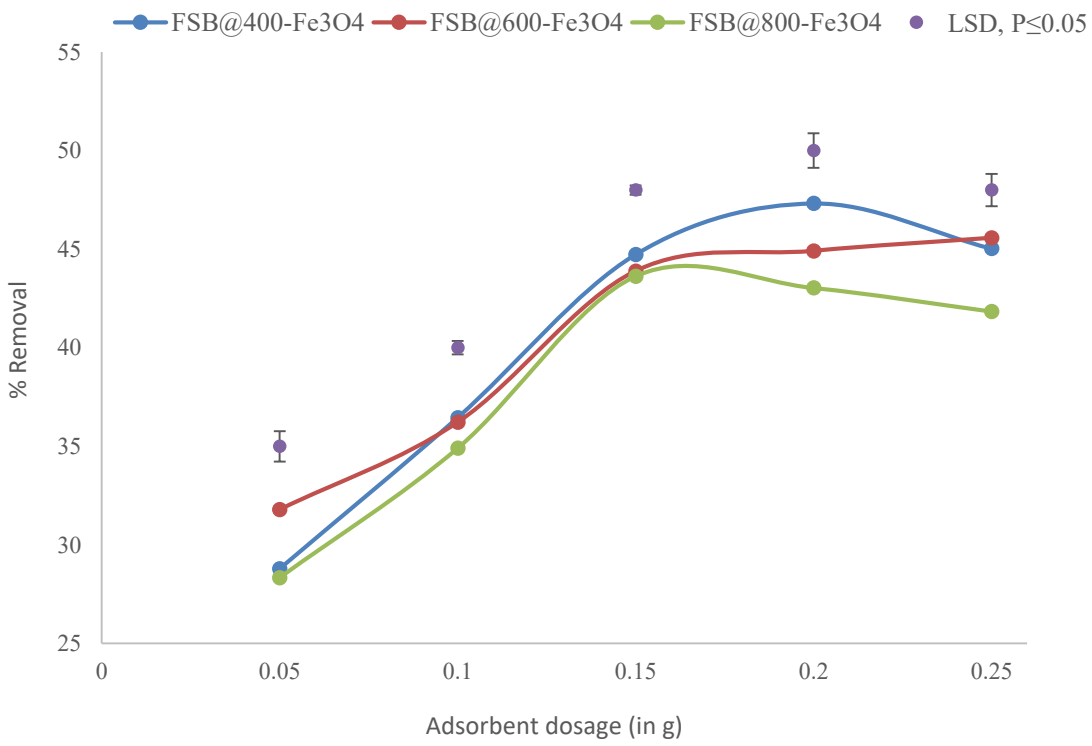

Figures 4.3.3g: Effects of adsorbent dosage on IC dye removal efficiency (%R)

The effect of pH on dye removal was examined within pH levels of 2, 4, 6, 8 and 10. The findings showed that removal efficiency (%R) of indigo carmine dye from the artificial wastewater declined with the rise in the considered pH levels for the magnetic composites under study (Table 4.3.3c and Figure 4.3.3h). Previous studies have proven that adsorption efficiency of an adsorbent at different pH levels is a function of surface charges, adsorption capacity and energetic sites of the adsorbent (Santhi *et al*., 2016).

Table 4.3.3c: Effect of initial solution pH on adsorption efficiency (%R) of indigo carmine (IC) dye onto magnetic composites

	Initial pH of indigo carmine dye solution				
Adsorbents	**2**	**4**	**6**	**8**	**10**
FSB@400 ºC-Fe_3O_4	47.89[a]	46.27[b]	42.78[b]	39.09[b]	38.45[b]
FSB@600 ºC-Fe_3O_4	48.10[a]	47.50[a]	44.35[a]	44.29[a]	40.66[a]
FSB@800 ºC-Fe_3O_4	46.35[b]	42.29[c]	40.24[c]	36.31[c]	35.90[c]
CV%	0.47	0.42	0.50	0.68	0.92
LSD, P≤0.05	0.45	0.38	0.42	0.54	0.70

[a, b, c] Data with different letters are significantly different; CV-coefficient of variation; LSD-least significant difference

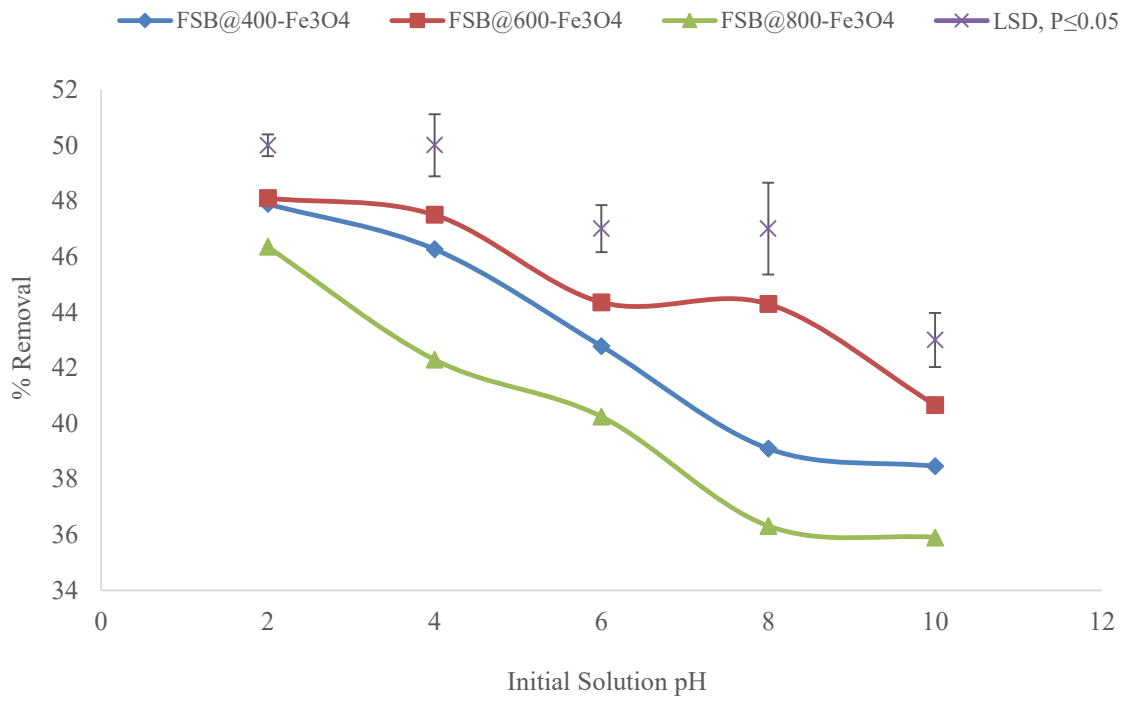

Figures 4.3.3h: Effects of initial solution pH on IC dye removal efficiency (%R)

Adsorbent FSB@600 ºC-Fe_3O_4, for instance, displayed a reduction in dye abstraction efficiency from 48.10 % at pH 2 to 40.66 % at pH 10. The observation herein is an affirmation that at a pH < 6, the adsorbents develop net positive charges on their surfaces as projected by the data from point of zero charge pH (pH_{pzc}) (Table 4.2.1 and Figure 4.2.1). Coulombic forces of attraction developed between the adsorbent and negatively charged indigo carmine dye particles, leading to a higher removal efficiency (Ayanda *et al*., 2019; Badeenezhad *et al*., 2019). Slimani *et al*. (2014) reported that higher pH levels effect a decrease in removal efficiency of calcined eggshells since there would be competition for active sites between hydroxyl (OH^-) ions and indigo carmine dye anions in aqueous solution. Higher pH levels (pH of 8) have been confirmed to reduce abstraction efficiency of methyl orange dye particles (Chakraborty *et al*., 2016). In another study, Konicki *et al*. (2017) investigated the adsorption of two anionic azo dyes, Acid Orange 8 (AO8) and Direct Red 23 (DR23), onto graphene oxide (GO) and reported that the adsorption capacity at equilibrium was favourable at acidic pH. Optimal pH 2 for removal of anionic indigo carmine dye so observed in the current research is in harmony with the conclusion made by Almoisheer *et al*. (2019). Figure 4.3.3j illustrates the mechanism involved in the adsorption of indigo carmine dye onto magnetic composite (FSB@Fe_3O_4). The surface of the magnetic composite developed positive charges in acidic pH since it was protonated causing an electrostatic interaction between the negatively charged indigo carmine dye particles and the positively charged adsorbent. Moreover, there will be forces of attraction between the dye particles and Fe-O in the

magnetic composite. Hydrogen bonding will also form between a hydrogen atom on the dye and -OH in the magnetic composite.

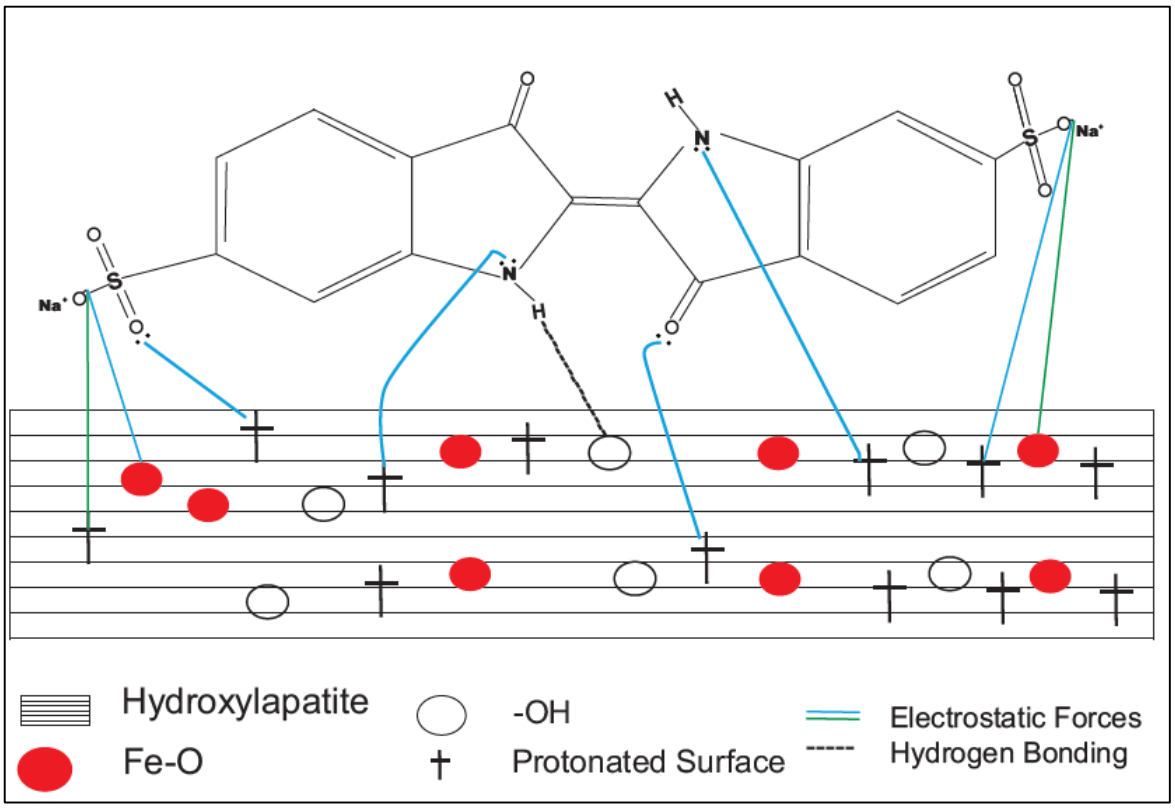

Figure 4.3.3i: Mechanism of indigo carmine dye adsorption onto magnetic composite

The temperature effect on indigo carmine dye abstraction from artificial dye wastewater was examined. Adsorption experiments for this physical parameter were monitored at 298 K, 303 K, 313 K and 323 K while varying initial dye concentrations, initial solution pH of 2 and adsorbent dose of 0.20 g per 30 mL of dye solution (Table 4.3.3d). Amount of dye removed by 0.20 g of FSB@600 ºC-Fe_3O_4 significantly ($p \leq 0.05$) augmented from 5.116 mg/g at 298 K to 5.551 mg/g at 323 K. These findings confirm that temperature rise improved adsorption process by increasing kinetic energy of dye and the surface activity of the adsorbent (Ho &

McKay, 2003) suggesting an endothermic state of dye removal (Kulkarni *et al*., 2017). The amount of indigo carmine dye adsorbed increased with increase in surface area and decrease in particle size as displayed by the adsorbents; FSB@600 ^{o}C-Fe_3O_4 > FSB@400 ^{o}C-Fe_3O_4 > FSB@800 ^{o}C-Fe_3O_4. This observation is attributed to the increase in the number of active sites on the surface of the adsorbent.

Table 4.3.3d: Effect of temperature on the quantity (mg/g) of indigo carmine dye onto magnetic composites

	Temperature (in K)			
Adsorbents	**298**	**303**	**313**	**323**
FSB@400 ^{o}C-Fe_3O_4	5.07^{b}	5.13^{c}	5.16^{c}	5.39^{b}
FSB@600 ^{o}C-Fe_3O_4	5.12^{a}	5.22^{a}	5.58^{a}	5.55^{a}
FSB@800 ^{o}C-Fe_3O_4	5.06^{c}	5.14^{b}	5.26^{b}	5.15^{c}
CV%	0.00	0.00	0.00	0.00
LSD, P≤0.05	0.00	0.00	0.00	0.00

$^{a, b, c}$ Data with different letters are significantly different; CV-coefficient of variation; LSD-least significant difference

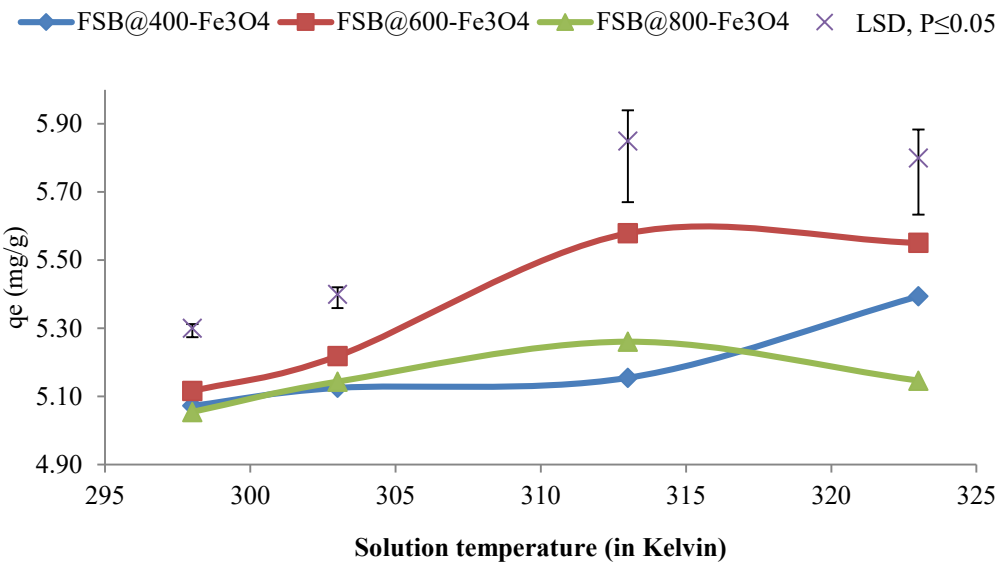

Figure 4.3.3j: Effects of temperature on adsorption of IC dye molecules

It is concluded that contact time, initial dye concentration, solution pH, temperature and adsorbent dosage have an influence on the adsorption of anionic indigo carmine dye by the adsorbents.

4.4 Batch adsorption process and conditions

4.4.1 Effect of contact time, initial dye concentration, adsorbent dosage, solution pH and temperature on adsorption of crystal violet

The working wavelength for crystal violet dye was experimentally obtained as 588 nm (Figure 4.4.1a).

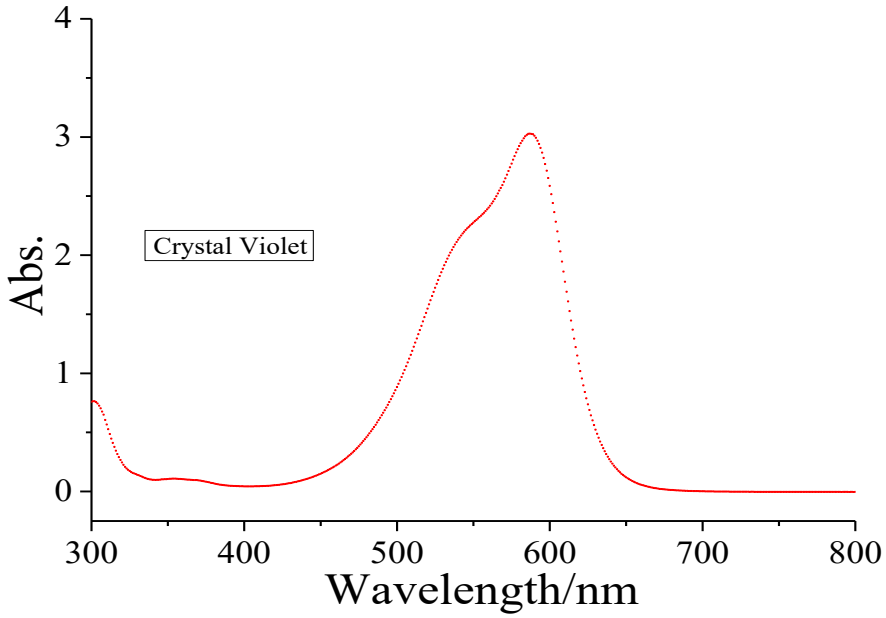

Figures 4.4.1a: Wavelength for crystal violet dye experiments

Removal efficiency (%R) of crystal violet dye from aqueous solution was studied as a function of contact time and initial dye concentration (Table 4.4.1a and Figure 4.4.1b). A dosage of 0.2 g of adsorbent in 30 mL of each of the four concentration levels 25 mg/L, 50 mg/L, 75 mg/L and 100 mg/L of dye solutions was agitated at 200 rpm from 0 to 180 minutes at 298 K. The adsorption process was very fast at the initial stages but gradually

declined as the system approached equilibrium. This observation was attributed to a large number of unoccupied adsorption sites at the onset of the process and reduced number of available binding sites towards equilibrium point. Maximum adsorptions were afforded after 160 min, 140 min, 140 min and 100 min, respectively, for 25 mg/L, 50 mg/L, 75 mg/L and 100 mg/L. A higher quantity of dye was abstracted at higher initial concentrations than at lower initial concentrations. This observation is ascribed to significant driving force due to increased mass gradient at higher initial dye concentrations that supports adsorption of dye molecules onto the adsorbents. This finding is in harmony with reports from other researchers (Rangabhashiyam *et al*., 2018; Adeyi *et al*., 2019).

Table 4.4.1a: Effect of initial dye concentration and contact time on adsorption of crystal violet dye (mg/g) onto FSB@600 ºC

Conc in mg/L	Contact time (in minutes)									CV%	LSD, P≤0.05
	20	40	60	80	100	120	140	160	180		
25	37.15^{g}	43.93^{f}	45.15^{e}	46.72^{d}	49.53^{c}	49.74^{c}	50.10^{a}	52.22^{a}	52.10^{a}	0.32	0.26
50	37.64^{h}	44.74^{g}	46.67^{f}	47.59^{e}	50.07^{d}	52.95^{c}	55.93^{a}	$55.72^{a,b}$	55.50^{b}	0.33	0.28
75	35.26^{g}	38.68^{f}	41.49^{e}	$41.65^{d,e}$	41.88^{d}	43.44^{c}	45.31^{a}	44.82^{b}	44.62^{b}	0.50	0.36
100	34.73^{f}	37.99^{e}	46.00^{d}	48.00^{c}	50.25^{a}	$50.12^{a,b}$	$50.15^{a,b}$	$50.09^{a,b}$	$50.09^{a,b}$	0.20	0.16

$^{a, b, c, d, e, f, g}$ Data with different letters are significantly different; CV-coefficient of variation; LSD-least significant difference

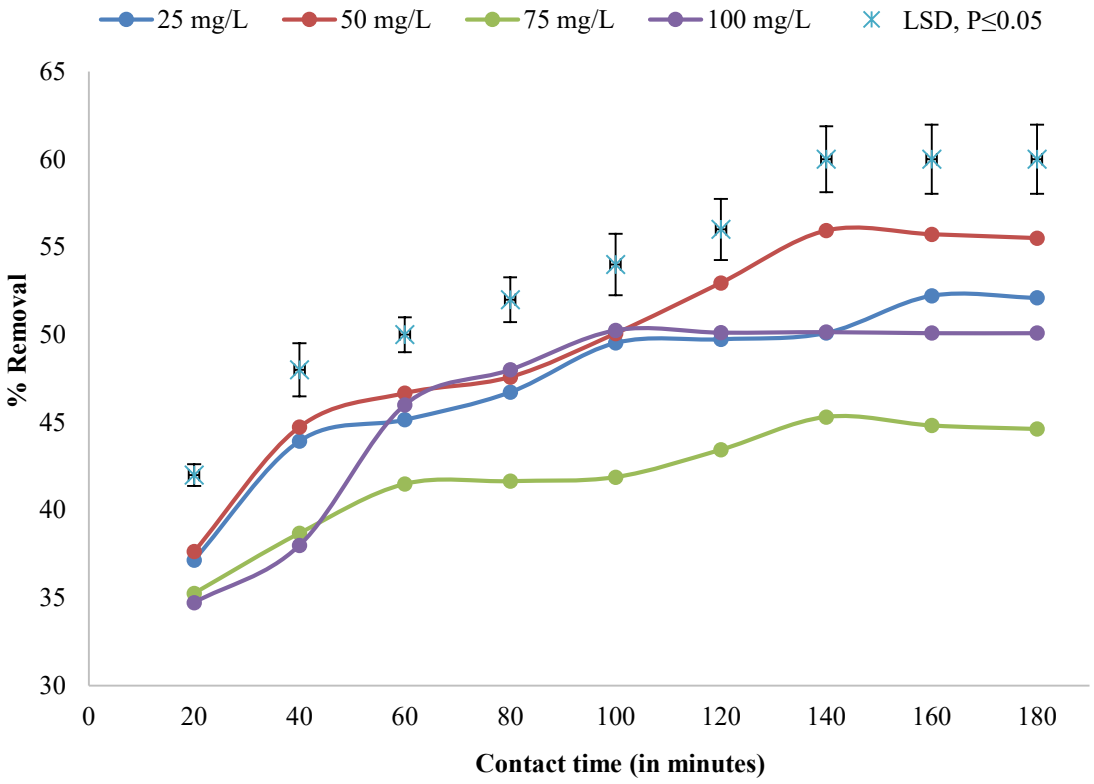

Figure 4.4.1b: Effect of initial dye concentration and contact time on adsorption efficiency (%R) of crystal violet (CV) dye onto fish scale biochar (FSB@600 ºC)

Adsorption efficiency of crystal violet dye as a function of adsorbent dosage was also studied by varying dosage from 0.05-0.25 g per 30 mL of dye solution. Removal efficiency (%R) of an adsorbent is highly dependent on adsorbent weight used. The results of the influence of adsorbent dose on removal efficiency of crystal violet dye is given in Table 4.4.2b and Figure 4.4.2c. Peak dosages were recorded at 0.20 g, 0.20 g, 0.20 g, 0.20 g, 0.20 g, 0.25 g and 0.25 g for Activated charcoal, FSB@400 ºC, FSB@600 ºC, FSB@800 ºC, FSB@400 ºC-Fe_3O_4, FSB@600 ºC-Fe_3O_4 and FSB@800 ºC-Fe_3O_4, respectively. This observation is attributed to the increase in the number of active sites on the surface of the adsorbents with the increase in adsorbent dosage which caused an

increase in the amount of dyes adsorbed (Badeenezhad *et al*., 2019; Temesgen *et al*., 2018). A decline in removal efficiency was registered past the peak dosages of the adsorbents, a characteristic that is tied to saturation of the active sites on the surface of the adsorbents with adsorbate (Ayanda *et al*., 2019).

Table 4.4.1b: Effect of adsorbent dose on adsorption efficiency (%R) of crystal violet dye onto the adsorbents

	Adsorbent Dosage (in g)						
Adsorbent	**0.05**	**0.10**	**0.15**	**0.20**	**0.25**	**CV%**	**LSD, P≤0.05**
Activated Charcoal	94.25^{e}	96.38^{d}	97.22^{c}	99.76^{a}	99.20^{b}	0.13	0.23
FSB@400 ºC	34.24^{e}	37.99^{d}	39.87^{c}	42.82^{a}	42.35^{b}	0.47	0.34
FSB@600 ºC	37.12^{e}	39.05^{d}	42.69^{c}	44.82^{a}	44.29^{b}	0.17	0.13
FSB@800 ºC	37.00^{e}	37.73^{d}	38.36^{c}	41.63^{a}	41.33^{b}	0.41	0.29
FSB@400 ºC-Fe_3O_4	38.37^{e}	38.87^{d}	39.32^{c}	41.23^{a}	40.92^{b}	0.31	0.23
FSB@600 ºC-Fe_3O_4	38.73^{e}	42.02^{d}	44.96^{c}	47.84^{b}	48.22^{a}	0.42	0.34
FSB@800 ºC-Fe_3O_4	40.80^{d}	43.25^{c}	43.60^{b}	45.62^{a}	45.86^{a}	0.36	0.29

[a, b, c, d, e] Data with different letters are significantly different; CV-coefficient of variation; LSD-least significant difference

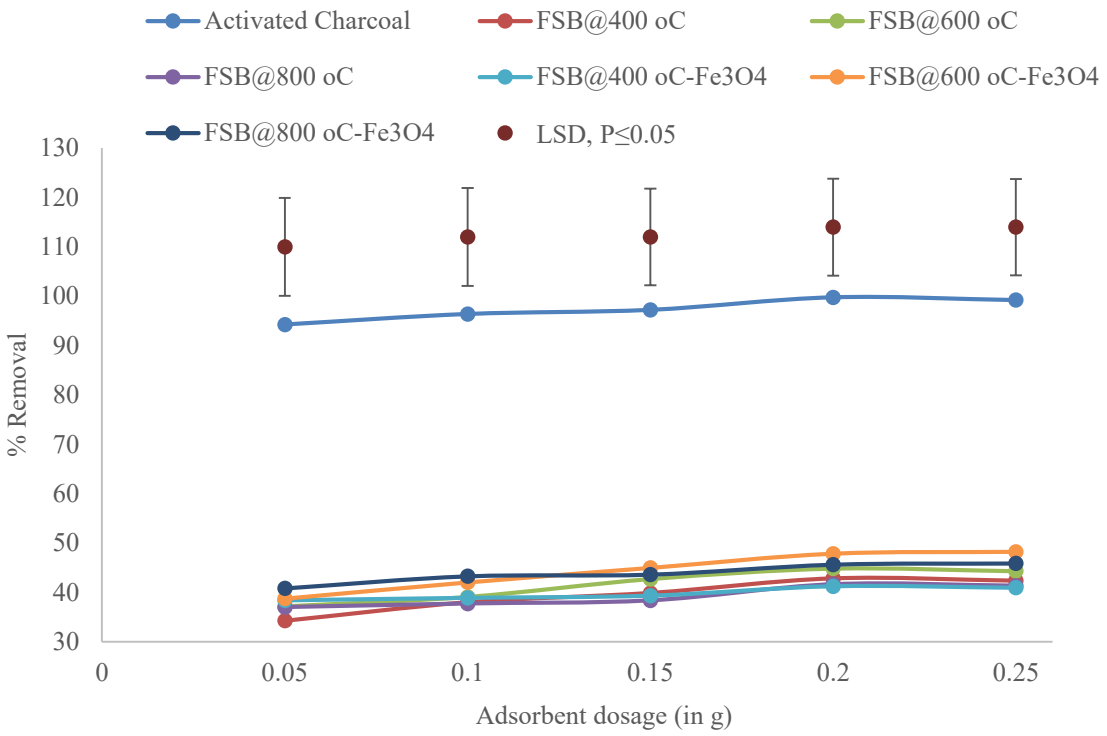

Figure 4.4.1c: Effect of adsorbent dosage on adsorption efficiency (%R) of crystal violet (CV) dye onto activated charcoal, fish scale biochars (FSB) and magnetic composites (FSB@Fe_3O_4)

The removal efficiency (%R) of crystal violet dye from aqueous solution onto the adsorbents increased with increase in solution pH (pHs) for all the tested adsorbents as illustrated in Table 4.4.1c and Figure 4.4.1d. The surface of the adsorbents acquired positive charges as confirmed by point of zero charge pH (pH_{pzc}) which contributed to repulsion forces between the adsorbent and CV molecules leading to a decrease in adsorption (Ayanda *et al*., 2019, Badeenezhad *et al*., 2019, Nnaemeka *et al*., 2016). However, adsorption process was favoured when the adsorbent surface was negatively charged due to attractive forces between the negative and positive charges on the surface

of the adsorbents and CV dye molecules, respectively (Ayanda *et al*., 2019, Badeenezhad *et al*., 2019, Nnaemeka *et al*., 2016). Significant differences (P≤0.05) in adsorbents performance was observed where the reference adsorbent (Activated Charcoal) did better than all the other adsorbents at all solution pH. The findings of this study on the effect of solution pH on the adsorption of crystal violet dye showed that pH 8 (activated charcoal, FSB@400 ºC, FSB@600 ºC and FSB@800 ºC) and pH 10 (FSB@400 ºC-Fe_3O_4, FSB@600 ºC-Fe_3O_4 and FSB@800 ºC-Fe_3O_4) were favourable for the adsorption process.

Table 4.4.1c: Effect of initial solution pH on adsorption efficiency (%R) of crystal violet (CV) dye onto fish scale biochars (FSB) and magnetic composites (FSB@Fe_3O_4)

Adsorbent	pH levels					CV%	LSD, P≤0.05
	2	4	6	8	10		
Activated Charcoal	88.68^{d}	96.39^{c}	98.47^{b}	98.65^{b}	99.05^{a}	0.22	0.39
FSB@400 ºC	38.21^{e}	39.24^{d}	39.67^{c}	41.24^{b}	42.13^{a}	0.49	0.36
FSB@600 ºC	38.69^{d}	40.23^{c}	43.41^{b}	45.23^{a}	45.34^{a}	0.69	0.53
FSB@800 ºC	35.58^{d}	36.76^{c}	40.82^{b}	41.59^{a}	42.00^{a}	0.62	0.44
FSB@400 ºC-Fe_3O_4	36.73^{d}	38.17^{c}	39.24^{b}	40.73^{a}	40.61^{a}	0.44	0.31
FSB@600 ºC-Fe_3O_4	39.48^{d}	42.14^{c}	45.08^{b}	47.82^{a}	47.75^{a}	0.61	0.49
FSB@800 ºC-Fe_3O_4	40.34^{d}	41.29^{c}	43.46^{b}	46.41^{a}	46.01^{a}	0.58	0.46

$^{a, b, c, d, e}$ Data with different letters are significantly different; CV-coefficient of variation; LSD-least significant difference

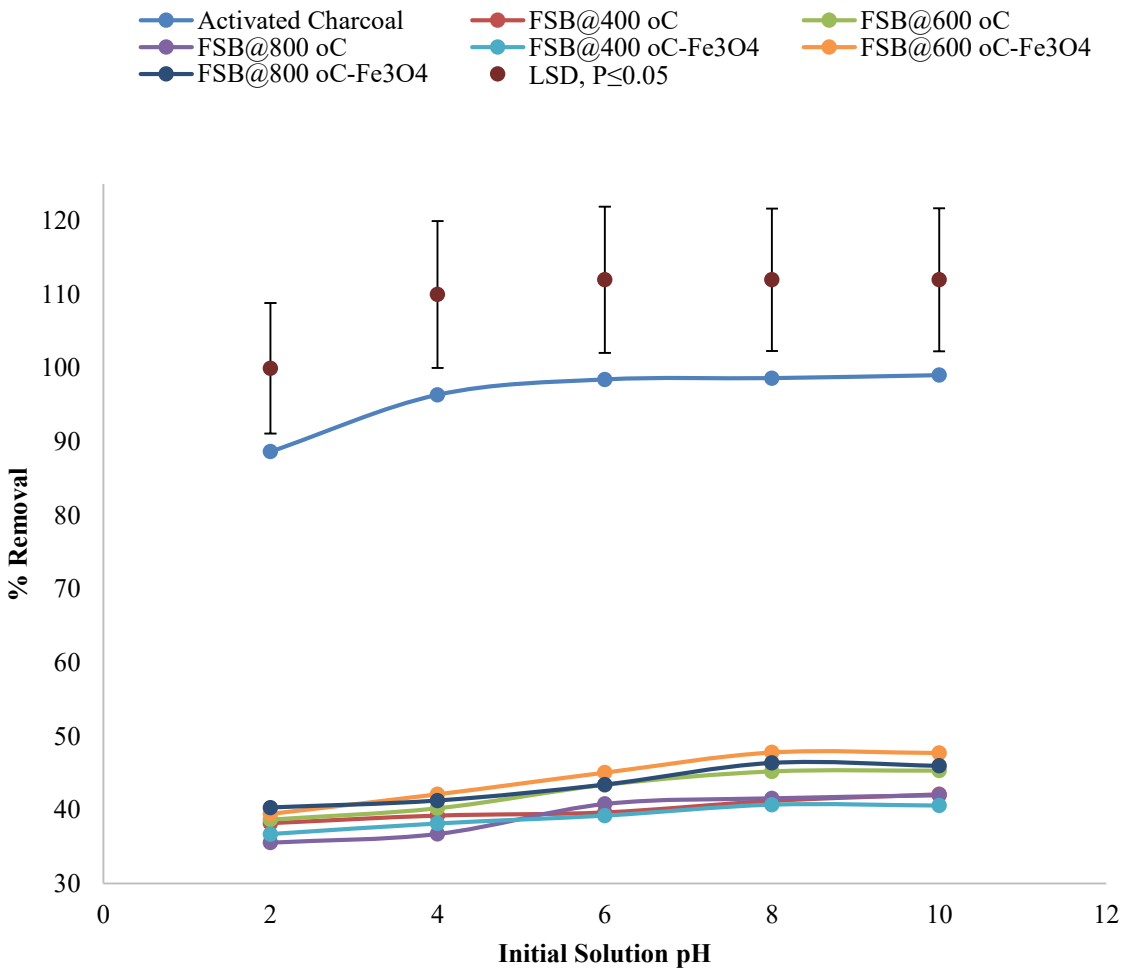

Figure 4.4.1d: Effect of initial solution pH on adsorption efficiency (%R) of crystal violet (CV) dye onto activated charcoal, fish scale biochars (FSB) and magnetic composites (FSB@Fe_3O_4)

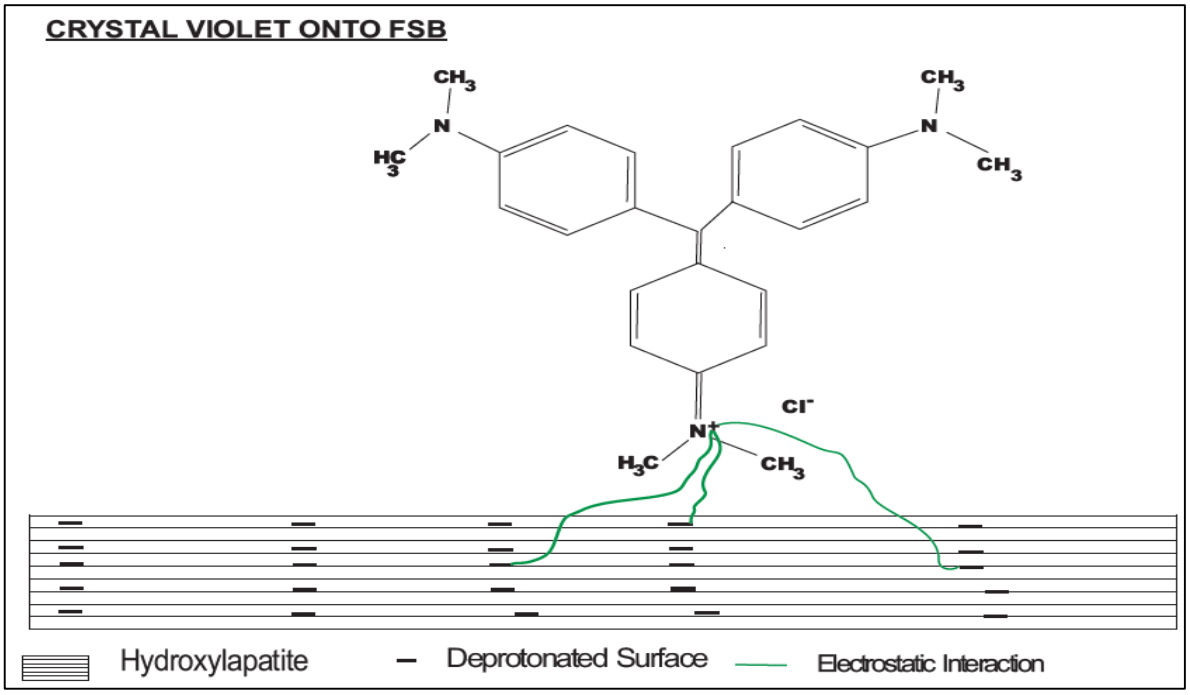

Figure 4.4.1e: Mechanism of crystal violet dye adsorption onto FSB

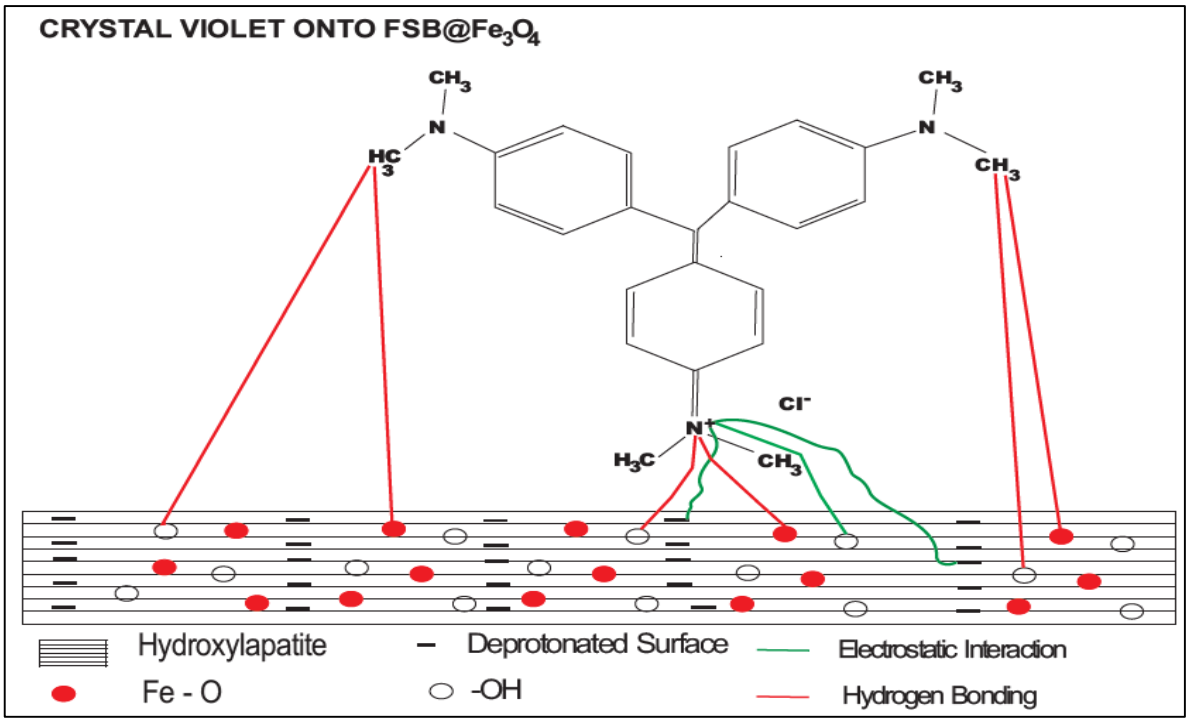

Figure 4.4.1f: Mechanism of crystal violet dye adsorption onto magnetic composite

In order to investigate the effect of temperature on the adsorption of CV dye, the adsorption experiments were carried out at 298, 303, 313 and 323 K for the different initial dye concentrations, and at an initial solution pH 10, adsorbent dosage of 0.2 g, 30 mL of dye solution volume, and agitation speed of 200 rpm, as illustrated in Figures 4.4.1g and h. The amount of dye removed increased with temperature for all the adsorbents, suggesting that the adsorption process was principally endothermic. This tendency is attributed to the strong bond between the binding sites of the adsorbents and dye molecules with concomitant shift of the equilibrium to the right at higher temperatures (Kulkarni *et al*., 2017). Ho & McKay (2003) also reported that higher temperatures usually enhance adsorption due to the increased kinetic energy of the adsorbate and adsorbent surface activity. In other words, increase in temperature will raise the rate of diffusion of the adsorbed dye molecules across the external boundary layer and the internal pores of the adsorbent particles due to the decrease in the viscosity of the solution.

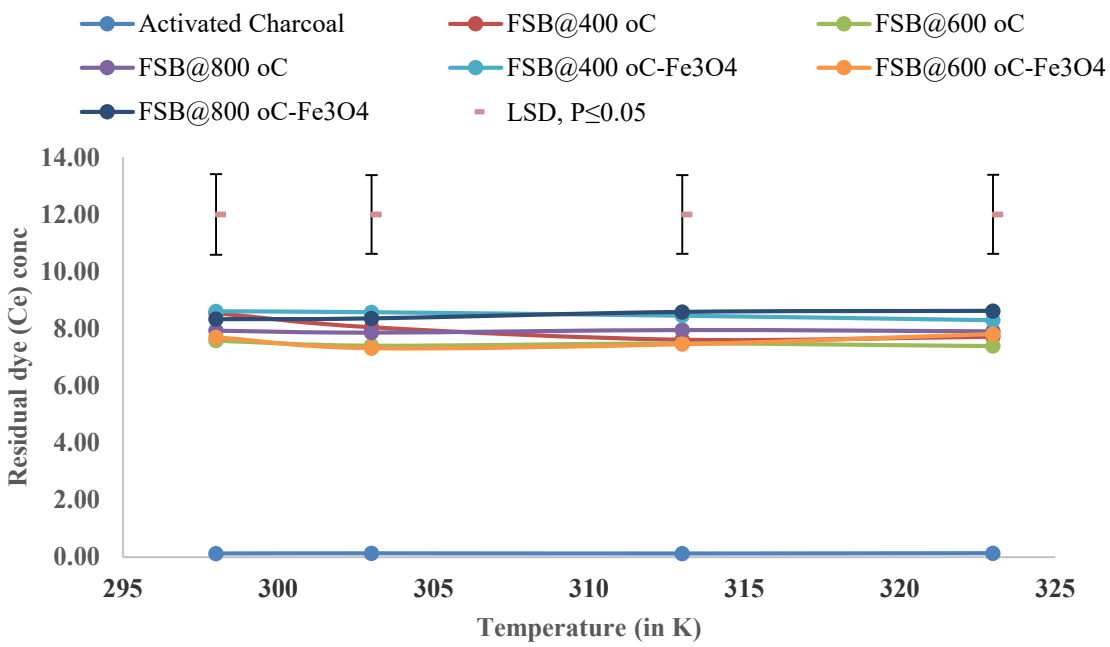

Figure 4.4.1g: Effect of temperature on CV dye removal (15 mg/L, 0.20 g/30 mL)

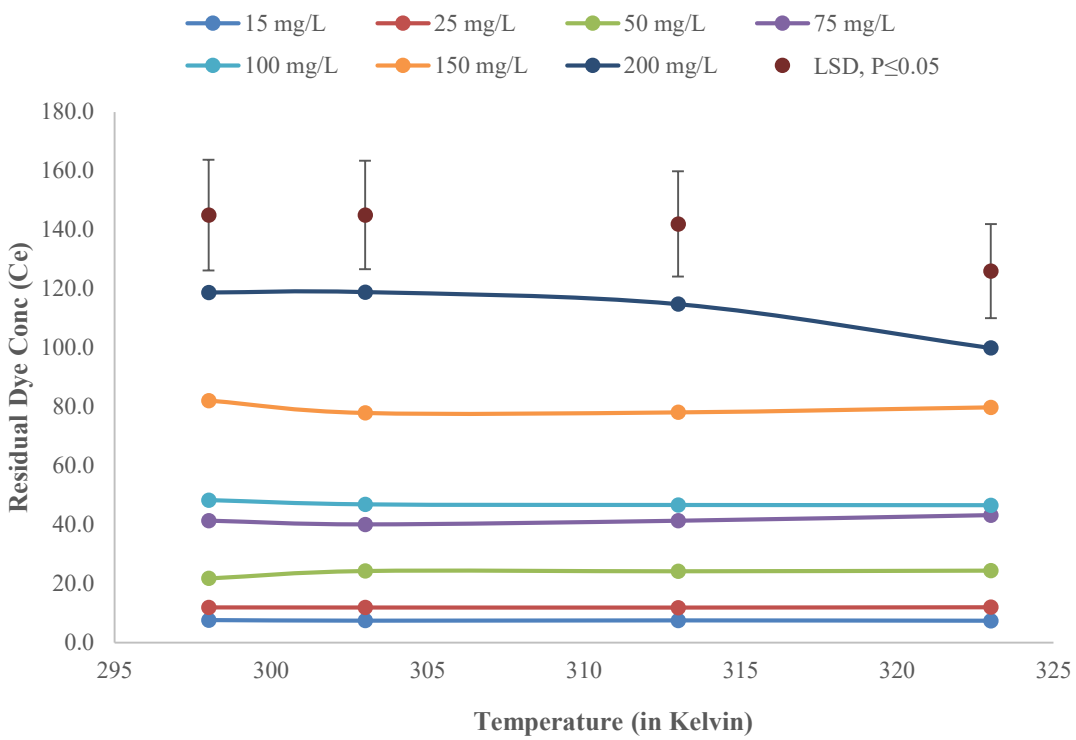

Figure 4.4.1h: Effect of temperature on CV dye removal (FSB@600 ºC; 0.20 g/30 mL)

It is concluded that contact time, initial dye concentration, solution pH, temperature and adsorbent dosage have an influence on the adsorption of cationic crystal violet dye by the adsorbents.

4.5 The kinetics and thermodynamics of adsorption

4.5.1 Kinetics and thermodynamics of adsorption of indigo carmine dye

Studying the kinetics of adsorption of indigo carmine dye removal onto the adsorbents (activated charcoal and fish scale biochars) involved fitting of the contact time data at various initial adsorbate concentrations onto *pseudo*-first-order, *pseudo*-second-order, and intraparticle diffusion models (Table 4.5.1a and Figure 4.5.1a). The R^2 values (for intraparticle diffusion model) for the indigo carmine dye concentrations of 25, 50, 75 and 100 mg/L were 0.987, 0.611, 0.811 and 0.947, respectively, signifying that q_t had a low linear dependency on $t^{0.5}$ (Table 4.5.1a and Figure 4.5.1a). From the data in Table 4.5.1a, it can be concluded that intra-particle diffusion (K_p) was not the sole operating rate controlling step, since the plot registered non-zero y-intercept values (El Haddad *et al*., 2013b; Kimosop *et al*., 2017). Comparison of R^2 values showed that equilibrium data best fitted the *pseudo*-first-order kinetic model since they are all close to unity.

Table 4.5.1a: Calculated parameters for kinetic models

	***Pseudo*-first order**			***Pseudo*-second order**			**Intraparticle**		
Conc (mg/L)	K_1 (1/min)	q_e (mg/g)	R^2	K_2 (g/mg.min)	q_e (mg/g)	R^2	K_P ($mg/g.min^{0.5}$)	I	R^2
25	58535	1.778	0.99999	0.00028	1.781	0.996711	0.062	1.426	0.987
50	58537	4.040	0.99999	0.00063	4.052	0.996630	0.075	3.767	0.611
75	58537	6.950	0.99999	0.00130	6.963	0.996629	0.100	6.735	0.801
100	58532	10.689	0.99999	0.00049	10.728	0.996671	0.179	9.683	0.947

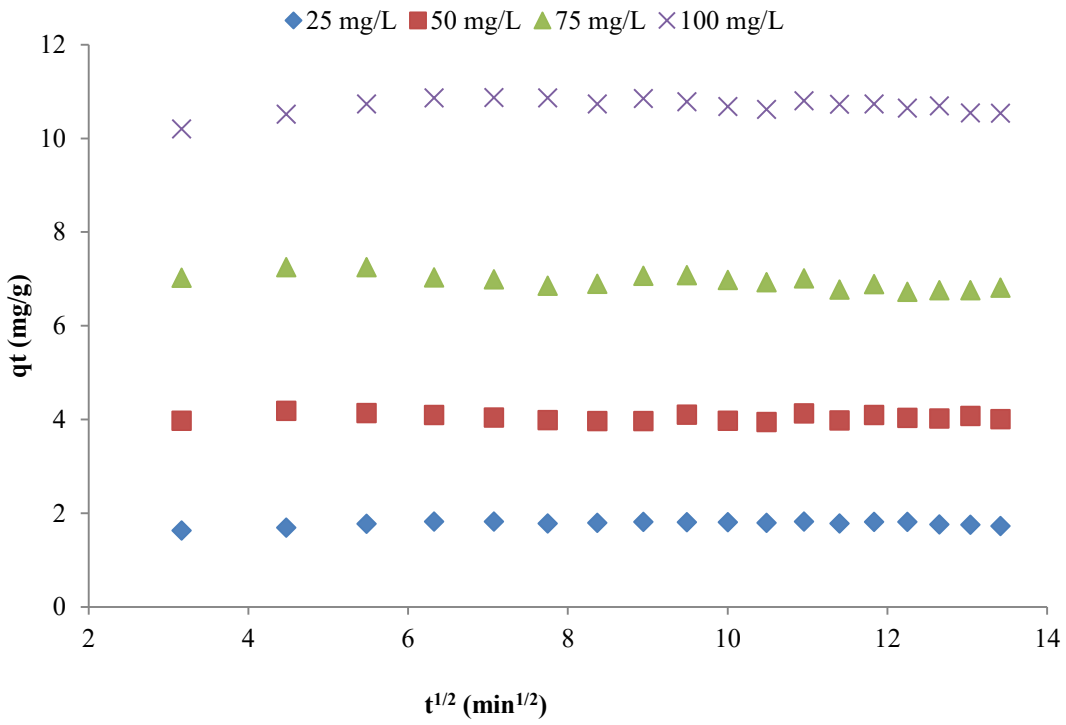

Figure 4.5.1a: Intra-particle diffusion model plot for FSB@600 °C. Experimental conditions include: 30 mL of 25, 50, 75 and 100 mg/L of indigo carmine, adsorbent dose of 0.2 g, 200 rpm and 298 K

Thermodynamic parameters such as ΔG, ΔH, and ΔS were calculated (Table 4.5.1b). Positive ΔH values indicated that the adsorption processes were endothermic corroborating the observed increase in adsorption with temperature. Similarly, the positive ΔS denoted increase in randomness at the solid-liquid interphase. Adsorption onto the activated charcoal was spontaneous at all temperatures as seen in the negative ΔG values. However, adsorptions onto the fish scales biochars were predominantly non-spontaneous and this non-spontaneity decreased with temperature. It is noteworthy that the spontaneity also varied with the initial concentration denoting its dependence on the equilibrium constant K. From the data, it can be deduced that chemisorption was the principal mechanism of indigo carmine dye removal from the aqueous solution onto the adsorbents (Kulkarni *et al*., 2017). Begum & Kabir (2013) reported that the functional groups in the fish scale structure, such as phosphates, carboxyls, amines and carbonyls, are supposed to be involved in the sorption process as confirmed by the FT-IR spectra in this study.

Table 4.5.1b: Thermodynamic parameters for biochars and activated charcoal for IC removal

		Adsorbents											
		Activated charcoal			**FSB@400 °C**			**FSB@600 °C**			**FSB@800 °C**		
Temp	Conc	ΔG	ΔH	ΔS	ΔG	ΔH	ΔS	ΔG	ΔH	ΔS	ΔG	ΔH	ΔS
(°K)	(mg/L)	kJ/mol	kJ/mol	J/mol/K	kJ/mol	kJ/mol	J/mol/K	kJ/mol	kJ/mol	J/mol/K	kJ/mol	kJ/mol	j/mol/K
	15	−2.349	4.232	24.642	1.900	14.772	42.909	1.969	0.580	−3.810	1.876	11.550	31.842
	25	−2.583	9.516	42.851	1.377	23.972	75.612	1.594	12.342	36.800	1.594	20.679	64.143
	50	−3.012	5.819	32.052	0.820	25.561	82.333	0.923	12.748	39.558	0.697	19.760	63.798
298	75	−3.356	18.014	73.774	0.834	42.277	137.764	0.428	34.541	113.581	0.385	30.712	100.159
	100	−4.243	7.201	38.984	−0.373	15.448	52.731	−0.384	14.113	48.998	−0.165	23.876	79.939
	150	−0.999	−2.849	−0.006	−1.365	5.193	0.021	−0.869	13.834	0.049	−0.906	18.232	0.063
	200	0.479	3.433	0.010	−0.078	0.011	−0.00013	0.030	11.052	0.037	0.472	27.719	0.091
	15	−3.697			1.704			1.232			1.832		
	25	−3.935			1.207			1.123			1.369		
	50	−4.512			0.683			0.742			0.324		
303	75	−4.514			0.746			0.203			0.865		
	100	−4.717			−0.664			−1.043			−0.336		
	150	−1.022			−8.502			−1.333			−0.950		
	200	0.253			6.104			0.147			0.339		
	15	−4.620			1.689			2.149			2.235		
	25	−4.708			0.239			0.363			0.353		
	50	−4.899			0.226			0.503			0.211		
313	75	−6.391			−0.245			−0.395			−0.295		
	100	−5.259			−0.490			−0.845			−0.470		
	150	−0.711			−1.435			−1.648			−1.507		
	200	0.711			−1.829			−0.472			−0.135		
	15	−2.903			0.696			1.686			0.862		
	25	−3.687			−0.419			0.764			0.123		
	50	−3.962			−1.321			−0.115			−1.074		
323	75	−4.933			−2.658			−2.541			−1.943		
	100	−5.204			−1.921			−1.882			−2.349		
	150	−0.930			−1.694			−2.110			−2.411		
	200	0.030			2.688			−0.776			−1.937		

Kinetics of indigo carmine dye adsorption by the magnetic composites were studied by fitting contact time data at different initial dye concentrations onto intra-particle diffusion, *pseudo*-first and second-order reaction models as highlighted in Table 4.5.1c and Figures 4.5.1a, b and c. The coefficient of determination, R^2, values attained were 0.6796, 0.6739, 0.4229 and 0.7870 for dye concentrations of 25, 50, 75 and 100 mg/L, correspondingly, demonstrating a low linear dependency of q_t on $t^{0.5}$ (Figure 4.5.1a).

Table 4.5.1c: Evaluated kinetic models parameters for the adsorption of indigo carmine

	***Pseudo*-first order**			***Pseudo*-second order**			**Intra-particle diffusion**		
Conc (mg/L)	K_1 (1/min)	q_e (mg/g)	R^2	K_2 (g/mg.min)	q_e (mg/g)	R^2	K_P ($mg/g.min^{0.5}$)	I	R^2
25	0.0311	0.306	0.9624	0.2762	1.606	0.9998	0.0177	1.3784	0.6796
50	0.0320	0.774	0.8567	0.0872	4.078	0.9998	0.0538	3.3837	0.6739
75	0.0421	0.9559	0.8247	0.1973	5.107	0.9997	0.0443	4.5788	0.4229
100	0.0702	8.696	0.8958	0.0306	7.874	0.9996	0.1270	6.1779	0.7870

Notably, Table 4.5.1c display data that evidently support the report by El Haddad *et al*. (2013a and b) that intraparticle diffusion constant (K_p) was not the only effective reaction rate-governing phase, since the plot recorded y-intercept values greater than zero. Furthermore, comparison of R^2 values showed the *pseudo*-second-order kinetic model values were close to 1, inferring that the model best described the equilibrium data since it demonstrated the best fit. Similar results were also reported for the adsorption of methylene blue, methyl violet, rhodamine B and orange G onto graphene and graphene oxide (Ramesha *et al*., 2011).

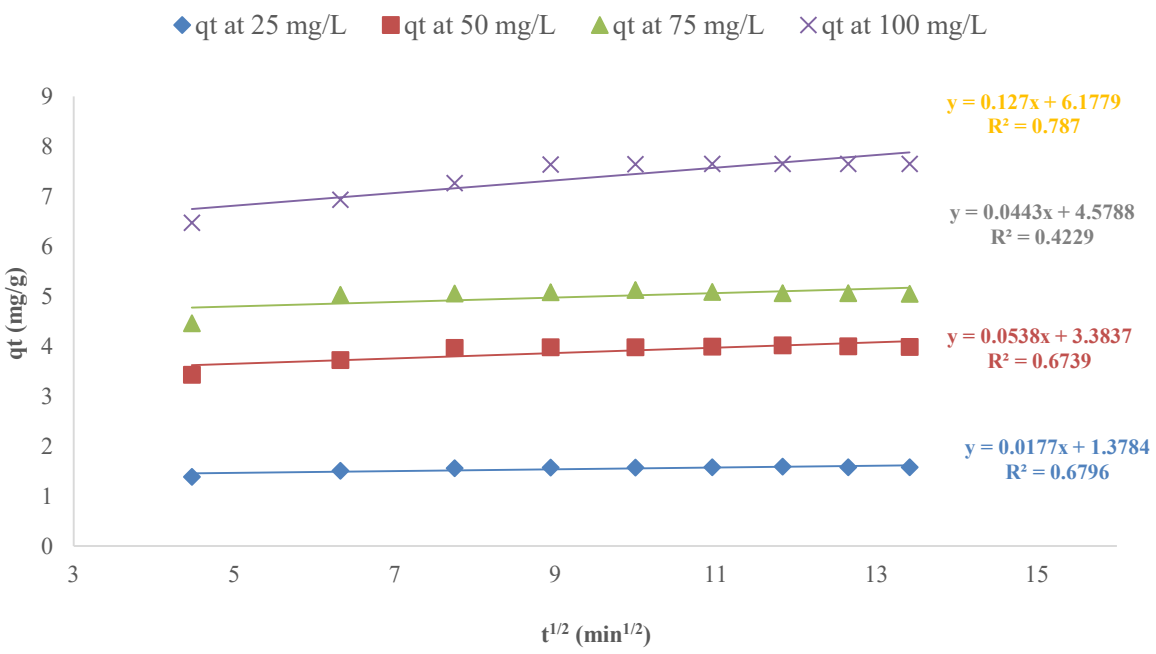

Figure 4.5.1b: Intra-particle diffusion model Plot for FSB@600 ºC-Fe_3O_4. Experimental conditions: 30 mL of 25, 50, 75 and 100 mg/L of indigo carmine, adsorbent dose of 0.2 g, 200 rpm and 298 K

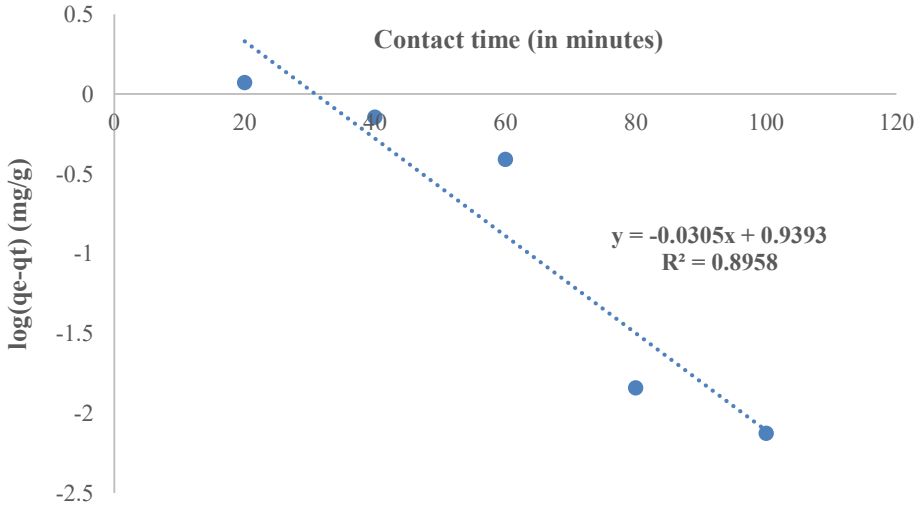

Figure 4.5.1c: Pseudo-first order kinetic plot for FSB@600 ºC-Fe_3O_4. Experimental conditions: 30 mL of 100 mg/L of indigo carmine solution, adsorbent dose of 0.2 g, 200 rpm, equilibration time of 2 h and 298 K

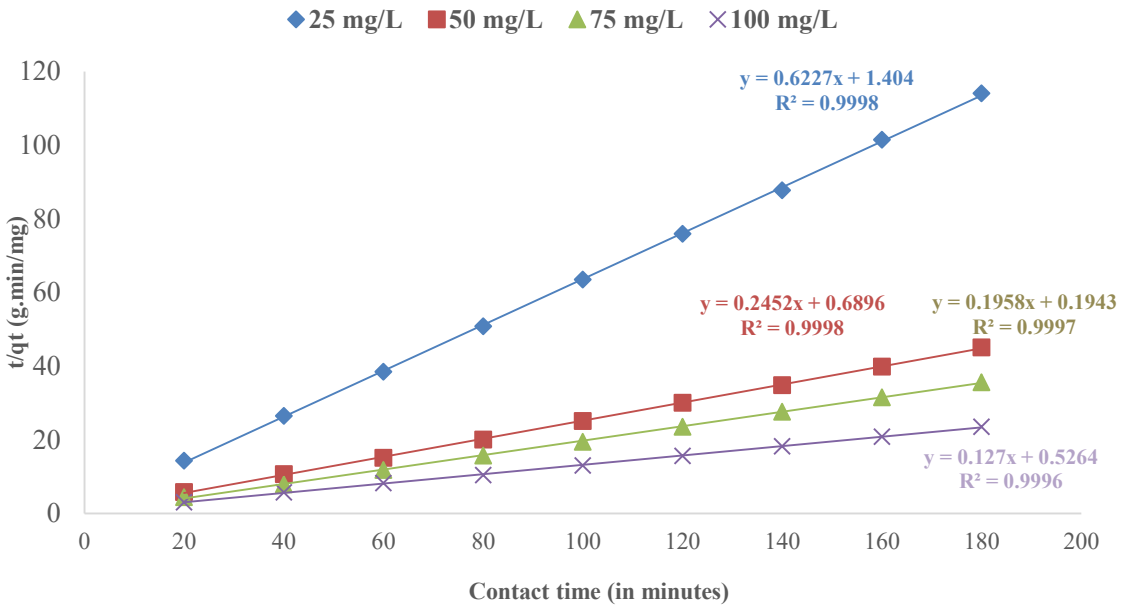

Figure 4.5.1d: Pseudo-second order kinetic plots for FSB@600 ºC-Fe_3O_4

Comparison of R^2 values (Table 4.5.1c and Figures 4.5.1b, c and d) was close to 1, inferring that the *pseudo*-second-order kinetic model best described the equilibrium data since it demonstrated the best fit. The findings of this study on kinetics corroborate the reports of other researchers. The *pseudo*-second-order kinetic model well described the adsorption of the anionic dye of Acid Black 210 (AB210) from aqueous solutions by a magnetically separable Fe_3O_4/CeO_2 (Fe/Ce) nanocomposite (Gao *et al*., 2019). Zhang *et al*. (2020) reported coefficient of determination (R^2) values that exceeded 0.99 for initial methyl orange dye concentrations (10, 30, 50, 100 and 150 mg/L) demonstrating that the *pseudo*-second-order kinetic model well described the adsorption of methyl orange dye onto porous carbon/Fe_3O_4-600 composite. The kinetics of methylene blue (MB) and malachite green (MG) biosorption onto *Carica papaya* wood (CPW) was studied and reported as better described by *pseudo*-second-order kinetic equation (Rangabhashiyam

et al., 2018). A study by Essandoh & Garcia (2018) on efficient removal of indigo carmine dye from aqueous solutions using a novel hemoglobin/iron oxide composite (Hb/Fe_3O_4) established that the adsorption process followed pseudo-second order kinetic model. In addition, the adsorption kinetics of synthetic methylene blue (MB) dye onto graphene oxide-magnetic iron oxide nanoparticles (GO-MNP) adsorbent follows *pseudo*-second order kinetics model (Othman *et al*., 2018). However, *pseudo*-first-order kinetic and Freundlich isotherm models described the removal of indigo carmine dye from simulated wastewater by *tilapia* fish scale biochars (FSB).

Three thermodynamic factors, which include changes in Gibb's free energy (ΔG), enthalpy (ΔH), and entropy (ΔS), were computed (Figure 4.5.1d). Resulting positive ΔH values showed that removal processes for indigo carmine dye were dominantly endothermic, confirming the witnessed rise in adsorption reaction with dye solution temperature. Again, positive ΔS signified a rise in a random collision of particles at the boundary of solid and liquid. Indigo carmine dye adsorptions onto the fish scales biochar magnetic composites ($FSB@Fe_3O_4$) were mostly non-spontaneous. The change in Gibb's free energy for the physisorption adsorption process is between -20 and 0 kJ mol^{-1} while the positive value of entropy suggests a good affinity of adsorbate towards the adsorbent as reported by Konicki *et al*. (2017) in their research. The findings are in agreement with a report by Yadav *et al*. (2020) for adsorption of methylene blue (MB) dye onto Magnetic/Activated Charcoal/β-Cyclodextrin/Alginate (Fe_3O_4/AC/CD/Alg) polymer nanocomposite. The adsorption thermodynamics data for the adsorption of indigo

carmine onto carbon-biomass from the seeds of *Moringa oleifera* and manganese ferrite ($MnFe_2O_4$@MOAC) revealed that the process was endothermic and spontaneous (Sirajudheen *et al*. 2021). On the contrary, Kulkarni *et al*. (2017) presented data from thermodynamic parameters in which chemisorption was the primary mechanism in the abstraction of indigo carmine dye from artificial dye wastewater by the adsorbents.

Table 4.5.1d: Thermodynamic parameters for biochar magnetic composites for IC removal

		FSB@400 ^{o}C-Fe_3O_4			**FSB@600 ^{o}C-Fe_3O_4**			**FSB@800 ^{o}C-Fe_3O_4**		
Temp	Conc	ΔG	ΔH	ΔS	ΔG	ΔH	ΔS	ΔG	ΔH	ΔS
(^{o}K)	(mg/L)	kj/mol	kj/mol	j/mol/K	kj/mol	kj/mol	j/mol/K	kj/mol	kj/mol	j/mol/K
	15	0.713	-0.218	-3.100	0.651	0.905	0.743	0.712	0.501	-0.770
	25	0.762	-0.423	-3.930	0.687	0.206	-1.640	0.826	0.061	-2573.18
	50	-0.379	0.202	1.926	-0.403	-0.126	0.942	-0.364	0.053	1.393
	75	0.387	3.385	9.658	0.229	5.519	17.096	0.418	1.191	2.452
	100	-0.103	-0.624	-1.670	-0.189	0.757	3.084	-0.107	0.373	1.567
	150	0.284	1.701	4.555	0.236	1.484	4.012	0.320	0.922	1.914
	200	1.816	2.579	-56.020	1.842	-1.783	-11.950	1.881	-1.724	-11890.7
	15	0.720			0.689			0.733		
	25	0.735			0.699			0.829		
298	50	-0.361			-0.399			-0.345		
	75	0.488			-0.434			0.504		
	100	-0.093			-0.133			-0.076		
	150	0.348			0.306			0.366		
	200	1.861			1.822			1.878		
	15	0.718			0.676			0.724		
	25	0.768			0.687			0.827		
303	50	-0.384			-0.416			-0.383		
	75	0.441			0.359			0.425		
	100	-0.123			-0.197			-0.114		
	150	0.322			0.264			0.331		
	200	1.785			1.742			1.805		
	15	0.659			0.609			0.693		
	25	0.768			0.680			0.824		
	50	-0.392			-0.399			-0.368		
313	75	0.415			0.041			0.322		
	100	-0.161			-0.228			-0.131		
	150	0.240			0.171			0.287		
	200	1.762			1.889			1.838		
	15	0.756			0.631			0.699		
	25	0.776			0.682			0.824		
	50	-0.379			-0.396			-0.360		
	75	0.204			0.066			0.423		
323	100	-0.034			-0.198			-0.108		
	150	0.225			0.202			0.295		
	200	1.856			1.917			2.002		

4.5.2 Kinetics and thermodynamics of adsorption of crystal violet dye

Fitting of the contact time data at initial adsorbate concentrations (25, 50, 75 and 100 mg/L) onto *pseudo*-first-order, *pseudo*-second-order, and intraparticle diffusion models formed the basis of the kinetics studies of crystal violet dye adsorption onto the adsorbents, as presented in Table 4.5.2. The intraparticle diffusion model plot data displayed R^2 values that signify a slight linear dependency of q_t on $t^{0.5}$ and non-zero *I* values implying that there were other reaction rate governing steps other than intraparticle diffusion model. The regression constant (R^2) values for the *pseudo*-first order and *pseudo*-second order models were compared to ascertain the one that displayed the best fit. The R^2 values ranged from 0.8247 to 0.9624 and 0.9996 to 0.9998 in *pseudo*-first order and *pseudo*-second order kinetic models, respectively. The *pseudo*-second order kinetic model achieved R^2 values close to 1 hence making it the best fit for describing the equilibrium data.

Table 4.5.2a: Evaluated kinetic models parameters for the adsorption of crystal violet

	***Pseudo*-first order**			***Pseudo*-second order**			**Intra-particle diffusion**		
Conc (mg/L)	K_1 (1/min)	q_e (mg/g)	R^2	K_2 (g/mg.min)	q_e (mg/g)	R^2	K_P (mg/g.min$^{0.5}$)	I	R^2
25	0.0311	0.306	0.9624	0.2762	1.606	0.9998	0.0009	1.4614	0.5460
50	0.0320	0.774	0.8567	0.0872	4.078	0.9998	0.0026	3.6363	0.5412
75	0.0421	0.9559	0.8247	0.1973	5.107	0.9997	0.0020	4.7993	0.3017
100	0.0702	8.696	0.8958	0.0306	7.874	0.9996	0.0064	6.7581	0.6649

4.6 Adsorption isotherm modelling

4.6.1 Isotherm modelling for adsorption of indigo carmine dye

Isotherm models are fundamental concepts of the adsorption phenomenon which explain the interaction between the adsorbate and adsorbent (Nia *et al*., 2017). Langmuir, Freundlich, Temkin, Sips, Toth, Hill and Redlich-Peterson were used to fit the adsorption data (Table 4.6.1a and b, and Figures 4.6.1a, b and c) for activated charcoal and fish scale biochars. The constants q_m, K_L, K_F and n are Langmuir maximum monolayer adsorption capacity (mg/g), Langmuir constant representing the energy of adsorption (L/mg), Freundlich constant (mg/g. Lmg$^{-1/n}$) and Freundlich model constant that indicates the intensity of the adsorption process. The Freundlich models displayed better fit for the data than Langmuir isotherm, based on R^2 values, suggesting multilayer adsorption. The magnitude of *n* describes the favorability of the adsorption process. The *n* values ranging 2-10 represent good, 1-2 for moderately difficult, and less than 1 for a poor adsorptive

potential (Treybal, 1980). In the present study, the magnitudes of *n* were averagely <1 suggesting a poor adsorptive potential.

Langmuir and Freundlich models were engaged to fit the adsorption statistics (Table 4.6.1b) for the biochar magnetic composites. Langmuir isotherm demonstrated a superior fit for the data relative to Freundlich models, established on the coefficient of determination, R^2, values, suggesting uniformly energetic adsorption sites and monolayer adsorption process. This finding is in harmony with other studies; Othman *et al*. (2016) reported Langmuir isotherm model as the best fit for the data in the application of waste *Mozambique tilapia (M. tilapia)* fish scale as a cost-effective adsorbent in removing zinc and ferum ion in wastewater.

Table 4.6.1a: Langmuir and Freundlich constants for biochars and activated charcoal for IC dye removal

Temp (in ^oK)	Activated charcoal	FSB@400 ^oC	FSB@600 ^oC	FSB@800 ^oC
298	Langmuir $q_m = 4315.397$ $K_L = 0.000148$ $R_L=0.074916$ $R^2 = 0.820294$ Freundlich $n = 0.593094$ $K_F = 0.1067498$ $R^2 = 0.89883$	Langmuir $q_m = 629.6546$ $K_L = 0.000213$ $R_L=0.052054$ $R^2 = 0.811603$ Freundlich $n = 0.583608$ $K_F = 0.0095526$ $R^2 = 0.885522$	Langmuir $q_m = 629.6552$ $K_L = 0.000223$ $R_L=0.049720$ $R^2 = 0.841889$ Freundlich $n = 0.515815$ $K_F = 0.0044185$ $R^2 = 0.970335$	Langmuir $q_m = 629.7558$ $K_L = 0.000219$ $R_L=0.050628$ $R^2 = 0.901544$ Freundlich $n = 0.604680$ $K_F = 0.0123151$ $R^2 = 0.992663$
303	Langmuir $q_m = 4315.397$ $K_L = 0.000214$ $R_L=0.051811$ $R^2 = 0.976442$ Freundlich $n = 0.817328$ $K_F = 0.5439812$ $R^2 = 0.996891$	Langmuir $q_m = 629.6547$ $K_L = 0.000229$ $R_L=0.048417$ $R^2 = 0.770375$ Freundlich $n = 0.966324$ $K_F = 0.1277959$ $R^2 = 0.7795$	Langmuir $q_m = 629.6553$ $K_L = 0.000261$ $R_L=0.042481$ $R^2 = 0.748598$ Freundlich $n = 0.463863$ $K_F = 0.002613$ $R^2 = 0.858256$	Langmuir $q_m = 629.7558$ $K_L = 0.000217$ $R_L=0.051094$ $R^2 = 0.836877$ Freundlich $n = 0.706431$ $K_F = 0.0293854$ $R^2 = 0.878623$
313	Langmuir $q_m = 4315.397$ $K_L = 0.000274$ $R_L=0.040466$ $R^2 = 0.839095$ Freundlich $n = 1.047963$ $K_F = 1.3028393$ $R^2 = 0.84032$	Langmuir $q_m = 629.6548$ $K_L = 0.000265$ $R_L=0.041840$ $R^2 = 0.946064$ Freundlich $n = 0.713828$ $K_F = 0.0391229$ $R^2 = 0.994573$	Langmuir $q_m = 629.6554$ $K_L = 0.00028$ $R_L=0.039598$ $R^2 = 0.868669$ Freundlich $n = 0.543744$ $K_F = 0.0088814$ $R^2 = 0.981609$	Langmuir $q_m = 629.7557$ $K_L = 0.000264$ $R_L=0.041998$ $R^2 = 0.936927$ Freundlich $n = 0.702358$ $K_F = 0.0359721$ $R^2 = 0.992653$
323	Langmuir $q_m = 4315.397$ $K_L = 0.000204$ $R_L=0.054351$ $R^2 = 0.840868$ Freundlich $n = 0.542483$ $K_F = 0.121834$ $R^2 = 0.969535$	Langmuir $q_m = 629.6525$ $K_L = 0.000483$ $R_L=0.022956$ $R^2 = 0.833006$ Freundlich $n = 0.787007$ $K_F = 0.1263237$ $R^2 = 0.86768$	Langmuir $q_m = 629.6544$ $K_L = 0.000412$ $R_L=0.026911$ $R^2 = 0.647737$ Freundlich $n = 0.623700$ $K_F = 0.0361503$ $R^2 = 0.73091$	Langmuir $q_m = 629.7541$ $K_L = 0.000471$ $R_L=0.023540$ $R^2 = 0.807417$ Freundlich $n = 0.475355$ $K_F = 0.0086858$ $R^2 = 0.996826$

Table 4.6.1b: Langmuir and Freundlich constants for biochar magnetic composites for IC dye removal

Temp (in ^oK)	FSB@400 ^oC-Fe_3O_4	FSB@600 ^oC-Fe_3O_4	FSB@800 ^oC-Fe_3O_4
298	Langmuir q_m=243.9 K_L=0.0377 R_L=0.3198 R^2=0.9755 Freundlich n=1.11 K_F=0.1713 R^2=0.9110	Langmuir q_m=238.1 K_L=0.0381 R_L=0.3178 R^2=0.9753 Freundlich n=1.11 K_F=0.1733 R^2=0.9108	Langmuir q_m=250.0 K_L=0.0373 R_L=0.3218 R^2=0.9739 Freundlich n=1.10 K_F=0.1671 R^2=0.9095
303	Langmuir q_m=227.3 K_L=0.0407 R_L=0.3057 R^2=0.9746 Freundlich n=1.09 K_F=0.1664 R^2=0.9129	Langmuir q_m=222.2 K_L=0.0408 R_L=0.3053 R^2=0.9756 Freundlich n=1.10 K_F=0.1705 R^2=0.9125	Langmuir q_m=227.3 K_L=0.0410 R_L=0.3044 R^2=0.9730 Freundlich n=1.09 K_F=0.1648 R^2=0.9105
313	Langmuir q_m=243.9 K_L=0.0372 R_L=0.3223 R^2=0.9748 Freundlich n=1.09 K_F=0.1676 R^2=0.9122	Langmuir q_m=217.4 K_L=0.0409 R_L=0.3049 R^2=0.9756 Freundlich n=1.11 K_F=0.1828 R^2=0.8967	Langmuir q_m=227.3 K_L=0.0406 R_L=0.3062 R^2=0.9736 Freundlich n=1.10 K_F=0.1676 R^2=0.9074
323	Langmuir q_m=200.0 K_L=0.0471 R_L=0.2799 R^2=0.9740 Freundlich n=1.09 K_F=0.1663 R^2=0.9060	Langmuir q_m=217.4 K_L=0.0411 R_L=0.3040 R^2=0.9754 Freundlich n=1.12 K_F=0.1832 R^2=0.8963	Langmuir q_m=250.0 K_L=0.0368 R_L=0.3243 R^2=0.9727 Freundlich n=1.12 K_F=0.1757 R^2=0.8972

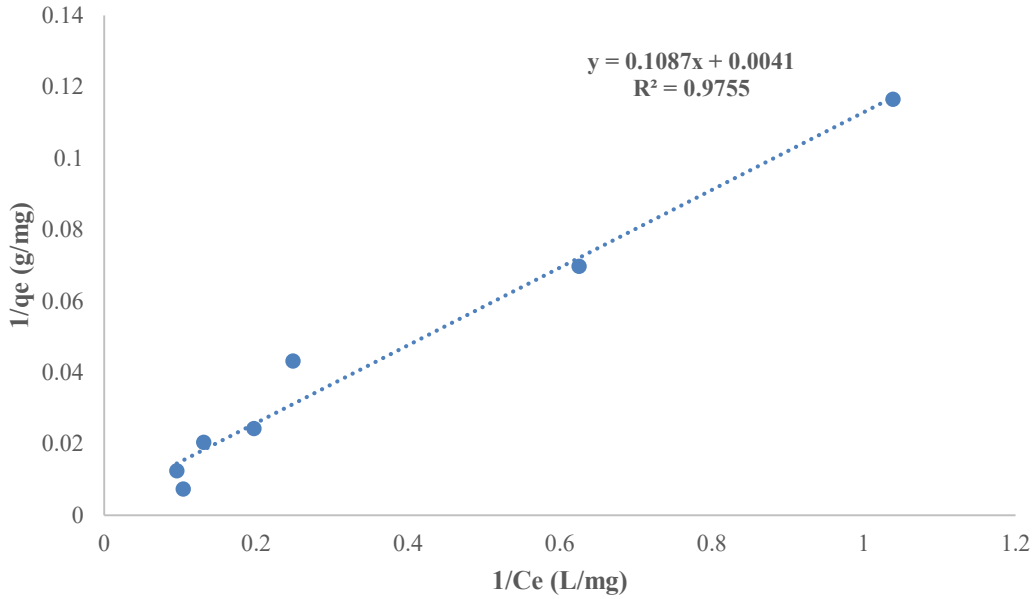

Figure 4.6.1a: Linear Langmuir plot for FSB@400 ºC-Fe_3O_4. Experimental conditions: 30 mL of 15, 25, 50, 75, 100, 150 and 200 mg/L of indigo carmine solution, adsorbent dose of 0.2 g, 200 rpm, and equilibration time of 2 h and 298 K

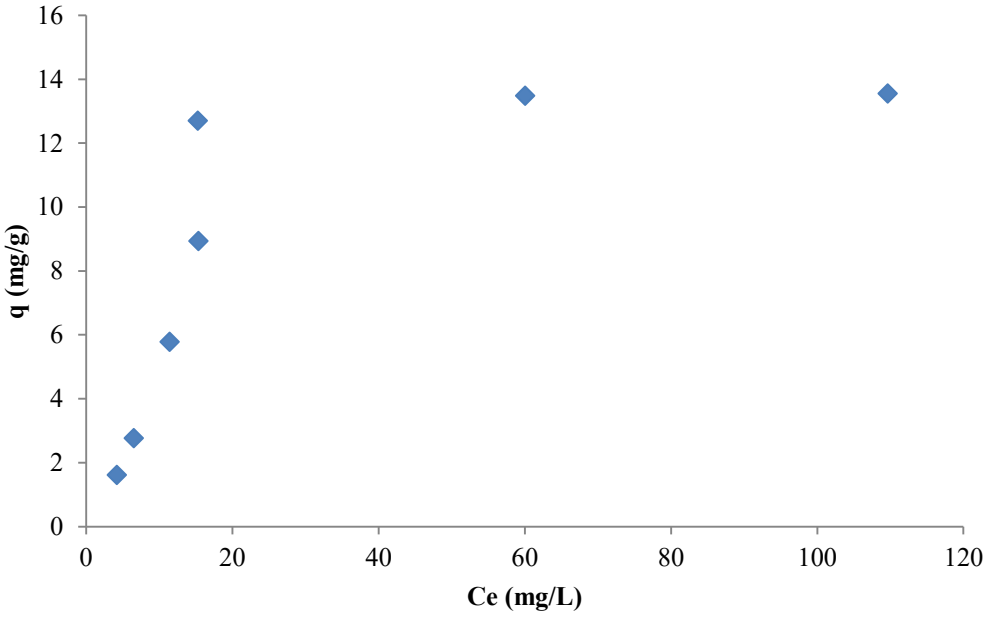

Figure 4.6.1b: Non-linear Langmuir plot for activated charcoal. Experimental conditions include 30 mL of 15, 25, 50, 75 and 100 mg/L of indigo carmine, adsorbent dose of 0.2 g, 200 rpm, equilibration time of 2 h and 298 K.

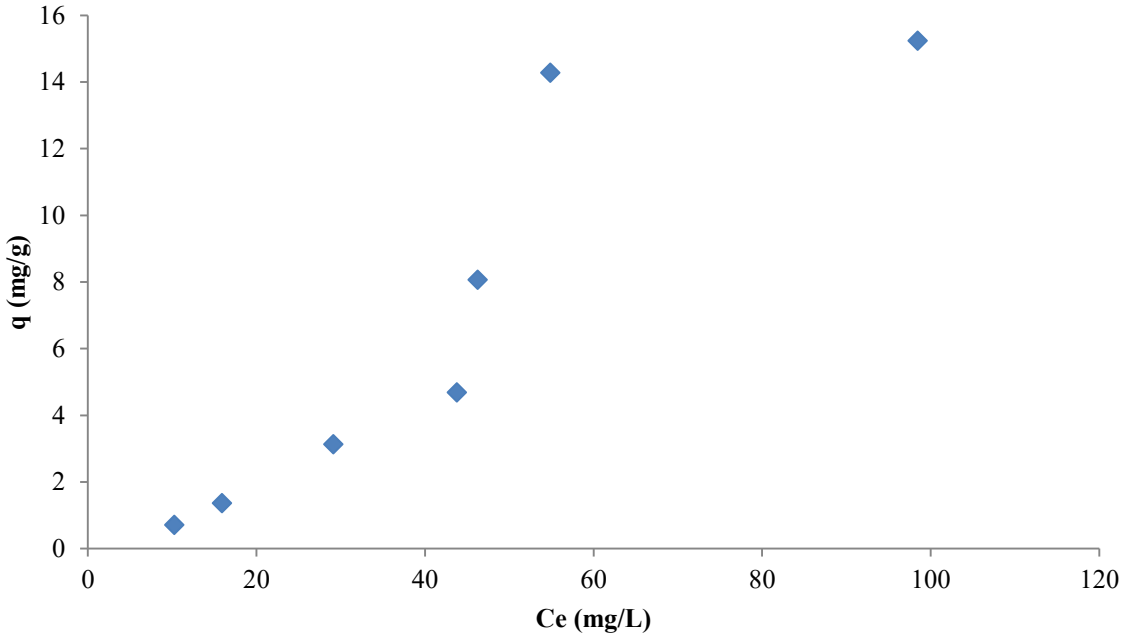

Figure 4.6.1c: Non-linear Langmuir plot for FSB@400 °C. Experimental conditions include: 30 mL of 15, 25, 50, 75 and 100 mg/L of indigo carmine dye, 0.2 g of FSB@400°C, 200 rpm and 298 K

Table 4.6.1c: Calculated parameters for Temkin, Sips, Toth, Redlich-Peterson, and Hill isotherm models for adsorption of indigo carmine dye by fish scale biochars (FSB), magnetic composites (FSB@Fe_3O_4) and activated charcoal (AC)

Adsorbents	Isotherm models for adsorption of indigo carmine dye				
	Temkin	**Sips**	**Toth**	**Redlich-Peterson**	**Hill**
FSB@400 ºC	$B=2.26x10^{8}$	$a_s=3.52x10^{-8}$	$z=11.7963$	$g=2.62218$	$n_H=3.282799$
	$A_T=1.84x10^{9}$	$q_{ms}=546.91$	$q_{mT}=2.29x10^{24}$	$a_R= 0$	$q_{SH}= 17.1048$
	$R^2= 0$	$B_s=3.9467$	$a_T=9.48x10^{23}$	$K_R=0.134684$	$K_D=2.065x10^{5}$
		$R^2=0.001$	$R^2= 0.593663$	$R^2= 0.637631$	$R^2=0.478516$
FSB@600 ºC	$B=2.26x10^{8}$	$a_s=3.52x10^{-8}$	$z=11.13524$	$g=2.62218$	$n_H= 4.8603$
	$A_T=1.84x10^{9}$	$q_{ms}=546.91$	$q_{mT}=2.81x10^{22}$	$a_R= 0$	$q_{SH}= 17.4848$
	$R^2= 0$	$B_s=3.9467$	$a_T=9.26x10^{21}$	$K_R=0.134684$	$K_D=1.989x10^{7}$
		$R^2=0.0024$	$R^2=0.62153$	$R^2=0.637408$	$R^2=0.475728$
FSB@800 ºC	$B=2.26x10^{8}$	$a_s=3.52x10^{-8}$	$z=4.289792$	$g=2.62218$	$n_H= 3.271708$
	$A_T=1.84x10^{9}$	$q_{ms}=546.91$	$q_{mT}=1.15x10^{9}$	$a_R= 0$	$q_{SH}= 16.87861$
	$R^2= 0$	$B_s=3.9467$	$a_T=1.33x10^{9}$	$K_R=0.134684$	$K_D=1.887x10^{5}$
		$R^2=0.001$	$R^2=0.598783$	$R^2=0.6379$	$R^2=0.483283$
Activated Charcoal	$B=2.26x10^{8}$	$a_s=3.52x10^{-8}$	$z=1.471726$	$g=2.62218$	$n_H= 2.568381$
	$A_T=1.84x10^{9}$	$q_{ms}=546.91$	$q_{mT}=195.78$	$a_R= 0$	$q_{SH}= 14.12795$
	$R^2= 0$	$B_s=3.9467$	$a_T=116.995$	$K_R=0.134684$	$K_D=1.624x10^{2}$
		$R^2=0.001$	$R^2=0.573629$	$R^2=0.319804$	$R^2=0.490635$

The adsorption of the anionic dye of Acid Black 210 (AB210) from aqueous solutions by a magnetically separable Fe_3O_4/CeO_2 (Fe/Ce) nanocomposite was well described by the Langmuir isotherm model (Gao *et al*., 2019). The extent of n defines favourability of adsorption route. Values of n between 2-10 denote good, 1-2 for moderately and energetically not favourable, and <1 for a reduced adsorptive potential (Treybal, 1981). This study registered average n values in the range 1-2, suggesting a moderately and energetically not favourable adsorption process. Relationship between R_L and C_o, which signify features of Langmuir isotherm for fish scales biochar magnetic composites (FSB@Fe_3O_4), is presented in Figure 4.6.1d. The R_L for initial indigo carmine dye concentrations fall between 0.022956-0.074916 and 0.2799-0.3243 for FSB and FSB@Fe_3O_4, respectively, signifying a favourable adsorption process of the indigo carmine dye under the considered experimental conditions.

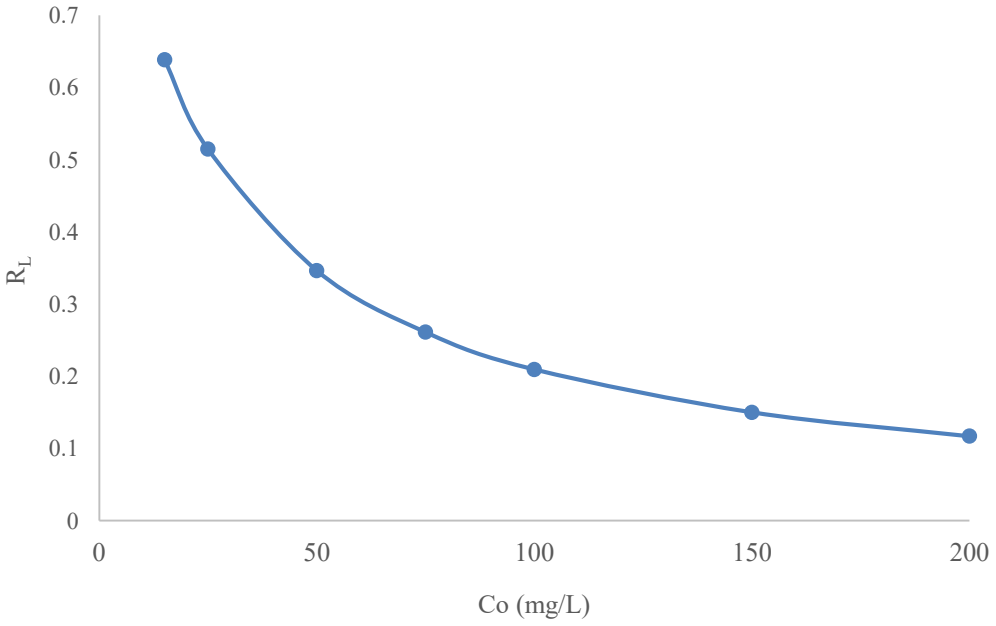

Figure 4.6.1d: Dimensionless separation factor (R_L) for the FSB@400 ºC-Fe_3O_4

Konicki *et al*. (2017) reported R_L values in the range of 0-1 for the adsorption of Acid Orange 8 (AO8) and Direct Red 23 (DR23) dyes onto graphene oxide (GO) suggesting a favourable process. The calculated value of $B_T \ln A_T$ for the Temkin isotherm model was 4.877 x 10^{-10} kJ mol^{-1}, presenting a very low energy value that suggests a physisorption interaction between the indigo carmine dye and the FSB@Fe_3O_4 adsorbing sites (Table 4.6.1c). Rahangdale & Kumar (2018) reported that adsorption energies ($B_T \ln A_T$) in the range of 8-16 kJ mol^{-1} denote chemisorption mechanisms. In this study, the positive b_T values are also attributed to thermodynamically exothermic processes (Miraboutalebi *et al*., 2017). However, the model recorded zero values for R^2, implying that it is not appropriate for explaining the adsorption of indigo carmine onto the magnetic composites. Konicki *et al*. (2017) reported experimental data whose Temkin model's correlation coefficient values were lower than those obtained for the Langmuir model for the adsorption of Acid Orange 8 (AO8) and Direct Red 23 (DR23) onto graphene oxide (GO). The Sips isotherm experimental data displayed a poor fitting as reflected by the low coefficient of determination, R^2, value (Table 4.6.1c). The surfaces of the magnetic composites were relatively heterogeneous as depicted by the very low positive values of the constant B_s. However, Gholami *et al*. (2018) reported experimental data on the application of nanomagnetic Fe_3O_4@Fish scale as a bio-adsorbent for removal of Methylene Blue (MB), which were well described by the Sips isotherm model. The calculated parameters for the Toth isotherm model are highlighted in Table 4.61c. The magnitude of *z* was above unity signifying a heterogeneous adsorption

system. Hossain *et al*. (2012) reported that a system becomes heterogeneous as z deviates from unity. The experimental data and the average value of the coefficient of determination indicated that the Toth isotherm model could be used to explain the adsorption process. The Redlich-Peterson isotherm displayed a moderate R^2 value (0.5342), inferring its attempt to describe the experimental data. The calculated g value shows the non-heterogeneity of the sorption system (Table 4.6.1c). Moreover, the extremely low predicted maximum adsorption capacity (0.155 mg/g) inconsistent with the equilibrium data signifies the inappropriateness of the Redlich-Peterson isotherm model to describe indigo carmine dye uptake onto FSB@Fe_3O_4. A relatively high value of the coefficient of determination (R^2=0.9952) for the Redlich-Peterson isotherm model was reported by Gholami *et al*. (2018) for the adsorption of methylene blue (MB) onto magnetic fish scales (MFS). Konicki *et al*. (2017) reported calculated values of g closer to unity for the adsorption of Acid Orange 8 (AO8) and Direct Red 23 (DR23) onto graphene oxide (GO) implying the applicability of the model in describing the adsorption process. The Hill isotherm model displayed an average R^2 value of 0.5016 and the calculated n_H value of 2.048 signifying positive cooperativity in the binding of indigo carmine dye particles onto the homogenous surface of FSB@Fe_3O_4. Positive cooperativity in binding was also documented for the adsorption of Cu^{2+} ions onto fish scale biochar (Achieng' & Shikuku, 2020). It is concluded that the removal mechanisms and kinetics of anionic indigo carmine dye onto activated charcoal, FSB and FSB@Fe_3O_4 were plausible. In addition, enthalpy and entropy were the main parameters that were driving the adsorption process.

4.6.2 Isotherm modelling for adsorption of crystal violet dye

The isotherm modelling was conducted to examine the model that best explained the adsorption process. The evaluated models were Langmuir, Freundlich, Temkin, Sips, Toth, Hill and Redlich-Peterson (Table 4.6.2a, b and c). Maximum adsorption capacity (q_m) afforded by the adsorbents ranged from 29.59 to 666.7 mg/g. The favourability of adsorption route, n, indicated that the adsorption process was moderately and energetically not favourable since the values of n recorded were in the range of 1-2. The coefficient of determination (R^2) for the models were compared and it was observed that the average R^2 values for Langmuir isotherm model was the closest to 1 amongst the surveyed models, implying that it best explained the adsorption process compared to the rest of the models. The R_L for initial crystal violet dye concentrations fall between 0.021985-0.022175 and 0.222172-0.022175 for FSB and FSB@Fe_3O_4, respectively, signifying a favourable adsorption process of the crystal violet dye under the considered experimental conditions (Figures 4.6.2a and b). The isotherm modelling for the adsorption of crystal violet dye from its aqueous solution onto tamarind (*Tamarindus indica)* fruit shell powder was investigated using Freundlich and Langmuir isotherms (Patel & Vashi, 2010). Freundlich isotherm was found to be most applicable in describing the adsorption process. Loulidi *et al*. (2020) reported that modulation of adsorption isotherms for crystal violet onto an agricultural waste residue followed the Langmuir model.

Table 4.6.2a: Langmuir and Freundlich constants for biochars and activated charcoal for CV dye removal

Temp (in ^oK)	Adsorbents			
	Activated Charcoal	**FSB@400 ^oC**	**FSB@600 ^oC**	**FSB@800 ^oC**
298	Langmuir q_m=169.49 K_L=0.10 R_L=0.022088 R^2=0.9375 Freundlich n=1.52 K_F=12.78 R^2=0.7923	Langmuir q_m=263.16 K_L=0.00044 R_L=0.022175 R^2=0.9770 Freundlich n=1.23 K_F=0.209 R^2=0.9129	Langmuir q_m=222.22 K_L=0.00069 R_L=0.022175 R^2=0.9821 Freundlich n=1.17 K_F=0.2330 R^2=0.9650	Langmuir q_m=29.59 K_L=0.0049 R_L=0.022171 R^2=0.9830 Freundlich n=1.35 K_F=0.2829 R^2=0.9399
303	Langmuir q_m=238.10 K_L=0.07 R_L=0.022113 R^2=0.9717 Freundlich n=1.51 K_F=12.49 R^2=0.8155	Langmuir q_m=57.47 K_L=0.0025 R_L=0.022173 R^2=0.9562 Freundlich n=1.36 K_F=0.3038 R^2=0.9099	Langmuir q_m=86.96 K_L=0.0018 R_L=0.022174 R^2=0.9945 Freundlich n=1.14 K_F=0.2181 R^2=0.9775	Langmuir q_m=34.48 K_L=0.0044 R_L=0.022171 R^2=0.9704 Freundlich n=1.34 K_F=0.2925 R^2=0.9441
313	Langmuir q_m=81.96 K_L=0.22 R_L=0.021985 R^2=0.9615 Freundlich n=1.52 K_F=12.23 R^2=0.8246	Langmuir q_m=89.29 K_L=0.0017 R_L=0.022174 R^2=0.9811 Freundlich n=1.26 K_F=0.2726 R^2=0.9204	Langmuir q_m=108.70 K_L=0.0014 R_L=0.022174 R^2=0.9915 Freundlich n=1.11 K_F=0.2047 R^2=0.9789	Langmuir q_m=53.48 K_L=0.0027 R_L=0.022173 R^2=0.9657 Freundlich n=1.30 K_F=0.2746 R^2=0.9413
323	Langmuir q_m=166.67 K_L=0.10 R_L=0.022088 R^2=0.9664 Freundlich n=1.49 K_F=12.18 R^2=0.8227	Langmuir q_m=57.14 K_L=0.0026 R_L=0.022173 R^2=0.9790 Freundlich n=1.23 K_F=0.2486 R^2=0.9478	Langmuir q_m=74.63 K_L=0.0021 R_L=0.022173 R^2=0.9919 Freundlich n=1.06 K_F=0.1765 R^2=0.9762	Langmuir q_m=51.02 K_L=0.0029 R_L=0.022173 R^2=0.9693 Freundlich n=1.28 K_F=0.2687 R^2=0.9555

Table 4.6.2b: Langmuir and Freundlich constants for magnetic composites for CV dye removal

	Adsorbents		
Temp (in ^oK)	**FSB@400 ^oC-Fe_3O_4**	**FSB@600 ^oC-Fe_3O_4**	**FSB@800 ^oC-Fe_3O_4**
298	Langmuir q_m=238.10 K_L=0.0005 R_L=0.022175 R^2=0.9785 Freundlich n=1.19 K_F=0.19 R^2=0.9611	Langmuir q_m=333.30 K_L=0.0004 R_L=0.022175 R^2=0.9883 Freundlich n=1.15 K_F=0.21 R^2=0.9437	Langmuir q_m=277.00 K_L=0.0004 R_L=0.022175 R^2=0.9921 Freundlich n=1.19 K_F=0.20 R^2=0.9463
303	Langmuir q_m=714.29 K_L=0.0002 R_L=0.022175 R^2=0.9754 Freundlich n=1.20 K_F=0.20 R^2=0.9427	Langmuir q_m=43.86 K_L=0.0036 R_L=0.022172 R^2=0.9918 Freundlich n=1.17 K_F=0.23 R^2=0.9618	Langmuir q_m=57.80 K_L=0.0021 R_L=0.022173 R^2=0.9960 Freundlich n=1.17 K_F=0.18 R^2=0.9647
313	Langmuir q_m=312.50 K_L=0.0004 R_L=0.022175 R^2=0.9849 Freundlich n=1.16 K_F=0.19 R^2=0.9591	Langmuir q_m=87.72 K_L=0.0017 R_L=0.022174 R^2=0.9930 Freundlich n=1.14 K_F=0.21 R^2=0.9585	Langmuir q_m=192.31 K_L=0.0006 R_L=0.022175 R^2=0.9948 Freundlich n=1.12 K_F=0.16 R^2=0.9810
323	Langmuir q_m=84.03 K_L=0.0015 R_L=0.022174 R^2=0.9930 Freundlich n=1.13 K_F=0.17 R^2=0.9644	Langmuir q_m=666.67 K_L=0.0002 R_L=0.022175 R^2=0.9951 Freundlich n=1.09 K_F=0.18 R^2=0.9579	Langmuir q_m=256.41 K_L=0.0005 R_L=0.022175 R^2=0.9931 Freundlich n=1.11 K_F=0.16 R^2=0.9796

Table 4.6.2c: Calculated parameters for Temkin, Sips, Toth, Redlich-Peterson, and Hill isotherm models for adsorption of crystal violet dyes by fish scale biochars (FSB), magnetic composites (FSB@Fe_3O_4) and activated charcoal (AC)

Adsorbents	Isotherm models for adsorption of indigo carmine dye				
	Temkin	**Sips**	**Toth**	**Redlich-Peterson**	**Hill**
FSB@400 ºC-Fe_3O_4	$B=2.26 \times 10^{-8}$ $A_T=2.35 \times 10^{9}$ $R^2= 0.000$	$a_s=3.52 \times 10^{-8}$ $q_{ms}=546.9$ $B_s=3.946$ $R^2= 0.0003$	$z=4.425$ $q_{mT}=1.68 \times 10^{9}$ $a_T=2.54 \times 10^{9}$ $R^2= 0.52065$	$g=2.915$ $a_R=6.53 \times 10^{-7}$ $K_R=0.155$ $R^2= 0.536321$	$n_H=1.950$ $q_{SH}=11.378$ $K_D=1028.91$ $R^2= 0.503825$
FSB@600 ºC-Fe_3O_4	$B=2.26 \times 10^{-8}$ $A_T=2.35 \times 10^{9}$ $R^2= 0.000$	$a_s=3.52 \times 10^{-8}$ $q_{ms}=546.9$ $B_s=3.947$ $R^2= 0.0003$	$z=4.108$ $q_{mT}=3.02 \times 10^{8}$ $a_T=4.65 \times 10^{8}$ $R^2= 0.522317$	$g=2.915$ $a_R=6.53 \times 10^{-7}$ $K_R=0.155$ $R^2= 0.53654$	$n_H=2.177$ $q_{SH}=10.81$ $K_D=1782.20$ $R^2= 0.498846$
FSB@800 ºC-Fe_3O_4	$B=2.26 \times 10^{-8}$ $A_T=2.35 \times 10^{9}$ $R^2= 0.000$	$a_s=3.52 \times 10^{-8}$ $q_{ms}=546.9$ $B_s=3.947$ $R^2= 0.0003$	$z=4.308$ $q_{mT}=9.05 \times 10^{8}$ $a_T=1.41 \times 10^{9}$ $R^2= 0.520043$	$g=2.915$ $a_R=6.53 \times 10^{-7}$ $K_R=0.155$ $R^2= 0.529614$	$n_H=2.017$ $q_{SH}=11.043$ $K_D=1217.04$ $R^2= 0.502098$

It is concluded that the removal mechanisms and kinetics of cationic crystal violet dye onto activated charcoal, FSB and FSB@Fe_3O_4 were plausible. In addition, enthalpy and entropy were the main parameters that were driving the adsorption process.

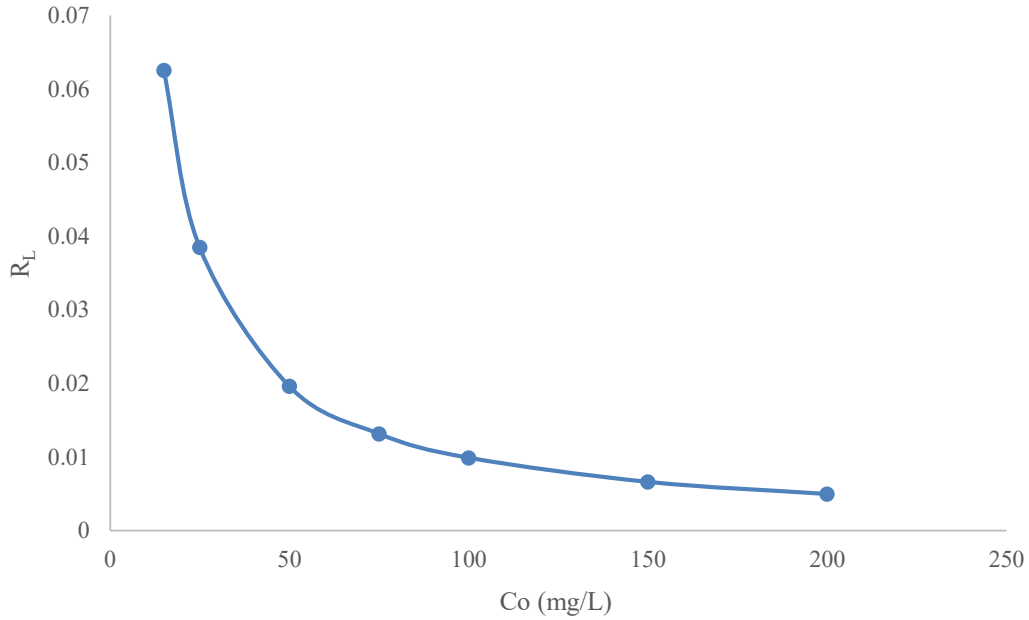

Figure 4.6.2a: Dimensionless separation factor (R_L) for the FSB@400 ºC for CV removal

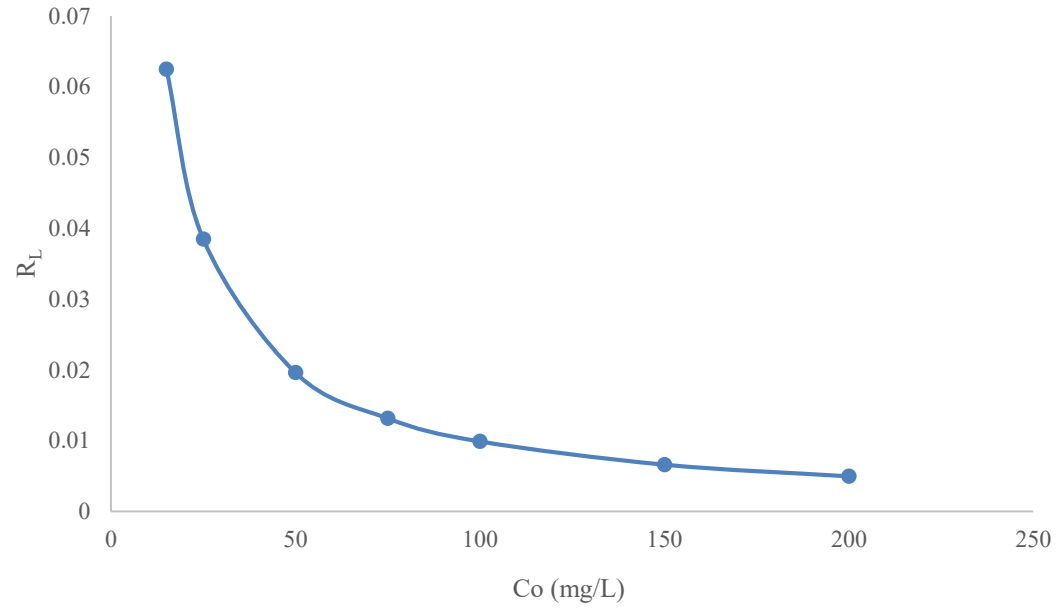

Figure 4.6.2b: Dimensionless separation factor (R_L) for the FSB@400 ºC-Fe_3O_4 for CV removal

4.7 Characterization of the spent adsorbents

4.7.1 Adsorbents spent on adsorption of indigo carmine dye

In attempts to establish any morphological and chemical changes to the adsorbents during adsorption, we analyzed the used adsorbents using FT-IR and SEM-EDX (Figure 4.7.1). Notably, SEM image of fresh FSB@400 ^{o}C exhibited morphologically different surfaces relative to the used FSB@400 ^{o}C-IC (Figure 4.7.1a). This is due to aggregation of adsorbate molecules on the adsorbent surface (Bordoloi *et al*., 2018). In addition, elemental composition analysis by EDX revealed the presence of N, H, S and Na (Table 4.2.4 and Figure 4.2.4) supporting the adsorption of indigo carmine dye onto FSB@400 ^{o}C. Gholami *et al*. (2018) reported the presence of N and S elements from methyl blue (MB) dye on the surface of used magnetic fish scales (UMFS) confirming the adsorption of the dye. In addition, the spots of FSB@400 ^{o}C-IC on the TEM micrograph were blurred due to surface coverage with dye molecules (Figure 4.7.1b). The FT-IR spectrum of the used adsorbent (Figure 4.7.1d) displayed some changes on the surface of the adsorbent. For instance, the peak at 872 cm^{-1} shifted to 876 cm^{-1}. Similarly, the observed reductions in the intensities of some peaks, demonstrates the interaction between the dye and the adsorbents (Ooi *et al*., 2017).

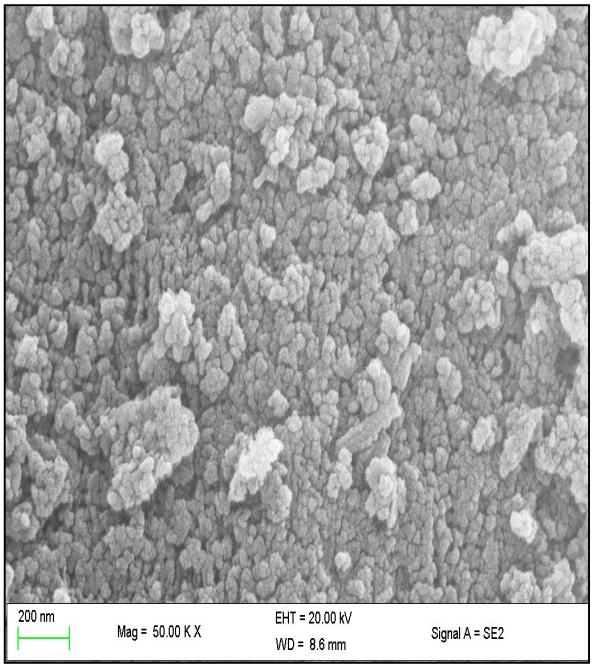
200 nm
Mag = 50.00 K X
EHT = 20.00 kV
WD = 8.6 mm
Signal A = SE2

(a)

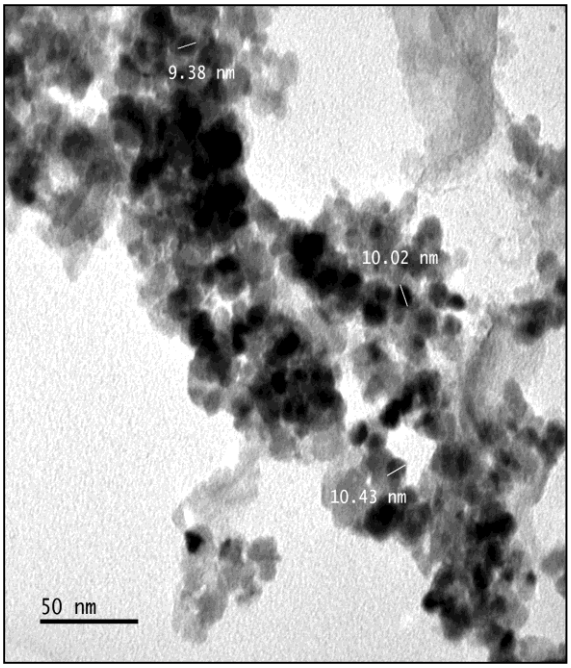
9.38 nm
10.02 nm
10.43 nm
50 nm

(b)

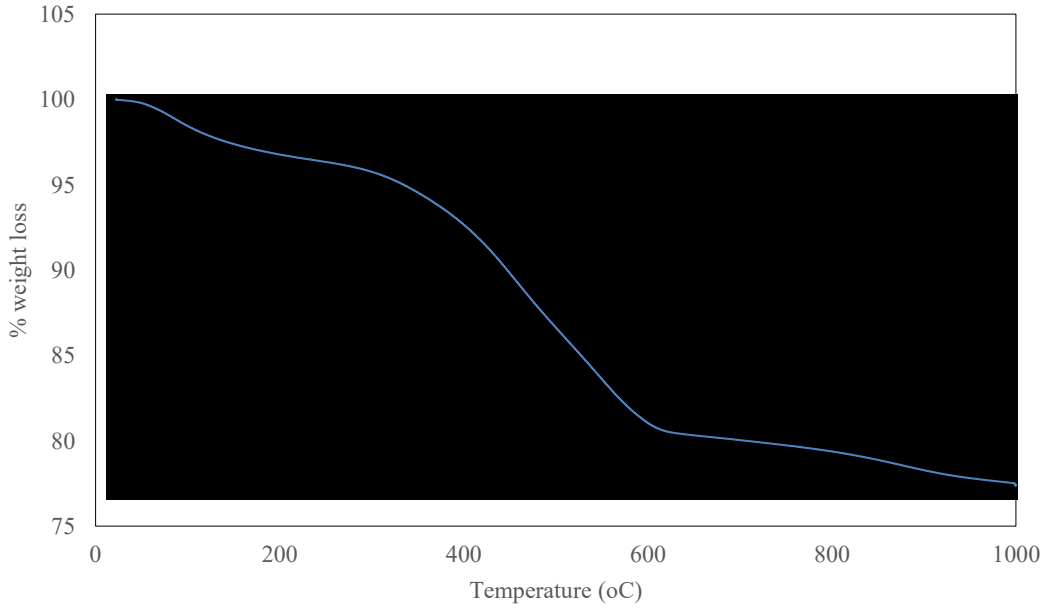
105
100
95
90
85
80
75
% weight loss
0
200
400
600
800
1000
Temperature (oC)

(c)

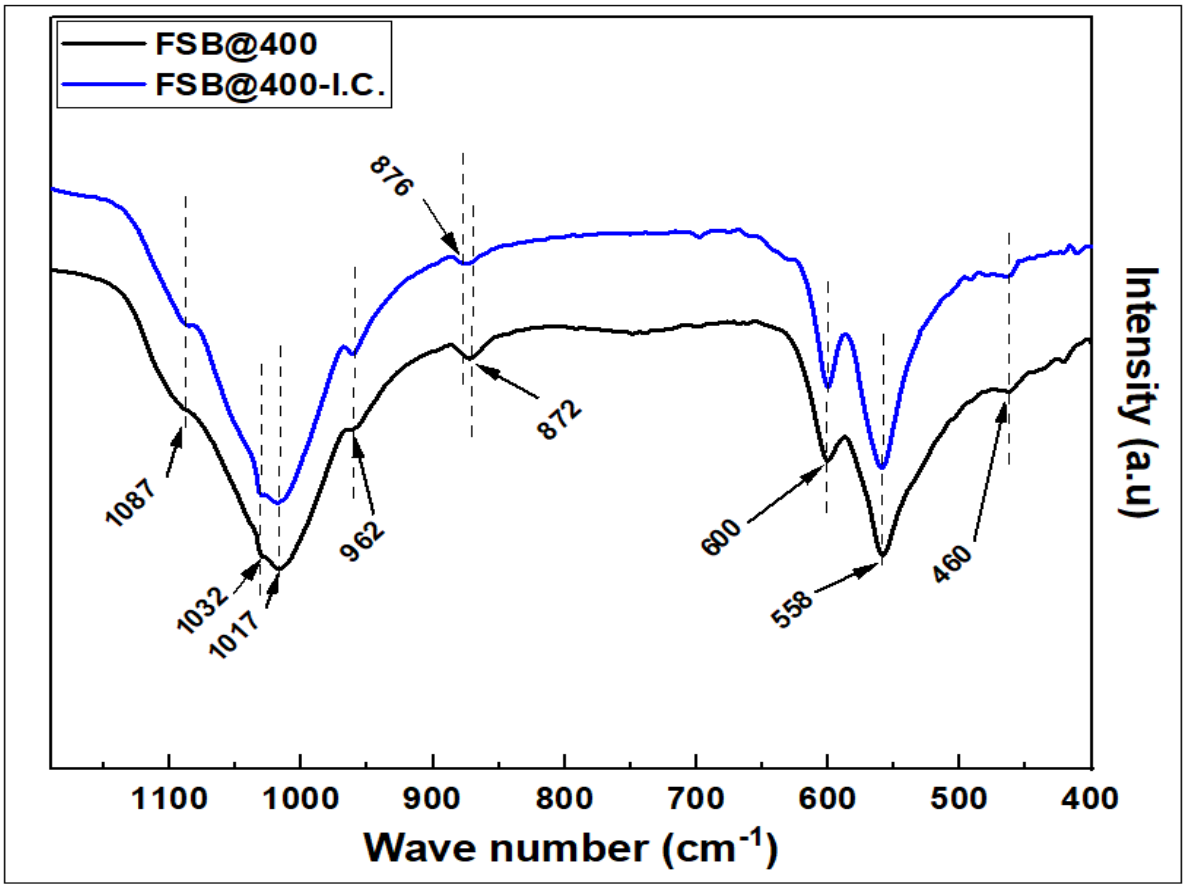

(d)

Figure 4.7.1: (a) SEM image of FSB@400ºC-IC, (b) TEM image of FSB@400 ºC-IC, (c) TGA of FSB@400 ºC-IC, (d) FT-IR of FSB@400 ºC and FSB@400 ºC-IC

Suspected morphological and chemical changes on the spent magnetic composites were analyzed on TEM, FT-IR and SEM-EDX (Table 4.2.4 and Figure 4.2.4). Notably, SEM micrograph of FSB@400 ºC-Fe_3O_4 displayed a morphologically dissimilar surface comparative to spent FSB@400 ºC-Fe_3O_4-I.C. (Figures 4.2.4b and c), an observation attributed to the accumulation of dye particles on the surface of the adsorbent (Bordoloi *et al*., 2018). Analysis of chemical constitution by EDX showed the existence of nitrogen, sulphur and sodium (Table 4.2.4 and Figure 4.2.4) proving that indigo carmine

dye was adsorbed onto FSB@400 ^{o}C-Fe_3O_4. In another study, existence of nitrogen and sulphur elements from methyl blue dye on the surface of spent fish scales magnetic composite was reported, thus, ratifying the adsorption of the dye (Gholami *et al*., 2018). Additionally, the spots of FSB@400 ^{o}C-Fe_3O_4-I.C. on TEM images were blurry owing to surface coverage with dye particles (Figure 4.2.4f). The FT-IR spectra of spent magnetic composite (Figure 4.2.2c) exhibited some differences on the surface in which the peaks of FSB@400 ^{o}C-Fe_3O_4-I.C appeared less intense than those in FSB@400 ^{o}C-Fe_3O_4. The observed declines in intensities of some peaks validate dye and adsorbents interaction (Ooi *et al*., 2017). To determine whether there was a chemical change on the adsorbed indigo carmine dye particles, desorption was done on the spent adsorbent using three runs of 10 mL ethyl alcohol. The desorbed dye solution was characterized on UV-Vis Spectrophotometer at wavelength 611 nm. The concentrations of the adsorbed and desorbed indigo carmine dyes were non-significantly different confirming that there was no chemical change on the dye molecule, further corroborating the physisorption nature of the adsorption process.

4.7.2 Adsorbents spent on adsorption of crystal violet dye

Characterization of the spent adsorbent was done to determine any morphological and chemical changes on its surface. The SEM micrograph of spent adsorbent (Figure 4.2.6f) showed that its surface was covered with dye particles. This observation was confirmed by the EDX spectrum of the spent adsorbent, which was characterized by increased concentrations of N and Cl atoms compared to the biochar FSB@400 ^{o}C (Table 4.2.4 and Figure 4.2.4). The FT-IR spectrum of FSB@400 ^{o}C displayed a shift of

wavenumbers from 872 cm^{-1} to 876 cm^{-1} in the spectrum of the spent adsorbent, FSB@400 ºC-C.V. (Figure 4.7.2).

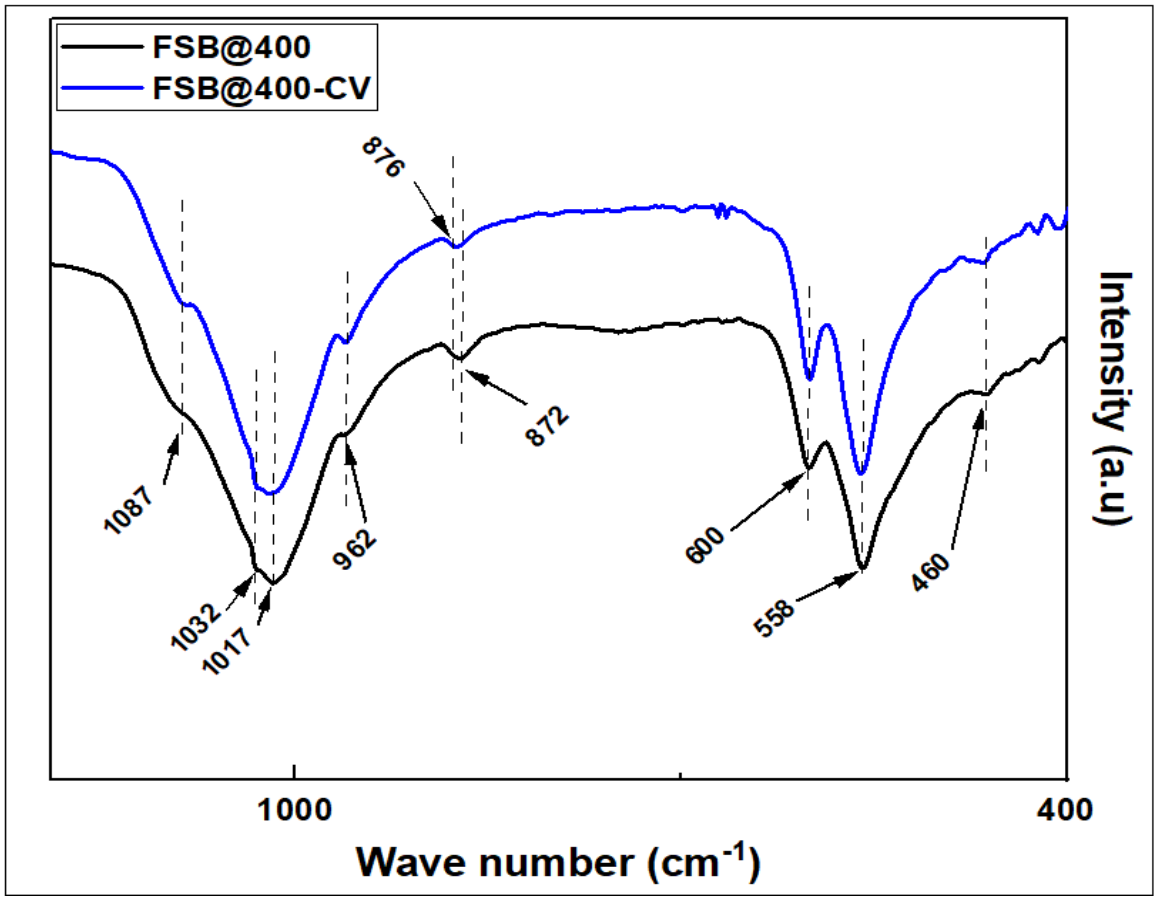

Figure 4.7.2: FT-IR spectra of FSB@400 ºC and FSB@400 ºC and FSB@400 ºC-CV

The desorbed crystal violet dye solution was characterized on UV-Vis Spectrophotometer at wavelength 588 nm. The concentrations of the adsorbed and desorbed crystal violet dye were non-significantly different confirming that there was no chemical change on the dye molecule, further corroborating the physisorption nature of the adsorption process.

4.8 Stability test and regeneration/recycling of FSB@Fe_3O_4 adsorbents

The results of the leaching test for the magnetic composites (FSB@Fe_3O_4) carried out at pH2 and 10 are given in Tables 4.8a and b. The concentrations of iron (Fe) in the supernatants were averagely 0.02 mg/L, an indication of the high stability of the synthesized composites. Leaching of Fe was effectively prevented at extremely acidic condition due to the protection of SiO_2 and anionic polyacrylamide-modified-chitosan (CS-PAA) (Zheng *et al*., 2020), as evidenced in the observed insignificant loss of Fe from anionic polyacrylamide-modified-chitosan magnetic (Fe_3O_4) composite (FS@CS-PAA) nanoparticles in the whole tested pH range signifying that FS@CS-PAA had good stability.

Table 4.8a: Leaching of metals (mg/L) from the magnetic composites at pH 2

Adsorbent	Concentrations			
	Ca	**Mg**	**Na**	**Fe**
FSB@400 ºC-Fe_3O_4	<0.01±0.00	0.77±0.06	0.63±0.01	0.02±0.00
FSB@600 ºC-Fe_3O_4	<0.01±0.00	0.34±0.01	0.63±0.01	0.02±0.00
FSB@800 ºC-Fe_3O_4	<0.01±0.00	0.55±0.02	0.63±0.02	0.02±0.00

Table 4.8b: Leaching of metals (mg/L) from the magnetic composites at pH 10

Adsorbent	Concentrations			
	Ca	**Mg**	**Na**	**Fe**
FSB@400 ºC-Fe_3O_4	<0.01±0.00	0.45±0.02	0.60±0.01	0.01±0.00
FSB@600 ºC-Fe_3O_4	<0.01±0.00	0.32±0.01	0.62±0.02	0.02±0.00
FSB@800 ºC-Fe_3O_4	<0.01±0.00	0.52±0.02	0.60±0.01	0.01±0.00

In another study, Song *et al*. (2014) investigated the stability of water-soluble polyacrylamide coated-Fe_3O_4 magnetic composites (Fe_3O_4@-PAM) and reported <1% leaching of Fe in 0.02 mol/L HCl solution for 96 hours, demonstrating that PAM coat prevented the dissolution of Fe_3O_4. Essandoh & Garcia (2018) reported a similar finding on a novel hemoglobin/iron oxide composite (Hb/Fe_3O_4). The observation made in the current research endorses the magnetic composite (FSB@Fe_3O_4) for industrial application in the treatment of dye wastewater. The reusability of an adsorbent is an important aspect in assessing its practicability for adsorbate removal from an aqueous solution. In this research, the spent adsorbents were separated from the adsorption mixture by an external magnet, washed three times using 10 mL of ethyl alcohol and dried in the oven. The adsorption experiment was then repeated five times by dispersing 0.2 g of the adsorbents in 30 mL of 25 mg/L indigo carmine dye solution. The analysis data on the reusability of the materials showed that the adsorbents conserved their

adsorption capacities for the abstraction of indigo carmine dye for five consecutive cycles without significant depletion (Figures 4.8a and b). Concerning adsorbent FSB@600 ^{o}C-Fe_3O_4, the adsorption capacities (q_e) were recorded as 1.6194, 1.6185, 1.6144, 1.6128 and 1.6094 mg/g, respectively, for cycles 1, 2, 3, 4 and 5. However, significant loss of adsorption capacity was recorded for crystal violet dye in the fifth cycle (Figure 4.8b). In a similar study, Zhang *et al*. (2020) reported that the prepared porous carbon/Fe_3O_4-600 composite retained an excellent adsorption capacity for the removal of methyl orange dye after four cycles, therefore, qualifying it as an outstanding material for recyclable dye adsorbent. Four adsorption and regeneration cycles on a novel hemoglobin/iron oxide composite (Hb/Fe_3O_4) established that the adsorption capacity for indigo carmine dye reduced by 2% of the initial capacity (Essandoh & Garcia, 2018). However, the researchers noted that the regeneration treatment was not effective for 300 mg/L dye solution leading to lose of reusability. Recycle adsorption experiments using calcination method also showed that the prepared monodisperse porous silica nanospheres (SiO_2 NSs) were recycled at least six times while the removal efficiencies for Alcian blue (AB) and methylene blue (MB) dyes had no significant decrease (Lv *et al*., 2018). In another study, reusability of fish (Dicentrarchus labrax) scales (FS) in the adsorption of Acid Blue (AB) 121 dye was surveyed (Uzunoğlu & Özer, 2016). The findings indicated that while the adsorbed AB 121 amount by FS in the first and eighth cycles were 98.5 and 39.9 mg/g, respectively. Since FS displayed high structural stability even after multi-cycles use, the researchers concluded that it could be considered as an adsorbent in the removal of the dye anions. Rangabhashiyam *et al*. (2018) investigated

the reusability of *Carica papaya* wood (CPW) for five successive cycles in the biosorption of methylene blue (MB) and malachite green (MG) dyes from simulated wastewater. The results of the regeneration of the dyes were more than 80% removal efficiency in all five cycles. A study by Gholami *et al*. (2018) on the reusability potential of magnetic fish scales (MFS) showed an efficiency of 59.63% in the adsorption of methylene blue (MB) dye. In addition, a regenerative study on adsorption of synthetic methylene blue (MB) dye onto graphene oxide-magnetic iron oxide nanoparticles (GO-MNP) adsorbent revealed a minor reduction in adsorption capacity of the regenerated adsorbent after 2 cycles (Othman *et al*., 2018).

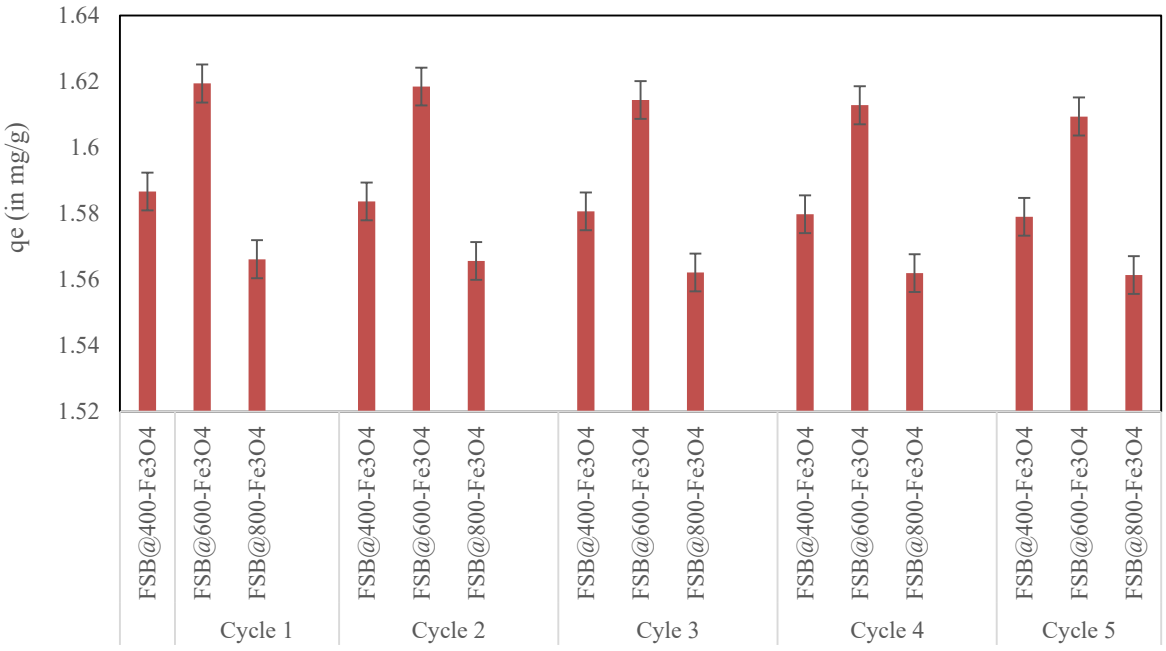

Figure 4.8a: Reusability of the adsorbents for the removal of indigo carmine dye from aqueous solution

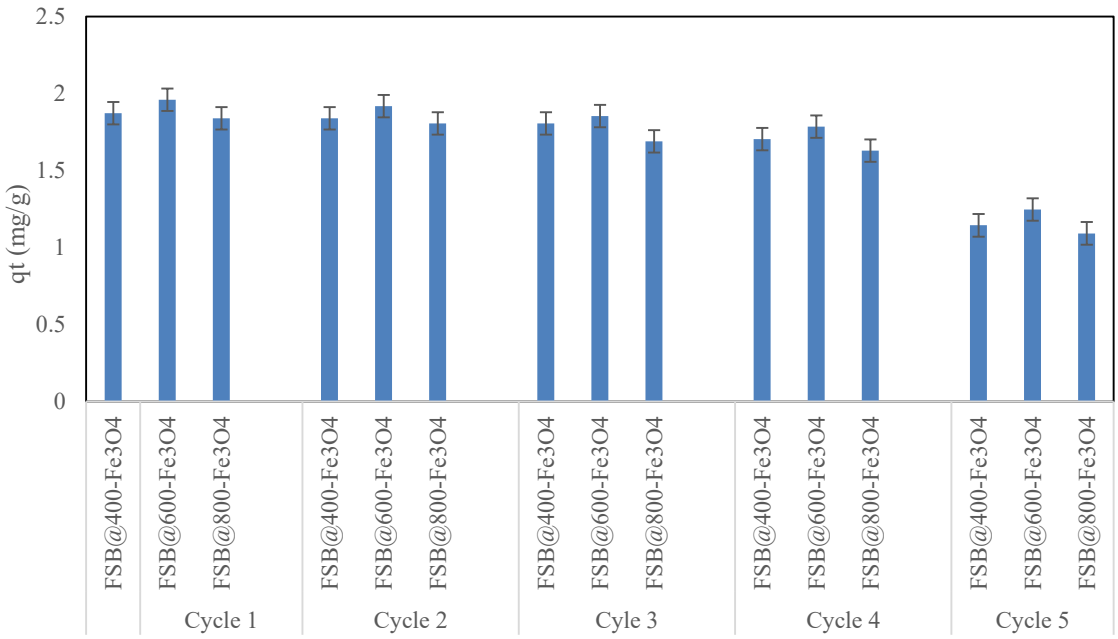

Figure 4.8b: Reusability of the adsorbents for the removal of crystal violet dye from aqueous solution

It is concluded that magnetic composites were stable under the reaction conditions and their regeneration/recyclability frequency was possible.

Targeting a clean environment with limited pollution is paramount. The proportion of the biochar in the magnetic composite is higher than that of the magnetic particles, since the magnetic particles are used to aid in recovery of the spent adsorbent, which would otherwise flow, with the treated wastewater. In the context of upscaling, the quantities of hydrated ferrous and ferric chlorides that would be used to produce the magnetite at a larger scale, definitely would predictably incur high costs. However, priorities have to be considered in that an option of a clean environment would warrant use of resources at any level of cost to actualize.

4.9 Treatment of dye wastewater using raw fish scales (RFS), Fish Scale Biochars (FSB), magnetic composites (FSB@Fe_3O_4) and activated charcoal

The collected raw wastewater samples exhibited blue colour indicating the possibility of the presence of indigo carmine and crystal violet dyes. The intensity of the blue colour varied amongst the sampling sites suggesting different concentrations of the dyes. The other parameters were equally significantly ($P \leq 0.05$) different in the five locations. A summary of the levels of pH, indigo carmine and crystal violet dyes in the characterized raw and control wastewater samples is presented in Table 4.9a and Figure 4.9a, b, c and d.

Table 4.9a: Levels of parameters in the characterized raw wastewater

PARAMETERS	SAMPLING LOCATIONS					CV%	LSD, P≤0.05
	A	B	C	D	E		
pH (Units)	5.05[d]	5.48[c]	5.42[c]	7.20[b]	10.28[a]	1.81	0.26
Temperature (^{o}C)	24.30[a]	21.63[c]	21.97[b]	22.13[b]	22.13[b]	0.64	0.26
Colour	blue	blue	blue	blue	blue	-	-
Indigo Carmine (mg/L)	259.33[b]	861.20[a]	0.74[d]	3.99[c,d]	19.82[c]	4.23	17.64
Crystal Violet (mg/L)	1.75[b,c]	3.67[b]	150.92[a]	0.61[c]	2.03[b,c]	5.23	3.02

[a, b, c, d] Data with different letters are significantly different (P≤0.05)

Table 4.9b: Levels of parameters in the control samples not treated with the adsorbents

PARAMETERS	SAMPLING LOCATIONS					CV%	LSD, P≤0.05
	A	B	C	D	E		
pH (Units)	4.95^{d}	5.55^{c}	5.44^{c}	7.18^{b}	10.25^{a}	1.80	0.25
Indigo Carmine (mg/L)	259.35^{b}	858.98^{a}	0.78^{d}	$4.04^{c,d}$	20.10^{c}	4.20	17.60
Crystal Violet (mg/L)	$1.72^{b,c}$	3.62^{b}	150.85^{a}	0.65^{c}	$2.10^{b,c}$	5.18	2.90

$^{a, b, c, d}$ Data with different letters are significantly different (P≤0.05)

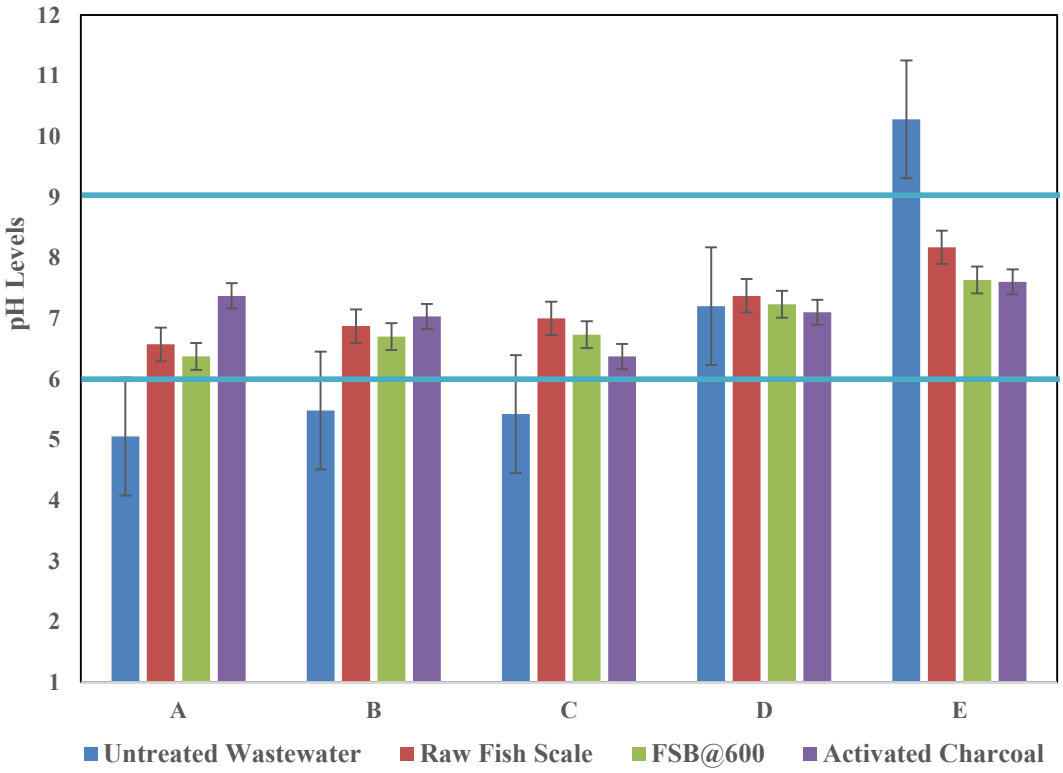

Figure 4.9a: Levels of pH in the characterized raw and treated wastewaters

The results of the concentrations of the selected parameters after treatment with the respective adsorbents are highlighted in Tables 4.9b, c and d, and Figures 4.9a and b. The pollutant concentrations within the control samples (Table 4.9b) that were not treated with the adsorbents in the experiment did not exhibit any significant disparity ($p \leq 0.05$) with the raw samples (Table 4.9b). The data show that all the adsorbents significantly ($p \leq 0.05$) improved the pH levels to WHO permissible confines and reduced the concentrations of indigo carmine and crystal violet dyes from the wastewater samples in all the locations. The removal efficiency (%R) of indigo carmine dye ranged from 42.70 % in RFS to 99.74 % in Activated Charcoal (AC) in location A, 36.37 % in RFS to 99.84 % in AC in location B, 66.84 % in FSB@800 ^{o}C-Fe_3O_4 to 100 % in AC in location C and 74.22 % in FSB@600 ^{o}C-Fe_3O_4 to 100 % in AC in location D, 58.45 % in raw fish scales (RFS) to 99.86 % in activated charcoal AC in location E. On the other hand, removal efficiency (%R) of crystal violet dye ranged from 54.15 % in raw fish scales (RFS) to 100.00 % in activated charcoal (AC) in location A, 56.84 % in RFS to 100.00 % in AC in location B, 52.91 % in RFS to 100.00 % in AC in location C, 75.49 % in RFS to 100.00 % in AC in location D and 74.22 % in RFS to 100.00 % in AC in location E. It is also remarkable that all the studied adsorbents recorded comparable removal efficiencies (%R), except for activated charcoal. The data, therefore, establish that the adsorbents were effective in the wastewater treatment process. Application of activated carbon to reduce the colour of textile wastewater samples was found to be effective (Panhwar *et al*., 2020). The efficiency of orange peel as an adsorbent for the removal of dyes from wastewater was investigated (Popuri *et al*., 2016) and established the maximum percentage of colour removal of 47.23, 52.59, 66.34 and 88.04 % for the textile

dyeing industry effluent respectively under optimum conditions of 90 rpm, 120 min, adsorbent dosage of 2.5 g/L and pH of 10. The study concluded that adsorption technique is the most suitable process for treatment of effluent from dyeing industry. In another study by Elango & Govindasamy (2018), the colour of industrial wastewater was effectively removed by activated carbon derived from temple waste flowers. In our study, the removal efficiencies (%R) attained by the adsorbents in the environmental wastewater were higher than synthetic dye wastewater from the laboratory batch experiments. Konan *et al*. (2020) reported a similar observation on adsorption of 2,4-dimethylphenol onto activated carbon. This observation was attributed to nitrite ions in the wastewater and organic materials adsorbed onto the adsorbent.

Appropriate disposal of the spent adsorbents is very important since this will ensure that the environment is not polluted again. In this regard, incineration of the used/spent adsorbents would be the best option.

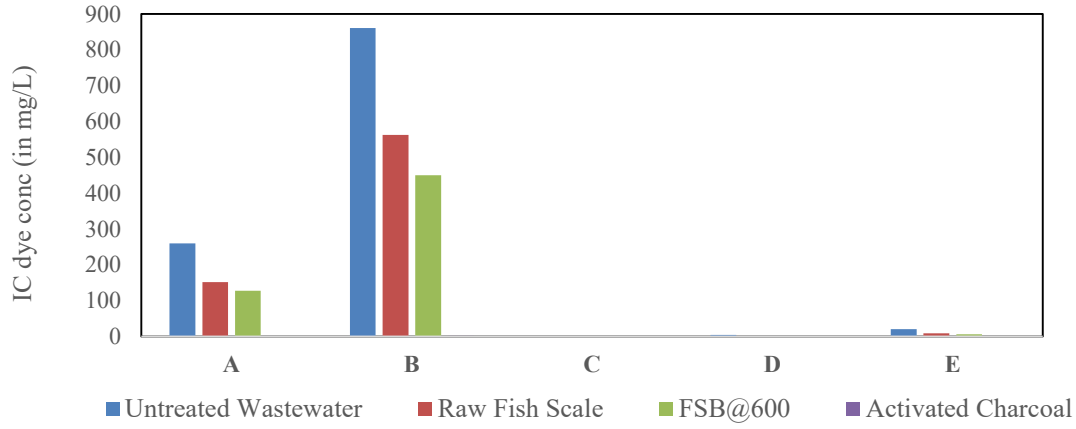

Figure 4.9b: Levels of IC dye in the characterized raw and treated wastewaters

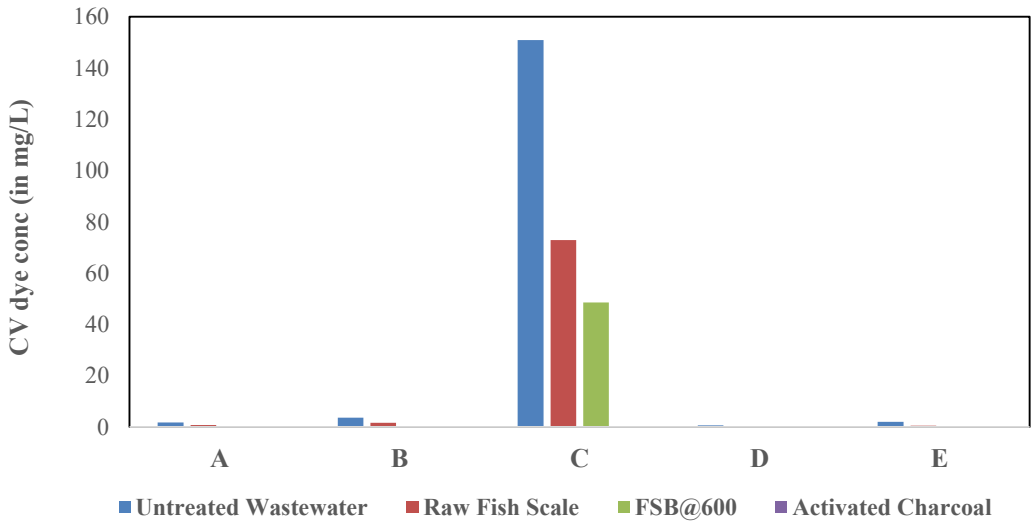

Figure 4.9c: Levels of CV dye in the characterized raw and treated wastewaters

Table 4.9c: Performance of adsorbents in improvement of pH and abstraction of indigo carmine dye from wastewater

ADSORBENT	PARAMETERS	LOCATIONS					CV%	LSD, P≤0.05
		A	B	C	D	E		
Raw Fish Scale	pH (Units)	6.57^{e}	6.87^{d}	7.00^{c}	7.37^{b}	8.17^{a}	0.95	0.12
	IC (mg/L)	151.79^{b}	563.0^{a}	0.13^{d}	0.71^{d}	8.25^{c}	1.42	3.74
	%R	42.70^{c}	36.37^{d}	81.05^{a}	81.44^{a}	58.45^{b}	0.44	0.48
Activated Charcoal	pH (Units)	7.37^{b}	7.03^{c}	6.37^{d}	7.10^{c}	7.60^{a}	1.09	0.14
	IC (mg/L)	0.69^{a}	1.42^{a}	0.00^{a}	0.00^{a}	0.03^{a}	229.4	1.79
	%R	99.74^{b}	$99.84^{a,b}$	100.00^{a}	100.00^{a}	$99.86^{a,b}$	0.11	0.21
FSB@400 ^{o}C	pH (Units)	6.43^{c}	6.34^{c}	6.71^{d}	7.27^{b}	7.97^{a}	1.07	0.13
	IC (mg/L)	130.91^{b}	508.54^{a}	0.02^{d}	0.74^{d}	7.02^{c}	1.04	2.44
	%R	50.58^{d}	42.53^{c}	97.05^{a}	80.57^{b}	64.63^{c}	0.90	1.10
FSB@600 ^{o}C	pH (Units)	6.37^{d}	6.70^{e}	6.73^{c}	7.23^{a}	7.63^{a}	0.74	0.09
	IC (mg/L)	127.50^{b}	449.85^{a}	0.02^{e}	0.75^{d}	5.56^{c}	0.16	0.33
	%R	51.87^{d}	49.16^{e}	96.64^{a}	80.26^{b}	72.00^{c}	0.29	0.37
FSB@800 ^{o}C	pH (Units)	6.27^{d}	6.87^{c}	6.13^{e}	7.33^{b}	7.53^{a}	0.86	0.11
	IC (mg/L)	132.46^{b}	456.61^{a}	0.138^{d}	0.797^{d}	4.87^{c}	1.16	2.52
	%R	50.00^{d}	48.39^{e}	79.73^{a}	79.12^{b}	75.47^{c}	0.35	0.42
FSB@400 ^{o}C-Fe_3O_4	pH (Units)	6.40^{d}	6.43^{d}	6.57^{c}	6.97^{b}	7.10^{a}	0.94	0.12
	IC (mg/L)	144.5^{b}	518.9^{a}	0.17^{d}	$0.96^{c,d}$	5.41^{c}	2.02	4.93
	%R	45.45^{c}	41.35^{d}	75.44^{a}	74.85^{a}	72.75^{b}	1.03	1.16
FSB@600 ^{o}C-Fe_3O_4	pH (Units)	6.57^{c}	6.33^{d}	6.17^{e}	7.13^{a}	6.93^{b}	0.87	0.11
	IC (mg/L)	136.8^{b}	526.7^{a}	0.197^{d}	0.984^{d}	5.81^{c}	1.34	3.28
	%R	48.37^{c}	40.47^{d}	70.96^{b}	74.22^{a}	70.75^{b}	0.49	0.55
FSB@800 ^{o}C-Fe_3O_4	pH (Units)	6.53^{d}	6.83^{c}	6.73^{c}	7.00^{b}	7.23^{a}	0.99	0.12
	IC (mg/L)	143.2^{b}	526.2^{a}	0.225^{d}	0.961^{d}	6.02^{c}	1.71	4.20
	%R	45.96^{d}	40.53^{e}	66.84^{c}	74.81^{a}	69.66^{b}	0.90	0.97

$^{a, b, c, d, e}$ Data with different letters are significantly different (P≤0.05); CV% - Percent coefficient of variation; LSD- least significant difference; pH-hydrogen concentration; IC-indigo carmine; %R-percent removal

Table 4.9d: Performance of adsorbents in abstraction of crystal violet dye from wastewater

Adsorbent	PARAMETER	LOCATIONS					CV%	LSD, P≤0.05
		A	B	C	D	E		
Raw Fish Scale	CV (mg/L)	0.71^{c}	1.56^{b}	72.90^{a}	0.088^{e}	0.45^{d}	0.93	0.26
	%R	54.15^{d}	56.84^{c}	52.91^{e}	75.49^{b}	76.56^{a}	0.29	0.34
Activated Charcoal	CV (mg/L)	0.00^{a}	0.00^{a}	0.00^{a}	0.00^{a}	0.00^{a}	0.00	0.00
	%R	100.00^{a}	100.00^{a}	100.00^{a}	100.00^{a}	100.00^{a}	0.00	0.00
FSB@400 ºC	CV (mg/L)	0.27^{c}	0.66^{b}	48.32^{a}	0.001^{d}	0.03^{d}	1.28	0.23
	%R	82.41^{c}	81.73^{d}	68.79^{e}	99.73^{a}	98.68^{b}	0.18	0.28
FSB@600 ºC	CV (mg/L)	$0.05^{b,c}$	$0.07^{b,c}$	48.52^{a}	0.00^{c}	0.21^{b}	1.04	0.19
	%R	96.96^{c}	98.09^{b}	68.65^{e}	100.00^{a}	88.81^{d}	0.40	0.67
FSB@800 ºC	CV (mg/L)	0.05^{b}	0.04^{b}	53.85^{a}	0.002^{b}	0.04^{b}	0.53	0.10
	%R	96.50^{d}	98.89^{b}	65.21^{e}	99.43^{a}	97.65^{c}	0.15	0.25
FSB@400 ºC- Fe_3O_4	CV (mg/L)	1.13^{b}	1.17^{b}	1.31^{b}	2.88^{a}	2.99^{a}	8.84	0.305
	%R	80.60^{d}	91.78^{a}	68.52^{e}	90.80^{b}	88.64^{c}	0.45	0.69
FSB@600 ºC- Fe_3O_4	CV (mg/L)	0.22^{c}	0.63^{b}	49.59^{a}	0.046^{c}	0.25^{c}	1.15	0.21
	%R	85.58^{c}	82.64^{d}	67.97^{e}	87.21^{a}	86.71^{b}	0.33	0.50
FSB@800 ºC- Fe_3O_4	CV (mg/L)	$0.23^{b,c}$	0.59^{b}	66.30^{a}	0.062^{c}	$0.36^{b,c}$	1.51	0.37
	%R	85.40^{a}	83.72^{b}	57.17^{e}	82.74^{c}	81.33^{d}	0.45	0.64

$^{a, b, c, d, e}$ Data with different letters are significantly different (P≤0.05); CV% - Percent coefficient of variation; LSD- least significant difference; CV-crystal violet; %R-percent removal

It is concluded that the prepared adsorbents were effective in treatment of industrial dye wastewater.

The contribution that this work presents is the potential application of fish scales in the remediation of wastewater containing dyes. By using fish scale wastes from the environment to remove dyes from wastewater, we are simply achieving doubly in terms of pollution abatement.

CHAPTER FIVE

SUMMARY, CONCLUSIONS, SIGNIFICANCE OF THE STUDY, RECOMMENDATIONS AND SUGGESTIONS FOR FUTURE RESEARCH

5.1 SUMMARY

Pulverized raw fish scale, fish scale biochars and magnetic composites were prepared and characterized for surface charge, functional groups, thermal stability, particle size and morphology, elemental composition, crystallinity, surface area, absorption peaks and magnetic properties. The materials were applied as adsorbents for the removal of indigo carmine and crystal violet dyes from aqueous solutions. The biochars and magnetic composites performed significantly better than raw fish scales in dye removal. However, the performance of activated charcoal was still the highest of all the adsorbents assessed. The percent removal (%R) on the surface of the biochar increased with increase in adsorbent dosage and initial dye concentration. The fish scale biochar magnetic composites (FSB@Fe_3O_4) were successfully synthesized using co-precipitation method and characterized for surface charges, optical absorbance, thermal stability, crystallinity, magnetic properties, surface area, surface morphology and functional groups. The investigated adsorption conditions revealed that the adsorption rate of indigo carmine and crystal violet dyes from aqueous solutions onto the adsorbents increased with contact time, initial dye solution, adsorbent dosage and solution temperature. However, the optimum adsorption of indigo carmine dye was at lower pH levels while the adsorption of crystal violet dye was favoured by high pH levels. The adsorption data for indigo carmine and crystal violet dyes were fitted into *pseudo*-first order, *pseudo*-second order,

and intra-particle diffusion models to evaluate the kinetics of the adsorption process. The magnetic composites (FSB@Fe_3O_4) were stable under reaction conditions, successfully recovered and regenerated/recycled. Besides, isotherm modeling for the adsorption of indigo carmine and crystal violet dyes was evaluated using Langmuir, Freundlich, Redlich-Peterson, Toth, Hill, Sips and Temkin models. The industrial dye wastewater was treated with raw fish scales (RFS), Fish Scale Biochars (FSB), magnetic composites (FSB@Fe_3O_4) and activated charcoal under ambient conditions to establish the efficiencies of the adsorbents in the treatment process.

5.2 CONCLUSIONS

i. Biochar generation from RFS improved the surface properties. Increase in pyrolysis temperature of RFS increases the thermal stability of the FSB. The generated FSB were crystalline in nature with the main compound identified being hydroxyl-apatite (HAp).

ii. Considering the RFS and FSB, FSB@600 ^oC posted the highest adsorption capacities (q) for indigo carmine and crystal violet dyes. However, the performance of the reference material (AC) surpassed all the adsorbents considered in this research.

iii. Fish scale biochar magnetic composites (FSB@Fe_3O_4) exhibited surface charges. The optical absorbance data of the three magnetic composites indicated that FSB@600 ^oC-Fe_3O_4 had the highest adsorption capacity. The thermal stability of the FSB and FSB@Fe_3O_4 increases with the increase in pyrolysis temperatures of the RFS. The data obtained from crystallinity, surface area, surface morphology and functional groups concluded that the FSB were crystalline in nature, their surface

properties were improved, and there was successful coupling between FSB and Fe_3O_4. The magnetic properties confirmed that the spent FSB@Fe_3O_4 would be easily recovered from the adsorption system.

iv. The initial indigo carmine dye concentrations of 25 mg/L, 50 mg/L, 75 mg/L and 100 mg/L attained maximum adsorptions after 40 min, 10 min, 40 min and 50 min, respectively, for FSB and 25, 50, 75 and 100 mg/L reached optimum adsorptions after 140, 140, 100 and 120 minutes, correspondingly, for FSB-Fe_3O_4. For crystal violet dye, maximum adsorptions were afforded after 160 min, 140 min, 140 min and 100 min, respectively, for 25 mg/L, 50 mg/L, 75 mg/L and 100 mg/L for FSB. More dye molecules were adsorbed at higher initial concentrations than at lower ones. Optimal adsorbent dosages were 0.10 g, 0.25 g, 0.20 g and 0.20 g per 30 mL, respectively, for activated charcoal, FSB@400 ºC, FSB@600 ºC, and FSB@800 ºC, respectively, and 0.20 g, 0.25 g, and 0.15 g for FSB@400 ºC-Fe_3O_4, FSB@600 ºC-Fe_3O_4, and FSB@800 ºC-Fe_3O_4, correspondingly, for the adsorption of indigo carmine dye. For the adsorption of crystal violet dye, peak dosages were recorded at 0.20 g, 0.20 g, 0.20 g, 0.20 g, 0.20 g, 0.25 g and 0.25 g for activated charcoal, FSB@400 ºC, FSB@600 ºC, FSB@800 ºC, FSB@400 ºC-Fe_3O_4, FSB@600 ºC-Fe_3O_4 and FSB@800 ºC-Fe_3O_4, respectively. The optimum pH 2 and pH 8-10 were favourable for the adsorption of IC and CV dyes, respectively.

v. The data fitted the *pseudo*-second-order kinetic equation while the Langmuir isotherm model presented the best fitting of the seven models considered suggesting uniformly energetic adsorption sites and monolayer adsorption. Indigo carmine (IC)

and crystal violet (CV) abstraction from artificial dye wastewater by fish scale biochars and magnetic composites were endothermic, non-spontaneous, and physisorption-moderated process involving electrostatic interactions. The FSB@Fe_3O_4 can be regenerated and reused/recycled upto the fifth and fourth cycles, respectively, for the abstraction of indigo carmine (IC) and crystal violet (CV) dyes. The magnetic composites were also stable under the considered adsorption conditions.

vi. The adsorbents recorded significant removal efficiencies, thus, were effective in the treatment of industrial dye wastewater.

5.3 SIGNIFICANCE OF THE STUDY

Modelling of a novel adsorbent from fish scale biomass has proved that it can aid in dye pollution remediation and create a clean environment free from the menace caused by decomposing heaps of fish scales. This study has also availed information on morphological and chemical properties of the prepared biochars and magnetic composites, the efficiencies of dye removal, kinetics and mechanisms of dye adsorption. These are summarized as followed:

i. The study has revealed that FSB generated from RFS exhibited improved surface properties that are important in adsorption of IC and CV from wastewater.

ii. The spent FSB immobilized with Fe_3O_4 was easily recovered from the adsorption system since the resulting FSB@Fe_3O_4 was stable and exhibited sufficient magnetic properties. Four and five reusability cycles were recorded for adsorption of CV and IC dyes, respectively.

iii. The adsorbents posted significant removal efficiencies. This indicated that they were effective in the treatment of industrial dye wastewater.

5.4 RECOMMENDATIONS

i. Thermal conversion of RFS to FSB is necessary since it improves the surface properties of the biochars that are required for better results during adsorption process.

ii. In order to realize better IC and CV removal efficiencies and capacities, biochars can be used owing to their improved surface properties.

iii. It is necessary to immobilize FSB with Fe_3O_4 since it creates properties that are necessary for adsorbent recovery after adsorption.

iv. Adsorbent dosages of 0.10 g, 0.25 g, 0.20 g and 0.20 g per 30 mL are recommended for activated charcoal, FSB@400 ºC, FSB@600 ºC, and FSB@800 ºC, respectively, while 0.20 g, 0.25 g, and 0.15 g for FSB@400 ºC-Fe_3O_4, FSB@600 ºC-Fe_3O_4, and FSB@800 ºC-Fe_3O_4, correspondingly, for the adsorption of 75 mg/L of indigo carmine dye. For the adsorption of crystal violet dye, the recommended dosages are 0.20 g, 0.20 g, 0.20 g, 0.20 g, 0.20 g, 0.25 g and 0.25 g for activated charcoal, FSB@400 ºC, FSB@600 ºC, FSB@800 ºC, FSB@400 ºC-Fe_3O_4, FSB@600 ºC-Fe_3O_4 and FSB@800 ºC-Fe_3O_4, respectively, for the adsorption of 75 mg/L of IC dye. The adsorption studies of indigo carmine and crystal violet dyes onto fish scale biochars (FSB) and magnetic composites (FSB@Fe_3O_4) should be done at pH 2 and pH 8-10, respectively.

A temperature of 313 K is recommended to be the most ideal for the adsorption of IC and CV dyes onto FSB and FSB@600 ºC-Fe_3O_4.

v. Immobilizing FSB with Fe_3O_4 is recommended for easy recovery of the spent adsorbent since the resulting FSB@Fe_3O_4 is stable and exhibit sufficient magnetic properties. Four and five reusability cycles are appropriate for adsorption of CV and IC dyes, respectively.

vi. The adsorbents RFS, FSB and FSB@Fe_3O_4 can be applied in the treatment of industrial wastewater containing IC and CV dyes.

5.5 SUGGESTIONS FOR FUTURE RESEARCH

i. Survey of properties of biochars prepared from fish scales of other species in comparison with properties of *Tilapia* fish scales.

ii. Investigate the influence of ionic strength and rotation speed on the adsorption capacity of fish scale biochars and magnetic composites.

iii. Evaluation of the efficacy of fish scale biochars and magnetic composites in remedying wastewater contaminated with pollutants other than dyes, such as metals, acid radicals such as sulphates, nitrates, phosphates etc., chemical oxygen demand (COD) and pharmaceutical active ingredients (PAI).

REFERENCES

Abdullah, B., & Vo, D. V. N. (2014). An evaluation of fish scales as potential adsorbents: pH and concentration effect. *Applied Mechanics and Materials*, *625*, 73–76.

Abd-Elhamid, A. I., Emran, M., El-Sadek, M. H., El-Shanshory, A. A., Soliman, H. M., Akl, M. A., & Rashad, M. (2020). Enhanced removal of cationic dye by eco-friendly activated biochar derived from rice straw. *Applied Water Science, 10*(1), 1-11. https://doi.org/10.1007/s13201-019-1128-0.

Abd Malek, N. N., Jawad, A. H., Abdulhameed, A. S., Ismail, K., & Hameed, B. H. (2020). New magnetic Schiff's base-chitosan-glyoxal/fly ash/Fe3O4 biocomposite for the removal of anionic azo dye: an optimized process. *International journal of biological macromolecules*, *146*, 530-539. https://doi.org/10.1016/j.ijbiomac.2020.01.020.

Achieng, G. O., & Shikuku, V. O. (2020). Adsorption of copper ions from water onto fish scales derived biochar: Isothermal perspectives. *Journal of Materials and Environmental Science, 11*(11), 1816-1827.

Adeyi, A. A., Jamil, S. N., Abdullah, L. C., & Choong, T. S. (2019). Adsorption of malachite green dye from liquid phase using hydrophilic thiourea-modified poly (acrylonitrile-co-acrylic acid): kinetic and isotherm studies. *Journal of Chemistry*, pp 14. https://doi.org/10.1155/2019/4321475.

Ahmadifar, Z., & Koohi, A. D. (2018). Characterization, preparation, and uses of nanomagnetic Fe_3O_4 impregnated onto fish scale as more efficient adsorbent for Cu^{2+} ion adsorption. *Environmental Science and Pollution Research, 25*(20), 19687–19700.

Ali, S. F. A., & Gad, E. S. (2020). Investigation of an adsorbent based on novel starch/chitosan nanocomposite in extraction of indigo carmine dye from aqueous solutions. *Biointerface Research in Applied Chemistry, 10*(3), 5556-5563. https://doi.org/10.33263/BRIAC103.556563.

Al-Deffeeri, N. S. (2013). Chemical analysis of distilled water: A case study. *Desalination and Water Treatment*, *51*(7-9), 1936-1940. https://doi.org/10.1080/19443994.2012.714737.

Alizadeh, N., Shariati, S., & Besharati, N. (2017). Adsorption of crystal violet and methylene blue on azolla and fig leaves modified with magnetite iron oxide nanoparticles. *International Journal of Environmental Research, 11*(2), 197-206. DOI 10.1007/s41742-017-0019-1.

Allen, S. J., Gan, Q., Matthews, R., & Johnson, P.A. (2003). Comparison of optimized isotherm models for basic dye adsorption by kudzu. *Bioresource Technology, 88*(2), 143–152. https://doi.org/10.1016/S0960-8524(02)00281-X.

Almoisheer, N., Alseroury, F., Kumar, R., Aslam, M., & Barakat, M. (2019). Adsorption and anion exchange insight of indigo carmine onto CuAl-LDH/SWCNTs nanocomposite: kinetic, thermodynamic and isotherm analysis. *RSC Advances, 9*(1), 560-568. 10.1039/C8RA09562K.

Ansari, R., Seyghali, B., Mohammad-khah, A., Zanjanchi, M. A. (2012). Application of Nano Surfactant Modified Biosorbent as an Efficient Adsorbent for Dye Removal. *Separation Science and Technology, 47*(12), 1802-1812. https://doi.org/10.1080/01496395.2012.658485.

Ayanda, O. S., Amodu, O. S., Adubiaro, H., Olutona, G. O., Ebenezer, O. T., Nelana, S. M., & Naidoo, E. B. (2019). Effectiveness of termite hill as an economic adsorbent for the adsorption of alizarin red dye. *Journal of Water Reuse and Desalination, 9*(1), 83-93. https://doi.org/10.2166/wrd.2018.026.

Azari, A., Nabizadeh, R., Mahvi, A. H., & Nasseri, S. (2021). Magnetic multi-walled carbon nanotubes-loaded alginate for treatment of industrial dye manufacturing effluent: adsorption modelling and process optimisation by central composite face-central design. *International Journal of Environmental Analytical Chemistry*, 1-21. https://doi.org/10.1080/03067319.2021.1877279.

Azizi, S. N., Colagar, A. H., & Hafeziyan, S. M. (2012). Removal of Cd(II) from Aquatic System Using *Oscillatoria* sp. Biosorbent. *The Scientific World Journal*, 2012: pp 7. https://doi.org/10.1100/2012/347053.

Badeenezhad, A., Azhdarpoor, A., Bahrami, S., & Yousefinejad, S. (2019). Removal of methylene blue dye from aqueous solutions by natural clinoptilolite and clinoptilolite modified by iron oxide nanoparticles. *Molecular Simulation, 45*, 564-571. https://doi.org/10.1080/08927022.2018.1564077.

Bafana, A., Devi, S. S., & Chakrabarti, T. (2011). Azo dyes: past, present and the future. *Environmental Reviews, 19*, 350-371. https://doi.org/10.1139/a11-018.

Bagtash, M., & Zolgharnein, J. (2017). Hybrid central composite design for simultaneous optimization of removal of methylene blue and alizarin red S from aqueous solutions using Vitis tree leaves. *Journal of Chemometrics, 32*: pp 13. https://doi.org/10.1002/cem.2960.

Bamukyaye, S., & Wanasolo, W. (2017). Performance of egg-shell and fish-scale as adsorbent materials for chromium (VI) removal from effluents of tannery industries in Eastern Uganda. *Open Access Library Journal, 4*(8), 1-12. 10.4236/oalib.1103732.

Begum, H. A., & Kabir, M. H. (2013). Removal of brilliant red from aqueous solutions by adsorption on fish scales. *Dhaka University Journal of Science, 61*(1), 7–12. https://doi.org/10.3329/dujs.v61i1.15089.

Bordoloi, N., Dey, M. D., Mukhopadhyay, R., & Kataki, R. (2018). Adsorption of Methylene blue and Rhodamine B by using biochar derived from Pongamia glabra seed cover. *Water Science and Technology, 77*, 638-646. https://doi.org/10.2166/wst.2017.579.

Bouteraa, S., Saiah, F. B. D., Hamouda, S., & Bettahar, N. (2020). Zn-M-CO_3 Layered Double Hydroxides (M= Fe, Cr, or Al): Synthesis, Characterization, and Removal of

Aqueous Indigo carmine. *Bulletin of Chemical Reaction Engineering & Catalysis, 15*(1), 43-54. 10.9767/bcrec.15.1.5053.43-54.

Carneiro, P. A., Umbuzeiro, G. A., Oliveira, D. P., & Zanoni, M. V. B. (2010). Assessment of water contamination caused by a mutagenic textile effluent/dyehouse effluent bearing disperse dyes. *Journal of hazardous materials*, *174*(1-3), 694-699. https://doi.org/10.1016/j.jhazmat.2009.09.106.

Chaki, S., Malek, T.J., Chaudhary, M., Tailor, J., & Deshpande, M. (2015). Magnetite Fe_3O_4 nanoparticles synthesis by wet chemical reduction and their characterization. *Advances in Natural Sciences: Nanoscience and Nanotechnology, 6*(3), 1-6. https://doi.org/10.1088/2043-6262/6/3/035009.

Chakraborty, J., Dey, S., & Halder, U. (2016). An eco-friendly bio-sorbent derived from fish (Carp) scale: A study of commercial dye removal. *International Journal of Scientific and Engineering Research, 7*, 72-76.

Chowdhury, S., Das Saha, P., & Ghosh, U. (2012). Fish (Labeo rohita) scales as potential low-cost biosorbent for removal of malachite green from aqueous solutions. *Bioremediation Journal, 16*(4), 235–242.

Cimò, G., Kucerik, J., Berns, A. E., Schaumann, G. E., Alonzo, G., & Conte, P. (2014). Effect of heating time and temperature on the chemical characteristics of biochar from poultry manure. *Journal of agricultural and food chemistry*, *62*(8), 1912-1918.

Couto, S. R. (2009). Dye removal by immobilised fungi. *Biotechnology Advances, 27*(3), 227-235. https://doi.org/10.1016/j.biotechadv.2008.12.001.

Dada, A. O., Adekola, F. A., & Odebunmi, E. O. (2014, March). Synthesis and characterization of iron nanoparticles and its ash rice husk supported nanocomposite. In *Proceedings of the 1st African international conference/workshop on application of nanotechnology to energy, health and environment, UNN,* 138-149.

Dai, Z., Meng, J., Muhammad, N., Liu, X., Wang, H., He, Y., Brookes, P. C., & Xu, J. (2013). The potential feasibility for soil improvement, based on the properties of biochars pyrolyzed from different feedstocks. *Journal of soils and sediments*, *13*(6), 989-1000. https://doi.org/10.1007/s11368-013-0698-y.

Das, S. K., Ghosh, G. K., Avasthe, R. K., & Sinha, K. (2021). Compositional heterogeneity of different biochar: Effect of pyrolysis temperature and feedstocks. *Journal of Environmental Management*, *278*, 1-12. https://doi.org/10.1016/j.jenvman.2020.111501.

Dastgerdi, Z. H., Meshkat, S. S., & Esrafili, M. D. (2019). Enhanced adsorptive removal of Indigo carmine dye performance by functionalized carbon nanotubes based adsorbents from aqueous solution: equilibrium, kinetic, and DFT study. *Journal of Nanostructure in Chemistry*, *9*(4), 323-334. https://doi.org/10.1007/s40097-019-00321-0.

Datta, D., Kerkez Kuyumcu, Ö., Bayazit, Ş. S., & Abdel Salam, M. (2017). Adsorptive removal of malachite green and Rhodamine B dyes on Fe3O4/activated carbon composite. *Journal of Dispersion Science and Technology*, *38*(11), 1556-1562. https://doi.org/10.1080/01932691.2016.1262776.

De Gisi, S., Lofrano, G., Grassi, M., & Notarnicola, M. (2016). Characteristics and adsorption capacities of low-cost sorbents for wastewater treatment: a review. *Sustainable Materials and Technologies, 9*, 10–40. https://doi.org/10.1016/j.susmat.2016.06.002.

De León-Condés, C. A., Roa-Morales, G., Martínez-Barrera, G., Menchaca-Campos, C., Bilyeu, B., Balderas-Hernández, P., Ureña-Núñez F, & Toledo-Jaldin, H. P. (2019). Sulfonated and gamma-irradiated waste expanded polystyrene with iron oxide nanoparticles, for removal of indigo carmine dye in textile wastewater. *Heliyon, 5*(7), 1-8. https://doi.org/10.1016/j.heliyon.2019.e02071.

Delgado, C. L., Wada, N., Rosegrant, M. W., Meijer, S., & Ahmed, M. (2003). The future of fish: issues and trends to 2020: pp 6. https://hdl.handle.net/20.500.12348/2179.

dos Santos, A. B., Bisschops, I. A., Cervantes, F. J., & van Lier, J. B. (2005). The transformation and toxicity of anthraquinone dyes during thermophilic (55 C) and mesophilic (30 C) anaerobic treatments. *Journal of Biotechnology*, *115*(4), 345-353. https://doi.org/10.1016/j.jbiotec.2004.09.007.

Dutta, S., Gupta, B., Srivastava, S. K., & Gupta, A. K. (2021). Recent advances on the removal of dyes from wastewater using various adsorbents: A critical review. *Materials Advances*. 2, 4497-4531. 10.1039/d1ma00354b.

Ebrahimian Pirbazari, A., Saberikhah, E., & Gholami Ahmad Gorabi, N. (2016). Fe_3O_4 nanoparticles loaded onto wheat straw: an efficient adsorbent for Basic Blue 9 adsorption from aqueous solution. *Desalination and Water Treatment*, *57*(9), 4110-4121. https://doi.org/10.1080/19443994.2014.989918.

Edwin, M., & Sekhar, S. J. (2015). Performance and chemical analysis of distilled saline water production using solar distillation system. *International Journal of ChemTech Research*, *8*(4), 1632-1637.

El Haddad, M., Slimani, R., Mamouni, R., ElAntri, S., & Lazar, S. (2013a). Removal of two textile dyes from aqueous solutions onto calcined bones. *Journal of the Association of Arab Universities for Basic and Applied Sciences*, *14*(1), 51-59. https://doi.org/10.1016/j.jaubas.2013.03.002.

El Haddad, M., Slimani, R., Mamouni, R., Laamari, M. R., Rafqah, S., & Lazar, S. (2013b). Evaluation of potential capability of calcined bones on the biosorption removal efficiency of

safranin as cationic dye from aqueous solutions. *Journal of the Taiwan Institute of Chemical Engineers*, *44*(1), 13-18. https://doi.org/10.1016/j.jtice.2012.10.003.

Elango, G., & Govindasamy, R. (2018). Removal of Colour from Textile Dyeing Effluent Using Temple Waste Flowers as Ecofriendly Adsorbent. *Journal Applied Chemistry*, *11*(6), 19-28. 10.9790/5736-1106011928.

Esakkiraj, P., Maruthiah, T., Nawas, P. M. A., Immanuel, G., & Palavesam, A. (2013). Solid-state protease production by Bacillus thuringiensis AP-CMST using trash fish meal as substrate. *Journal of Pure and Applied Microbiology*, *7*(4), 1-8.

Essandoh, M., Garcia, R. A. (2018). Efficient removal of dyes from aqueous solutions using a novel hemoglobin/iron oxide composite. *Chemosphere,* 206, 502-512. https://doi.org/10.1016/j.chemosphere.2018.04.182.

Federation WE, APH Association (2005). Standard methods for the examination of water and wastewater. American Public Health Association (APHA): Washington, DC, USA.

Fegousse, A., El Gaidoumi, A., Miyah, Y., El Mountassir, R., & Lahrichi, A. (2019). Pineapple bark performance in dyes adsorption: optimization by the central composite design. *Journal of Chemistry, 2019*, pp 11. https://doi.org/10.1155/2019/3017163.

Foo, K. Y., & Hameed, B. H. (2010). Insights into the modeling of adsorption isotherm systems. *Chemical engineering journal*, *156*(1), 2-10. https://doi.org/10.1016/j.cej.2009.09.013.

Fraga, T. J. M., de Lima, L. E. M., de Souza, Z. S. B., Carvalho, M.N., Freire, E. M. P. D. L., Ghislandi, M. G., & da Motta, M. A. (2019). Amino-Fe_3O_4-functionalized graphene oxide as a novel adsorbent of Methylene Blue: kinetics, equilibrium, and recyclability aspects. *Environmental Science and Pollution Research*, *26*(28), 28593-28602. https://doi.org/10.1016/j.jhazmat.2011.06.068.

Freundlich, H. (1907). Über die adsorption in lösungen. *Zeitschrift für physikalische Chemie, 57*:385-470. https://doi.org/10.1515/zpch-1907-5723.

Gao, S., Zhang, W., An, Z., Kong, S., & Chen, D. (2019). Adsorption of anionic dye onto magnetic Fe_3O_4/CeO_2 nanocomposite: Equilibrium, kinetics, and thermodynamics. *Adsorption Science & Technology*, *37*(3-4), 185-204. https://doi.org/10.1177/0263617418819164.

Gautam, D., & Hooda, S. (2020). Magnetic graphene oxide/chitin nanocomposites for efficient adsorption of methylene blue and crystal violet from aqueous solutions. *Journal of Chemical & Engineering Data*, *65*(8), 4052-4062. https://dx.doi.org/10.1021/acs.jced.0c00350.

Gholami, N., Dadvand Koohi, A., & Ebrahimian Pirbazari, A. (2018). Fabrication, characterization, regeneration and application of nanomagnetic Fe_3O_4@fish scale as a bio-adsorbent for removal of methylene blue. *Journal of Water and Environmental Nanotechnology*, *3*(3), 219-234. 10.22090/jwent.2018.03.003.

Gonçalves, A. H., Siciliano, P. H., Alves, O. C., Cesar, D. V., Henriques, C. A., & Gaspar, A. B. (2020). Synthesis of a magnetic Fe_3O_4/RGO composite for the rapid photo-fenton discoloration of indigo carmine dye. *Topics in Catalysis*, *63*(11), 1017-1029. https://doi.org/10.1007/s11244-020-01277-0.

Gupta, V. K., Jain, R., & Varshney, S. (2007). Removal of Reactofix golden yellow 3 RFN from aqueous solution using wheat husk—an agricultural waste. *Journal of Hazardous Materials*, *142*(1-2), 443-448. https://doi.org/10.1016/j.jhazmat.2006.08.048.

Gupta, V. K. (2009). Application of low-cost adsorbents for dye removal–a review. *Journal of environmental management*, *90*(8), 2313-2342. https://doi.org/10.1016/j.jenvman.2008.11.017.

Guz, L., Curutchet, G., Sanchez, R. T., & Candal, R. (2014). Adsorption of crystal violet on montmorillonite (or iron modified montmorillonite) followed by degradation through Fenton or Photo-Fenton type reactions. *Journal of Environmental Chemical Engineering*, *2*(4), 2344-2351. https://doi.org/10.1016/j.jece.2014.02.007.

Han, Y., Cao, X., Ouyang, X., Sohi, S. P., & Chen, J. (2016). Adsorption kinetics of magnetic biochar derived from peanut hull on removal of Cr (VI) from aqueous solution: effects of production conditions and particle size. *Chemosphere*, *145*, 336-341 https://doi.org/10.1016/j.chemosphere.2015.11.050.

Heitkötter, J., & Marschner, B. (2015). Interactive effects of biochar ageing in soils related to feedstock, pyrolysis temperature, and historic charcoal production. *Geoderma*, *245*, 56-64. https://doi.org/10.1016/j.geoderma.2015.01.012.

Hessel, C., Allegre, C., Maisseu, M., Charbit, F., & Moulin, P. (2007). Guidelines and legislation for dye house effluents. *Journal of environmental management*, *83*(2), 171-180. https://doi.org/10.1016/j.jenvman.2006.02.012.

Ho, Y. S., & McKay, G. (2003). Sorption of dyes and copper ions onto biosorbents. *Process Biochemistry*, *38*(7), 1047-1061. https://doi.org/10.1016/S0032-9592(02)00239-X.

Ho, L. N., Ong, S. A., Osman, H., & Chong, F. M. (2012). Enhanced photocatalytic activity of fish scale loaded TiO_2 composites under solar light irradiation. *Journal of Environmental Sciences*, *24*(6), 1142-1148. https://doi.org/10.1016/S1001-0742(11)60872-3.

Hossain, M. A., Ngo, H. H., Guo, W. S., & Nguyen, T. V. (2012). Palm oil fruit shells as biosorbent for copper removal from water and wastewater: experiments and sorption models. *Bioresource technology*, *113*, 97-101. https://doi.org/10.1016/j.biortech.2011.11.111.

Huang, E. (2007). Use of fish scales as biosorbent for the removal of copper in water. *Water Research, 30*, 1985–1990.

Ismail, M., Akhtar, K., Khan, M.I., Kamal, T., Khan, M.A., M Asiri, A., Seo, J., & Khan, S.B. (2019). Pollution, toxicity and carcinogenicity of organic dyes and their catalytic bio-remediation. *Current pharmaceutical design*, *25*(34), 3645-3663. https://doi.org/10.2174/1381612825666191021142026.

Jindo, K., Mizumoto, H., Sawada, Y., Sanchez-Monedero, M. A., & Sonoki, T. (2014). Physical and chemical characterization of biochars derived from different agricultural residues. *Biogeosciences*, *11*(23), 6613-6621. https://doi.org/10.5194/bg-11-6613-2014.

Keypour, H., Saremi, S. G., Noroozi, M., & Veisi, H. (2017). Synthesis of magnetically recyclable Fe_3O_4@[$(EtO)_3$Si-L1H]/Pd(II) nanocatalyst and application in Suzuki and Heck coupling reactions. *Applied Organometallic Chemistry*, *31*(2), 1-7. https://doi.org/10.1002/aoc.3558.

Khenifi, A., Bouberka, Z., Sekrane, F., Kameche, M., & Derriche, Z. (2007). Adsorption study of an industrial dye by an organic clay. *Adsorption*, *13*(2), 149-158. https://doi.org/10.1007/s10450-007-9016-6.

Kimosop, S. J., Okello, V. A., Getenga, Z. M., Orata, F. & Shikuku, V. O. (2017). Green remediation of carbamazepine from water using novel magnetic iron modified carbonized baggasse: kinetics, equilibrium and mechanistic studies. *Chemical Science International Journal, 18*(3), 1-9. 10.9734/CSIJ/2017/32444.

Konan, A. T. S., Richard, R., Andriantsiferana, C., Yao, K. B., & Manero, M. H. (2020). Recovery of borassus palm tree and bamboo waste into activated carbon: application to the phenolic compound removal. *Journal of Materials and Environmental Science*, *11*(10), 1584-1598.

Konicki W, Aleksandrzak M, Moszyński D, Mijowska E (2017) Adsorption of anionic azo-dyes from aqueous solutions onto graphene oxide: Equilibrium, kinetic and thermodynamic studies. J. Colloid Interface Sci. 496:188-200. https://doi.org/10.1016/j.jcis.2017.02.031.

Konicki, W., Aleksandrzak, M., Moszyński, D., & Mijowska, E. (2017). Adsorption of anionic azo-dyes from aqueous solutions onto graphene oxide: equilibrium, kinetic and thermodynamic studies. *Journal of colloid and interface science*, *496*, 188-200. https://doi.org/10.1016/j.reffit.2017.01.009.

Kulkarni, S., & Kaware, J. (2014). Regeneration and recovery in adsorption-a review. *International Journal of Innovative Science Engineering and Technology*, *1*(8), 61-64.

Kumar, K. V., & Kumaran, A. (2005). Removal of methylene blue by mango seed kernel powder. *Biochemical Engineering Journal*, *27*(1), 83-93. https://doi.org/10.1016/j.bej.2005.08.004.

Lafi, R., Montasser, I., & Hafiane, A. (2019). Adsorption of congo red dye from aqueous solutions by prepared activated carbon with oxygen-containing functional groups and its regeneration. *Adsorption Science & Technology*, *37*(1-2), 160-181. http://dx.doi.org/10.1177/0263617418819227.

Langmuir, I. (1916). The constitution and fundamental properties of solids and liquids. Part I. Solids. *Journal of the American chem society, 38*(11), 2221-2295. https://doi.org/10.1021/ja02268a002.

Li, F., Shen, K., Long, X., Wen, J., Xie, X., Zeng, X., Liang, Y., Wei, Y., Lin, Z., Huang, W., & Zhong, R. (2016). Preparation and characterization of biochars from Eichornia crassipes for cadmium removal in aqueous solutions. *PloS one*, *11*(2), pp 13. https://doi.org/10.1371/journal.pone.0148132.

Liu, L., Chen, P., Sun, M., Shen, G., & Shang, G. (2015). Effect of biochar amendment on PAH dissipation and indigenous degradation bacteria in contaminated soil. *Journal of Soils and Sediments*, *15*(2), 313-322. https://doi.org/10.1016/j.chemosphere.2018.08.106.

Loulidi, I., Boukhlifi, F., Ouchabi, M., Amar, A., Jabri, M., Kali, A., Chraibi, S., Hadey, C. & Aziz, F. (2020). Adsorption of crystal violet onto an agricultural waste residue: kinetics, isotherm, thermodynamics, and mechanism of adsorption. *The Scientific World Journal*, *2020,* 1-9. https://doi.org/10.1155/2020/5873521.

Luo, M., Huang, Y., Zhu, M., Tang, Y. N., Ren, T., Ren, J., Wang, H., & Li, F. (2018). Properties of different natural organic matter influence the adsorption and aggregation behavior of TiO_2 nanoparticles. *Journal of Saudi Chemical Society*, *22*(2), 146-154. doi: 10.1016/j.jscs.2016.01.007.

Lv, X., Zhao, M., Chen, Z., Zhang, J., Tian, X., Ren, X., & Mei, X. (2018). Prepare porous silica nanospheres for water sustainability: high efficient and recyclable adsorbent for cationic organic dyes. *Colloid and Polymer Science*, *296*(1), 59-70. https://doi.org/10.1007/s00396-017-4224-4.

Mahdavi, M., Namvar, F., Ahmad, M. B., & Mohamad, R. (2013). Green biosynthesis and characterization of magnetic iron oxide (Fe_3O_4) nanoparticles using seaweed (Sargassum muticum) aqueous extract. *Molecules*, *18*(5), 5954-5964. https://doi.org/10.1021/cm200397g.

Marrakchi, F., Ahmed, M. J., Khanday, W. A., Asif, M., & Hameed, B. H. (2017). Mesoporous carbonaceous material from fish scales as low-cost adsorbent for reactive orange 16 adsorption. *Journal of the Taiwan Institute of Chemical Engineers*, *71*, 47-54. https://doi.org/10.1016/j.jtice.2016.12.026.

Mimmo, T., Panzacchi, P., Baratieri, M., Davies, C. A., & Tonon, G. (2014). Effect of pyrolysis temperature on miscanthus (Miscanthus× giganteus) biochar physical, chemical and functional properties. *Biomass and Bioenergy*, *62*, 149-157. https://doi.org/10.1016/j.biombioe.2014.01.004.

Miraboutalebi, S. M., Nikouzad, S. K., Peydayesh, M., Allahgholi, N., Vafajoo, L., & McKay, G. (2017). Methylene blue adsorption via maize silk powder: Kinetic, equilibrium, thermodynamic studies and residual error analysis. *Process Safety and Environmental Protection*, *106*, 191-202. https://doi.org/10.1016/j.psep.2017.01.010.

Mohammed, R., Mohamed, F., Mohamed, E., El, H. B., Mohamed, F., & Mohamed, O. (2008). Protein rich ingredients from fish waste for sheep feeding. *African Journal of Microbiology Research*, *2*(4), 73-77.10.5897/AJMR.

Monalisa, P., & Nayak, P. L. (2013). Ecofriendly green synthesis of iron nanoparticles from various plants and spices extract. *International Journal of Plant, Animal and Environmental Sciences*, *3*(1), 68-78.

Mtshatsheni, K. N., Naidoo, B. E., & Ofomaja, A. E. (2020). Characterization of grafted acrylamide onto pine magnetite composite for the removal of methylene blue from wastewater. *Waste in Textile and Leather Sectors, 2020*, pp 15. http://dx.doi.org/10.5772/intechopen.92114.

Mushtaq, W., Rafiq, M., Mushtaq, Z., Nadeem, F., & Abdul, H. (2019). Wastewater Treatment and Dye Sequestration using Potential Magnetic Composites–A Comprehensive Review. *International Journal of Chemical and Biochemical Sciences, 15*, 74-86.

Mustafiz, S. (2003). The application of fish scales in removing heavy, metals from energy-produced waste streams: the role of microbes. *Energy Sources, 25*(9), 905–916. https://doi.org/10.1080/00908310390221255.

Neves, C. V., Scheufele, F. B., Nardino, A. P., Vieira, M. G. A., da Silva, M. G. C., Módenes, A. N., & Borba, C. E. (2018). Phenomenological modeling of reactive dye adsorption onto fish scales surface in the presence of electrolyte and surfactant mixtures. *Environmental technology*, *39*(19), 2467-2483. https://doi.org/10.1080/09593330.2017.1356876.

Nnaemeka, O. J., Josphine, O. J., & Charles, O. (2016). Adsorption of basic and acidic dyes onto agricultural wastes. *International Letters of Chemistry, Physics and Astronomy*, *70*, 12-26. doi:10.18052/www.scipress.com/ILCPA.70.12.

Ngeno, E. C., Orata, F., Lilechi, D. B., Shikuku, V. O., & Kimosop, S. (2016). Adsorption of caffeine and ciprofloxacin onto pyrolytically derived water hyacinth biochar: Isothermal, kinetics and thermodynamics. *Journal of Chemistry and Chemical Engineering, 10*, 185-194. doi: 10.17265/1934-7375/2016.04.006.

Nooraee Nia, N., Rahmani, M., Kaykhaii, M., & Sasani, M. (2017). Evaluation of eucalyptus leaves as an adsorbent for decolorization of methyl violet (2B) dye in contaminated waters: thermodynamic and kinetics model. *Modeling Earth Systems and Environment*, *3*(2), 825-829. https://doi.org/10.1007/s40808-017-0338-4.

Nnadozie, E. C., & Ajibade, P. A. (2021). Isotherm, kinetics, thermodynamics studies and effects of carbonization temperature on adsorption of Indigo Carmine (IC) dye using C. odorata biochar. *Chemical Data Collections*, *33*, 1-11. https://doi.org/10.1016/j.cdc.2021.100673.

Nnadozie, E. C., & Ajibade, P. A. (2020). Adsorption, kinetic and mechanistic studies of Pb (II) and Cr (VI) ions using APTES functionalized magnetic biochar. *Microporous and Mesoporous Materials, 309*, 1-9. https://doi.org/10.1016/j.micromeso.2020.110573.

Noor, N. M., Shariff, A., Abdullah, N., & Aziz, N. S. M. (2019). Temperature effect on biochar properties from slow pyrolysis of coconut flesh waste. *Malaysian Journal of Fundamental and Applied Sciences*, *15*(2), 153-158.

Ogugbue, C. J., & Sawidis, T. (2011). Bioremediation and detoxification of synthetic wastewater containing triarylmethane dyes by Aeromonas hydrophila isolated from industrial effluent. *Biotechnology research international*, *2011*, 1-11. https://doi.org/10.4061/2011/967925.

Ooi, J., Lee, L. Y., Hiew, B. Y. Z., Thangalazhy-Gopakumar, S., Lim, S. S., & Gan, S. (2017). Assessment of fish scales waste as a low cost and eco-friendly adsorbent for removal of an azo dye: Equilibrium, kinetic and thermodynamic studies. *Bioresource Technology*, *245*, 656-664. https://doi.org/10.1016/j.biortech.2017.08.153.

Othman, N., Abd-Kadir, A., & Zayadi, N. (2016). Waste fish scale as cost effective adsorbent in removing zinc and ferum ion in wastewater. *Journal of Engineering and Applied Sciences*, *11*(3), 1584-1592.

Owens, J. W. (2002). Chemical toxicity indicators for human health: case study for classification of chronic noncancer chemical hazards in life-cycle assessment. *Environmental Toxicology and Chemistry: An International Journal*, *21*(1), 207-225. https://doi.org/10.1002/etc.5620210129.

Panhwar, A., Faryal, K., Kandhro, A., Brohi, N., Khanzada, S., Ahmed, K. (2020). Removal of Color from Textile Industry Effluent. *Journal of Chemical Biological and physical sciences, 10*, 299-304. 10.24214/jcbps.D.10.3.29904.

Patel, H., & Vashi, R. T. (2010). Adsorption of crystal violet dye onto tamarind seed powder. *E-Journal of Chemistry*, *7*(3), 975-984. https://doi.org/10.1155/2010/143439.

Pati, F., Adhikari, B., & Dhara, S. (2010). Isolation and characterization of fish scale collagen of higher thermal stability. *Bioresource technology*, *101*(10), 3737-3742. https://doi.org/10.1016/j.biortech.2009.12.133.

Prasad, A., & Rao, K. V. B. (2011). Physicochemical analysis of textile effluent and decolorization of textile azo dye by Bacillus Endophyticus strain VITABR13. *The IIOAB Journal*, *2*(2), 55-62.

Pereira, P. C. G., Reimão, R. V., Pavesi, T., Saggioro, E. M., Moreira, J. C., & Correia, F. V. (2017). Lethal and sub-lethal evaluation of Indigo Carmine dye and byproducts after TiO_2 photocatalysis in the immune system of *Eisenia andrei* earthworms. *Ecotoxicology and Environmental Safety, 143*(2017), 275-282. https://doi.org/10.1016/j.ecoenv.2017.05.043.

Pereira L, Alves M (2012) Dyes-environmental impact and remediation. In Environmental protection strategies for sustainable development. Springer, Dordrecht pp 111-162. https://doi.org/10.1007/978-94-007-1591-2_4.

Paul, S., Pal, A., Choudhury, A. R., Bodhak, S., Balla, V. K., Sinha, A., & Das, M. (2017). Effect of trace elements on the sintering effect of fish scale derived hydroxyapatite and its bioactivity. *Ceramics International*, *43*(17), 15678-15684. https://doi.org/10.1016/j.ceramint.2017.08.127.

Popuri, A. K., Mandapati, R. N., Pagala, B., & Guttikonda, P. (2016). Colour removal from dye wastewater using adsorption. *International Journal of Pharmaceutical Sciences Review and Research*, *39*(23), 115-118.

Rafiq, M. K., Bachmann, R. T., Rafiq, M. T., Shang, Z., Joseph, S., & Long, R. (2016). Influence of pyrolysis temperature on physico-chemical properties of corn stover (Zea mays L.) biochar and feasibility for carbon capture and energy balance. *PloS one*, *11*(6), 1-17. https://doi.org/10.1371/journal.pone.0156894.

Rahangdale, D., & Kumar, A. (2018). Chitosan as a substrate for simultaneous surface imprinting of salicylic acid and cadmium. *Carbohydrate polymers*, *202*, 334-344. https://doi.org/10.1016/j.carbpol.2018.08.129.

Ramesha, G. K., Kumara, A. V., Muralidhara, H. B., & Sampath, S. (2011). Graphene and graphene oxide as effective adsorbents toward anionic and cationic dyes. *Journal of colloid and interface science*, *361*(1), 270-277. https://doi.org/10.1016/j.jcis.2011.05.050.

Ramesh, T. N., Kirana, D. V., Mohana Kumari, T. N., & Ashwini, A. (2013). Adsorption studies of indigo caramine dye by magnesium oxide. *International Journal of Science Research*, *1*(4), 495-501.

Ramesh, T. N., & Sreenivasa, V. P. (2015). Removal of indigo carmine dye from aqueous solution using magnesium hydroxide as an adsorbent. *Structure*, *33*(35), 1-10. http://dx.doi.org/10.1155/2015/753057.

Rangabhashiyam, S., Lata, S., & Balasubramanian, P. (2018). Biosorption characteristics of methylene blue and malachite green from simulated wastewater onto Carica papaya wood biosorbent. *Surfaces and Interfaces*, *10*, 197-215. https://doi.org/10.1016/j.surfin.2017.09.011.

Redlich O., & Peterson, D. L. (1959). A useful adsorption isotherm. *Journal of Physical Chemistry, 63*(6), 1024-1026. https://doi.org/10.1021/j150576a611.

Ribeiro, A. R., & de Aragão Umbuzeiro, G. (2014). Effects of a textile azo dye on mortality, regeneration, and reproductive performance of the planarian, Girardia tigrina. *Environmental Sciences Europe, 26*(1), 1-8. https://doi.org/10.1186/s12302-014-0022-5.

Robinson, T., Chandran, B., & Nigam, P. (2002). Removal of dyes from a synthetic textile dye effluent by biosorption on apple pomace and wheat straw. *Water research*, *36*(11), 2824-2830. https://doi.org/10.1016/S0043-1354(01)00521-8.

Rustad, T. (2003). Utilisation of marine by-products. *Electronic Journal of Environmental, Agricultural and Food Chemistry*, *2*(4), 458-463.

Sahoo, S. R., Sri, A. G., & Mishra, C. (2019). Preparation of activated carbon from fish scale. *Journal of Advance Research and Development, 4*(4), 1-2.

Santhi, T., Manonmani, S., Vasantha, V. S., & Chang, Y. T. (2016). A new alternative adsorbent for the removal of cationic dyes from aqueous solution. *Arabian journal of chemistry*, *9*, 466-474. https://doi.org/10.1016/j.arabjc.2011.06.004.

Sharma, P., & Kaur, H. (2011). Sugarcane bagasse for the removal of erythrosin B and methylene blue from aqueous waste. *Applied water science*, *1*(3), 135-145. https://doi.org/10.1007/s13201-011-0018-x.

Shikuku, V. O., Zanella, R., Kowenje, C. O., Donato, F. F., Bandeira, N. M., & Prestes, O. D. (2018). Single and binary adsorption of sulfonamide antibiotics onto iron-modified clay: linear and nonlinear isotherms, kinetics, thermodynamics, and mechanistic studies. *Applied Water Science*, *8*(6), 1-12. https://doi.org/10.1007/s13201-018-0825-4.

Shikuku, V. O., Achieng, G. O., & Kowenje, C. O. (2020). Removal of Dyes From Wastewater by Adsorption Onto Low-Cost Adsorbents. In Impact of Textile Dyes on Public Health and the Environment (pp. 239-257). IGI Global. 10.4018/978-1-7998-0311-9.ch011.

Sips, R. (1948). On the structure of a catalyst surface. *The journal of chemical physics*, *16*(5), 490-495. https://doi.org/10.1063/1.1746922.

Sirajudheen, P., Karthikeyan, P., Ramkumar, K., Nisheetha, P., & Meenakshi, S. (2021). Magnetic carbon-biomass from the seeds of Moringa oleifera@ $MnFe_2O_4$ composite as an effective and recyclable adsorbent for the removal of organic pollutants from water. *Journal of Molecular Liquids*, *327*, 1-11. https://doi.org/10.1016/j.molliq.2020.114829.

Slimani, R., El Ouahabi, I., Abidi, F., El Haddad, M., Regti, A., Laamari, M. R., El Antri, S., & Lazar, S. (2014). Calcined eggshells as a new biosorbent to remove basic dye from aqueous solutions: thermodynamics, kinetics, isotherms and error analysis. *Journal of the Taiwan Institute of Chemical Engineers*, *45*(4), 1578-1587. https://doi.org/10.1016/j.jtice.2013.10.009.

Song, W., Liu, M., Hu, R., Tan, X., & Li, J. (2014). Water-soluble polyacrylamide coated-Fe_3O_4 magnetic composites for high-efficient enrichment of U (VI) from radioactive wastewater. *Chemical engineering journal*, *246*, 268-276. https://doi.org/10.1016/j.cej.2014.02.101.

Srivastava, S. (2012). Synthesis and characterization of iron oxide nanoparticle from FeCl3 by using polyvinyl alcohol. *International Journal of Physical and Social Sciences*, *2*(5), 161-184.

Sun, P., Hui, C., Azim Khan, R., Du, J., Zhang, Q., & Zhao, Y. H. (2015). Efficient removal of crystal violet using Fe_3O_4-coated biochar: the role of the Fe_3O_4 nanoparticles and modeling study their adsorption behavior. *Scientific reports*, *5*(1), 1-12. 10.1038/srep12638 (2015).

Temesgen, F., Gabbiye, N., & Sahu, O. (2018). Biosorption of reactive red dye (RRD) on activated surface of banana and orange peels: economical alternative for textile effluent. *Surfaces and interfaces*, *12*, 151-159. https://doi.org/10.1016/j.surfin.2018.04.007.

Temkin, M. I. (1940). Kinetics of ammonia synthesis on promoted iron catalysts. *Acta physiochim. URSS*, *12*, 327-356.

Teshale, F., Karthikeyan, R., & Sahu, O. (2020). Synthesized bioadsorbent from fish scale for chromium (III) removal. *Micron*, *130*, 102817. https://doi.org/10.1016/j.micron.2019.102817.

Toth, J. (1971). State equations of the solid-gas interface layer. *Acta Chem. Acad Hung,* 69, 311-317.

Treybal, R. E. (1981). Mass-transfer operations, McGraw-Hill. Using tree fern as a biosorbent. *Process Biochemistry*, *40*(1), 119-124.

Tsolele, R., Mtunzi, F. M., Klink, M. J. & Pakade, V. E. (2019). An alternative low-cost adsorbent for gold recovery from cyanide-leached liquors: adsorption isotherm and kinetic studies. *Adsorption Science & Technology,* *37*(1-2), 3–23. https://doi.org/10.1177/0263617418802557.

Uzunoğlu, D., & Özer, A. (2016). Adsorption of Acid Blue 121 dye on fish (Dicentrarchus labrax) scales, the extracted from fish scales and commercial hydroxyapatite: equilibrium, kinetic, thermodynamic, and characterization studies. *Desalination and Water Treatment*, *57*(30), 14109-14131. https://doi.org/10.1080/19443994.2015.1063091.

Uchimiya, M., Wartelle, L. H., Klasson, K. T., Fortier, C. A., & Lima, I. M. (2011). Influence of pyrolysis temperature on biochar property and function as a heavy metal sorbent in soil.

Journal of agricultural and food chemistry, *59*(6), 2501-2510. https://doi.org/10.1021/jf104206c.

Vanitha, T. (2014). Removal of crystal violet from wastewater. *Scrutiny International Research Journal of Advanced Zoology, Animal Science and Nutriotion*, *1*(1), 2349-4263.

Vikrant, K., Giri, B. S., Raza, N., Roy, K., Kim, K. H., Rai, B. N., & Singh, R. S. (2018). Recent advancements in bioremediation of dye: current status and challenges. *Bioresource Technology, 253*, 355–367.

Villanueva-Espinosa, J. F., Hernandez-Esparza, M., & Ruiz-Trevino, F. A. (2001). Adsorptive properties of fish scales of Oreochromis Niloticus (Mojarra Tilapia) for metallic ion removal from wastewater. *Industrial & Engineering Chemistry Research*, *40*(16), 3563-3569

Wagh, P. B., & Shrivastava, V. S. (2015). Removal of indigo carmine dye by using palm wood cellulose activated carbon in aqueous solution: a kinetic and equilibrium study. *International Journal of Latest Technology in Engineering, Management & Applied Science*, *4*(7), 106-114.

Wang, S., Zhao, X., Xing, G., & Yang, L. (2013). Large-scale biochar production from crop residue: A new idea and the biogas-energy pyrolysis system. *BioResources*, *8*(1), 8-11.

Wang, X., Zhou, W., Liang, G., Song, D., & Zhang, X. (2015). Characteristics of maize biochar with different pyrolysis temperatures and its effects on organic carbon, nitrogen and enzymatic activities after addition to fluvo-aquic soil. *Science of The Total Environment, 538*, 137–144. https://doi.org/10.1016/j.scitotenv.2015.08.026.

Wu, N., Liu, X., Zhao, C., Cui, C., & Xia, A. (2016). Effects of particle size on the magnetic and microwave absorption properties of carbon-coated nickel nanocapsules. *Journal of Alloys and Compounds*, *656*, 628-634. https://doi.org/10.1016/j.jallcom.2015.10.027.

Xie, T., Reddy, K. R., Wang, C., Yargicoglu, E., & Spokas, K. (2015). Characteristics and applications of biochar for environmental remediation: a review. *Critical Reviews in Environmental Science and Technology*, *45*(9), 939-969. https://doi.org/10.1080/10643389.2014.924180.

Xiu, S., Shahbazi, A., & Li, R. (2017). Characterization, modification and application of biochar for energy storage and catalysis: a review. *Trends in renewable energy*, *3*(1), 86-101. 10.17737/tre.2017.3.1.0033.

Xu, Y., & Wang, E. (2012). Electrochemical biosensors based on magnetic micro/nano particles. *Electrochimica Acta*, *84*, 62-73. https://doi.org/10.1016/j.electacta.2012.03.147.

Xu, Y., & Chen, B. (2013). Investigation of thermodynamic parameters in the pyrolysis conversion of biomass and manure to biochars using thermogravimetric analysis. *Bioresource technology*, *146*, 485-493. https://doi.org/10.1016/j.biortech.2013.07.086.

Yadav, S., Asthana, A., Chakraborty, R., Jain, B., Singh, A. K., Carabineiro, S. A., & Susan, M. A. B. H. (2020). Cationic dye removal using novel magnetic/activated charcoal/β-cyclodextrin/alginate polymer nanocomposite. *Nanomaterials*, *10*(1), 170-189. https://doi.org/10.3390/nano10010170.

Yuan, X., Xia, W., An, J., Yin, J., Zhou, X., & Yang, W. (2015). Kinetic and thermodynamic studies on the phosphate adsorption removal by dolomite mineral. *Journal of Chemistry*, 1–8.

Yu, X., Tong, S., Ge, M., Zuo, J., Cao, C., & Song, W. (2013). One-step synthesis of magnetic composites of cellulose@ iron oxide nanoparticles for arsenic removal. *Journal of Materials Chemistry A*, *1*(3), 959-965. https://doi.org/10.1039/C2TA00315E.

Zainon, I., Alwi, N., Abidin, M., Haniza, H., Ahmad, M. & Ramli, A. (2012). Physicochemical properties of hydroxyapatite extracted from fish scales. *Advanced Materials Research, 545*, 235–239. https://doi.org/10.4028/www.scientific.net/AMR.545.235.

Zhang, B., Zeng, X., Xu, P., Chen, J., Xu, Y., Luo, G., Xu, M, & Yao, H. (2016). Using the novel method of nonthermal plasma to add Cl active sites on activated carbon for removal of mercury from flue gas. *Environmental science & technology*, *50*(21), 11837-11843. https://doi.org/10.1021/acs.est.6b01919.

Zhang, J., Zhang, P., Zhang, S., & Zhou, Q. (2014). Comparative study on the adsorption of tartrazine and indigo carmine onto Maize Cob Carbon. *Separation Science and Technology*, *49*(6), 877-886. https://doi.org/10.1080/01496395.2013.863340.

Zhang, M., Gao, B., Varnoosfaderani, S., Hebard, A., Yao, Y., & Inyang, M. (2013). Preparation and characterization of a novel magnetic biochar for arsenic removal. *Bioresource Technology*, *130*, 457-462. https://doi.org/10.1016/j.biortech.2012.11.132.

Zhang, Y., Xu, Q., Zhang, S., Liu, J., Zhou, J., Xu, H., Xiao, H., & Li, J. (2013). Preparation of thiol-modified Fe_3O_4@ SiO_2 nanoparticles and their application for gold recovery from dilute solution. *Separation and Purification Technology*, *116*, 391-397. https://doi.org/10.1016/j.seppur.2013.06.018.

Zhang, Q., Cheng, Y., Fang, C., Chen, J., Chen, H., Li, H., & Yao, Y. (2020). Facile synthesis of porous carbon/Fe_3O_4 composites derived from waste cellulose acetate by one-step carbothermal method as a recyclable adsorbent for dyes. *Journal of Materials Research and Technology*, *9*(3), 3384-3393. https://doi.org/10.1016/j.jmrt.2020.01.074.

Zhao, S. X., Ta, N., & Wang, X. D. (2017). Effect of temperature on the structural and physicochemical properties of biochar with apple tree branches as feedstock material. *Energies*, *10*(9), 1-15. https://doi.org/10.3390/en10091293.

Zheng, Y., Yang, Y., Zhang, Y., Zou, W., Luo, Y., Dong, L., & Gao, B. (2019). Facile one-step synthesis of graphitic carbon nitride-modified biochar for the removal of reactive red 120 through adsorption and photocatalytic degradation. *Biochar*, *1*(1), 89-96. https://doi.org/10.1007/s42773-019-00007-4.

Zheng, X., Zheng, H., Xiong, Z., Zhao, R., Liu, Y., Zhao, C., & Zheng, C. (2020). Novel anionic polyacrylamide-modify-chitosan magnetic composite nanoparticles with excellent adsorption capacity for cationic dyes and pH-independent adsorption capability for metal ions. *Chemical Engineering Journal*, *392*, 1-55. https://doi.org/10.1016/j.cej.2019.123706.

Zhu, K., Gong, X., He, D., Li, B., Ji, D., Li, P., Peng, Z., & Luo, Y. (2013). Adsorption of Ponceau 4R from aqueous solutions using alkali boiled Tilapia fish scales. *RSC advances*, *3*(47), 25221-25230. 10.1039/c3ra43817a.

APPENDICES

Appendix 1a: Nitrogen sorption isotherm for FSB@400 ºC

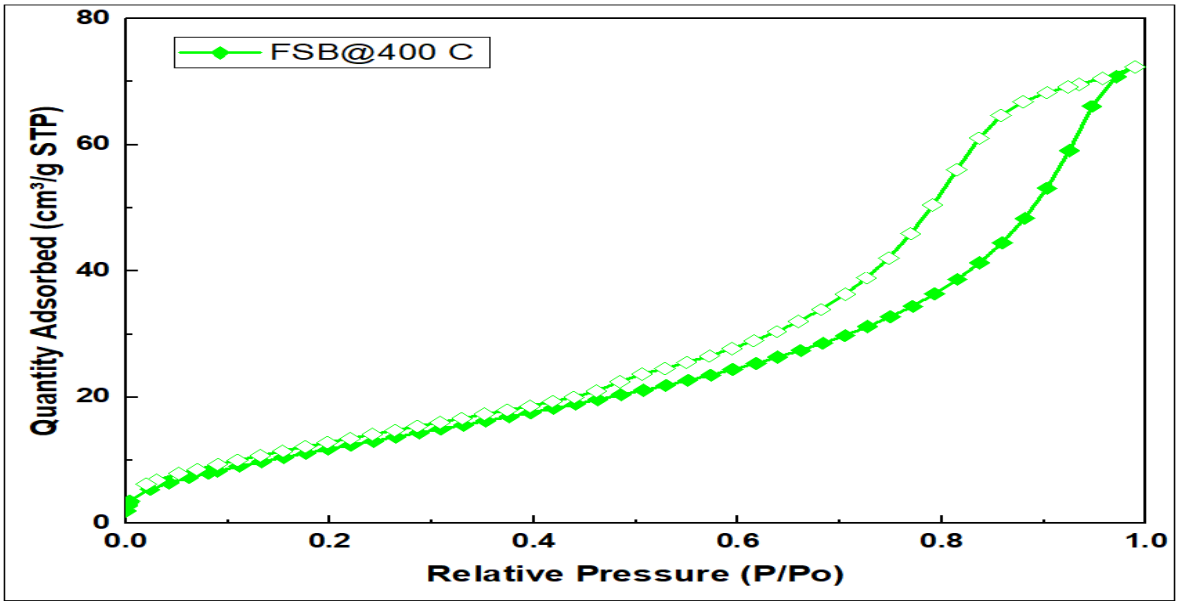

Appendix 1b: Nitrogen sorption isotherm for FSB@400 ºC-Fe_3O_4

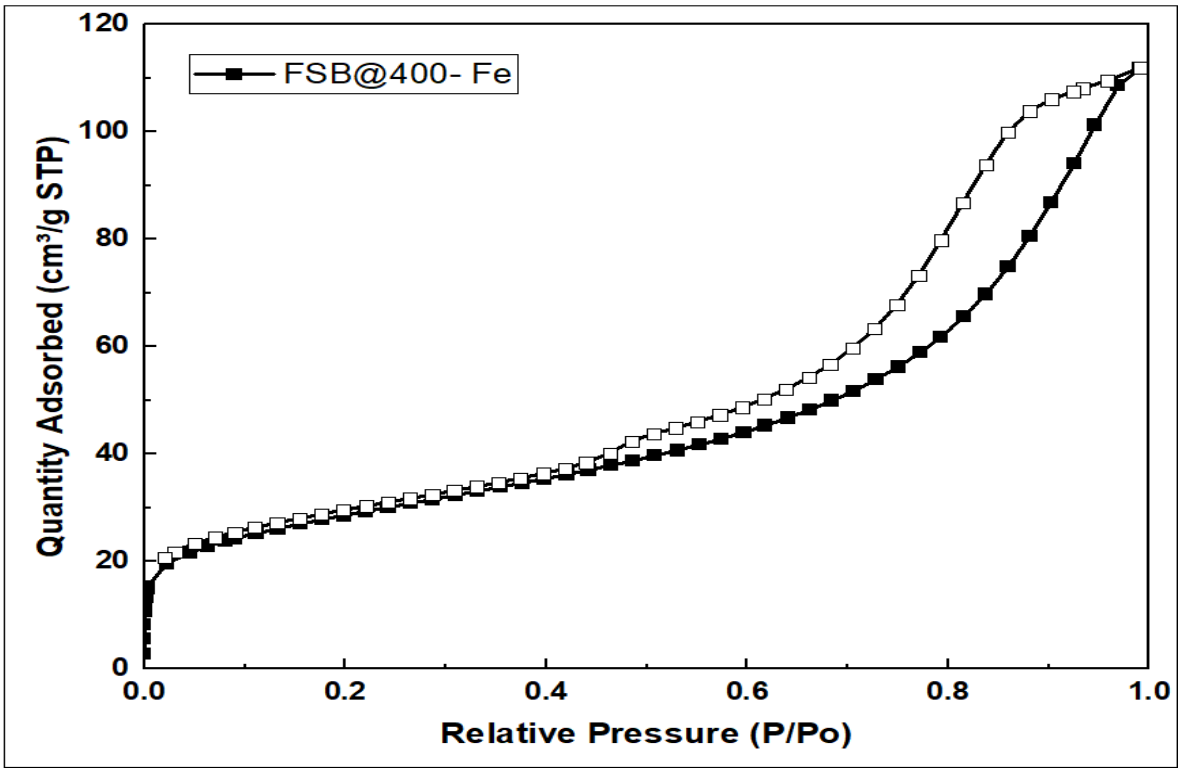

Appendix 1c: Nitrogen sorption isotherm for FSB@400 ºC-CV

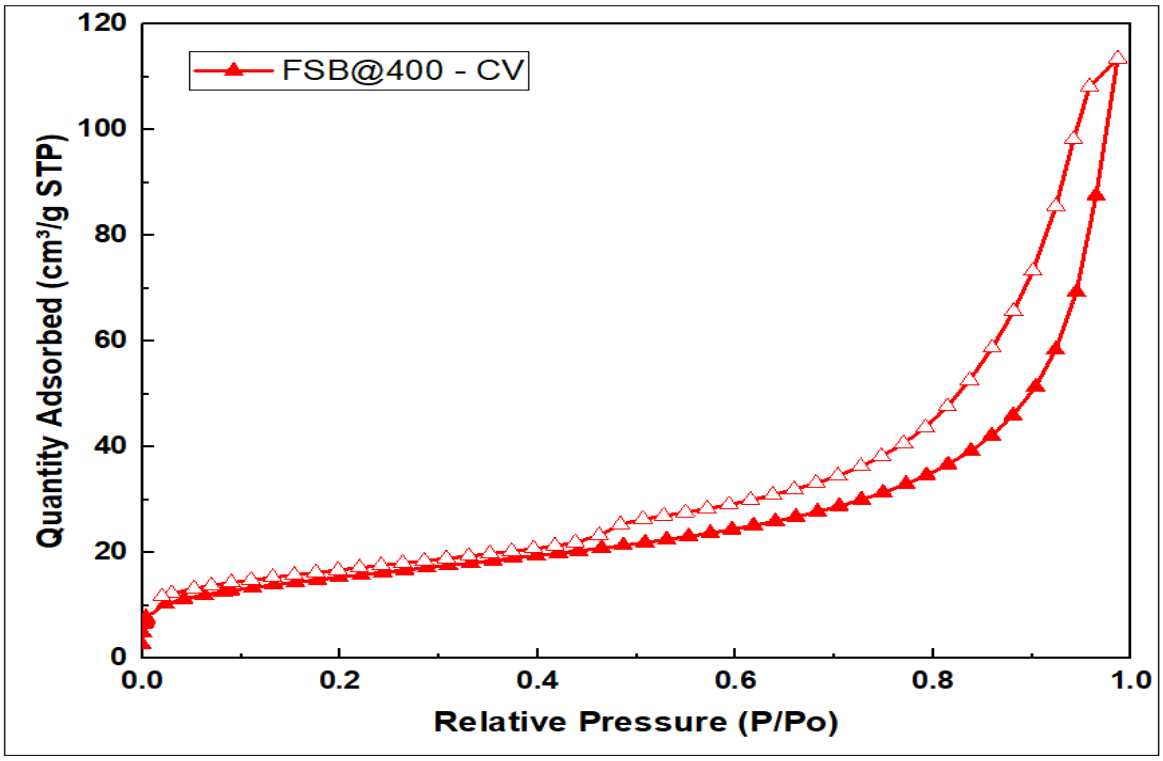

Appendix 1d: Nitrogen sorption isotherm for FSB@600 ºC

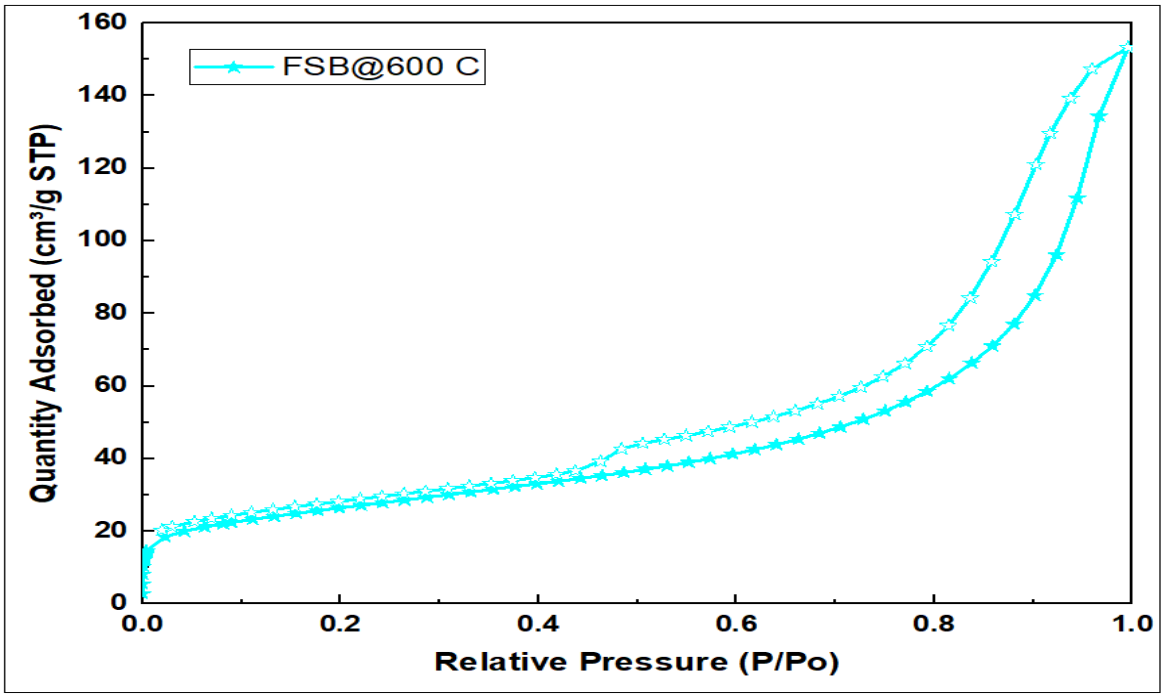

Appendix 1e: Nitrogen sorption isotherm for FSB@600 ºC-Fe_3O_4

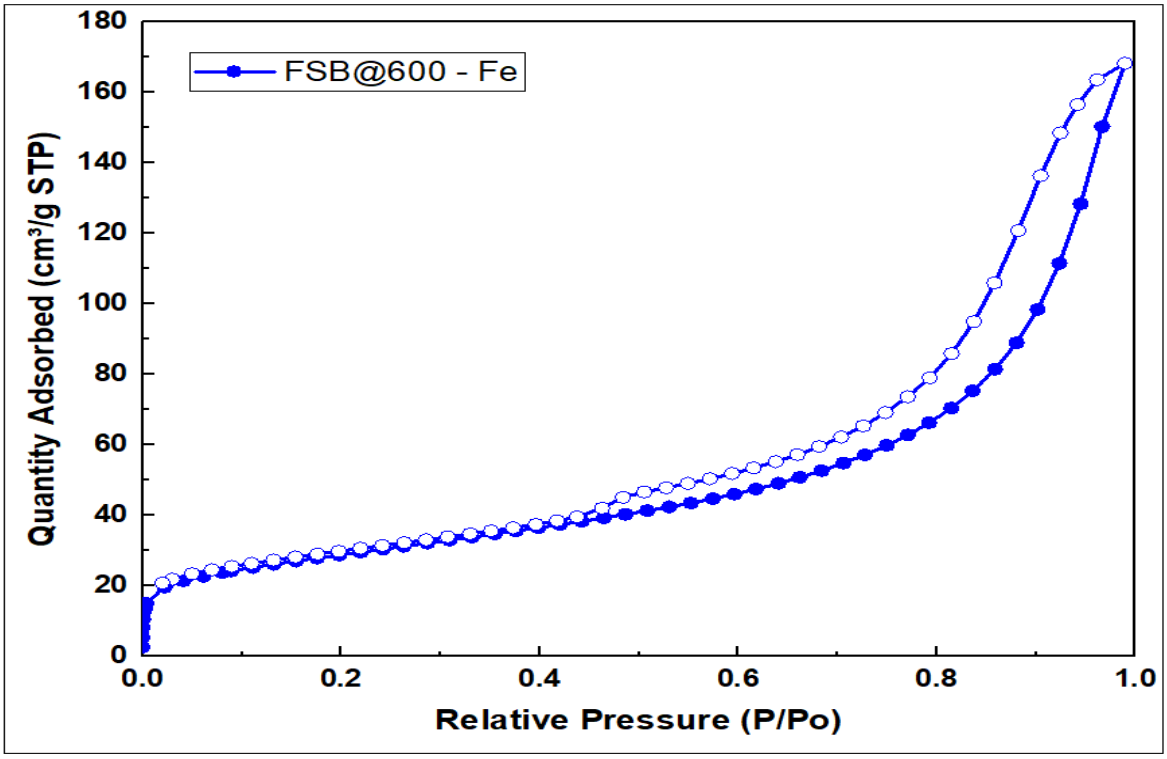

Appendix 1f: Nitrogen sorption isotherm for FSB@800 ºC

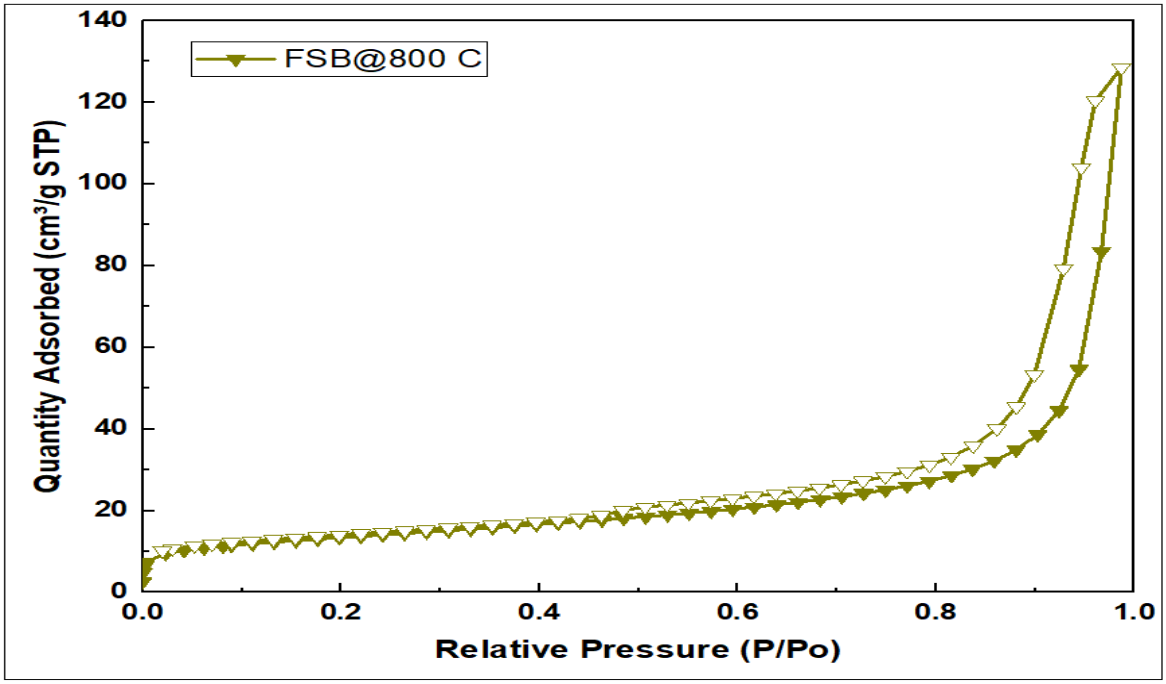

Appendix 1g: Nitrogen sorption isotherm for FSB@800 ºC-Fe_3O_4